UNIVERSITY OF OKLAHOMA

GRADUATE COLLEGE

WEAK SCALE SUPERSYMMETRY FROM THE MULTIVERSE

A DISSERTATION

SUBMITTED TO THE GRADUATE FACULTY

in partial fulfillment of the requirements for the

Degree of

DOCTOR OF PHILOSOPHY

By

DIBYASHREE SENGUPTA

Norman, Oklahoma

2020

WEAK SCALE SUPERSYMMETRY
FROM THE MULTIVERSE

A DISSERTATION APPROVED FOR THE
HOMER L. DODGE DEPARTMENT OF PHYSICS AND ASTRONOMY

BY THE COMMITTEE CONSISTING OF

Dr. Howard Baer, Chair

Dr. Lucy Lifschitz

Dr. Chung Kao

Dr. Patrick Skubic

Dr. Bruno Uchoa

Table of Contents

List of Acronyms

1. AdS : Anti de Sitter
2. AMSB : Anomaly Mediated Supersymmetry Breaking
3. ATLAS : A Toroidal LHC ApparatuS
4. BBN : Big Bang Nucleosynthesis
5. BCM : Bosonic Coherent Motion
6. BG : Background
7. BK : Bastero-Gil-King model
8. BSM : Beyond Standard Model
9. CC : Cosmological Constant
10. CCB : Color or Charge Breaking
11. CCK : Choi-Chun-Kim model
12. CCL : Choi-Chun-Lee model
13. CDEEL : Cvetic-Demir-Espinosa-Everett-Langacker model
14. CDM : Cold Dark Matter
15. CERN : Conseil européen pour la recherche nucléaire (European Organization for Nuclear Research)
16. CKM : Cabibbo–Kobayashi–Maskawa
17. CKN : Chun-Kim-Nilles model

18. CM : Casas-Munoz model

19. CMB : Cosmic Microwave Background

20. CMS : Compact Muon Solenoid

21. cMSSM : Constrainted Minimal Supersymmetric Standard Model

22. CO : Coherent Oscillation

23. CP : Charge-Parity

24. DE : Dark Energy

25. DFSZ : Dine-Fischler-Srednicki-Zhitnitsky model

26. DM : Dark Matter

27. ECAL : Electromagnetic Calorimeter

28. EW : Electroweak

29. EWK : Eyton-Williams-King model

30. EWSB : Electroweak Symmetry Breaking

31. FCNC : Flavor Changing Neutral Current

32. GM : Giudice-Masiero model

33. GMSB : Gauge Mediated Supersymmetry Breaking

34. GSW : Glashow-Salam-Weinberg model

35. GUT : Grand Unified Theory

36. HCAL : Hadronic Calorimeter

37. HE-LHC : High Energy-Large Hadron Collider

38. HFD : Higgs Flavor Democracy model

39. HL-LHC : High Luminosity-Large Hadron Collider

40. HPT : Hundi-Pakvasa-Tata model

41. hyCCK : Hybrid Choi-Chun-Kim model

42. hyMSY : Hybrid Murayama-Suzuki-Yanagida model

43. hySPM : Hybrid S.P. Martin model

44. IDD : Indirect Detection

45. IL : Integrated Luminosity

46. IR : Infrared

47. KKLT : Kachru-Kallosh-Linde-Trivedi

48. KMR : Kamionkowski and March-Russell

49. KN : Kim-Nilles model

50. KSVZ : Kim-Shifman-Vainshtein-Zakharov model

51. LH : Little Hierarchy

52. LHA : Les Houches Accord

53. LHC : Large Hadron Collider

54. LHC14 : Large Hadron Collider at 14 TeV

55. LO : Leading Order

56. LSP : Lightest Supersymmetric Particle

57. mAMSB : Minimal Anomaly Mediated Supersymmetry Breaking model

58. MBGW : Martin-Babu-Gogoladze-Wang model

59. MET : Missing Transverse Energy

60. MI : Model Independent

61. MM : Mirage Mediation

62. m_P : Reduced Planck Mass

63. MSSM : Minimal Supersymmetric Standard Model

64. mSUGRA : minimal Supergravity model

65. MSY : Murayama-Suzuki-Yanagida model

66. nAMSB : natural Anomaly Mediated Supersymmetry Breaking model

67. nGMM : natural General Mirage Mediation model

68. NLO : Next-to-Leading Order

69. NMSSM : Next-to-Minimal Supersymmetric Standard Model

70. nMSSM : Nearly-Minimal Supersymmetric Standard Model

71. $\mu\nu$SSM : μ-from-ν Supersymmetric Standard Model

72. NUHM2,3 : Two or Three extra parameter non-Universal Higgs models

73. OS : Opposite Sign

74. OU : Our Universe

75. pMSSM : Phenomenological Minimal Supersymmetric Standard Model

76. PQ : Peccei-Quinn

77. PU : Pocket Universe

78. QCD : Quantum ChromoDynamics

79. RGE : Renormalization Group Equation

80. RH : Right-Handed

81. RHN : Right-Handed Neutrino

82. RNS : Radiatively-Driven Natural Supersymmetry

83. RPV : R-Parity Violation

84. SD : Spin Dependent

85. SD DD : Spin Dependent Direct Detection

86. SF : Same Flavor

87. SI : Spin Independent

88. SI DD : Spin Independent Direct Detection

89. SM : Standard Model

90. sMSSM : Secluded sector Minimal Supersymmetric Standard Model

91. SPM : S.P.Martin model

92. SS : Same Sign

93. SSB : Soft Supersymmetry Breaking

94. SSdB : Same sign diBoson

95. SUGRA : Supergravity

96. SUSY : Supersymmetry

97. UV : Ultraviolet

98. VEV : Vacuum Expectation Value

99. WIMP : Weakly Interacting Massive Particle

100. WTN : Well Tempered Neutralino

Abstract

The CERN Large Hadron Collider (LHC) has not found any experimental evidence yet for Supersymmetric (SUSY) particles. This has pushed the limits on the masses of SUSY particles in the multi-TeV region high enough to question whether nature is finetuned for SUSY to exists. However, with the introduction of the Electroweak (EW) fine tuning measure Δ_{EW}, some distinct SUSY models are found to be natural even if they involve highly massive SUSY particles.

Naturalness require the superpotential μ parameter $\mu \approx 110$ - 350 GeV. However, it is not straightforward to explain the origin of such low value of μ and this leads to the SUSY μ-problem. These natural SUSY models provide a higgsino-like Lightest Supersymmetric Particle (LSP) which can serves as a possible DM candidate (considering R-parity conservation) if it has no color or electric charge. In chapter II of this thesis, it has been shown that such a thermally-produced LSP alone cannot account for the entire DM content of the universe. At this point the Axion, arising in a different context, rescues the model from under-producing DM. The PQ solution to the strong CP problem, that gives rise to Axion, requires implementation of $U(1)_{PQ}$ symmetry as the fundamental symmetry, which being a global symmetry, is incompatible with the inclusion of gravity. Hence the model suffers from a gravity-spoliation problem.

Chapter III focuses on solving the SUSY μ problem, and the gravity-spoliation problem while still solving the strong CP problem and giving rise to axion to fulfill the DM content of our universe. To serve this purpose I introduce here two new SUSY DFSZ axion models based on a fundamental discrete R-symmetry $\mathbf{Z}_{24}^{R}$-which may emerge from compactification of 10-d Lorentzian spacetime in string theory. String theory, expected to be an ultraviolet complete theory, generates the PQ breaking scale (f_a) as high as $f_a \sim m_{\rm GUT}$ to $m_{\rm string}$. However, for mixed axion-neutralino dark matter, cosmological (dark matter) constraints require the PQ breaking scale $f_a \sim 10^{11} - 10^{12}$ GeV.

Since, the string landscape approach arising from multiverse argument could successfully predict the value of the Cosmological Constant (Λ), so in chapter IV, I explore the possibility that the magnitude of the Peccei-Quinn (PQ) scale f_a is also set within the cosmological sweet spot $f_a \sim 10^{11} - 10^{12}$ GeV by string landscape considerations within the framework of a compelling SUSY axion model. Rather general considerations of the string theory landscape imply a mild statistical draw towards large soft SUSY breaking terms (m^n_{soft}) tempered by requiring $\Delta_{EW} < 30$ so as to not violate the (anthropic) atomic principle. Chapter IV also shows how the string theory landscape affects the mirage mediated SUSY breaking framework and how it leads to a natural mixed decoupling/quasi-degeneracy solution to the SUSY flavor problem and a decoupling solution to the SUSY CP problem.

Chapter V provides detailed phenomenological study of two important SUSY search channels in the LHC : 1. Gluino pair production and 2. Wino pair production for the natural SUSY models which has higgsino-like LSP. Two other important channel for SUSY searches in LHC are top squark pair production and higgsino pair production. All of these search channels have been confronted with current LHC constraints and projected constraints from High Luminosity LHC (HL-LHC) and High Energy LHC (HE-LHC) to show what sort of upgradation is needed for LHC to discover or falsify natural supersymmetry.

I. Introduction

I.1. Standard Model

Till today, the Standard Model (SM) is the most celebrated theory that explains nature almost completely. However, the SM cannot explain some phenomena observed in nature and that is why it is needed to look for theories beyond the Standard Model (BSM). In this section, the SM will be briefly discussed followed by its drawbacks and BSM theories.

I.1.1. Forces, Particles and Symmetries

Nature consists of matter and forces. The four forces in nature are : Strong nuclear force, Weak nuclear force, Electromagnetic force and Gravitational force. Each force is mediated by some fundamental particles, named the gauge bosons, which are present in the particle spectrum of the Standard Model.

- The strong force holds the nucleons together to form a nucleus. It is attractive in nature at small distance but only acts over nuclear distance scales. The gauge boson which mediates the strong force is called the Gluon. Only those particles which have color charge can interact via strong interaction i.e., via exchange of gluons.

- Weak force or weak interaction between subatomic particles manifests itself through radioactive decay of nuclei. It is mediated through $W^{\pm}$ and Z bosons. Its effective range is less than the diameter of a proton.

- Electromagnetic force is responsible for the interaction between electrically charged particles. Its range is infinity. However, its strength reduces as the distance between the interacting particles increases. Since atoms are electrically neutral, we

often don't notice the long range of this force. It is mediated through the photon (γ).

- Gravitational force is attractive in nature and is always present between any two massive particles. It also has a range of infinity and its strength decreases as the distance between the interacting particles increases. It is mediated through a hypothetical particle called the graviton.

Beside the bosons, the SM also contains fermions. All the fundamental particles can be broadly classified into bosons (integer spin) and fermions (half-integer spin). Bosons obey Bose-Einstein quantum statistics while fermions obey Fermi-Dirac statistics. Bosons have been already discussed above. Fermions can again be classified into leptons and quarks.

Quarks have color charge and electric charge and hence participate in strong, weak, electromagnetic and gravitational interaction. There are six flavors of quarks, namely, up (u), down (d), strange (s), charm (c), top (t) and bottom (b). These six quarks can be classified into three generations as shown in Fig 1.

Leptons do not have color charge. Hence they do not participate in strong interactions. There are three electrically charged leptons, namely, electron (e), muon (μ) and tau (τ), and three electrically neutral leptons, namely, electron neutrino (ν_e), muon neutrino (ν_μ) and tau neutrino (ν_τ).

All the above described particles (bosons and fermions) have their anti-particles as well. Beside these bosons and fermions, the SM includes a spin-0 particle called the Higgs boson which is responsible for mass of all the above particles (except possibly the neutrinos). In 2012, the discovery of the Higgs boson with mass $m_h \sim 125$ GeV by the Atlas [1] and the CMS [2] collaboration at LHC completed the expected matter content of the SM.

The Standard Model is a non-Abelian gauge theory based on the group $SU(3)_C \times$

$SU(2)_L \times U(1)_Y$ with $SU(2)_L \times U(1)_Y$ broken to $U(1)_{em}$. $SU(3)_C$ is unbroken. The representations in the SM for the first generation fermions and bosons along with their quantum numbers under $SU(3)_C \times SU(2)_L \times U(1)_Y$ is given in Table 1 :

	$SU(3)_C \times SU(2)_L \times U(1)_Y$
Fermions	$Q = \begin{pmatrix} u_L \\ d_L \end{pmatrix} \sim (3, 2, \frac{1}{3}), u_R \sim (3, 1, \frac{4}{3}), d_R \sim (3, 1, -\frac{2}{3})$ $L = \begin{pmatrix} \nu_L^e \\ e_L \end{pmatrix} \sim (1, 2, -1), e_R \sim (1, 1, -2)$
Gauge Bosons	$G_{a,a=1-8}, A_{i,i=1-3}, B$
Higgs	$\Phi = \begin{pmatrix} \phi^+ \\ \phi^0 \end{pmatrix} \sim (1, 2, 1)$

Table 1: Matter, gauge boson and higgs contents of the SM.

The Particle spectrum of The Standard Model is given in Fig 1. The $SU(3)_C$ gauge theory is Quantum Chromodynamics (QCD). The $SU(2)_L$ X $U(1)_Y$ symmetry underlies the electroweak model also known as the Glashow-Salam-Weinberg (GSW) model [3, 4, 5].

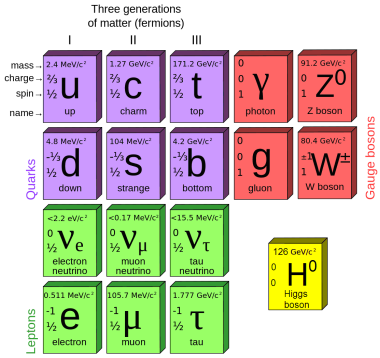

Figure 1: Particle spectrum of The Standard Model.

I.1.2. Electroweak Symmetry Breaking

At low energy, $SU(2)_L \times U(1)_Y$ breaks down to $U(1)_{em}$ which explains the electromagnetic interactions. This symmetry breaking is spontaneous and is known as Electroweak symmetry breaking or Brout-Englert-Higgs-Kibble mechanism [6, 7] (The Higgs mechanism for short). This process occurs when the Higgs boson, which is a spin 0 field with gauge quantum numbers as shown in Table 1, acquires a Vacuum Expectation Value (VEV). The Lagrangian Density for the Higgs field $\Phi = \begin{pmatrix} \phi^+ \\ \phi^0 \end{pmatrix}$ is given by

$$\mathcal{L}_{higgs} = (D_\mu \Phi)^\dagger (D_\mu \Phi) - V(\Phi) \tag{1}$$

with,

$$V(\Phi) = \mu^2 \Phi^\dagger \Phi + \lambda (\Phi^\dagger \Phi)^2 \tag{2}$$

This potential $V(\Phi)$ is the famous mexican hat potential. For $\mu^2 > 0$ the minima of $V(\Phi)$ is at $\Phi = \begin{pmatrix} 0 \\ 0 \end{pmatrix}$ but for $\mu^2 < 0$ the field Φ develops a non-zero Vacuum Expectation Value at $|\Phi| = (-\frac{\mu^2}{2\lambda})^{1/2}$.

The Higgs field can be redefined as

$$\Phi = \begin{pmatrix} 0 \\ \frac{H(x)+V}{\sqrt{2}} \end{pmatrix} \tag{3}$$

where H is a real field with zero VEV. From Equation (1) and (3), we can obtain masses of $W^\pm$ and Z bosons by plugging in $V = 246$ GeV while photon (γ) remains massless. Similarly, the fermions also gain mass through the Higgs mechanism except the neutral leptons i.e., the neutrinos since the SM does not include right-handed neutrinos. However, it is straight forward to include either Dirac or Majorana massive neutrinos

by adding three generations of gauge singlet right-handed neutrinos ν_i^R.

I.1.3. Physics Beyond Standard Model

Following are some of the questions that the SM cannot solve:

- Radiative corrections to the Higgs boson mass are quadratically divergent : $\delta m_H^2 \sim \Lambda^2$. The theoretically obtained Higgs boson mass from the SM is $m_H^2 = m_{H_0}^2 + \delta m_H^2$. Hence, $m_{H_0}^2$ must be incredibly fine-tuned in order to match the experimentally obtained mass of Higgs boson $m_h \sim 125$ GeV [1, 2, 8]. This discrepancy between theory and experiment is named the Big Hierarchy Problem.

- The particle content of the SM can explain only 5% of the universe. 27% of the Universe consists of Dark Matter (DM) and 68% of the Universe consists of Dark Energy (DE) [9]. The SM does not have a viable DM candidate.

- The SM assumes neutrinos to be massless. However, experimentally it was determined that neutrinos have tiny mass [10].

- The Universe is made of matter only and it does not contain any anti-matter. SM also cannot explain this matter-antimatter asymmetry [11].

- Out of the four forces in nature, namely : Strong force, Weak force, Electromagnetic force and Gravitational force, the SM can explain the first three but the quantum Gravitational force is non-renormalizable.

- There are gauge couplings associated with each force which accounts for the strength of the corresponding interaction. At higher energies it is expected that due to restoration of symmetry the gauge couplings for Strong force, Weak force and Electromagnetic force should unify. This phenomena is called Gauge Coupling Unification which cannot be explained by SM.

- The SM requires Electroweak Symmetry Breaking (EWSB) [6] to theoretically explain the experimentally obtained values of the masses of SM particles. However, the SM allows for but does not explain EWSB.

- In the QCD sector of SM, the $U(1)_A$ problem which arise due to the appearance of 4 Goldstone bosons (or four pions) on breaking $U(2)_A$ spontaneously was solved by 't Hooft via the discovery of the QCD θ vacuum which does not respect $U(1)_A$ symmetry. This led to an additional term in the QCD Lagrangian : $\theta \frac{g^2}{32\pi^2} F_a^{\mu\nu} \tilde{F}_{a\mu\nu}$, which turns out to be a CP-violating term. On including weak interaction effects this term in the Lagrangian gets modified as : $\bar{\theta} \frac{g^2}{32\pi^2} F_a^{\mu\nu} \tilde{F}_{a\mu\nu}$, where $\bar{\theta} = \theta + |M|$, with $|M|$ being the diagonalized quark mass matrix. Thus the CP-violating term in the complete Lagrangian is $\bar{\theta} \frac{g^2}{32\pi^2} F_a^{\mu\nu} \tilde{F}_{a\mu\nu}$. In order to match experiments, $\bar{\theta}$ should be very small ($\bar{\theta} << 10^{-10}$). Such a small value of $\bar{\theta}$ requires a large amount of fine-tuning. This is known as the "Strong CP-Problem" [12].

- The measured value of the cosmological constant $\Lambda \simeq 10^{-120} m_P^4$ whereas naively it is expected that $\Lambda \simeq m_P^4$ with m_P being the reduced Planck mass. This is the cosmological constant (CC) problem [65].

The above unsolved questions are the inspiration behind the requirement of Beyond Standard Model (BSM) theories.

I.2. Supersymmetry

Out of many BSM theories, Supersymmetry (SUSY) is a well-motivated extension of the SM that can provide solutions for most of the problems discussed in Sec I.1.3. SUSY requires that for each SM fermion (boson) there exist a boson (fermion). The superpartner of the SM fermions have spin-0 and are called *sfermions*. Analogously, superpartner of quarks are *squarks* and that of leptons are *sleptons*. The superpartner of the SM bosons are spin-1/2 particles. The superpartner of the gauge bosons are

called the *gauginos* namely : *gluino*, *wino* and *bino*, and that of higgs boson are called the *higgsinos*. The *gauginos* and the *higgsinos* are in mathematical basis. They mix and in the physical basis, we have the *charginos* and the *neutralinos*.

I.2.1. Motivation

The assumption of presence of a boson(fermion) for each SM fermion (boson) is motivated by solution to Big Hierarchy Problem. Under SUSY, the quadratic divergences in Higgs mass calculation that arise due to SM particles are cancelled by their corresponding SUSY particles. In addition to this, following are several experimental arguments that also support supersymmetric models.

1. **Unification of gauge couplings** : The values of running gauge couplings do not unify if we evolve the weak scale values to high energies using Renormalization Group Equations (RGEs) of the SM but they unify remarkably well if we use supersymmetric RGEs provided the superpartner masses are in the range 100 GeV-10 TeV.

2. **Cold Dark Matter** : All supersymmetric models with a conserved R-parity quantum number include a stable massive particle. If it is electrically and color neutral then it is a suitable candidate for being a Dark Matter particle.

3. **Radiative breakdown of electroweak symmetry** : In the SM, EWSB can be accommodated by appropriate choice of the scalar potential parameters without any explanation for this choice. But in supersymmetric models, renormalization effects triggered by the large top quark Yukawa coupling results in the observed electroweak symmetry breaking.

4. **Mass of the Higgs Boson** : Quadratic divergences are cancelled in any supersymmetric model. This offers the opportunity for a natural (i.e., no fine-tuning) value of the measured Higgs mass.

I.2.2. Minimal Supersymmetric Standard Model

The Minimal Supersymmetric Standard Model (MSSM) is the simplest supersymmetric extension of the SM [13]. The gauge symmetry group chosen for MSSM is that of the Standard Model : $SU(3)_C \times SU(2)_L \times U(1)_Y$. Each SM field is promoted to its corresponding superfield. The gauge bosons of the SM are promoted to gauge superfields as follows :

$$\hat{g}_A \ni (\tilde{g_A}, G_{A\mu}, \mathcal{D}_{gA}), A = 1 - 8$$

$$\hat{W_A} \ni (\lambda_A, W_{A\mu}, \mathcal{D}_{WA}), A = 1 - 3$$

$$\hat{B} \ni (\lambda_0, B_\mu, \mathcal{D}_B)$$

The matter superfields are :

$$\begin{pmatrix} \nu_{iL} \\ e_{iL} \end{pmatrix} \rightarrow \hat{L}_i \equiv \begin{pmatrix} \hat{\nu}_{iL} \\ \hat{e}_{iL} \end{pmatrix},$$

$$\left(e^c_{iR}\right) \rightarrow \hat{E}^c_i,$$

$$\begin{pmatrix} u_{iL} \\ d_{iL} \end{pmatrix} \rightarrow \hat{Q}_i \equiv \begin{pmatrix} \hat{u}_{iL} \\ \hat{d}_{iL} \end{pmatrix},$$

$$\left(u^c_{iR}\right) \rightarrow \hat{U}^c_i,$$

$$\left(d^c_{iR}\right) \rightarrow \hat{D}^c_i,$$

where i = 1, 2, 3 is the generation index.

Since the superpotential must be a function of just left-chiral superfields, instead of using the right-handed SM fermions, we shall use their left-handed charge conjugates

as shown above.

Each superfield consists of the SM particle and its SUSY partner in addition to the corresponding auxiliary field. Explicitly, if the superfield expansion of electron is written :

$$\hat{e}_L = \tilde{e}_L(\hat{x}) + i\sqrt{2}\bar{\theta}\psi_{eL}(\hat{x}) + i\bar{\theta}\theta_L\mathcal{F}_e(\hat{x}) \tag{4}$$

where, $\tilde{e}_L$ is the selectron field, ψ_{eL} is the left-handed SM electron field and $\mathcal{F}_e$ is the corresponding auxiliary field.

The Higgs doublet of the SM is promoted to a doublet of left-chiral superfields :

$$\phi \equiv \begin{pmatrix} \phi^+ \\ \phi^0 \end{pmatrix} \rightarrow \hat{H}_u \equiv \begin{pmatrix} \hat{h}_u^+ \\ \hat{h}_u^0 \end{pmatrix}.$$

It carries a weak hypercharge of Y = 1. The VEV of the scalar component of $\hat{h}_u^0$ gives mass to up-type quark but cannot give mass to down-type quark because a field with Y=-1 is needed for this purpose. The scalar component of the right-chiral superfield $\hat{h}_u^{0\dagger}$ would have served the purpose but since right-chiral superfields are not allowed in the superpotential, so we need to introduce a second left chiral scalar doublet superfield :

$$\hat{H}_d \equiv \begin{pmatrix} \hat{h}_d^- \\ \hat{h}_d^0 \end{pmatrix}.$$

This has a weak hypercharge Y =-1 and hence the VEV of the scalar component of $\hat{h}_d^0$ gives mass to down-type quark and the charged leptons.

The introduction of this additional Higgs doublet in the theory beside giving mass to all the SM quarks and leptons under proper electroweak symmetry breaking, also cancel triangle anomalies.

The matter, gauge and Higgs superfield content of MSSM for a single generation with

their quantum numbers under $SU(3)_C \times SU(2)_L \times U(1)_Y$ is given in Table 2. The

	$SU(3)_C \times SU(2)_L \times U(1)_Y$
Fermions	$\hat{Q} = \begin{pmatrix} \hat{u}_L \\ \hat{d}_L \end{pmatrix} \sim (3, 2, \frac{1}{3}), \hat{U}^c \sim (3^*, 1, -\frac{4}{3}), \hat{D}^c \sim (3^*, 1, \frac{2}{3})$ $\hat{L} = \begin{pmatrix} \hat{\nu}_{eL} \\ \hat{e}_L \end{pmatrix} \sim (1, 2, -1), \hat{E}^c \sim (1, 1, 2)$
Gauge Bosons	$\hat{g}_A \ni (\tilde{g_A}, G_{A\mu}, \mathcal{D}_{gA}), A = 1 - 8$ $\hat{W}_A \ni (\lambda_A, W_{A\mu}, \mathcal{D}_{WA}), A = 1 - 3$ $\hat{B} \ni (\lambda_0, B_\mu, \mathcal{D}_B)$
Higgs	$\hat{H}_u = \begin{pmatrix} \hat{h}_u^+ \\ \hat{h}_u^0 \end{pmatrix} \sim (1, 2, 1)$ $\hat{H}_d = \begin{pmatrix} \hat{h}_d^- \\ \hat{h}_d^0 \end{pmatrix} \sim (1, 2^*, -1)$

Table 2: Matter, gauge boson and Higgs contents of the MSSM.

interaction between matter and Higgs chiral superfields, called the Yukawa interaction, can be represented by the following superpotential :

$$W_{Yukawa} = \mu \hat{H}_u^a \hat{H}_{da} + \Sigma_{i,j=1,3}[(\mathbf{f}_u)_{ij} \epsilon_{ab} \hat{Q}_i^a \hat{H}_u^b \hat{U}_j^c + (\mathbf{f}_d)_{ij} \hat{Q}_i^a \hat{H}_{da} \hat{D}_j^c + (\mathbf{f}_e)_{ij} \hat{L}_i^a \hat{H}_{da} \hat{E}_j^c] \quad (5)$$

The superpotential in Eqn. (5) respects baryon and lepton number conservation, where baryon and lepton numbers for the superfields are defined similar to that in the SM, i.e., baryon number B = 1/3 (-1/3) for quark (antiquark) superfields, lepton number L = 1 (-1) for the lepton (antilepton) superfields, and zero for the Higgs and gauge superfields. Within the SM, baryon and lepton number is automatically conserved through gauge invariance. However, it is not the same in supersymmetry. There are certain terms that are allowed in the superpotential through gauge invariance but do not conserve baryon and lepton number. Including these terms, therefore, the complete superpotential of MSSM which would describe the interaction between the chiral superfields can

be written as :

$$
\begin{aligned}
W_{MSSM} \ni\ & \mu H_u H_d + \kappa_i L_i H_u + m_N^{ij} N_i^c N_j^c \\
& + f_e^{ij} L_i H_d E_j^c + f_d^{ij} Q_i H_d D_j^c + f_u^{ij} Q_i H_u U_j^c + f_\nu^{ij} L_i H_u N_j^c \\
& + \lambda_{ijk} L_i L_j E_k^c + \lambda'_{ijk} L_i Q_j D_k^c + \lambda''_{ijk} U_i^c D_j^c D_k^c \\
& + \frac{\kappa^{(1)}_{ijkl}}{m_P} Q_i Q_j Q_k L_l + \frac{\kappa^{(2)}_{ijkl}}{m_P} U_i^c U_j^c D_k^c E_l^c .
\end{aligned}
\tag{6}
$$

where a and b are $SU(2)$ doublet indices and i and j are generation indices.

The MSSM superpotential depicted in Eqn. (6) contains all terms allowed by gauge invariance. The κ_i, λ_{ijk}, λ'_{ijk} and λ''_{ijk} terms violate either baryon number B or lepton number L or both and can, if unsuppressed, lead to rapid proton decay and an unstable lightest SUSY particle (LSP). The $f^{ij}_{u,d,e}$ are the quark and lepton Yukawa couplings and must be allowed to give the SM fermions mass via the Higgs mechanism. The $\kappa^{(1,2)}_{ijkl}$ terms lead to dimension-five proton decay operators and are required to be either highly suppressed or forbidden.

The unwanted terms described above cannot be forbidden by imposing baryon and lepton number conservation because these symmetries are broken via non-perturbative effects and hence are not exact. Also, these symmetries are not sufficient to forbid the dangerous dimension-five proton decay operator. All of these undesirable terms can be forbidden by imposing a symmetry called R-parity, which is defined as $R = (-1)^{3(B-L)+2s}$, where s is the spin of the field. Assuming R-parity conservation can help us to get rid of the baryon and lepton number violating terms, dimension-five proton decay operators and leave the theory with a stable LSP which can serve as a good cold dark matter candidate, provided it is electrically and color neutral. Although, at this stage, imposing R-parity conservation may seem ad-hoc, but it will be shown in Sec III. that R-parity arises accidentally out of a more fundamental symmetry.

After we have obtained the MSSM superpotential, we can use Eqn. (6.44) in Ref [13]

to obtain the complete globally supersymmetric Lagrangian.

The SM has 19 free parameters, while the MSSM has 124 at the weak scale. In order to simplify, it is a common practice to assume unification of parameters at the GUT scale from which weak scale parameters are derived through Renormalization Group Equations (RGE).

This assumption of unification of parameters at the GUT scale is based on one of the most distinctive feature/motivation of SUSY : Unification of gauge coupling, as discussed in Sec I.2.1. Unification of other parameters at the GUT are more model dependent and will be discussed in detail in Sec. I.3

In order to ensure proper electroweak symmetry breaking in the MSSM, scalar potential must develop a non-zero VEV. It has been assumed that the matter scalars do not develop VEVs because this would lead to electric charge or color or lepton number breaking minima. Hence, it is sufficient to examine the scalar potential for Higgs scalar fields only. This scalar potential is given by :

$$\begin{aligned} V_{scalar} &= (m_{H_u}^2 + \mu^2)|h_u^0|^2 + (m_{H_d}^2 + \mu^2)|h_d^0|^2 \\ &- B\mu(h_u^0 h_d^0 + h.c.) + \frac{1}{8}(g^2 + g'^2)(|h_u^0|^2 - |h_d^0|^2)^2 \end{aligned} \tag{7}$$

After minimizing the above potential and defining a new parameter

$$tan\,\beta = \frac{< h_u^0 >}{< h_d^0 >} = \frac{v_u}{v_d} \tag{8}$$

the potential minimization conditions are obtained as :

$$B\mu = \frac{(m_{H_u}^2 + m_{H_d}^2 + 2\mu^2) sin\,2\beta}{2} \tag{9}$$

and

$$\mu^2 = \frac{m_{H_d}^2 - m_{H_u}^2 tan^2\,\beta}{tan^2\,\beta - 1} - \frac{M_z^2}{2} \tag{10}$$

Eqn (10) plays an important role in determining naturalness of a SUSY model which will be discussed in detail in Sec I.2.4

I.2.3. Supersymmetry Breaking

Since, *sparticles* have not been found experimentally yet, hence it is obvious that the superpartners of the SM particles are heavier than the corresponding SM particles. This implies SUSY is broken. Though SUSY is broken, it is broken *softly* which means quadratic divergences that were cancelled in a SUSY model to explain stability of Higgs mass, are still cancelled but log divergences are introduced. These divergences, which are introduced in *softly* broken SUSY, are logarithmic and logarithmic divergences may still render the Higgs mass natural at $\sim$ 125 GeV. The Lagrangian containing all possible gauge invariant SUSY breaking terms is provided in Eqn. (8.10) in ref. [13].
The mechanism of SUSY breaking is not yet known. Hence, it is necessary to assume a "hidden sector" which would couple only indirectly to the "observable sector" of SM particles and their superpartners and some dynamics in the "hidden sector" would break supersymmetry and the effect would be communicated to the "observable sector" as Soft SUSY Breaking (SSB) parameters through interactions between observable sector superfields and hidden sector fields. Depending on how the SUSY breaking effects are communicated to the observable sector, SUSY breaking mechanisms can be broadly classified into four categories which are discussed as follows :

Gravity-mediated SUSY breaking

In SUSY models with gravity-mediated SUSY breaking, the SSB parameters arise from tree level gravitational interactions between observable sector superfields and gauge singlet hidden sector fields. The minimal SUSY model with gravity-mediated SUSY breaking called the minimal supergravity (mSUGRA) or the Constrained MSSM

(CMSSM) model is discussed as follows : [15].

CMSSM/mSUGRA model : The Constrainted MSSM (CMSSM) or the minimal supergravity (mSUGRA) model arise within this framework of gravity mediated SUSY breaking when a flat Kahler metric is chosen. This choice leads to a common mass for all scalars of

$$m_0^2 = m_{3/2}^2 + V_0/M_P^2$$

where V_0 is the minimum of the scalar potential. This "minimal" choice of the Kahler potential leads to the "minimal" supergravity model. Gaugino mass unification at the GUT scale may arise due to grand unification of gauge interactions or by assuming that the gauge kinetic function has the same field dependence on the hidden sector fields, for each factor of gauge symmetry. In this model, the parameters are unified as follows :

$$\begin{aligned} Gauge\, couplings &: g_C = g_L = g_Y \equiv g_{GUT} \\ Matter\, scalars &: m_{Q_i}^2 = m_{U_i}^2 = m_{D_i}^2 = m_{L_i}^2 = m_{E_i}^2 = m_{H_u}^2 = m_{H_d}^2 \equiv m_0^2 \\ Gaugino\, mass &: M_1 = M_2 = M_3 \equiv m_{1/2} \\ Trilinear\, couplings &: A_t = A_b = A_\tau \equiv A_0 \end{aligned} \tag{11}$$

Thus, the parameter set that completely specify the mSUGRA model is :

$$m_0,\ m_{1/2},\ A_0,\ \tan\beta,\ \mathrm{sign}(\mu).$$

where, m_0, $m_{1/2}$ and A_0 are the unified values for scalar masses, gaugino masses and trilinear couplings respectively at m_{GUT}, $\tan\beta$ and $\mathrm{sign}(\mu)$ are two factors necessary for electroweak symmetry breaking.

There are several such SUSY models in which SSB parameters are generated through gravity-mediation. Two such models namely : The two- or three- extra parameter non-universal Higgs models, NUHM2 or NUHM3 [40], which are generalizations of the aforementioned CMSSM/mSUGRA model have been discussed in Sec. I.3.1.

Anomaly-mediated SUSY breaking

In SUSY models with gravity-mediated SUSY breaking, the SSB parameters arise from tree level gravitational interactions between observable sector superfields and gauge singlet hidden sector fields. But an additional one-loop contribution to SSB parameters, originating in the super-Weyl anomaly, are always present when SUSY is broken [43]. This contribution in the SSB parameters is called the anomaly-mediated SUSY breaking contribution. Though, generally, such contributions are loop suppressed, certain models where the usual gravity-mediated contribution to SSB parameters get suppressed by an additional factor, then the anomaly-mediated contribution dominate.
SUSY models with pure anomaly-mediated SUSY breaking mecahnism have been discussed in Sec. I.3.2.

Gauge-mediated SUSY breaking

In gauge-mediated SUSY breaking (GMSB), [196] in addition to the hidden sector and the observable sector, there is a third sector, called the messenger sector. The fields in the messenger sector has SM gauge interactions with the observable sector and also couple to the hidden sector fields. When some dynamics in the hidden sector breaks SUSY, it is first felt by the fields in the messenger sector and then communicated to the observable sector through SM gauge interactions.

Gaugino-mediated SUSY breaking

In this mechanism, gauginos acquire a mass due to their direct coupling to the SUSY breaking sector and MSSM scalars acquire SUSY breaking masses via their interactions with gauginos.

These various mechanisms, in which SUSY can be *softly* broken give rise to various

SUSY models. Depending on these mechanisms, the low energy phenomenology can change drastically. Some of such different SUSY models which differ in terms of SUSY breaking mechanism and its consequences have been discussed in Sec. I.3.
In the rest of this text, models with gauge-mediated and gaugino-mediated SUSY breaking mechanisms are not discussed because such models have been rendered *unnatural/finetuned* according to the naturalness notion discussed in the following section.

I.2.4. Naturalness

The notion of **practical naturalness** is that

> the *independent* contributions to any observable $\mathcal{O}$ must be comparable to or less than $\mathcal{O}$.

Since sparticles are bound to have much higher mass than their SM counterparts, as discussed in Sec. I.2.3, their contribution in the calculation of various observables can render the model unnatural or fine-tuned. Thus, the requirement of naturalness puts an upper bound on the sparticle masses. Since, sparticles are still beyond the reach of the Large Hadron Collider (LHC), which gives the lower bound on the sparticle masses, it must be ensured in all SUSY models that the sparticle spectrum obtained from those models respect the lower mass bound as constrained by the LHC and also the upper mass bound as required by naturalness. In this section, various naturalness measures and their effect on the sparticle mass bounds have been discussed.

Δ_{EW}: electroweak naturalness

The simplest naturalness measure Δ_{EW}[16, 17] arises from the form of the Higgs potential in the MSSM. By minimizing the weak-scale SUSY Higgs potential, including radiative corrections, as obatined in Eqn (10), one may relate the measured value of

the Z-boson mass to the various SUSY contributions:

$$m_Z^2/2 = \frac{m_{H_d}^2 + \Sigma_d^d - (m_{H_u}^2 + \Sigma_u^u)\tan^2\beta}{\tan^2\beta - 1} - \mu^2 \simeq -m_{H_u}^2 - \mu^2 - \Sigma_u^u(\tilde{t}_{1,2}).$$

The measure

$$\Delta_{EW} = |(max\ RHS\ contribution)|/(m_Z^2/2) \tag{12}$$

is then a measure of how much $m_Z^2/2$ differ from the SUSY contributions to it. If Δ_{EW} is low then the model is said to be natural according to the notion of practical naturalness. The Σ_u^u and Σ_d^d contain over 40 radiative corrections which are listed in the Appendix of Ref. [17].

Δ_{HS}: tuning dependent contributions

It is also common in the literature to apply practical naturalness to the Higgs mass:

$$m_h^2 \simeq m_{H_u}^2(weak) + \mu^2(weak) + mixing + rad.\ corr. \tag{13}$$

where the mixing and radiative corrections are both comparable to m_h^2. Also, $m_{H_u}^2(weak) = m_{H_u}^2(\Lambda) + \delta m_{H_u}^2$ where it is common to estimate $\delta m_{H_u}^2$ using its renormalization group equation (RGE) which is as follows :

$$\frac{dm_{H_u}^2}{dt} = \frac{2}{16\pi^2}(-\frac{3}{5}g_1^2M_1^2 - 3g_2^2M_2^2 + \frac{3}{10}g_1^2S + 3f_t^2X_t^2) \tag{14}$$

where,

$$X_t = m_{Q_3}^2 + m_{U_3}^2 + m_{H_u}^2 + A_t^2 \tag{15}$$

$$S = m_{H_u}^2 - m_{H_d}^2 + Tr[\mathbf{m_Q^2} - \mathbf{m_L^2} - \mathbf{2m_U^2} + \mathbf{m_D^2} + \mathbf{m_E^2}] \tag{16}$$

$$t = \ln\frac{Q^2}{Q_0^2} \tag{17}$$

By setting S = 0 and neglecting gauge terms and $m_{H_u}^2$ contribution in X_t and then

integrating Eqn. (14) from m_{SUSY} to the cutoff Λ yields:

$$\delta m_{H_u}^2 \sim -\frac{3f_t^2}{8\pi^2}(m_{Q_3}^2 + m_{U_3}^2 + A_t^2)\ln\left(\Lambda^2/m_{soft}^2\right). \tag{18}$$

Taking $\Lambda \sim m_{GUT}$ and requiring the high scale measure

$$\Delta_{HS} \equiv \delta m_{H_u}^2/m_h^2 \tag{19}$$

$\Delta_{HS} \leq 1$ then requires three third generation squarks lighter than 500 GeV[18, 19] (now highly excluded by LHC top-squark searches) and small A_t terms (whereas $m_h \simeq 125$ GeV typically requires large mixing and thus multi-TeV values of A_0[20, 21]). The simplifications made in this calculation ignore the fact that $\delta m_{H_u}^2$ is highly dependent on $m_{H_u}^2(\Lambda)$ (which is set to zero in the simplification)[22, 23, 24]. In fact, the larger one makes $m_{H_u}^2(\Lambda)$, then the larger becomes the cancelling correction $\delta m_{H_u}^2$ as shown in Fig. 5 of Ref. [24]. Thus, these terms are *not independent*: one cannot tune $m_{H_u}^2(\Lambda)$ against a large contribution $\delta m_{H_u}^2$. Thus, weak-scale top squarks and small A_t are not required by naturalness.

Δ_{BG}: the problem with parameters

The more traditional measure Δ_{BG} was proposed by Ellis *et al.*[25] and later investigated more thoroughly by Barbieri and Giudice[26]. The starting point is to express m_Z^2 in terms of weak scale SUSY parameters as in Eq. (12):

$$m_Z^2 \simeq -2m_{H_u}^2 - 2\mu^2 \tag{20}$$

where the partial equality obtains for moderate-to-large $\tan\beta$ values and where we assume for now that the radiative corrections are small. An advantage of Δ_{BG} over the previous large-log measure is that it maintains the correlation between $m_{H_u}^2(\Lambda)$ and $\delta m_{H_u}^2$ by replacing $m_{H_u}^2(m_{weak}) = \left(m_{H_u}^2(\Lambda) + \delta m_{H_u}^2\right)$ by its expression in terms of

high scale parameters. To evaluate Δ_{BG}, one needs to know the explicit dependence of $m_{H_u}^2$ and μ^2 on the fundamental parameters. Semi-analytic solutions to the one-loop renormalization group equations for $m_{H_u}^2$ and μ^2 can be found for instance in Ref's [27]. For the case of $\tan\beta = 10$, then[28, 29, 30]

$$\begin{aligned} m_Z^2 \simeq & -2.18\mu^2 + 3.84M_3^2 + 0.32M_3M_2 + 0.047M_1M_3 \\ & - 0.42M_2^2 + 0.011M_2M_1 - 0.012M_1^2 - 0.65M_3A_t \\ & - 0.15M_2A_t - 0.025M_1A_t + 0.22A_t^2 + 0.004M_3A_b \\ & - 1.27m_{H_u}^2 - 0.053m_{H_d}^2 \\ & + 0.73m_{Q_3}^2 + 0.57m_{U_3}^2 + 0.049m_{D_3}^2 - 0.052m_{L_3}^2 + 0.053m_{E_3}^2 \\ & + 0.051m_{Q_2}^2 - 0.11m_{U_2}^2 + 0.051m_{D_2}^2 - 0.052m_{L_2}^2 + 0.053m_{E_2}^2 \\ & + 0.051m_{Q_1}^2 - 0.11m_{U_1}^2 + 0.051m_{D_1}^2 - 0.052m_{L_1}^2 + 0.053m_{E_1}^2 \end{aligned} \tag{21}$$

where all terms on the right-hand-side are understood to be GUT scale parameters.

Then, the proposal is that the variation in m_Z^2 with respect to parameter variation be small:

$$\Delta_{BG} \equiv max_i\left[c_i\right] \quad \text{where} \quad c_i = \left|\frac{\partial \ln m_Z^2}{\partial \ln p_i}\right| = \left|\frac{p_i}{m_Z^2}\frac{\partial m_Z^2}{\partial p_i}\right| \tag{22}$$

where the p_i constitute the fundamental parameters of the model. Thus, Δ_{BG} measures the fractional change in m_Z^2 due to fractional variation in the high scale parameters p_i. The c_i are known as *sensitivity coefficients*[30].

The requirement of low Δ_{BG} is then equivalent to the requirement of no large cancellations on the right-hand-side of Eq. (21) since (for linear terms) the logarithmic derivative just picks off coefficients of the relevant parameter. For instance, $c_{m_{Q_3}^2} = 0.73 \cdot (m_{Q_3}^2/m_Z^2)$. If one allows $m_{Q_3} \sim 3$ TeV (in accord with requirements from the measured value of m_h), then one obtains $c_{m_{Q_3}^2} \sim 800$ and so $\Delta_{BG} \geq 800$. In this case, SUSY would be electroweak fine-tuned to about 0.1%. If instead one sets

$m_{Q_3} = m_{U_3} = m_{H_u} \equiv m_0$ at GUT scale as in models with scalar mass universality, then the various scalar mass contributions to m_Z^2 largely cancel and $c_{m_0^2} \sim -0.017 m_0^2/m_Z^2$: the contribution to Δ_{BG} from scalars drops by a factor ~ 50.

The above argument illustrates the extreme model-dependence of Δ_{BG} for multi-parameter SUSY models.

Conclusion on Naturalness

As argued in Ref [24], for correlated (i.e., inter-dependent) soft terms as should occur in any more fundamental theory such as SUGRA with a well-specified SUSY breaking sector, or in string theory, Δ_{HS} and Δ_{BG} collapse to Δ_{EW} so that Δ_{EW} is sufficient as both an infra-red (IR) and ultra-violet (UV) fine-tuning measure. Thus, Δ_{EW} is adopted as a measure of naturalness in fundamental theories with the MSSM as the weak scale effective theory. A value of $\Delta_{EW} < 30$ is adopted as a conservative choice for natural models of SUSY. Later in Sec I.6, it will be shown that this choice $\Delta_{EW} < 30$ is not ad-hoc, rather it has some serious implication in the formation of our universe. It corresponds to independent contributions to the weak scale no more than a factor of 4 beyond the measured value of the weak scale.

Thus, it can be seen from Eq. (12) that the conditions for natural SUSY (i.e., $\Delta_{EW} < 30$)[1] requires:

- The superpotential μ parameter has magnitude not too far from the weak scale, $|\mu| \leq 300$ GeV[33, 34]. This implies the existence of light higgsinos $\tilde{\chi}_{1,2}^0$ and $\tilde{\chi}_1^{\pm}$ with $m(\tilde{\chi}_{1,2}^0, \tilde{\chi}_1^{\pm}) \sim 100 - 300$ GeV.

- $m_{H_u}^2$ is radiatively driven from large high scale values to *small* negative values at the weak scale as shown in Fig 2 (this is SUSY with *radiatively-driven naturalness* or RNS [16] discussed in Sec. I.3).

- Large cancellations occur in the $\Sigma_u^u(\tilde{t}_{1,2})$ terms for large A_t parameters which then

[1]The onset of finetuning for $\Delta_{EW} \geq 30$ is visually displayed in Fig. 1 of Ref. [32].

allow for $m_{\tilde{t}_1} \sim 1-3$ TeV for $\Delta_{EW} < 30$. The large A_t term gives rise to large mixing in the top-squark sector and thus lifts the Higgs mass m_h into the vicinity of 125 GeV. The gluino contribution to the weak scale is at two-loop order so its mass can range up to $m_{\tilde{g}} \leq 6-9$ TeV (depending on the details of the model) with little cost to naturalness[17, 32, 35].

- Since first/second generation squarks and sleptons contribute to the weak scale at one-loop through (mainly cancelling) D-terms and at two-loops via RGEs, they can range up to 10-30 TeV with little cost to naturalness (thus helping to alleviate the SUSY flavor and CP problems)[36, 37].

The first condition requires $\mu \sim$ 100-300 GeV, while the first term in Eqn. (6) leads one to expect that the dimensionful parameter μ should be of order $m_P \sim 2.4 \times 10^{18}$ GeV. This is the famous SUSY μ problem [38, 120]. A promising approach to solve the SUSY μ problem is to first forbid μ, perhaps via some symmetry, and then regenerate it of order the scale of soft SUSY breaking terms. However, present LHC limits suggest the soft breaking scale m_{soft} lies in the multi-TeV regime whilst naturalness requires $\mu \sim m_{W,Z,h} \sim 100$ GeV so that a Little Hierarchy (LH) appears with $\mu \ll m_{soft}$. Solutions to the SUSY μ problem and whether or not these solutions admit Little Hierarchy have been discussed in detail in Sec. III.

Since Δ_{EW} is determined by the weak scale SUSY parameters, then different models which give rise to exactly the same sparticle mass spectrum will have the same fine-tuning value (model independence). Using the naturalness measure Δ_{EW}, then it has been shown in Sec. V.3, that plenty of SUSY parameter space remains natural even in the face of LHC Run 2 Higgs mass measurements and sparticle mass limits[17].

I.3. Radiatively-Driven Natural Supersymmetric (RNS) Models

As seen in Sec I.2.4, naturalness requires $m^2_{H_u}$ to be a small negative value at the weak scale. This requirement is fulfilled when $m^2_{H_u}$ is radiatively driven from large high scale values to *small* negative values at the weak scale as shown in Fig 2. The SUSY models that are characterized by this kind of behaviour of $m^2_{H_u}$ are called Radiatively-Driven Natural Supersymmetric (RNS) Models. In this section, a few such RNS models and their low scale phenomenology will be discussed.

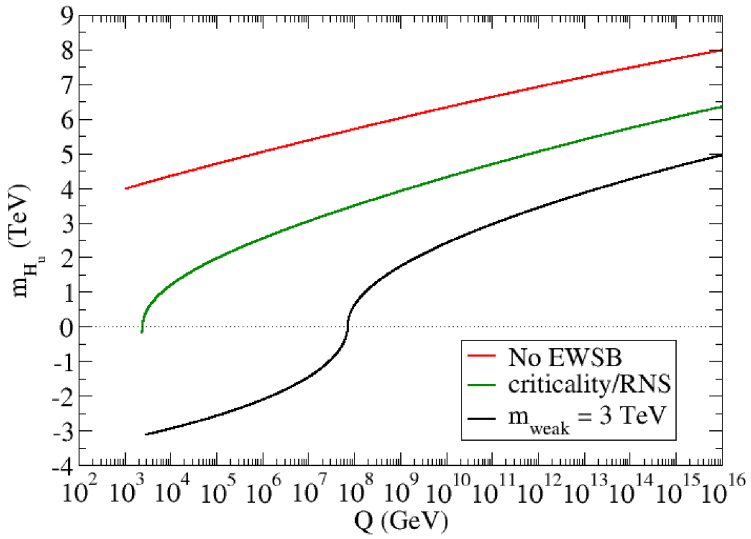

Figure 2: Evolution of the term $sign(m^2_{H_u})\sqrt{m^2_{H_u}}$ for the case of $No\ EWSB$, criticality as in RNS and $m_{weak} = 3$ TeV [39].

I.3.1. NUHM2 & NUHM3

The two- or three- extra parameter non-universal Higgs models, NUHM2 or NUHM3 [40] are slight generalizations of the CMSSM/mSUGRA model [15] where gaugino masses are unified to $m_{1/2}$ at the GUT scale as shown in Fig. 3, but where the soft Higgs masses m_{H_u} and m_{H_d} are instead independent of the matter scalar soft masses m_0. This is well

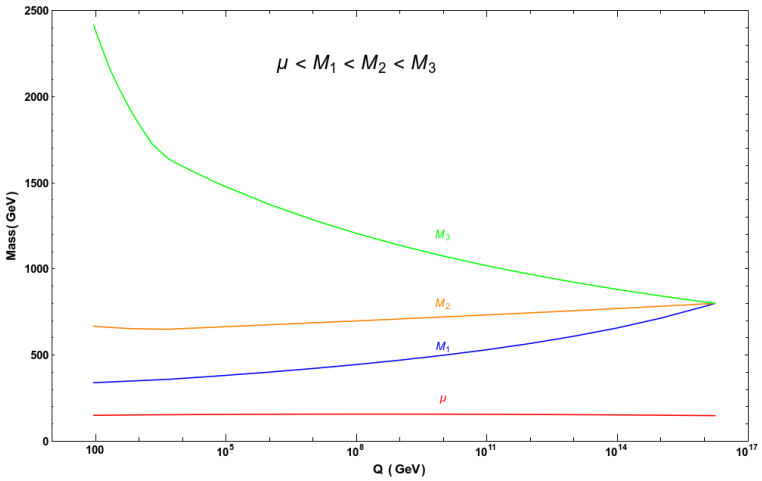

Figure 3: Gaugino mass unification at GUT scale in NUHM2 model

justified since the Higgs superfields necessarily live in different GUT multiplets than the matter superfields. In the NUHM3 model, it is further assumed that the third generation matter scalars are split from the first two generation $m_0(1,2) \neq m_0(3)$. In these models, typically the parameter freedom in m_{H_u} and m_{H_d} is traded for the more convenient weak scale parameters μ and m_A.

Thus, the parameter space for NUHM2 model is :

$$m_0,\ m_{1/2},\ A_0,\ \tan\beta,\ \mu,\ m_A$$

and, the parameter space for NUHM3 model is :

$$m_0(1,2),\ m_0(3),\ m_{1/2},\ A_0,\ \tan\beta,\ \mu,\ m_A$$

I.3.2. nAMSB

In the original minimal anomaly-mediated SUSY breaking model[43] (mAMSB) gaugino masses were calculated to be proportional to the corresponding gauge group beta functions times the gravitino mass.

$$M_i = \frac{\beta_i}{g_i} m_{3/2} \tag{23}$$

where, $\beta_i = \frac{g_i^3}{16\pi^2} b_i$ with b_i = (6.6,1,-3) and i labels the gauge group. This leads to wino being the LSP and hence the dark matter of the model. In addition, in AMSB the soft breaking scalar masses were computed to be :

$$m_{\tilde{f}}^2 = -\frac{1}{4}(\frac{d\gamma}{dg}\beta_g + \frac{d\gamma}{df}\beta_f)m_{3/2}^2 \tag{24}$$

where β_f is the beta function for the corresponding superpotential Yukawa coupling and anomalous dimension $\gamma = \partial \mathrm{lnZ}/\partial \mathrm{ln}\mu$ with Z the wave function renormalization constant and μ is the running energy scale. The AMSB contribution to trilinear soft SUSY breaking terms is given by

$$A_f = \frac{\beta_f}{f} m_{3/2} \tag{25}$$

where f is the corresponding Yukawa coupling. An annoyance with mAMSB is that the slepton masses turn out to be tachyonic with negative mass-squared leading to an electric charge breaking minimum for the scalar potential. In the original Randall-Sundrum paper, the authors suggest additional bulk contributions m_0^2 to scalar mass-squared values to solve the problem of tachyonic sleptons.

Thus, the parameter space for mAMSB model is given by :

$$m_0,\ m_{3/2},\ \tan\beta,\ \mathrm{sign}(\mu)$$

However, mAMSB now seems excluded since wino-only dark matter should have been detected by indirect dark matter searches[44, 45, 46]. Also, in mAMSB the anomaly-mediated contribution to the trilinear soft term A is usually too small to boost the Higgs mass $m_h \to 125$ Gev unless stop masses lie in the hundred-TeV range. Finally, the mAMSB model typically has a large μ term. The latter two situations lead to mAMSB being highly unnatural, especially if $m_h \simeq 125$ GeV is required as shown in Fig. 4.

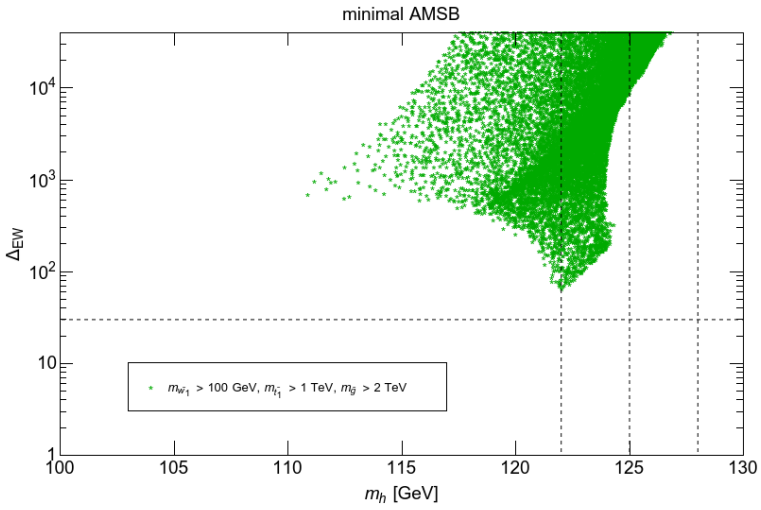

Figure 4: Plot of points from a scan over mAMSB parameter space in the Δ_{EW} vs. m_h plane

If the bulk contributions to $m_{H_u}^2$ and $m_{H_d}^2$ are non-universal with the matter scalars, then one can allow for a small natural μ term. Also, if bulk contributions to the A terms are allowed, (as suggested in the Randall-Sundrum paper), then large stop mixing can occur which both reduces the $\Sigma_u^u(\tilde{t}_{1,2})$ terms in Eq. (12) while lifting $m_h \to 125$ GeV as shown in Fig. 5. In that case, natural AMSB models can be generated with small $\Delta_{EW} < 30$ and with $m_h \simeq 125$ GeV[47].

Thus, the parameter space for nAMSB model is :

$$m_0,\ m_{3/2},\ A_0,\ \tan\beta,\ \mu,\ m_A$$

The phenomenology of *natural* AMSB (nAMSB) is quite different from mAMSB: in nAMSB, the higgsinos are the lightest electroweakinos so one has a higgsino-like LSP even though the winos are still the lightest gauginos. Axions are assumed to make up the bulk of dark matter[48].

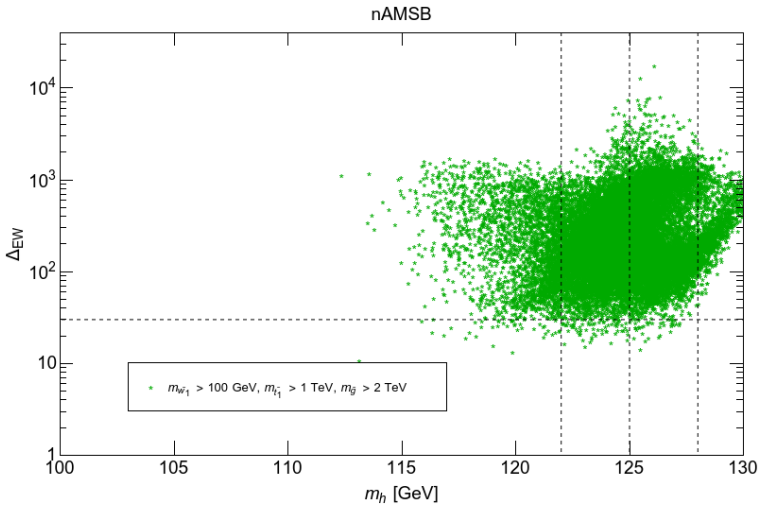

Figure 5: Plot of points from a scan over nAMSB parameter space in the Δ_{EW} vs. m_h plane

I.3.3. nGMM′

The scheme of mirage-mediation (MM) posits soft SUSY breaking terms which are suppressed compared to the gravitino mass $m_{3/2}$ so that moduli/gravity mediated contributions to soft terms are comparable to AMSB contributions[41]. The original mirage mediation scheme grew out of the Kachru-Kallosh-Linde-Trivedi (KKLT) proposal[241] for moduli stabilization accompanied by some uplifting mechanism to gain a de Sitter minimum, *i.e.* a small cosmological constant from the landscape [Sec. I.6]. The KKLT proposal was made in the context of IIB string theory compactified on an orientifold containing D3 and D7 branes. The complex structure or shape moduli and the dilaton could be stabilized by introducing NS and RR three-form fluxes with masses near the string scale. A remaining single Kähler modulus T would be stabilized by non-perturbative effects such as gaugino condensation or brane instantons, with $m_T \sim m_{3/2} \log(m_P/m_{3/2})$, leading to a supersymmetric AdS vacuum. As a final step, an uplifting mechanism– here the addition of an anti-D3 brane near the tip of a Klebanov-Strassler throat– would raise the scalar potential of the theory to gain a de Sitter vacuum with softly broken

$N = 1$ supersymmetry.

In the KKLT scheme, a little hierarchy

$$m_T \sim (4\pi^2) m_{3/2} \sim (4\pi^2) m_{soft} \tag{26}$$

was expected to ensue[242, 245], where $\log(m_P/m_{3/2}) \sim 4\pi^2$ and where m_{soft} is the expected scale of moduli (gravity)- mediated soft terms. Since m_{soft} was suppressed relative to $m_{3/2}$, then the moduli-mediated soft terms are expected to be comparable to contributions from anomaly-mediation (which are suppressed relative to $m_{3/2}$ by $\sim 1/(16\pi^2)$ loop factor). The resultant model has been dubbed mirage-mediation[243] (MM) due to the distinctive feature that gaugino (and scalar) masses evolve from non-universal values at the GUT scale to apparently universal values at some intermediate scale

$$\mu_{mir} = m_{GUT} \cdot e^{(-8\pi^2/\alpha)} \tag{27}$$

where the introduced parameter α measures the relative moduli- versus anomaly-mediated contributions to gaugino masses[244, 78].

Upon integrating out the heavy dilaton field and the shape moduli, one is left with an effective broken supergravity theory of the observable sector fields denoted by $\hat{Q}$ and the size modulus field $\hat{T}$. The Kähler potential depends on the location of matter and Higgs superfields in the extra dimensions via their modular weights $n_i = 0$ (1) for matter fields located on $D7$ ($D3$) branes, or $n_i = 1/2$ for chiral multiplets on brane intersections, while the gauge kinetic function $f_a = \hat{T}^{l_a}$, where a labels the gauge group, is determined by the corresponding location of the gauge supermultiplets, since the power $l_a = 1$ (0) for gauge fields on $D7$ ($D3$) branes [244, 78].

Within the MM model, the SSB gaugino mass parameters, trilinear SSB parameters and sfermion mass parameters, all renormalized just below the unification scale (taken

to be $Q = m_{\rm GUT}$), are given by,

$$M_a = M_s \left(l_a \alpha + b_a g_a^2 \right), \tag{28}$$

$$A_{ijk} = M_s \left(-a_{ijk} \alpha + \gamma_i + \gamma_j + \gamma_k \right), \tag{29}$$

$$m_i^2 = M_s^2 \left(c_i \alpha^2 + 4 \alpha \xi_i - \dot{\gamma}_i \right), \tag{30}$$

where $M_s \equiv \frac{m_{3/2}}{16\pi^2}$, b_a are the gauge β function coefficients for gauge group a and g_a are the corresponding gauge couplings. The coefficients that appear in (28)–(30) are given by $c_i = 1 - n_i$, $a_{ijk} = 3 - n_i - n_j - n_k$ and $\xi_i = \sum_{j,k} a_{ijk} \frac{y_{ijk}^2}{4} - \sum_a l_a g_a^2 C_2^a(f_i)$. Finally, y_{ijk} are the superpotential Yukawa couplings, C_2^a is the quadratic Casimir for the a^{th} gauge group corresponding to the representation to which the sfermion $\tilde{f}_i$ belongs, γ_i is the anomalous dimension and $\dot{\gamma}_i = 8\pi^2 \frac{\partial \gamma_i}{\partial \log \mu}$. Expressions for the last two quantities involving the anomalous dimensions can be found in the Appendices of Ref's. [78, 79]. In the earliest models the coefficients that appear in (29) and (30) took on values determined by discrete values of the modular weights n_i which depended on the location of fields in the original II-B string model and The MM model is then specified by the parameters

$$m_{3/2},\ \alpha,\ \tan\beta,\ \mathrm{sign}(\mu),\ n_i,\ l_a.$$

The mass scale for the SSB parameters is dictated by the gravitino mass $m_{3/2}$. The phenomenological parameter α, which could be of either sign, determines the relative contributions of anomaly mediation and gravity mediation to the soft terms, and is expected to be $|\alpha| \sim \mathcal{O}(1)$. Grand unification implies matter particles within the same GUT multiplet have common modular weights, and that the l_a are universal. We will assume here that all $l_a = 1$. These original MM models have been shown to be unnatural under LHC Higgs mass and sparticle limit constraints[23].

However, in more realistic compactifications with many Kähler moduli, then a more

general framework where the discrete modular weights a_{ijk} and c_i are elevated from discrete to continuous parameters in order to accommodate more general string theories and more general compactification schemes results in the generalized mirage-mediation model (GMM). This modification will not affect the result Eqn. (28) for gaugino mass parameters which is the most robust prediction in the MM mechanism. Thus, the GMM model has the parameter space :

$$\alpha,\, m_{3/2},\, c_m,\, c_{m3},\, a_3,\, c_{H_u},\, c_{H_d},\, \tan\beta$$

where a_3 is short for $a_{Q_3 H_u U_3}$ (appearing in Eq. (29)) and c_m, c_{m3}, c_{H_u} and c_{H_d} arise in Eq. (30). Here, an independent value c_m for the first two matter-scalar generations is adopted whilst the parameter c_{m3} applies to third generation matter scalars. Different modular weights c_{H_u} and c_{H_d} for each of the two Higgs doublets are also allowed. Such choices for the scalar field modular weights are motivated for instance by $SO(10)$ SUSY GUT models where the MSSM Higgs doublets may live in different **10**-dimensional Higgs reps. The GMM model maintains the phenomena of mirage unification of gaugino masses while allowing the flexibility of generating $m_h \simeq 125$ GeV while maintaining naturalness in the face of LHC sparticle mass limits. In *natural* GMM models (nGMM)[42], the gaugino spectrum is still compressed as in usual MM, but now the higgsinos lie at the bottom of the spectra. Consequently, the collider and dark matter phenomenology is modified from previous expectations.

The independent values of c_{H_u} and c_{H_d}, in the GMM model, which set the moduli-mediated contribution to the soft Higgs mass-squared soft terms, may conveniently be traded for weak scale values of μ and m_A as is done in the two-parameter non-universal Higgs model (NUHM2)[40] resulting in the $nGMM'$ model which thus has the parameter space :

$$\alpha,\, m_{3/2},\, c_m,\, c_{m3},\, a_3,\, \tan\beta,\, \mu,\, m_A.$$

This procedure allows to accommodate Little Hierarchy (LH) which requires $\mu \sim$

100−300 GeV and thus render the model *natural* in accord with *naturalness* as described in Sec. I.2.4.

Thus, our final formulae for the soft terms are given by

$$\begin{aligned}
M_a &= \left(\alpha + b_a g_a^2\right) m_{3/2}/16\pi^2, && (31)\\
A_\tau &= \left(-a_3\alpha + \gamma_{L_3} + \gamma_{H_d} + \gamma_{E_3}\right) m_{3/2}/16\pi^2, && (32)\\
A_b &= \left(-a_3\alpha + \gamma_{Q_3} + \gamma_{H_d} + \gamma_{D_3}\right) m_{3/2}/16\pi^2, && (33)\\
A_t &= \left(-a_3\alpha + \gamma_{Q_3} + \gamma_{H_u} + \gamma_{U_3}\right) m_{3/2}/16\pi^2, && (34)\\
m_i^2(1,2) &= \left(c_m\alpha^2 + 4\alpha\xi_i - \dot{\gamma}_i\right)(m_{3/2}/16\pi^2)^2, && (35)\\
m_j^2(3) &= \left(c_{m3}\alpha^2 + 4\alpha\xi_j - \dot{\gamma}_j\right)(m_{3/2}/16\pi^2)^2, && (36)\\
m_{H_u}^2 &= \left(c_{H_u}\alpha^2 + 4\alpha\xi_{H_u} - \dot{\gamma}_{H_u}\right)(m_{3/2}/16\pi^2)^2, && (37)\\
m_{H_d}^2 &= \left(c_{H_d}\alpha^2 + 4\alpha\xi_{H_d} - \dot{\gamma}_{H_d}\right)(m_{3/2}/16\pi^2)^2, && (38)
\end{aligned}$$

where, for a given value of α and $m_{3/2}$, the values of c_{H_u} and c_{H_d} are adjusted so as to fulfill the input values of μ and m_A. In the above expressions, the index i runs over first/second generation MSSM scalars $i = Q_{1,2}, U_{1,2}, D_{1,2}, L_{1,2}$ and $E_{1,2}$ while j runs overs third generation scalars $j = Q_3, U_3, D_3, L_3$ and E_3.

A schematic sketch of the three spectra from NUHM2, nGMM′ and nAMSB is shown in Fig. 6. The models are hardwired in the Isajet SUSY spectrum generator Isasugra[49].

As seen in Fig. 6, the three RNS models mentioned above have qualitatively different patterns of gaugino and higgsino masses which in turn determines the nature of the LSP i.e., dark matter in the model.

- For NUHM2 [40], because of gaugino mass unification assumption, one expects weak scale gaugino masses in the ratio $M_1 : M_2 : M_3 \sim 1 : 2 : 7$.
- For Natural (generalized) anomaly-mediated SUSY breaking model[47] (nAMSB), one expects weak scale gaugino masses in the ratio $M_1 : M_2 : M_3 \sim 3 : 1 : 8$ but

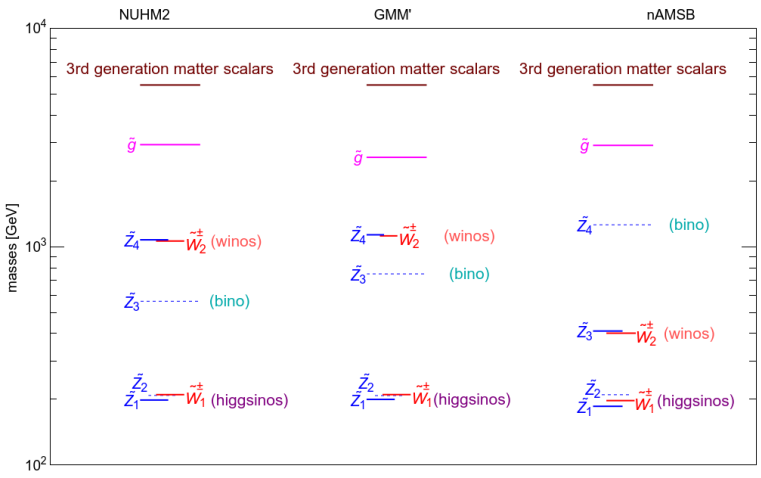

Figure 6: Typical mass spectra from natural SUSY in the case of NUHM2 (with gaugino mass unification), nGMM′ with mirage unification and compressed gauginos and natural AMSB where the wino is the lightest gaugino. In all cases, the higgsinos lie at the bottom of the spectra.

now with $\mu < M(gauginos)$ so that a higgsino-like neutralino (mixed with some wino component) is the LSP instead of the neutral wino.

- For Natural generalized mirage mediation model (nGMM′) [42] where both gravity- and anomaly-mediated contributions to soft terms are comparable, one expects the weak scale gaugino masses with $M_1 < M_2 < M_3$ but with compressed spectra depending on relative contribution from gravity- and anomaly-mediation which determines the intermediate scale of gaugino mass unification.

In Sec II., the dark matter content of these RNS models have been compared with various experimentally measured properties of dark matter.

These RNS models have been confronted by the LHC higgs and sparticles mass constraints in Sec. V. These models have a distinctive feature that the LSP is higgsino-like owing to smaller value of μ as compared to Bino, Wino and Gluino which is required to meet the naturalness constraints. This hierarchy leads to a novel, rather clean, same-sign diboson signature from wino pair production at hadron colliders. Besides, these RNS models have allowed gluino mass well-above the LHC reach as will be seen in

Sec. V. A gluino mass reach study followed by collider phenomenology of the same-sign diboson signature from wino pair production in these RNS models have also been done in detail in Sec. V.

I.4. Dark Matter in Supersymmetry

Almost 27 % of our Universe consists of Dark Matter (DM) which cannot be explained by the SM. So, an absolute requirement of any BSM theory is to provide a suitable DM particle whose relic density must match the experimentally measured dark matter density of our Universe.

The theory behind relic density calculation is that in the very early Universe, when temperature was very hot (T $\gg$ m_{DM}), these DM particles were created and annihilated, but were in thermal equilibrium with the cosmic soup. As the Universe expanded and cooled, the temperature reduced such that these DM particles cannot be pair-produced but they can still annihilate with one another. Finally, the Universe expanded so much that these DM particles cannot find each other and their annihilation rate gradually dropped to 0. Thus the relic density of the DM particle became fixed which is now the experimentally measured dark matter density of our Universe. Above is the description of *thermally-produced* DM relics. *Non-thermally produced* DM relics include production from bosonic field coherent motion or from out-of-equilibrium decays of heavier states or from bosonic coherent motion.

Such a scenario requires the DM particle electrically and color neutral. If the DM particle has electrical and color charge then, it would have become bound in nuclei and atoms and would have been detected [14]. Additionally, the DM particles must also be non-relativistic (hence massive) since relativistic particles (such as neutrinos) would exceed the escape velocity of clumping baryons and thus could not produce the gravitational wells needed for structure formation. DM particles should also be stable (at least long-lived so that its lifespan would be more than the age of our Universe) so

that the constancy of its density in the Universe can be justified.

In Supersymmetry, R-parity conservation ensures the stability of the Lightest Supersymmetric Particle (LSP) and the requirement of absence of electric and color charge leaves a sneutrino or the lightest neutralino or the gravitino as a valid candidate for the LSP and hence the DM particle. However, it will be seen in Sec. I.4.2., that dark matter detection techniques have ruled out sneutrinos as LSP and have rendered gravitinos undetectable. Hence, lightest neutralino is typically the best choice as LSP (and hence DM) in SUSY models. So, in the rest of this thesis, we will consider the case of neutralino LSP.

I.4.1. Neutralino LSP

In the MSSM, the *gauginos* and the *higgsinos* mix to give the *neutralinos* and the *charginos*. Thus, the neutralino mass matrix is given by [13]:

$$M_{Neutral} = \begin{bmatrix} 0 & \mu & -\frac{gv_u}{\sqrt{2}} & \frac{g'v_u}{\sqrt{2}} \\ \mu & 0 & -\frac{gv_d}{\sqrt{2}} & -\frac{g'v_d}{\sqrt{2}} \\ -\frac{gv_u}{\sqrt{2}} & \frac{gv_d}{\sqrt{2}} & M_2 & 0 \\ \frac{g'v_u}{\sqrt{2}} & -\frac{g'v_d}{\sqrt{2}} & 0 & M_1 \end{bmatrix} \tag{39}$$

Where, M_1, M_2 and μ are the bino, wino and higgsino mass parameters respectively. This matrix is real and hermitian and hence can be diagonalized. The smallest eigenvalue of this matrix is the mass of the lightest neutralino. The neutralino mass eigenstates can be expressed as linear combination of basis states, an admixture of higgsino/bino/wino states :

$$X = \alpha\tilde{H}_u + \beta\tilde{H}_d + \gamma\tilde{B} + \delta\tilde{W} \tag{40}$$

with $|\alpha|^2 + |\beta|^2 + |\gamma|^2 + |\delta|^2 = 1$. The type of the lightest neutralino is determined by the hierarchy among M_1, M_2 and μ. The neutralino LSP can be bino-like, wino-like or

higgsino-like :

$$\begin{aligned} |M_2|, |\mu| \gg |M_1| &: \text{LSP is bino-like} \\ |M_1|, |\mu| \gg |M_2| &: \text{LSP is wino-like} \\ |M_{1,2}| \gg |\mu| \quad &: \text{LSP is higgsino-like .} \end{aligned} \tag{41}$$

If naturalness is not considered, then the higgsino mass parameter μ can be much higher than the gaugino mass parameters M_1, M_2 and M_3. If such a case is considered in gravity-mediated (NUHM2,3) or mirage-mediated model (GMM), then, as can be seen from Fig. 6, the LSP is bino-like while in anomaly-mediated model (AMSB), the LSP is wino-like.

But since we are considering naturalness, so for all *natural* SUSY models $\mu \ll M_{1,2}$ and hence the LSP is higgsino-like.

Relic Density of Neutralino LSP

The total matter/energy density of the Universe is written as :

$$\Omega = \frac{\rho}{\rho_c} \tag{42}$$

where ρ_c is the critical closure density [2] given by :

$$\rho_c = 3H_0^2/8\pi G_N \sim 1.88 \times 10^{-29} h^2 gcm^{-3} \tag{43}$$

where, $H_0 \sim 71 \text{kms}^{-1}\text{Mpc}^{-1} \equiv 100\text{hkms}^{-1}\text{Mpc}^{-1}$ is the present value of the Hubble parameter, with h being a dimensionless scaling constant and G_N is Newton's gravitational constant. Thus, the constant DM relic density is expressed as Ωh^2 and various experiments confirm its value to be $\Omega h^2 \sim 0.12$.

The relic density of the LSP can be theoretically calculated by solving the Boltzmann

[2] Critical closure density is the maximum total mass-energy density that the Universe can have and still be an open or unbound Universe like ours. Thus to have a Universe like our Universe $\rho \leq \rho_c$.

equation encoded in the computer code Isajet7.88 [49].

I.4.2. Dark Matter Detection

Many experiments have searched for Weakly Interacting Massive Particles (WIMPs) as relic dark matter from the Big Bang. There are several search channels for DM which can be broadly classified into three categories depending on what type of interaction between DM and SM particles have been considered :

- Collider Search
- Direct Detection
- Indirect Detection

Fig. 7 shows a compact summary of all of these search channels.

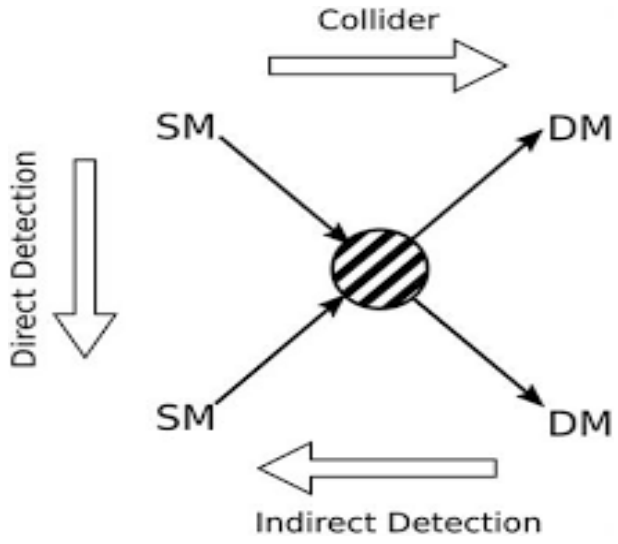

Figure 7: Various methods of Dark Matter Detection

Direct Detection

The general idea behind Direct Detection of Dark Matter [31] is that when WIMPs in our Universe scatter from nuclei of any material on earth, it deposits typically a

few keVs of energy. Detection of this deposited energy provide hints for presence of DM. Sneutrinos have a large scattering cross-section and absence of any such signal experiments has ruled out sneutrinos as a possible DM candidate (and hence as a LSP) [13]. Gravitinos are undetectable in these experiments [13]. Neutralino LSP has sufficiently small scattering cross-section and are yet to be probed.
Since the interaction between WIMPs and nuclei are not yet known so considering all possibilities, the scattering cross-section has both spin-independent (SI) and spin-dependent (SD) terms. These terms are discussed as follows :

- *spin-independent (SI) terms :* The scalar interaction term $\mathcal{L}_S = \bar{\chi}\chi\bar{q}q$ and the vector interaction term $\mathcal{L}_V = \bar{\chi}\gamma^\mu\chi\bar{q}\gamma^\mu q$ are the spin-independent terms. Here, χ denotes the DM particle and q denotes the SM particle in the scattering nucleus. The scattering cross-section calculated from these terms is denoted by σ^{SI}.

- *spin-dependent (SD) terms :* The Axial-vector interaction term $\mathcal{L}_A = \bar{\chi}\gamma^\mu\gamma_5\chi\bar{q}\gamma^\mu\gamma_5 q$ is the spin-dependent term. The scattering cross-section calculated from this term is denoted by σ^{SD}.

σ^{SI} and σ^{SD} can be experimentally measured from the energy deposited when WIMPs scatter from nuclei. These quantities can be theoretically calculated using the general feynman rules to calculate a scattering cross-section. These formulas are encoded in the computer code Isajet7.88 [49] which have been used here to calculate these quantities.

Indirect Detection

Indirect searches of Dark Matter involve search of SM particles produced via annihilation of DM particles. When WIMPs annihilate in the galactic core, they produce SM particles, for eg: high energy photons. These photons are examined in gamma ray observatories to derive limits on mass of the annihilating WIMPs. Here the measurable

quantity is $<\sigma v_{rel}>$ which is the thermally averaged WIMP-WIMP annihilation cross-section times relative velocity between WIMPs [3].

As argued above, neutralino qualifies as the most preferred LSP (hence the DM) in SUSY models and *Natural* SUSY models require the LSP to be higgsino-like with non-negligible gaugino components. In Sec. II, three RNS models : nNUHM2 [40], nAMSB [47] and nGMM′ [42] (discussed in Sec. I.3) which have such a LSP as the DM, will be used to calculate Ωh^2, σ^{SI}, σ^{SD} and $<\sigma v_{rel}>$ using Isajet 7.88 [49] and confront them with the values and limits derived from various experiments to check the validity of these models in context of DM.

I.5. Strong CP Problem & its solution

While we require naturalness in the electroweak sector, it is important to recall that there is also a naturalness problem in the QCD sector of the SM. In the early days of QCD, it was a mystery why the two-light-quark chiral symmetry $U(2)_L \times U(2)_R$ gave rise to three and not four light pions[50]. The mystery was resolved by 't Hooft's discovery of the QCD theta vacuum which allows for the emergence of three pseudo-Goldstone bosons– the pion triplet– from the spontaneously broken global $SU(2)_{axial}$ symmetry, but that didn't respect the remaining $U(1)_A$ symmetry[51]. As a consequence of the theta vacuum, one expects the presence of a term

$$\mathcal{L} \ni \frac{\bar{\theta}}{32\pi^2} F_{A\mu\nu} \tilde{F}_A^{\mu\nu} \tag{44}$$

in the QCD Lagrangian (where $\bar{\theta} = \theta + arg(det(\mathcal{M}))$ and $\mathcal{M}$ is the quark mass matrix). Experimental observation like neutron electric dipole moment $d_n < 2.9 \times 10^{-26}$ ecm , gives the bound $\bar{\theta} < 10^{-9}$ - 10^{-10}. Now the question arises why is $\bar{\theta}$ is so tiny ? This is

[3]Except for s-wave scattering, σv_{rel} depends on v_{rel} and hence $<\sigma v_{rel}>$ depends on temperature

the strong CP problem.

I.5.1. Peccei-Quinn Symmetry

A promising approach to solve the strong CP problem is to introduce a spontaneously broken global Peccei-Quinn (PQ) symmetry. Introduction of a global $U(1)_{PQ}$ symmetry dynamically drives $\bar{\theta} \to 0$ by replacing the static CP violating phase $\bar{\theta}$ by a dynamical CP conserving field : the axion.

Under $U(1)_{PQ}$ transformation, the axion field a(x) transforms as :

$$a(x) \to a(x) + \alpha f_a \tag{45}$$

To make the Lagrangian invariant under $U(1)_{PQ}$ symmetry, it must be augmented with axion interaction terms. One such term is

$$\xi \frac{a}{f_a} \frac{g^2}{32\pi^2} F_a^{\mu\nu} \tilde{F}_{a\mu\nu}$$

When $U(1)_{PQ}$ symmetry breaks, the axion field gets a vev such that

$$\bar{\theta} + \xi \frac{<a>}{f_a} = 0$$

Since, at minimum the $\bar{\theta}$ term is cancelled out, hence this provides a dynamical solution to the strong CP problem.

Various models solving the strong CP problem using this approach have been discussed in Sec. III.2.4. where it has also been shown that these models simultaneously solve the aforementioned SUSY μ problem as well.

I.5.2. Gravity-spoliation problem

Unfortunately, solution to the strong CP problem require the global $U(1)_{PQ}$ symmetry to be the fundamental symmetry of the model. But quantum gravity effects spoil the PQ solution to the strong CP problem. Hence, global symmetries are not compatible with

inclusion of quantum gravity, and hence these models suffers from **gravity-spoliation problem**. As shown in [58], in order to avoid gravity spoliation problem, the PQ violating terms in the scalar potential must be at least suppressed by $1/m_p^8$ i.e., the fundamental symmetry should not be an exact global symmetry, rather it should lie in the lavender region in Fig 8.

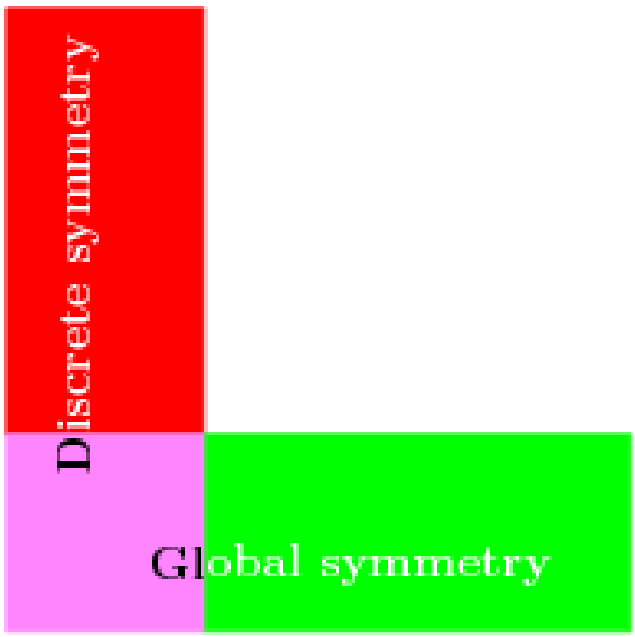

Figure 8: Kim diagram where the column represents an infinite sequence of lagrangian terms obeying gravity-safe discrete symmetry while the row represents an infinite sequence of terms obeying the global symmetry. The green region terms are gravity-unsafe while red region violates the global symmetry. The lavender terms are gravity-safe and obey the global symmetry.

One way to deal with the gravity spoliation problem is to assume a gravity-safe symmetry [4] to be the fundamental symmetry of the model and out of this fundamental symmetry, the PQ symmetry would emerge as an accidental approximate global symmetry

[4] various gravity-safe symmetries are discussed in Sec. III.3.1.

i.e., the scalar potential should contain terms allowed by the gravity safe fundamental symmetry only and these terms should be such that they will obey the global $U(1)_{PQ}$ symmetry accidentally if they are suppressed by $1/m_p^n$ with $n < 8$, and the scalar potential should contain at least one term which will violate the global $U(1)_{PQ}$ symmetry and such PQ violating terms must be suppressed by $1/m_p^n$ with $n \geq 8$.
Such gravity safe models which simulateously solve the strong CP problem and the SUSY μ problem are discussed in Sec. III.3 where it has also been shown why the "hybrid models" are preferred by nature than any other gravity safe model.

I.6. Stringy Naturalness

In the previous two sections we were concerned with naturalness of the EW scale and QCD naturalness involving the CP-violating $\bar{\theta}$ term respectively. If gravity is included in the SM, then a third naturalness problem emerges: why is the vacuum energy density ρ_{vac} so tiny, or alternatively, why is the cosmological constant (CC) Λ so tiny when there is no known symmetry to suppress its magnitude? Naively, one would expect $\Lambda \simeq m_P^4$ whereas experiments suggest $\Lambda \simeq 10^{-120} m_P^4$. Assuming a multiverse [61] with a huge (of order 10^{500} [62] or far greater? [63]) assortment of vacua states with cosmological constant uniformly distributed across the decades, then those pocket universes with Λ somewhat larger than our measured value would lead to such rapid expansion that galaxies wouldn't condense, and presumably observors wouldn't arise. Weinberg used such reasoning to predict the value of Λ to within a factor of several well before it was experimentally measured [64, 65].

Given the success of the landscape in predicting Λ, can multiverse arguments also be used to predict the scale of SUSY breaking [67, 68]? A statistical approach to understand the SUSY breaking scale has been advocated by Douglas [68, 69]. In this approach, naturalness is replaced by stringy naturalness [70, 71] wherein

observable $\mathcal{O}_2$ is more natural than observable $\mathcal{O}_1$ if more *phenomenologically viable* vacua lead to $\mathcal{O}_2$ than to $\mathcal{O}_1$.

The key phrase "phenomenologically viable" can be used here in an anthropic sense, as in the case of the cosmological constant, in that such vacua lead to pocket universes that can admit life as we understand it.

Specifically, the distribution of vacua might be written as [68]

$$dN_{vac}[m^2_{hidden}, m_{weak}, \Lambda] = f_{SUSY}(m^2_{hidden}) \cdot f_{EWSB} \cdot f_{CC} \cdot dm^2_{hidden} \tag{46}$$

where m_{hidden} is a mass scale associated with hidden sector SUSY breaking which gives rise to (in gravity mediation, which is assumed here) a gravitino mass $m_{3/2} \simeq m^2_{hidden}/m_P$ via the super-Higgs mechanism. In such models, then it is expected that the soft SUSY breaking terms, collectively denoted here as m_{soft}, will appear of order $m_{soft} \sim m_{3/2}$ [72, 73, 74].

For the prior distribution f_{SUSY}, Douglas proposed on rather general grounds a power law ansatz [68, 67]

$$f_{SUSY}(m^2_{hidden}) \sim (m^2_{hidden})^{2n_F+n_D-1} \tag{47}$$

where n_F is the number of hidden sector F-breaking fields and n_D is the number of contributing D-breaking fields. This is reflective of general string theory models which typically contain of order 10 hidden sectors some or all of which might contribute to SUSY breaking. Only for $n_F = 0$; $n_D = 1$ would we obtain (the usually assumed) uniform distribution of soft breaking terms. Already for $n_D = 0$; $n_F = 1$, we would expect a *linear* statistical draw towards large soft terms. For more complicated hidden sectors, then the statistical draw toward large soft terms would be even stronger.

Early on, these considerations led to extensive debate over whether to expect high

scale or weak scale SUSY breaking [68, 67, 75]. Such debate was in part predicated on the influence of cosmological constant selection on the SUSY breaking scale. Initial expectations were that $f_{CC} \sim \Lambda/m_{hidden}^4$. Following Douglas [68], the consensus emerged that f_{CC} would be independent of the SUSY breaking sector, and that $f_{CC} \sim \Lambda/m_{string}^4$.

The third element in Eq. (46) is f_{EWSB}. This function contains any anthropic requirements. For the case of SUSY, it also depends on the anticipated solution to the SUSY μ problem: why is the SUSY conserving μ parameter of order the weak scale rather than the Planck scale [38]? Here, a *natural* solution to the SUSY μ problem will be assumed, *i.e.* that $|\mu| \sim m_{weak}$. If $|\mu| \gg m_{weak}$, then some finetuning would be required to gain a value of m_{weak} close to the 100 GeV scale. Such finetuning requires a tiny range of compensating opposite-sign soft terms to maintain the weak scale not-too-far from its measured value [71]. And as shown by nuclear physics calculations of Agrawal *et al.* [76], the pocket universe value of the weak scale m_{weak}^{PU} should be within a factor of a few from our measured value of the weak scale. If $m_{weak}^{PU} \geq (2-5)m_{weak}^{OU}$ (OU stands for *our universe*) then stable nucleons are all Δ^{++} baryons. Complex nuclei will not form and consequently atoms as we know them will not form in such a universe. This anthropic requirement is known as the *atomic principle* in that in order to have a universe with observers, then likely atoms (and consequently chemistry) as we understand them would have to be formed [66].

To ameliorate this situation, it was proposed in Ref's [39, 77] to instead veto any non-standard EW vacua and also to veto any vacua with $m_Z^{PU} > 4\ m_Z^{OU}$ where m_Z^{PU} stands for the mass of Z boson in several pocket universes of the multiverse and m_Z^{OU} stands for the mass of Z boson in our Universe. For a fixed natural value of μ, this latter condition corresponds to vetoing pocket universes with $\Delta_{EW} > 30$. Thus, we also implement

$$f_{EWSB} = \Theta(30 - \Delta_{EW}). \tag{48}$$

Stringy naturalness will be discussed in detail in Sec. IV where, we shall see how the landscape approach affects the low scale phenomenology of various RNS models and provide a systematic and logical reasoning to predict different energy scales associated with these RNS models.

II. Is natural higgsino-only dark matter excluded?

As seen in Sec. I.2.4, electroweak naturalness (i.e., $\Delta_{EW} < 30$) requires the superpotenial μ parameter not too far from the weak scale. This implies the existence of light higgsinos with mass $\sim$ 100-300 GeV. The lower limit on the mass of higgsinos is obtained from the LEP2 experiment from chargino pair production searches. However, sparticle searches in the LHC have resulted in gluino mass limits $m_{\tilde{g}} \geq 2.2$ TeV [80] and stop mass limits $m_{\tilde{t}_1} \geq 1.1$ TeV [81] which pushes the SUSY breaking scale in the multi-TeV regime. Under such conditions, the lightest SUSY particle (LSP) is expected to be a mainly higgsino-like neutralino with non-negligible gaugino components. The LSP considered here, being a neutralino, does not have electric and color charge and also it cannot decay into SM particles due to conservation of R-parity (necessity of R-parity conservation has been discussed in Sec. I.2.2). Thus, the LSP is a stable neutral particle and hence it can serve as a good cold dark matter candidate. The computed thermal WIMP abundance in natural SUSY models is then found to be typically a factor 5-20 below its measured value. To gain concordance with observations, either an additional DM particle must be present or additional non-thermal mechanisms must augment the neutralino abundance. In this section, measured dark matter relic density and present direct and indirect WIMP detection limits (discussed in Sec. I.4) have been compared with these quantities calculated for three RNS models, namely, NUHM2, nAMSB and nGMM$'$ (discussed in Sec. I.3) using Isajet 7.88 [49]. It will be shown in this section that the case of natural higgsino-only dark matter where non-thermal production mechanisms augment its relic density, is essentially excluded by a combination of direct detection constraints from PandaX-II [83], LUX [82] and Xenon-1t [84] experiments, and by bounds from Fermi-LAT/MAGIC [85] observations of gamma rays from dwarf spheroidal galaxies. So, the only other possibility for the RNS models to satisfy the DM content of the universe is the presence of an additional DM candidate and axion,

being a solution to the Strong CP problem, is a well-motivated candidate.
Taken together, direct and indirect detection limits (discussed in Sec. I.4) have eliminated two previously well-regarded hypotheses for SUSY WIMP dark matter.

- The well-tempered neutralino (WTN)[86], wherein the bino and higgsino or wino components were adjusted to comparable values so as to obtain the required relic density, predicted $\sigma^{SI}(\tilde{z}_1 p) \sim 10^{-8}$ pb relatively independently of $m_{\tilde{z}_1}$. This adjustment was typical of the so-called focus point region[87] of the mSUGRA/CMSSM model[88]. This region is now solidly excluded[82, 83, 84, 89].

- The case of wino-like WIMP-only dark matter, which is characteristic of anomaly-mediated SUSY breaking models, predicts rather large rates for WIMP-WIMP annihilation into WW, leading to gamma ray production in areas of the universe where increased WIMP densities are expected (such as galactic cores and dwarf galaxies). Recent limits from Fermi-LAT (at lower $m_{\tilde{z}_1}$) and HESS (at $m_{\tilde{z}_1} \sim$ TeV-scale) have seemingly excluded this possibility if one includes Sommerfeld enhancement effects in the annihilation cross sections.[90, 91, 89]

The three RNS models examined here, as shown in Fig. 6, have qualitatively different patterns of gaugino and higgsino masses which in turn determines the nature of the SUSY WIMP.

II.1. Dark matter relic density in RNS models

For these RNS models, since $\mu \ll m_{soft}$ (as required by naturalness), then one expects the lightest SUSY particle (LSP) to be *mainly* higgsino-like, but with a non-negligible gaugino component (lest $\Sigma_u^u(m_{\tilde{w}_2})$ becomes large for too large wino masses). The first question then is: do the natural SUSY models produce the measured relic abundance of dark matter in the universe given by $\Omega_{DM}h^2 \equiv (\rho_{DM}/\rho_c)h^2$ where ρ_c is the critical closure density of dark matter and h is the scaled Hubble constant. Of course, since

higgsinos annihilate with full gauge strength in the early Universe, it is not expected that the relic density of *thermally produced*, light higgsinos to saturate the observed relic density, but it is nonetheless instructive to examine the expectations for the thermal relic density in well-motivated natural SUSY models.

To answer this question, the thermally-produced relic density for various SUSY models has been computed. The computer code Isajet 7.88 has been used to compute sparticle mass spectra for the nNUHM2, nAMSB and nGMM$'$ models[49].

For nNUHM2 model, a random scan in addition to a focused scan is performed over parameters

$$\begin{aligned} m_0: &\ 0-10\ \text{TeV}, \\ m_{1/2}: &\ 0.5-3\ \text{TeV}, (0.7-2\ \text{TeV}), \\ A_0: &\ -20\ \rightarrow\ +20\ \text{TeV}, ((-1\ \rightarrow\ -3)m_0), \\ \tan\beta: &\ 4-58, \\ \mu: &\ 100-500\ \text{GeV}, (100-360\ \text{GeV}), \\ m_A: &\ 0.25-10\ \text{TeV}. \end{aligned} \tag{49}$$

For nAMSB model, a random and a focused scan is done over

$$\begin{aligned} m_{3/2}: &\ 80-1000\ \text{TeV}, (80-300\ \text{TeV}), \\ m_0(3): &\ 1-10\ \text{TeV}, \\ m_0(1,2): &\ m_0(3)-20\ \text{TeV}, \\ A_0: &\ -20\ \rightarrow\ +20\ \text{TeV}, ((+0.5\ \rightarrow\ +2)m_0(3)), \\ \tan\beta: &\ 4-58, \\ \mu: &\ 100-500\ \text{GeV}, (100-350\ \text{GeV}), \\ m_A: &\ 0.25-10\ \text{TeV}. \end{aligned} \tag{50}$$

For the nGMM$'$ model, a scan is done over

$$\begin{aligned}
\alpha: &\ 2-40\\
m_{3/2}: &\ 3-65 \text{ TeV}\\
c_m = &\ (16\pi^2/\alpha)^2\\
c_{m3}: &\ 1-\min[40,(c_m/4)],\\
a_3: &\ 1-12,\\
\tan\beta: &\ 4-58,\\
\mu: &\ 100-360 \text{ GeV},\\
m_A: &\ 0.3-10 \text{ TeV}.
\end{aligned} \tag{51}$$

For each solution, the light Higgs boson mass m_h is required to be within 122 GeV and 128 GeV (allowing for ± 3 GeV error in the Isajet m_h calculation). To enforce naturalness, each solution must have $\Delta_{EW} < 30$. It is also required that $m_{\tilde{g}} > 2$ TeV and $m_{\tilde{t}_1} > 1$ TeV in order to satisfy LHC sparticle search limits.

The results of these calculations of the thermal LSP relic density $\Omega^{TP}_{\tilde{z}_1}h^2$ (using the Isajet subcode IsaReD[92]) are shown versus $m_{\tilde{z}_1}$ in Fig. 9 for the three natural SUSY models. The points from the above-mentioned scan that yield $\Delta_{\rm EW} \leq 30$ and also satisfy the Higgs boson mass and LHC sparticle mass constraints has been plotted as blue pluses (nGMM$'$ model), green stars (nAMSB model) and yellow crosses (nNUHM2 model). It can be seen that $m_{\tilde{z}_1}$ is bounded from below by $m_{\tilde{z}_1} \geq 100$ GeV due to LEP2 limits on $m_{\tilde{w}_1} \geq 100$ GeV (which has been set as the lower limit on the μ parameter scan). Also, $m_{\tilde{z}_1}$ is bounded from above by $m_{\tilde{z}_1} \leq 350$ GeV from the naturalness constraint, $\Delta_{EW} < 30$. For the lower range of $m_{\tilde{z}_1}$ values, then $\Omega^{TP}_{\tilde{z}_1}h^2$ is typically a factor ~ 20 below the measured value $\Omega_{\rm CDM} = 0.1199 \pm 0.0022$ [93] while for the high range of $m_{\tilde{z}_1}$ then the calculated relic abundance is about a factor ~ 4 below the measured result. The range of under-abundance just mentioned applies to all three

models with the possible exception of nAMSB where some of the green stars lie at even lower $\Omega_{\tilde{z}_1}^{TP}h^2$ values. The reason for this is that in nAMSB models, for a lower range of $m_{3/2}$ values then the wino can range down to $M_2 : 200 - 300$ GeV so that for this model the $\tilde{z}_1$ can be mixed higgsino-wino variety: then the neutralino annihilation rate in the universe is enhanced even beyond the higgsino-like case leading to even lower relic density. Thus, natural SUSY models typically predict an under-abundance of *thermally produced neutralinos* in standard Big Bang cosmology by a factor $\sim 5 - 25$. Other mechanisms are required to bring the expected DM abundance into accord with data. Two well-motivated classes of mechanisms have been proposed to bring the thermally-

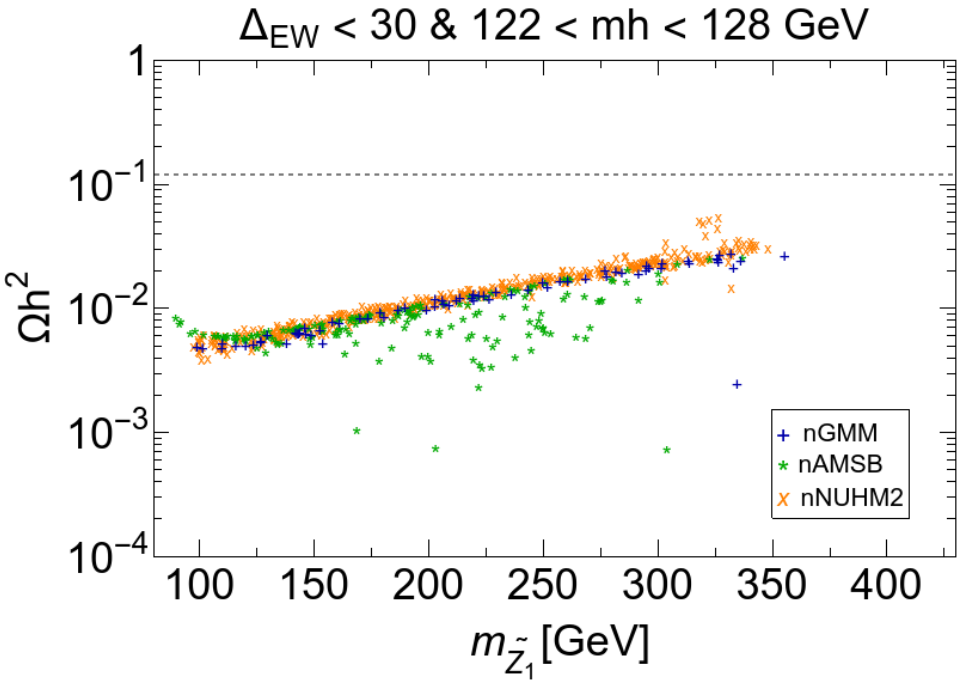

Figure 9: Plot of points in the $\Omega_{\tilde{z}_1}h^2$ vs. $m_{\tilde{z}_1}$ plane from a scan over NUHM2, nGMM′ and nAMSB model parameter space. The dashed line shows the measured value.

produced under-abundance of neutralinos into accord with the measured dark matter abundance. In the first class, the dark matter is *multi-component* with thermal higgsinos comprising only a fraction of the observed dark matter, with the remainder consisting of other particle(s). The axion is perhaps the best-motivated candidates for the remainder

of the dark matter (for a review, see *e.g.* Ref. [94]). In the second class of models, the dark matter is *all neutralinos*, with a non-thermal component from late decays (to neutralinos) of heavy particles making up the balance of the observed relic density. We will see below that if the neutralino is dominantly the higgsino of natural SUSY, the second class of models is essentially ruled out by the data.

Mixed axion/WIMP dark matter

As mentioned, one possibility is that the total WIMP abundance does not saturate the measured relic density but that, like visible matter, the dark matter is comprised of several particles. A very natural choice for a second dark matter particle is the QCD axion which also seems to be required to solve the strong CP problem in QCD. In a supersymmetric context, then the axion should occur as but one element of an axion superfield which would also necessarily contain a spin-0 R-parity even saxion field s and a spin-$\frac{1}{2}$ R-parity-odd axino field $\tilde{a}$. Both saxion and axino are expected to gain masses of order the gravitino mass $m_{3/2}$ in supergravity models[95].

In SUSY axion models, the axions can be produced via 1. vacuum misalignment, 2. thermally, and also 3. non-thermally via (late time) saxion decay $s \to aa$. The latter two may lead to relativistic axions whose population is limited by strict bounds on the effective number of relativistic degrees of freedom $N_{\rm eff} = 3.15 \pm 0.23$ derived from fits to CMB and other cosmological data [93]. Axinos can be thermally produced in the early universe and then augment the WIMP abundance via decays after thermal WIMP freeze-out. Saxions can be produced both thermally and non-thermally and then decay to SM particles (resulting in *entropy dilution* of all relics from their value at the time of decay), SUSY particles (which augment the WIMP abundance) or to axions as mentioned above. WIMPs can be produced thermally or non-thermally via axino, saxion or gravitino decay. The resultant mixed axion-WIMP abundance has been evaluated by solving eight-coupled Boltzmann equations[96]. The Boltzmann equations

track the interrelated abundances of

- thermally and non-thermally produced WIMPs,
- thermally and decay-produced axions,
- axions from vacuum mis-alignment/bosonic coherent motion (BCM),
- thermal production and decay of axinos,
- thermal production and decay of saxions,
- saxion BCM production and decay,
- thermal gravitino production and decay and
- production of radiation at re-heat and from saxion/axino decay.

The exact rates also depend on the underlying SUSY axion model assumed (KSVZ or DFSZ), as well as on other parameters such as $m_{\tilde{a}}$, m_s, θ_s, $m_{3/2}$, the re-heat temperature T_R, the initial axion mis-alignment andgle θ_i and the SUSY particle mass spectrum (which influences the saxion, axino and gravitino decay branching fractions)[96]. Points in parameter space may become excluded via overproduction of WIMPs or axions, or by increasing ΔN_{eff} via relativistic axion production from saxion decays or by violation of BBN constraints. For low values of the axion decay constant[5], $f_a \leq 10^{11}$ GeV, the WIMP abundance is its thermal value since axinos and saxions tend to decay before WIMP freeze-out so that $\xi = \xi_{TP} \equiv \Omega_{\tilde{z}_1}^{TP} h^2/0.12$. If $f_a \geq 10^{11}$ GeV, then post-freeze out saxion and axino decays may augment the WIMP abundance so that $\xi_{TP} < \xi < 1$. For very large $f_a \geq 10^{14}$ GeV, then almost always WIMPs are overproduced via saxion and

[5]The axion decay constant f_a is defined via its coupling to two gluons: $\mathcal{L} \ni \frac{\alpha_s}{8\pi(f_a/N_{DW})} a G^A_{\mu\nu} \tilde{G}^{A\mu\nu}$ where f_a can range from $\sim 10^9$ GeV (from SN1987A energy loss rate) up to possibly beyond the Planck scale (for tiny initial mis-alignment angle θ_i). Here, $N_{DW} = 6$ is the domain wall number for the DFSZ axion.

axino decays ($\xi > 1$), ΔN_{eff} becomes too large and BBN constraints on late-decaying neutral relics are violated.

For the non-excluded points $\xi \leq 1$, the upshot is that the expected rates for direct and indirect WIMP detection now depend on the fractional WIMP abundance denoted by $\xi = \Omega_{\tilde{z}_1} h^2/0.12 < 1$ since now there are fewer target WIMPs compared to the WIMP-only hypothesis for dark matter. For spin-independent (SI), spin-dependent (SD) detection rates, and also the neutrino detection rate at IceCube, the target event rates must be scaled by a factor[6] ξ while for indirect WIMP detection (IDD) via WIMP-WIMP annihilation into gamma-rays or particle-antiparticle pairs, the event rates must be scaled by a factor ξ^2. To be conservative, for mixed axion/WIMP dark matter, it has been assumed that $\xi = \xi_{TP} = \Omega_{\tilde{z}_1}^{TP} h^2/0.12$ which is usually the lower bound on ξ.

Non-thermally produced WIMP-only dark matter

Another option is to assume WIMP-only dark matter where the additional WIMP abundance is assumed to arise from non-thermal processes. The prototypical non-thermal WIMP production process occurs from light modulus field ϕ production in the early universe via the BCM (which also occurs for saxion and cold axion production). If the modulus field (of mass m_ϕ) then decays after WIMP freeze-out but before the onset of BBN, then it may augment the thermally-produced abundance to gain accord with the measured density of dark matter. This mechanism was originally suggested by Moroi and Randall [98] to account for how wino-like LSPs from AMSB models could account for the observed dark matter. It was later emphasized by Gondolo and Gelmini[99] that the measured relic density could be achieved for any value of $\Omega_{\tilde{z}_1}^{TP} h^2 > 10^{-5}(100\ GeV/m_{\tilde{z}_1})$ by adjusting just two parameters: b/m_ϕ and T_{R2} where b is the number of neutralinos produced per ϕ decay and T_{R2} is the (second) reheat

[6]Assuming the WIMP density in the sun is in equilibrium, the WIMP annihilation rate used to determine the (bound on the) spin-dependent cross section at IceCube is fixed by the WIMP *capture rate* which scales linearly as ξ, and has no further dependence on the WIMP annihilation cross section.

temperature arising from ϕ decay. This reheating temperature is related to the ϕ field energy density as $T_{R2} \sim \rho_\phi^{-1/4}$. Non-thermal WIMP production has also been recently invoked to reconcile an underproduced WIMP relic density with measured value in string-motivated models with a wino-like LSP[100, 101, 102]. For the case of natural WIMP-only dark matter, it has been assumed that the thermal and non-thermal relic density contributions sum to the measured dark matter density so that $\xi = 1$ for this case.

II.2. Bounds on natural SUSY WIMPs from direct and indirect WIMP searches

Direct WIMP detection bounds

In Fig. 10, the value of $\xi\sigma^{SI}(\tilde{z}_1 p)$ vs. $m_{\tilde{z}_1}$ is shown for *a*) the case with $\xi = \Omega_{\tilde{z}_1}^{TP}h^2/0.12 < 1$ (corresponding to mixed axion/WIMP DM with no non-thermal WIMP production or dilution) while in frame *b*) the case with natural WIMP-only DM and $\xi = 1$ is shown. Here, the Isajet subcode IsaReS[103] has been used for direct and indirect relic scattering calculations.[7] In both frames, the current SI DD bounds from LUX, PandaX and Xe-1ton (solid curves), along with a future projected bound from Xe-1ton (dashed) is also plotted. From frame *a*), we see that present bounds already exclude many natural SUSY model points even with $\xi < 1$, if we assume that the neutralino relic density is given by its thermal value. Especially, a large fraction of nAMSB model points are excluded. This is because in nAMSB the winos can be relatively light compared to $m_{\tilde{g}}$ and the $h\tilde{z}_1\tilde{z}_1$ coupling occurs as a product of gaugino times higgsino components (see Eq. (8.117) of Ref. [13]). The enhanced $\tilde{z}_1 p$ scattering rate for nAMSB more than compensates for the somewhat diminished relic abundance. For the nNUHM2 and nGMM

[7]The IsaReS SI direct detection cross sections depend sensitively on the strange quark content of the proton[104]. For IsaReS, the central values of updated quark mass fractions and moments as tabulated by Hisano *et al.*[105] has been used.

models, the major portion of model points survive the current SI DD bounds. But future ton-scale noble liquid search experiments will cover the remainder of parameter space, assuming that the neutralino relic density is not diluted from its thermal value by entropy injection in the early Universe.

In frame *b*), for WIMP-only DM with $\xi = 1$, then we see that current bounds exclude almost every point of all three models. A single point from the scan with $m_{\tilde{z}_1} \sim 250$ GeV has survived. The surviving point lies within the future reach of ton-scale noble liquid detectors. Thus, it appears from this plot alone that natural WIMP-only DM appears to be essentially excluded (but for one nNUHM2 point which has gaugino masses close to their naturalness upper limit, and hence a reduced gaugino content and correspondingly reduced neutralino coupling to h).[8] It is also shown in frame *b*) the latest Xe-1ton bound with an added factor of two uncertainty in the experimental bound. In this case, one additional point with $m_{\tilde{z}_1} \sim 205$ GeV could barely be allowed as it is just inside the limit band.

In Fig. 11, $\xi\sigma^{SD}(\tilde{z}_1 p)$ vs. $m_{\tilde{z}_1}$ is shown. Again, in frame *a*) $\xi = \Omega^{TP}_{\tilde{z}_1}h^2/0.12 < 1$ is taken while in *b*) the natural WIMP-only case with $\xi = 1$ is shown. The current SD limits from the PICO-60 experiment[106] and from IceCube[107] (the latter assuming dominant WIMP annihilation within the solar core into WW final states) is also shown. From frame *a*), we see that, save for a few points around $m_{\tilde{z}_1} \simeq 100$ GeV, all points avoid the present SD DD bounds.

We also see that the bulk of natural SUSY points will be probed by PICO-500 [108] (subject to the caveats mentioned above) although some points might still elude SD detection.

In frame *b*), the $\xi = 1$ case for natural WIMP-only DM is shown. In this case, we see that a combination of PICO-60 and IceCube have already ruled out a significant

[8]The outlier point with $m_{\tilde{z}_1} \simeq 250$ GeV was generated with $m_{\tilde{g}} = 6.2$ TeV and $\Delta_{\rm EW} = 29$ and $m_h = 122.5$ GeV. Thus, it inhabits the outermost extremity of the naturalness and Higgs mass allowed regime.

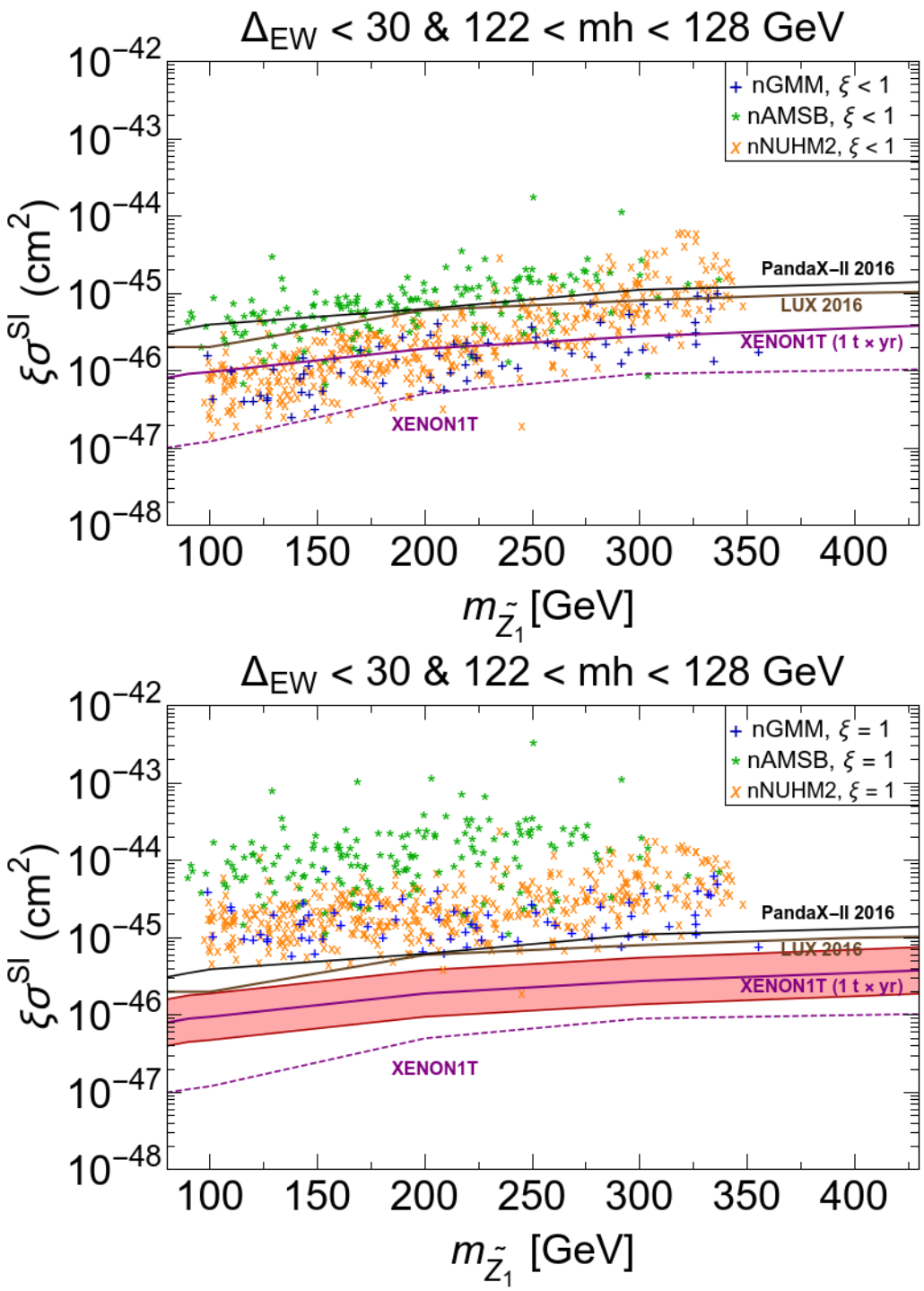

Figure 10: Plot of points in the $\sigma^{SI}(\tilde{z}_1 p)$ vs. $m_{\tilde{z}_1}$ plane from a scan over the natural NUHM2, nGMM and nAMSB model parameter space for *a*) $\xi < 1$, assuming the neutralino relic density is given by its thermal value, and *b*) $\xi = 1$.

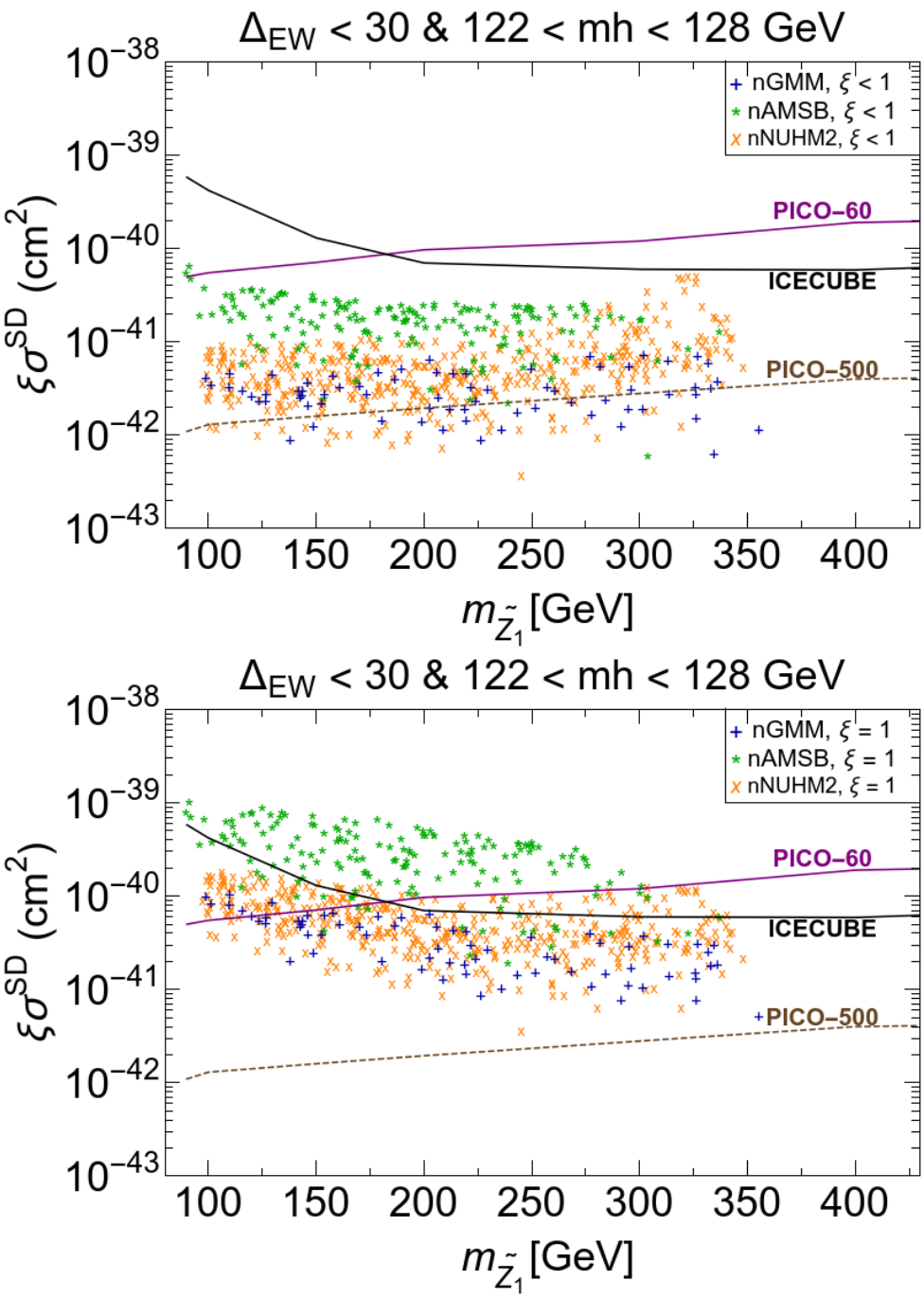

Figure 11: Plot of points in the $\sigma^{SD}(\tilde{z}_1 p)$ vs. $m_{\tilde{z}_1}$ plane from scans over the parameter space of the the natural NUHM2, nGMM and nAMSB models for *a*) $\xi < 1$, assuming the neutralino relic density is given by its thermal value, and *b*) $\xi = 1$.

fraction of natural SUSY model points. The projected reach of PICO-500 should probe the remaining possibilities.

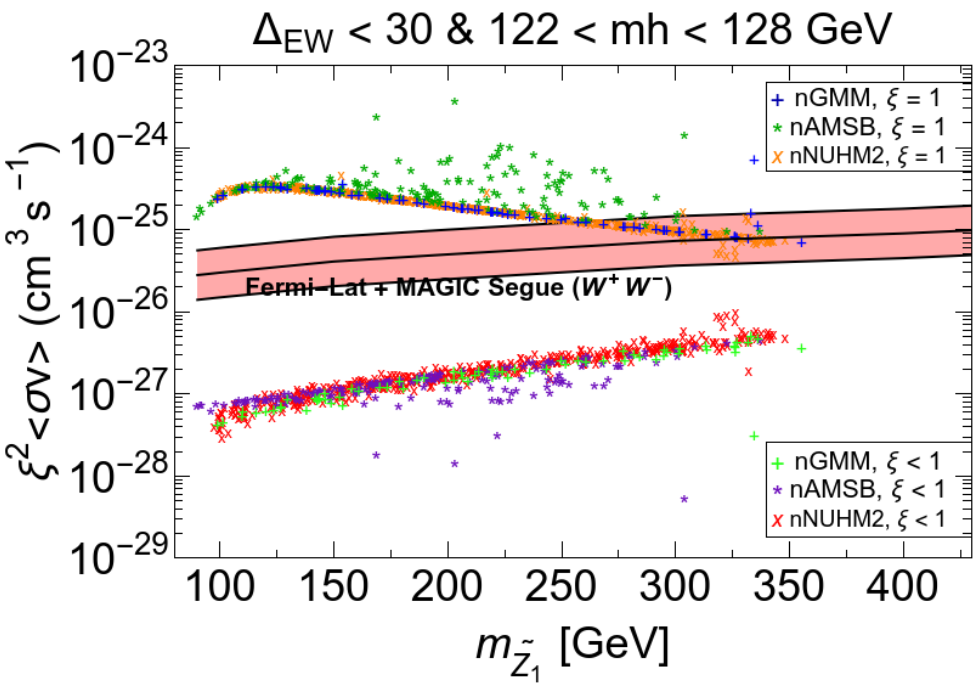

Figure 12: The scaled values $\xi^2\langle\sigma v\rangle$ from scans over the parameter space of the the natural NUHM2, nGMM and nAMSB models for $\xi < 1$, assuming the neutralino relic density is given by its thermal value (lower set), and $\xi = 1$ (upper set). The Fermi-LAT+MAGIC bound including the central value along with a possible factor of two uncertainty has been plotted.

Indirect WIMP detection bounds

In Fig. 12, the quantity $\xi^2\langle\sigma v\rangle$, the thermally averaged WIMP-WIMP annihilation cross section times velocity, evaluated as $v \to 0$, scaled by the square of the depleted relic abundance, vs. $m_{\tilde{z}_1}$ is shown.

In this figure, the mixed axion/WIMP dark matter points with $\xi \ll 1$ (lower set of points), again assuming the thermal neutralino relic density is close to its real value, are neatly separated from the $\xi = 1$ points for WIMP-only dark matter (upper set of points). The present bounds from the combined Fermi-LAT and MAGIC collaborations derived from observations of gamma rays from dwarf spheroidal galaxies is also shown.[9]

[9]For this case of mainly higgsino-like WIMPs, it has been checked that the WIMP-WIMP annihilation takes place almost entirely into the WW and ZZ channels along with a smaller component into Zh. Thus, the Fermi-LAT/MAGIC channel to be compared against is their result for annihilation ito

A possible "factor of two" uncertainty has been added here in the experimental limit so that it can also be interpreted as a limit band. Corresponding limits from HESS are relevant only for higher, unnatural values of $m_{\tilde{z}_1}$, and not shown in the figure. We see that *all* of the mixed axion/WIMP dark matter points fall well below the experimental bounds. However, we also see that all the natural WIMP-only points with $\xi = 1$ points are excluded by present bounds save for a few points with $m_{\tilde{z}_1} > 300$ GeV. If we instead use the limit band, then points with $m_{\tilde{z}_1} \geq 250$ GeV are still allowed.

It has been checked that the $m_{\tilde{z}_1} > 250$ GeV points are excluded by the SI DD band from Fig. 10*b*). Likewise, it has been checked that the two nNUHM2 point with $m_{\tilde{z}_1} \sim 200,\ 250$ GeV are excluded by the IDD limit band with $\xi = 1$.

Summary : In this section, dark matter relic density and the direct- and indirect-WIMP detection rates[10] for three different natural SUSY models with very different gaugino spectra: nNUHM2, nAMSB and nGMM$'$ have been calculated and confronted with the corresponding experimental limits. The three models all have higgsino-like LSPs but qualitatively different and non-negligible gaugino components. They have suppressed values of *thermally produced* neutralino relic abundances – lower than the measured abundance of CDM by factors ranging from 5-25. For these three models, the WIMP SI- and SD- direct detection rates and also their indirect detection rates have been examined for two different possibilities: 1. mixed axion-WIMP dark matter where only a fraction ξ, determined by the thermal neutralino relic abundance, is assumed to be due to WIMPs, while the remainder is axions, and 2. the case of WIMP-only dark matter where the thermal relic abundance is supplemented by non-thermal production from processes like modulus field decay in the early universe. In this second case, then

WW since the gammas come primarily from $V \to q\bar{q} \to \pi^0 s \to \gamma\gamma$ and these configurations are similar for $V = W$ or $V = Z$.

[10]For related recent work on AMS-02 bounds using $\bar{p}$ rates on non-natural SUSY models, see Ref's [110] and [111]. For recent work on direct, indirect and collider constraints on thermal-only SUSY WIMPs, see *e.g.* [112]. For general constraints on higgsino dark matter, see Ref. [113].

the fractional WIMP abundance is then taken to be $\xi = 1$.

From the scans of the parameter space of natural SUSY models, as mentioned above, we find that models where the WIMP relic density (taken to be its thermal value) forms just ∼5-20% of the measured CDM density comfortably survive constraints from LHC as well as those from direct and indirect searches. Direct searches at ton-sized detectors (Xenon-nT or LZ) will probe the entire natural SUSY parameter space, *assuming that the relic abundance is given by its thermal expectation.* In this case, future experiments such as PICO-500 – designed to measure the spin-dependent neutralino-nucleon scattering – will also probe a large part (but not all) of the parameter space. Otherwise, future colliders such as an electron-positron collider with $\sqrt{s} \geq 500 - 600$ GeV [109], or a high energy pp collider operating at $\sqrt{s} \sim 27 - 33$ TeV[114] will be necessary for a definitive probe of the natural SUSY scenario with multi-component dark matter.

The situation for natural SUSY models where the neutral higgsino-like WIMP saturates the observed relic density is qualitatively different. These scenarios are essentially excluded both by bounds from direct detection experiments as well as by *independent* bounds from Fermi-Lat + Magic observations of high energy gamma rays from dwarf galaxies. More correctly, while a few points from our scans survive the indirect searches, these are excluded by direct detection, and vice-versa. Such models would also be decisively probed by spin-dependent direct-detection at PICO-500. Thus, the answer to the question posed in the title is: yes, it appears the case of natural higgsino-like-WIMP-only dark matter is indeed excluded. Unnatural higgsino-like WIMP dark matter can still survive as detailed in Ref. [115, 116] although these models would have a difficult time explaining why it is that the weak scale is a mere 100 GeV instead of lying in the multi-TeV range. Another possibility is to have models with non-universal gaugino masses where $M_3 > 2$ TeV to satisfy LHC gluino mass bounds but where $M_1 \sim 50 - 150$ GeV with $|M_1| < |\mu|$. This case, explored with running non-universal gaugino masses in Ref. [117] and in the pMSSM context in the first of Ref. [118], has a mainly bino-like

LSP while still satisfying naturalness bounds. It is unclear as to the origin of the rather large mass gap between bino and gluino.

As a whole, the results obtained here seem to bolster the case for a second dark matter particle such as the axion. While the remainder of the dark matter could be in the hidden sector, the axion is a very well motivated candidate which may well constitute the bulk of dark matter in our Universe. Prospects for the complementary axion searches in SUSY axion models have been examined in Ref. [119].

III. Simultaneous solution to SUSY μ problem, strong CP problem and gravity-spoliation problem

III.1. Revisiting the SUSY μ problem in the LHC era

As discussed in Sec I.2.4, one of the naturalness conditions requires $\mu \sim$ 100-300 GeV, while the first term in Eqn. (6) leads one to expect that the dimensionful parameter μ should be of order $m_P \sim 2.4\times 10^{18}$ GeV. This is the famous SUSY μ problem [38, 120, 56] Here, we focus attention on the SUSY μ problem as occurs in gravity-mediation. The SUSY μ problem in gauge-mediated supersymmetry breaking (GMSB) is summarized in Ref. [121]. In GMSB, since the trilinear soft terms are expected to be tiny, then sparticle masses must become huge with highly unnatural contributions to the weak scale in order to accommodate a light Higgs boson with $m_h \simeq 125$ GeV [122, 123].[11]

There are two parts to solving the SUSY μ problem:

- First, one must forbid the appearance of μ, usually via some symmetry such as Peccei-Quinn (PQ) or better a continuous or discrete gauge or R-symmetry, and then
- re-generate μ at the much lower weak scale $|\mu| \sim 100 - 300$ GeV (the lower the more natural) via some mechanism such as symmetry breaking.

Many solutions to the SUSY μ problem have been proposed, and indeed later in this section we will review twenty of these. In most of these solutions, the goal (for gravity-mediation) was to re-generate $\mu \sim m_{3/2}$ where $m_{3/2}$ is the gravitino mass which arises from SUGRA breaking and which sets the mass scale for the soft SUSY breaking terms. When many of these μ solutions were proposed– well before the LHC era– it was

[11] We also do not consider SUSY models with non-holonomic soft terms[124] or multiple μ terms; it is not clear whether such models have viable UV completions[125, 126].

commonly accepted that $m_{3/2} \sim m_{weak}$ which would also solve the SUSY naturalness problem. However, absence of any direct signal for SUSY at LHC has pushed current sparticles mass limits to $m_{\tilde{g}} \geq 2.2$ TeV and $m_{\tilde{t}_1} \geq 1.1$ TeV which suggest that the soft SUSY breaking scale m_{soft} lies in the multi-TeV regime. Thus in the LHC era $\mu \ll m_{soft} \leq m_{3/2}$. This hierarchy is the so-called Little Hierarchy (LH). Hence, the SUSY μ problem needs a reformulation for the LHC era: any solution to the SUSY μ problem should first forbid the appearance of μ, but then re-generate it at the weak scale, *which is now hierarchically smaller than the soft breaking scale* m_{soft}:

$$|\mu| \sim m_{weak} \sim 100 - 300 \text{ GeV} \ll m_{soft} \sim \text{multi} - \text{TeV} \leq m_{3/2}. \tag{52}$$

Here, we shall review various proposed solutions to the SUSY μ problem and confront them with the Little Hierarchy as established by LHC data and as embodied by Eq. (52). While many solutions can be *tuned* to maintain the Little Hierarchy, others may offer compatibility with or even a mechanism to generate Eq. (52). Thus, present LHC data may be pointing to favored solutions to the SUSY μ problem which may be reflective of the way nature actually works.

III.2. Previously devised solutions to the SUSY μ problem

In this Section, some solutions to the SUSY μ problem have been reviewed. In the solutions reviewed here, the μ-term is typically generated by breaking the symmetry which originally prohibits the μ-term at the tree-level. Depending on the source of such symmetry breaking, the solutions have been categorized according to 1. those from supergravity/superstring models, 2. those from (visible-sector) extensions of the MSSM, 3. those including an extra local $U(1)'$ and 4. those which include also a solution to the strong CP problem with Peccei-Quinn symmetry breaking

III.2.1. Solutions in supergravity/string construction

Giudice-Masiero (GM)

In supergravity models the Kähler function $G = K + \log|W|^2$ is written in terms of the real Kähler potential K and the holomorphic superpotential W. If we posit some symmetry (PQ or R-symmetry as suggested in Ref. [127]) to forbid the usual MSSM μ term, then one may regenerate it via the Higgs fields coupling to hidden sector fields h_m via non-renormalizable terms in K [127]:

$$K \ni H_u^\dagger H_u + H_d^\dagger H_d + \left(\frac{\lambda_\mu}{m_P} H_u H_d h^\dagger + h.c.\right). \tag{53}$$

If we arrange for SUSY breaking in the hidden sector, then the auxilliary component of h develops a vev $\langle F_h\rangle \sim m_{hidden}^2$ so that the gravitino gets a mass $m_{3/2} \sim m_{hidden}^2/m_P$. A μ term is generated of order

$$\mu_{\rm eff} = \lambda_\mu \frac{\langle F_h^*\rangle}{m_P} \sim \lambda_\mu m_{hidden}^2/m_P \sim \lambda_\mu m_{3/2} \sim m_{soft}. \tag{54}$$

Thus, in the GM case, the μ parameter arises which is typically of order the soft breaking scale unless the coupling λ_μ is suppressed at the $\sim 0.01 - 0.1$ level.

Casas-Munoz (CM)

Casas and Munoz [128] propose a string theory inspired solution to the SUSY μ problem. In string theory, dimensionful couplings such as μ are already forbidden by the scale invariance of the theory so no new symmetries are needed to forbid it. They begin with a superpotential of the form

$$W = W_0 + \lambda_\mu W_0 H_u H_d/m_P^2 \tag{55}$$

where W_0 is the usual superpotential of the MSSM (but without the μ term) along with the hidden sector component which is responsible for SUSY breaking: $W_0 = W_0^{vis}(z_i) + W_0^{hid}(h_m)$ where the z_i comprise visible sector fields while the h_m denote hidden sector fields. While the scale-variant μ term is forbidden in W_0^{vis}, the non-renormalizable contribution in Eq. (55) is certainly allowed and, absent any symmetries which could forbid it, probably mandatory. Under, for instance, F-term SUSY breaking in the hidden sector, then W_0^{hid} gains a vev $\langle W_0^{hid}\rangle \sim m_{hidden}^2 m_P$ (as is easy to see in the simplest Polonyi model for SUSY breaking with $W_{Polonyi} = m_{hidden}^2(h + \beta m_P)$ where β is a dimensionless constant). Under these conditions, then a μ term develops with

$$\mu_{\rm eff} \sim \lambda_\mu m_{hidden}^2/m_P \sim \lambda_\mu m_{3/2} \sim m_{soft}. \tag{56}$$

Ref. [128] goes on to show that the CM solution can easily emerge in models of SUSY breaking due to hidden sector gaugino condensation at some intermediate mass scale Λ_h (where then we would associate $m_{hidden}^2 \simeq \Lambda_h^3/m_P$).

A benefit of the CM solution is that it should be consistent with any stringy UV completion [129] as it avoids the presence of some global (PQ) symmetry. A possible drawback to CM is that the μ term is naturally expected to be of order m_{soft} instead of m_{weak} unless λ_μ is suppressed (as in GM). One way to falsify the CM solution would be to discover a DFSZ-like axion with consistent mass and coupling values. Such a discovery would exclude the second term in Eq. (55) since it would violate the PQ symmetry.

μ and a big hierarchy from approximate R-symmetry

In string theory models, approximate R-symmetries are expected to develop from overall Lorentz symmetry of the 10-dimensional spacetime when compactified to four dimensions. Under a continuous $U(1)_R$ symmetry, the superspace co-ordinates transform non-trivially and hence so do the bosonic and fermionic components of superfields.

Thus, these symmetries can be linked to overall Lorentz symmetry where also bosons and fermions transform differently.

Under exact R-symmetry and supersymmetry, then the superpotential μ term is forbidden since the gauge-invariant bilinear term of Higgs pair $H_u H_d$ carries zero R-charge while the superpotential must have $R_W = +2$. However, $H_u H_d$ may couple to various other superfields ϕ_i which carry non-trivial R-charges so that

$$W \ni P_\mu(\phi_i) H_u H_d \tag{57}$$

where $P_\mu(\phi_i)$ is a sum over monomials in the fields ϕ_i^n. Unbroken R-symmetry requires a vanishing $\langle P_\mu(\phi_i)\rangle$ but if the R-symmetry is approximate then non-vanishing $P_\mu(\phi_i)$ contributions will develop at higher orders in powers of the field vevs $\langle(\phi_i/m_P)\rangle \leq 1$. Thus, a mild hierarchy in the field vevs $\langle\phi_i/m_P\rangle \leq 1$, when raised to higher powers $\langle(\phi_i/m_P)^{n_i}\rangle \ll 1$, can generate a much larger hierarchy of scales [130]. In this solution to the μ problem, which is essentially a UV completion of the CM solution, then $\mu \sim m_{3/2} \sim \langle W\rangle$ is expected to arise.

Solution via the discrete R-symmetry $\mathbb{Z}_4^R$

A particularly attractive way to solve the μ problem in some string constructions is via a discrete Abelian R-symmetry $\mathbb{Z}_4^R$ [131, 132, 134]. Such R-symmetries may arise as discrete remnants of the Lorentz symmetry of extra dimensional ($d = 10$) models upon compactification to $d = 4$ [133]. In Ref. [135], the $\mathbb{Z}_4^R$ symmetry was invoked to forbid the μ term as well as dimension-4 baryon- and lepton-number violating operators while dangerous dimension-5 operators leading to proton decay are highly suppressed [136, 137]. The desirable Weinberg neutrino mass operator is allowed. The $\mathbb{Z}_4^R$ charges are assigned so that all anomalies cancel by including Green-Schwarz terms (and extra R-charged singlets for gravitational anomalies). The R-charge assignments for R-symmetry $\mathbb{Z}_4^R$ are shown in second row of Table 3.

multiplet	H_u	H_d	Q_i	L_i	U_i^c	D_i^c	E_i^c	N_i^c
$\mathbb{Z}_4^R$ charge	0	0	1	1	1	1	1	1

Table 3: $\mathbb{Z}_4^R$ charge assignments for various superfields of the Lee-Raby-Ratz-Ross-Schieren-Schmidt-Hoberg-Vaudrevange model[136].

The charge assignments are consistent with embedding the matter superfields into a single **16** of $SO(10)$ while the split Higgs multiplets would arise from Wilson-line breaking of gauge symmetry. The $\mathbb{Z}_4^R$ symmetry may be broken via non-perturbative effects such as gaugino condensation breaking of SUGRA in the hidden sector so that a gravitino mass $m_{3/2}$ is induced along with soft terms $m_{soft} \sim m_{3/2}$. A μ term may arise via GM and/or CM (as discussed above) so that $\mu \sim \langle W \rangle / m_P^2 \sim m_{3/2} \sim m_{soft}$. Although the discrete $\mathbb{Z}_4^R$ R-symmetry is broken, the discrete matter/R-parity remains unbroken so that the LSP remains absolutely stable. This sort of solution to the μ problem is expected to be common in heterotic string models compactified on an orbifold [137]. Other possibilities for $\mathbb{Z}_N^R$ with $N > 4$ also occur[137] and in fact any N value is possible under anomaly cancellations provided one includes additional exotic matter into the visible sector [138].

A further concern is that a spontaneously broken discrete symmetry may lead to formation of domain walls in the early universe which could dominate the present energy density of the universe [139, 140, 141]. For the case of gravity mediation, the domain walls would be expected to form around the SUSY breaking scale $T \sim 10^{12}$ GeV. However, if inflation persists to lower temperatures, then the domain walls may be inflated away. It is key to observe that many mechanisms of baryogenesis are consistent with inflation persisting down to temperatures of $T \sim 10^6$ GeV [142].

String instanton solution

In string theory models, it is possible for superpotential terms to arise from non-perturbative instanton effects. These are particularly well suited for open strings in

braneworld scenarios such as IIA and IIB string theory. Intriguing applications of stringy instanton effects include the generation of Majorana neutrino mass terms, generation of Yukawa couplings and generation of the μ term in the superpotential [143, 144]. In some D-brane models which include the MSSM at low energy, then the superpotential μ term may be forbidden by $U(1)$ symmetries but then it is generated non-perturbatively via non-gauge D-brane instanton effects. In this case, then a μ term of the form

$$W \sim \exp(-S_{\rm cl}) M_s H_u H_d \tag{58}$$

can be induced where then $\mu \simeq \exp(-S_{\rm cl}) M_s$ and M_s is the string mass scale. The exponential suppression leads to the possibility of a μ term far below the string scale. Of course, in this case one might expect the μ term to arise at any arbitrary mass scale below the string scale rather than fortuitously at the weak scale. If the μ term does arise at the weak scale from stringy instanton effects, then that value may act as an attractor such that soft terms like $m_{H_u}^2$ are pulled statistically to large values by the string theory landscape, but not so large that EW symmetry doesn't break. Then its weak scale value is of comparable (negative) magnitude to μ (the naturalness condition) to ensure a universe with anthropically required electroweak symmetry breaking [39, 77].

Mu solution in G_2MSSM

In Ref. [145] (Acharya *et al.*), the authors consider 11-dimensional M-theory compactified on a manifold of G_2 holonomy, and derive various phenomenological implications. They consider fields living in multiplets of $SU(5)$ so the doublet-triplet splitting problem is present. As opposed to string theory models compactified on orbifolds, in M-theory the matter fields live only in four dimensions so a different solution to the μ problem is required. Witten suggested the existence of an additional discrete symmetry which forbids the μ term from appearing but which allows the Higgs triplets to gain large enough masses so as to evade proton decay constraints [146]. In Ref. [147], it is

shown that a $\mathbb{Z}_4$ symmetry is sufficient to forbid the μ term and other dangerous RPV operators while allowing massive Higgs triplets. The $\mathbb{Z}_4$ discrete symmetry is assumed to be broken via moduli stabilization so that a small μ term develops.

In the G_2MSSM, the gravitino gains mass from non-perturbative effects (such as gaugino condensation) in the hidden sector so that $m_{3/2} \sim \Lambda_h^3/m_P^2 \sim 10 - 200$ TeV. Matter scalar soft masses are expected at $m_\phi \sim m_{3/2}$ so should be very heavy (likely unnatural in the context of Eq. (12)). In contrast, gauginos gain mass from the gauge kinetic function which depends on the vevs of moduli fields so they are expected to be much lighter: m_λ $\sim$TeV scale and in fact these may have dominant AMSB contributions [43] (with comparable moduli-mediated SUSY breaking contributions) so that the wino may be the lightest of the gauginos. The dominant contribution to the μ parameter arises from Kähler contributions ala Giudice-Masiero and these are expected to be $\mu \sim c\frac{\langle S_i \rangle}{m_p} m_{3/2} \sim 0.1 m_{3/2}$ (where c is some constant ~ 1) and thus is suppressed compared to scalar soft masses, but perhaps comparable to gaugino masses.

III.2.2. Extended MSSM-type solutions

NMSSM: Added singlet with $\mathbb{Z}_3$ discrete symmetry

The case of adding an additional visible-sector gauge singlet superfield S to the MSSM leads to the next-to-minimal SSM or NMSSM [148]. Some motivation for the NMSSM can originate in string theory models such as heterotic orbifolds where the μ-term arises as an effective term from couplings of Higgs pair to a singlet field [129]. Without imposing any symmetry to forbid singlet couplings, we can write a generic NMSSM superpotential as follows:

$$W_{NMSSM} = W_{MSSM}(\mu = 0) + \lambda_\mu S H_u H_d + \xi_F S + \frac{1}{2}\mu_S S^2 + \frac{1}{3}\kappa S^3 \qquad (59)$$

and corresponding soft terms

$$\mathcal{L}_{soft}^{NMSSM} = \mathcal{L}_{soft}^{MSSM} - (a_\lambda S H_u H_d + B\mu H_u H_d + \frac{1}{3} a_\kappa S^3 + \frac{1}{2} b_S S^2 + tS + c.c.) - m_S^2 |S|^2. \quad (60)$$

Here $W_{MSSM}(\mu = 0)$ denotes the superpotential for the MSSM without mu-term. The tadpole t in Eq. (60) may have destabilizing quadratic divergences and must be suppressed [149]. A $\mathbb{Z}_3$ discrete symmetry is usually imposed wherein chiral superfields transform as $\phi \to e^{2\pi i/3}\phi$ which sends the dimensionful couplings ξ_F, μ, μ_S, $B\mu$, b_S and t to zero (only cubic couplings are allowed) at the expense of possibly introducing domain walls into the early universe after the electroweak phase transition [150]. (Some means of avoidance of domain walls are proposed in Ref's [151].) By minimizing the scalar potential, now including the new singlet scalar S, then vevs v_u, v_d and v_s are induced. An effective μ term emerges with

$$\mu_{\rm eff} = \lambda_\mu v_s. \quad (61)$$

An attractive alternative choice for μ-forbidding symmetry than the (perhaps ad-hoc) $\mathbb{Z}_3$ would be one of the anomaly-free discrete R-symmetries $\mathbb{Z}_4^R$ or $\mathbb{Z}_8^R$ [137]. Like the $\mathbb{Z}_3$ discrete symmetry, the $\mathbb{Z}_8^R$ symmetry also forbids the dangerous divergent tadpole term. The $\mathbb{Z}_4^R$ symmetry would allow the linear singlet term, but it can be argued that in the effective theory the linear term appears when the fields with which the singlet field is coupled acquire VEVs. If these fields belong to the hidden sector, then the coupling will be suppressed by some high mass scale ranging as high as m_P in the case of gravity-mediation. In this case the linear singlet term will be present but it will be highly suppressed [137].

Thus, all the advantages of the $\mathbb{Z}_3$ discrete symmetry can be obtained by imposing instead either a $\mathbb{Z}_4^R$ or $\mathbb{Z}_8^R$ symmetry which avoids the disadvantages : ad-hocness and

introduction of domain walls into the early universe after electroweak phase transition inherent in the $\mathbb{Z}_3$ discrete symmetry.

The added singlet superfield S in the NMSSM leads to new scalar and pseudoscalar Higgs fields which can mix with the usual MSSM Higgses for $v_s \sim v_{u,d}$. So far, LHC Higgs coupling measurements favor a SM-like Higgs so one might expect $v_s \gg v_{u,d}$ which may lead one to an unnatural value of $\mu_{\rm eff}$. The superfield S also contains a spin-$\frac{1}{2}$ singlino $\tilde{s}$ which may mix with the usual neutralinos and might even be the LSP [152]. In the NMSSM, additional Higgs quartic potential is generated from the F-term of singlet superfield, and thus the SM-like Higgs mass 125 GeV is explained more easily without introducing large one-loop corrections. It can make this theory more attractive to those who are uncomfortable with a MSSM Higgs of mass $m_h \simeq 125$ GeV[153].

nMSSM

An alternative singlet extension of the MSSM is the Nearly-Minimal Supersymmetric Standard Model (nMSSM) (also sometimes called Minimal Nonminimal Supersymmetric Standard Model or MNSSM) [154, 155]. The nMSSM, like the NMSSM, solves the μ problem via an added singlet superfield S. But in the nMSSM, the model is founded on a discrete R-symmetry either $\mathbb{Z}_5^R$ or $\mathbb{Z}_7^R$. Discrete R-charge assignments for $\mathbb{Z}_5^R$ are shown in Table 4. The tree level superpotential is given by

$$W_{nMSSM} \ni \lambda_\mu S H_u H_d + f_u Q H_u U^c + f_d Q H_d D^c + f_\ell L H_d E^c + f_\nu L H_u N^c + \frac{1}{2} M_N N^c N^c$$

so that unlike the NMSSM with $\mathbb{Z}_3$ symmetry, the κS^3 term is now forbidden. This is why the model is touted as a more minimal extension of the MSSM. The discrete R symmetry is broken by SUSY breaking effects in gravity-mediation. Then, in addition

to the above terms, an effective potential tadpole contribution

$$W_{nMSSM}^{tad} \ni \xi_F S \tag{62}$$

is induced at six-loop or higher-loop level where $\xi_F \sim m_{3/2}^2$ (along with a corresponding soft SUSY breaking term). Due to lack of the discrete global $\mathbb{Z}_3$ symmetry, the nMSSM then avoids the domain wall and weak scale axion problems that might afflict the NMSSM.

multiplet	H_u	H_d	Q_i	U_i^c	D_i^c	L_i	E_i^c	N^c	S
$\mathbb{Z}_5^R$	2	2	4	6	6	4	6	6	3

Table 4: Charge assignments for various superfields of nMSSM with a $\mathbb{Z}_5^R$ discrete R-symmetry.

Like the NMSSM, the nMSSM will include added scalar and pseudoscalar Higgs particles along with a fifth neutralino. However, due to lack of S self-coupling term and presence of the tadpole term, the mass eigenstates and couplings of the added matter states will differ from the NMSSM [156, 157, 158, 159, 160]. The neutralino in nMSSM is very light, mostly below 50 GeV, but it is hard to get lower than 30 GeV due to the dark matter relic density constraint. Since the neutralinos are so light it is very likely that a chargino will decay into either a MSSM-like χ_2^0 and a singlino χ_1^0, giving rise to a 5 lepton final state. A further decay of the neutralino can give rise to a 7 lepton state. These kinds of multilepton events are more likely in nMSSM than in the NMSSM. Also, since in the nMSSM the neutralino can be so light, then deviations in Higgs boson h decay branching fractions become more likely than in the case of the NMSSM[158, 159].

Mu-from-nu SSM ($\mu\nu$SSM)

The μ-from-νSSM ($\mu\nu$SSM) [161] is in a sense a more minimal version of the NMSSM in that it makes use of the gauge singlet right-hand-neutrino superfields N_i^c to generate

a μ term. The $\mu\nu$SSM first requires a $\mathbb{Z}_3$ symmmetry to forbid the usual μ term (and also a usual Majorana neutrino mass term $M_i N^c N^c$). The superpotential is given by

$$W \ni f_u Q H_u U^c + f_d Q H_d D^c + f_\ell L H_d E^c + f_\nu L H_u N^c \\ + \lambda_{\mu i} N_i^c H_u H_d + \frac{1}{3}\kappa_{ijk} N_i^c N_j^c N_k^c.$$

If the scalar component of one of the RHN superfields $\tilde{\nu}_{Ri}$ of N_i^c gains a weak scale vev, then an effective μ term develops:

$$\mu_{\rm eff} = \lambda_{\mu i}\langle\tilde{\nu}_{Ri}\rangle \tag{63}$$

along with a weak scale Majorana neutrino mass term $M_{Njk} \sim \kappa_{ijk}\langle\tilde{\nu}_{Ri}\rangle$. By taking small enough neutrino Yukawa couplings, then a weak scale see-saw develops which can accommodate the measured neutrino masses and mixings.

The $\mu\nu$SSM develops bilinear R-party violating terms via the superpotential $f_\nu L H_u N^c$ term so that the lightest $\mu\nu$SSM particle is not stable and doesn't comprise dark matter: $\tilde{z}_1 \to W^{(*)}\ell$ and other modes. As an alternative, a gravitino LSP is suggested with age longer than the age of the universe: it could decay as $\tilde{G} \to \nu\gamma$ and possibly yield gamma ray signals from the sky [162]. The phenomenology of the $\mu\nu$SSM also becomes more complex: now the neutrinos inhabit the same mass matrix as neutralinos, leptons join charginos in another mass matrix and Higgs scalars and sneutrinos inhabit a third mass matrix (albeit with typically small mixing effects). Collider signals are strongly modified from usual MSSM expectations [163].

While the $\mu\nu$SSM may be considered the most minimal model to solve the μ problem, it suffers the same $\mathbb{Z}_3$ domain wall problem as the NMSSM (and perhaps the sames routes to avoidance [151]). Also, in the context of GUTs, the role that the N_i^c field plays in the **16**-dimensional spinor of $SO(10)$ woud have to be abandoned.

III.2.3. μ from an extra local $U(1)'$

In this class of models [164, 165, 166, 167, 168], a SM singlet superfield S is introduced which is charged under a new $U(1)'$ gauge interaction, so terms with mass dimensions in Eq. (59) are forbidden. Due to the $U(1)'$ gauge charges of S, the cubic coupling S^3 is also absent. We will see below three representative realizations of this class of model.

CDEEL model

Cvetic-Demir-Espinosa-Everett-Langacker [164] (CDEEL) propose a $U(1)'$ extended gauge symmetry model as emblematic of fermionic orbifold string compactifications. While the usual μ term is forbidden by the extended gauge symmetry, the superpotential term

$$W \ni \lambda_\mu S H_u H_d \tag{64}$$

is allowed and under $U(1)'$ breaking then S develops a vev $\langle S \rangle \sim m_{weak}$ such that a μ term is generated $\mu_{\rm eff} = \lambda_\mu \langle S \rangle$ along with an additional weak scale Z' gauge boson. Forbidding the μ term via a gauge symmetry avoids the gravity spoliation/global symmetry problem. In addition, the μ term is linked to EW symmetry breaking and this would be expected to occur at m_{weak} rather than m_{soft}. The $U(1)'$ breaking can occur either via large soft SUSY breaking trilinear couplings or via radiative corrections driving certain mass-squared terms negative. A way to test this class of models, in the exotica decoupling limit, is to search for new Z' gauge bosons with exotic decays to light higgsinos [167].

To maintain anomaly cancellation, a variety of (intermediate scale) exotic quark and lepton fields must be introduced along with extra SM gauge singlets. If these new states come in GUT representations, then gauge coupling unification can be maintained. A set of possible $U(1)'$ gauge charges are listed in Table 5.

multiplet	H_u	H_d	Q_i	U_i^c	D_i^c	L_i	E_i^c	S
$(2\sqrt{10})Q'$	-2	-3	1	1	2	2	1	5

Table 5: Charge assignments for various superfields of a $U(1)'$ model [167, 166].

sMSSM model

An alternative $U(1)'$-extended MSSM (abbreviated as sMSSM)[169, 170] also solves the μ problem by invoking multiple SM singlet superfields charged under $U(1)'$ symmetry. In this model, a visible-sector singlet field S directly couples to Higgs doublets but avoids stringent constraints on having an additional weak scale Z' gauge boson by introducing as well a *secluded sector* containing three additional singlets $S_1,\ S_2,\ S_3$ charged under $U(1)'$. The superpotential is given by

$$W_{sMSSM} \ni \lambda_\mu S H_u H_d + \lambda_s S_1 S_2 S_3 \tag{65}$$

so that the secluded sector has a nearly F- and D-flat scalar potential. The $U(1)'$ and electroweak symmetry breaking then occur as a result of SUSY breaking A-terms. Then the secluded sector scalars can obtain vevs much larger than the weak scale; if also the trilinear singlet coupling, λ_s is small then the additional Z' essentially decouples. Nonetheless, additional Higgs and singlinos appear in the weak scale effective theory so that this model phenomenologically resembles the aforementioned nMSSM model which has very different manifestations from what is expected from the CDEEL $U(1)'$ model.

HPT model

The Hundi-Pakvasa-Tata (HPT) model [165] also solves the SUSY μ problem by positing an additional $U(1)'$ gauge symmetry in a supergravity context. The $U(1)'$ charges of the multiplets in the HPT scheme are shown in Table 6. With these

$U(1)'$ charge assignments, the μ term is forbidden in the superpotential but (unlike the CDEEL model) a dim-4 term as μ solution à la Kim-Nilles is allowed:

$$W \ni \lambda_\mu S^2 H_u H_d / M_p. \tag{66}$$

The $U(1)'$ gauge symmetry also forbids trilinear RPV couplings and dangerous p-decay operators. When the $U(1)'$ breaks (at an intermediate scale $Q \sim 10^{11}$ GeV), the S field acquires a vev to yield an effective μ parameter of the required magnitude.

A distinctive feature of the HPT model is that a bilinear RPV (bRPV) term, LH_u is allowed at the right magnitude so as to generate phenomenologically-allowed neutrino masses [171]. The desired pattern of neutrino masses and mixing angles are also accommodated through radiative corrections. The bRPV leads to an unstable lightest neutralino which decays via $\tilde{z}_1 \to \ell W^{(*)}$ or $\nu Z^{(*)}$ and may lead to displaced vertices in collider events. Dark matter must be comprised of some other particles (*e.g.* axions). Also, the $U(1)'$ is broken at the intermediate scale $Q \sim 10^{11}$ GeV so that the additional Z' has a mass far beyond any collider reach.

Since solving the μ problem as well as generating the neutrino mass scale of suitable order requires introduction of a new gauge group $U(1)'$, care must be taken so that associated anomalies are cancelled. Anomaly cancellation requires introducing various additional exotic fields including color triplets K_i and K_i' states. The lightest of these leads to stable weak-scale exotic hadrons which may also yield highly-ionizing tracks at collider experiments. In the HPT scheme, gauge coupling unification may be upset.

multiplet	H_u	H_d	Q_i	U_i^c	D_i^c	L_i	E_i^c	S
Q'	25	-31	0	-25	31	2	29	3

Table 6: Charge assignments for various superfields of the HPT $U(1)'$ supergravity model [165].

III.2.4. Solutions related to Peccei-Quinn symmetry breaking

In this subsection, we examine natural μ solutions related to Peccei-Quinn (PQ) symmetry used to solve the strong CP problem. In this class of models, the μ-term is forbidden by the PQ symmetry, but generated once PQ symmetry is broken. These models then, beside providing a solution to the SUSY μ problem, also provides a solution to the strong CP problem and generates axion dark matter, which is very much necessary to account for the entire dark matter content of the universe as argued in Sec. II. There are various sources of PQ breaking. Here, we review various models which differ from each other in source of PQ breaking.

Meanwhile, imposing global symmetry causes the 'quality' issues of the symmetry which spoil the PQ solution to the strong CP problem, since it is not protected from quantum gravity effect. This is the gravity-spoliation problem. As discussed in Sec. I.5.2., a model can be protected from this gravity-spoliation problem if the underlying fundamental symmetry of the model is not an exact global symmetry.

Kim-Nilles solution

Kim and Nilles (KN) [56] presented the first formulation of the SUSY μ problem along with a proposed solution. In Ref. [56], it is proposed that there exists a global Peccei-Quinn (PQ) symmetry $U(1)_{PQ}$ which is needed at first as a solution to the strong CP problem. The PQ symmetry is implemented in the context of the supersymmetrized version of the DFSZ [172] axion model[12] wherein the Higgs multiplets carry PQ charges *e.g.* $Q_{PQ}(H_u) = Q_{PQ}(H_d) = -1$ so that the μ term is forbidden by the global $U(1)_{PQ}$. Next, the Higgs multiplets are coupled via a non-renormalizable interaction to a SM

[12]In the DFSZ axion model [172], the SM is extended to include two Higgs doublets which then couple to singlets which contain the axion.

gauge singlet field X which carries a PQ charge $Q_{PQ}(X) = +2/(n+1)$:

$$W_\mu \ni \frac{\lambda_\mu}{m_P^n} X^{n+1} H_u H_d \tag{67}$$

for $n \geq 1$.

It is arranged to spontaneously break PQ by giving the X field a vev $\langle X \rangle$ which also generates a (nearly) massless axion a which solves the strong CP problem. To obtain cosmologically viable axions– with $\langle X \rangle \sim 10^{11}$ GeV and with $m_p \simeq 2.4 \times 10^{18}$ GeV, we can obtain the μ parameter of the order of $m_{3/2}$ only if $n = 1$ (for which $Q_{PQ}(X) = +1$). The matter superfields also carry appropriate PQ charge so as to allow the MSSM trilinear superpotential terms: see Table 7.

multiplet	H_u	H_d	Q_i	L_i	U_i^c	D_i^c	E_i^c	X	Y	Z
PQ charge	-1	-1	$+1$	$+1$	0	0	0	$+1$	-1	0

Table 7: PQ charge assignments for various superfields of the KN model with $n = 1$. One may add multiples of weak hypercharge or $B - L$ to these so their values are not unique.

The intermediate PQ breaking scale can be gained from a PQ superpotential of the form:

$$W_{PQ} = \lambda_{PQ} Z \left(XY - v_{PQ}^2 \right). \tag{68}$$

The scalar components of X and Y develop vevs $\langle X \rangle = \langle Y \rangle = v_{PQ}$ such that a μ term is generated:

$$\mu = \lambda_\mu \langle X \rangle^2 / m_P. \tag{69}$$

This value of the μ term $\mu \sim \lambda_\mu v_{PQ}^2 / m_P$ is to be compared to the soft breaking scale in models of gravity-mediation: $m_{soft} \sim m_{3/2} \sim m_{hidden}^2 / m_P$. Here, v_{PQ} is identified as $v_{PQ} \sim m_{hidden}$ and thus μ is obtained as $\mu \sim m_{3/2}$. But, a value $\mu \sim m_{weak} \ll m_{soft} \sim m_{3/2}$ can be accomodated for $v_{PQ} \ll m_{hidden}$, *i.e.* if the

scale of PQ breaking lies somewhat below the mass scale associated with hidden sector SUSY breaking.[13] [14] A virtue of the KN solution is that it combines a solution to the strong CP problem with a solution to the SUSY μ problem which also allows for a Little Hierarchy. A further benefit is that it provides an additional dark matter particle, namely the DFSZ [172] axion, to co-exist with the (thermally under-produced) higgsino-like WIMP from natural SUSY. Thus, dark matter is then expected to be comprised of a WIMP/axion admixture [175, 176]. For the lower range of PQ scale v_{PQ}, then the dark matter tends to be axion dominated with typically 10-20% WIMPs by mass density [177]. For larger v_{PQ} values, then non-thermal processes such as saxion and axino [179] decay augment the WIMP abundance while for even larger values of v_{PQ} the Higgsino-like WIMPs are overproduced and one typically runs into big bang nucleosynthesis constraints from late-decaying neutral particles (saxions and axinos) or overproduction of relativistic axions from saxion decay which contribute to the effective number of neutrino species N_{eff} (which is found to be $N_{eff} = 3.13 \pm 0.32$ from the recent Particle Data Group tabulation [180]). In the context of the DFSZ model embedded within the MSSM, then the presence of Higgsinos in the $a\gamma\gamma$ triangle diagram is expected to reduce the axion-photon-photon coupling to levels below present sensitivity making the SUSY DFSZ axion very challenging to detect [181].

Chun-Kim-Nilles Model

In the CKN model [182], it is assumed that SUSY is broken in the hidden sector due to gaugino condensation $\langle\lambda\lambda\rangle \sim \Lambda_h^3 \sim (10^{13}\ \text{GeV})^3$ in the presence of a hidden $SU(N)_h$ gauge group. Furthermore, there may be vector-like hidden sector quark chiral superfields present Q and Q^c which transform as N and N^* under $SU(N)_h$. The Higgs

[13] In models with SUSY breaking arising from *e.g.* gaugino condensation at an intermediate scale Λ_h, then $m_{3/2} \sim \Lambda_h^3/m_P^2$ in which case we would define $m_{hidden}^2 \sim \Lambda_h^3/m_p$.

[14] The model [173] shows a more complete ultraviolet theory which includes a mechanism to get v_{PQ} in the intermediate scale through the introduction of a chiral superfield in the hidden brane, yielding a ultraviolet suppressed term in the hidden brane which gives rise to $\mu \sim m_{weak}$ when SUSY is broken in the hidden brane through shining mechanism [174].

and hidden quark superfields carry PQ charges as in Table 8: This allows for the

multiplet	H_u	H_d	Q	Q^c	Q_i	U_i^c	D_i^c
PQ charge	-1	-1	1	1	0	1	1

Table 8: PQ charge assignments for various superfields of the CKN model.

presence of a superpotential term

$$W_{CKN} \ni \frac{\lambda_\mu}{m_P} Q Q^c H_u H_d. \tag{70}$$

Along with gauginos condensing at a scale Λ_h to break SUGRA with $m_{3/2} \sim \Lambda_h^3/m_P^2$, the hidden sector scalar squarks condense at a scale $\Lambda < \Lambda_h$ to break the PQ symmetry and to generate a μ term

$$\mu_{\rm eff} \sim \lambda_\mu \Lambda^2/m_P. \tag{71}$$

Thus, this model provides a framework for $\mu < m_{soft}$. It also generates a DFSZ axion to solve the strong CP problem along with a string model-independent (MI) axion which could provide a quintessence solution for the cosmological constant (CC) [183]. The CC arises from the very low mass MI axion field slowly settling to the minimum of its potential.

Bastero-Gil-King/Eyton-Williams-King solution linked to inflation and strong CP

In Ref's [184, 185], a model is proposed with superpotential

$$W_{EWK} \ni \lambda_\mu \phi H_u H_d + \kappa \phi N^2 \tag{72}$$

where the ϕ field plays the role of inflaton and the N field is a waterfall field leading to hybrid inflation in the early Universe [186]. Although the model appears similar to

the NMSSM, it is based on a PQ rather than $\mathbb{Z}_3$ symmetry with charges as in Table 9. Thus, it avoids the NMSSM domain wall problems which arise from a postulated global $\mathbb{Z}_3$ symmetry. By augmenting the scalar potential with soft breaking terms, the ϕ and N fields gain VEVs of order some intermediate scale $Q \sim 10^{12}$ GeV so that Yukawa couplings λ_μ and κ are of order 10^{-10}. Such tiny Yukawa couplings might arise from type-I string theory constructs [187]. To fulfill the inflationary slow-roll conditions, the field ϕ must gain a mass of less than $5 - 10$ MeV and a reheat temperature of $1 - 10$ GeV. Domain walls from breaking of the PQ symmetry are inflated away.

multiplet	H_u	H_d	ϕ	N
PQ charge	-1	-1	$+2$	-1

Table 9: PQ charge assignments for various superfields of the EWK model.

Natural Higgs-Flavor-Democracy (HFD) solution to the SUSY μ problem

In Ref. [194], the μ problem is solved by introducing additional identical Higgs doublet superfields to those of the MSSM. The theory then contains a direct product of discrete interchange symmetries $S_2(H_u) \times S_2(H_d)$. This is *Higgs flavor democracy* (HFD). Besides solving the μ problem, this mechanism also gives rise to an approximate PQ symmetry and hence a light QCD axion, thereby solving the strong CP problem whilst avoiding the gravity spoliation problem. The HFD discrete symmetry can be found in several string theory models.

HFD: One starts by introducing two pairs of Higgs doublets at the GUT scale m_G namely : $\{H_u^{(1)}, H_d^{(1)}\}$ and $\{H_u^{(2)}, H_d^{(2)}\}$. However, the weak scale MSSM requires only one pair of Higgs doublets: $\{H_u, H_d\}$. If, at the GUT scale, the two pairs of Higgs doublets : $H_u = \{H_u^{(1)}, H_u^{(2)}\}$ and $H_d = \{H_d^{(1)}, H_d^{(2)}\}$ are indistinguishable then there must the permutation symmetries $S_2(H_u) \times S_2(H_d)$. Then, the Higgsino mass matrix

has a democratic form given by:

$$\left\{ \begin{array}{cc} m_G/2 & m_G/2 \\ m_G/2 & m_G/2 \end{array} \right\}.$$

Thus, the Higgs mass eigenvalues are m_G and 0. Hence, the Higgs pair in the weak scale MSSM is obtained to be massless. Still, the model construction of the MSSM requires a massive Higgs pair at the weak scale with mass value μ. In order to fulfill this criteria, the HFD must be broken and this mechanism results in $\mu \approx \mathcal{O}(\text{TeV})$.

Generation of μ: The minimal Kahler potential is considered as $K = \Phi_i \Phi_i^\dagger$ where Φ_i (i =1, 2) is a doublet under the gauge group such as the Higgs superfield and X_i and $\bar{X}_i$ (i=1,2) are singlets under the gauge group. Both Φ_i and X_i and the corresponding barred fields obey the $S_2 \times S_2$ symmetry. $X^{(0)}$ and $\bar{X}^{(0)}$ are SM singlet fields containing a very light QCD axion for 10^9 GeV $\leq v_{PQ} \leq 10^{12}$ GeV. With this construct, the $S_2(L) \times S_2(R)$ symmetric nonrenormalizable term is :

$$W^{(nonrenormalizable)} = \sum_{i,j=1,2} \left(\frac{X^{(i)} \bar{X}^{(j)}}{m_P} \right) H_u^{(i)} H_d^{(j)} + \sum_{ij} \sum_{kl} \left(\frac{X^{(i)} \bar{X}^{(j)}}{m_P} \right) H_u^{(k)} H_d^{(l)} \quad (73)$$

With the HFD breaking minimum at $\langle X_1 \rangle = \langle \bar{X}_1 \rangle = v_{PQ}$ and $\langle X_2 \rangle = \langle \bar{X}_2 \rangle = 0$, Eq. (73) becomes

$$W^{(nonrenormalizable)} = \frac{\lambda_\mu v_{PQ}^2}{2 m_P} (H_u^{(0)} + H_u^{(M_G)})(H_d^{(0)} + H_d^{(M_G)}) \quad (74)$$

This choice of HFD breaking minimum is spontaneous. Thus we obtain $\mu = \frac{\lambda_\mu v_{PQ}^2}{2 m_P}$. With 10^{10} GeV $\leq v_{PQ} \leq 10^{12}$ GeV and $\lambda_\mu \approx \mathcal{O}(1)$, we obtain $\mu \approx \mathcal{O}(0.1 - 10^3$ TeV). Thus, the LH can be accomodated for the lower range of v_{PQ} or if $\lambda_\mu < 1$.

Light QCD Axion - Integrating out the heavy fields in Eq. (74), one obtains

$$W = \frac{\lambda_\mu X^{(0)} \bar{X}^{(0)}}{2m_P} H_u^{(0)} H_d^{(0)}. \tag{75}$$

The PQ charges of Higgs multiplets are obtained from their interaction with the quarks and PQ charges of $X^{(0)}$ and $\bar{X}^{(0)}$ are defined by Eq. (75). Thus, a term $m_{3/2}\frac{\lambda^2}{4m_P^2}\frac{1}{M_G}H_u H_d (X X^c)^2$ is obtained which violate PQ and hence add a tiny correction to μ. Here, M_G is the GUT scale higgsino mass. Hence, PQ symmetry emerges as an approximate symmetry, thereby giving rise to a light QCD axion which does not suffer from the gravity-spoliation problem.

Radiative PQ breaking from SUSY breaking

The above models are particularly compelling in that they include supersymmetry which solves the gauge hierarchy problem, but also include the axion solution to the strong CP problem of QCD. In addition, they allow for the required Little Hierarchy of $\mu \ll m_{soft}$. A drawback to the KN model is that it inputs the PQ scale "by hand" via the superpotential Eq. (68). It is desireable if the PQ scale can be generated via some mechanism and furthermore, the emergence of three *intermediate mass scales* in nature– the hidden sector SUSY breaking scale, the PQ scale and the Majorana neutrino scale– begs for some common origin. A model which accomplishes this was first proposed by Murayama, Suzuki and Yanagida (MSY) [53].

In radiative PQ breaking models, the MSSM superpotential is

$$W_{MSSM} = \sum_{i,j=1}^{3} \left[(\mathbf{f}_u)_{ij} Q_i H_u U_j^c + (\mathbf{f}_d)_{ij} Q_i H_d D_j^c + (\mathbf{f}_e)_{ij} L_i H_d E_j^c + (\mathbf{f}_\nu)_{ij} L_i H_u N_j^c \right] \tag{76}$$

where we explicitly include the right hand neutrino superfields N_i and the generation indices i, j run from $1-3$. To this, we add a PQ superpotential containing new PQ-

charged fields X and Y of the form

$$W_{PQ} \ni \frac{1}{2} h_{ij} X N_i^c N_j^c + \frac{f}{m_P} X^3 Y + W_\mu \tag{77}$$

and where

$$W_\mu^{MSY} = \frac{g_{MSY}}{m_P} X Y H_u H_d, \tag{78}$$

where the PQ charges $Q_{PQ}(matter) = 1/2$, $Q_{PQ}(Higgs) = -1$, $Q_{MSY}(X) = -1$ and $Q_{PQ}(Y) = 3$. Along with the MSY superpotential terms, we include the corresponding soft SUSY breaking terms

$$\begin{aligned} V_{MSY} \ni\ & m_X^2 |\phi_X|^2 + m_Y^2 |\phi_Y|^2 + m_{N_i}^2 |\phi_{N_i}|^2 \\ & + \left(\frac{1}{2} h_i A_i \phi_{N_i}^2 \phi_X + \frac{f}{m_P} A_f \phi_X^3 \phi_Y + \frac{g_{MSY}}{m_P} A_g H_u H_d \phi_X \phi_Y + h.c. \right). \end{aligned}$$

For simplicity, we assume a diagonal coupling $h_{ij} = h_i \delta_{ij}$. The model may be defined as applicable at the reduced Planck scale $m_P \simeq 2.4 \times 10^{18}$ GeV and the corresponding Renormalization Group Equations (RGEs) can be found in Ref. [53] at 1-loop and Ref. [55] at 2-loop order. Under RG evolution, the large Yukawa coupling(s) h_i push the soft mass m_X^2 to negative values at some intermediate mass scale resulting in the radiatively-induced breakdown of PQ symmetry as a consequence of SUSY breaking. The scalar potential consists of the terms $V = V_F + V_D + V_{\rm soft}$. The Higgs field directions can be ignored since these develop vevs at much lower energy scales. Then the relevant part of the scalar potential is just

$$V_F \ni \frac{|f|^2}{m_P^2} |\phi_X^3|^2 + \frac{9|f|^2}{m_P^2} |\phi_X^2 \phi_Y|^2. \tag{79}$$

Augmenting this with $V_{\rm soft}$, we minimize V at a scale $Q = v_{PQ}$ to find the vevs of ϕ_X

and ϕ_Y (v_X and v_Y):

$$0 = \frac{9|f|^2}{m_P^2}|v_X^2|^2 v_Y + f^* \frac{A_f^*}{m_P} v_X^{*3} + m_Y^2 v_Y \tag{80}$$

$$0 = \frac{3|f|^2}{m_P^2}|v_X^2|^2 v_X + \frac{18|f|^2}{m_P^2}|v_X|^2|v_Y|^2 v_X + 3f^* \frac{A_f^*}{m_P} v_X^{*2} v_Y^* + m_X^2 v_X. \tag{81}$$

The first of these may be solved for v_Y. Substituting into the second, we find a polynomial for v_X which may be solved for numerically. The potential has two minima in the v_X and v_Y plane symmetrically located with respect to the origin. For practical purposes, we use the notation v_X=$|v_X|$ and v_Y=$|v_Y|$.

The fields ϕ_X and ϕ_Y obtains vevs v_X and v_Y at the intermediate mass scale, taken here to be $v_{PQ} = \sqrt{v_X^2 + 9v_Y^2}$. The corresponding axion decay constant is given by $f_a = \sqrt{2}v_{PQ}$.[15] A DFSZ-like axion a arises as the pseudo-Goldstone boson of spontaneous PQ breaking, thus solving the strong CP problem. A μ parameter, which is originally forbidden by PQ symmetry, is generated with a value

$$\mu_{\text{eff}} = g_{MSY} \frac{v_X v_Y}{m_P} \tag{82}$$

and a Majorana neutrino mass, also initially forbidden by PQ symmetry, is generated at

$$M_{N_i} = h_i|_{Q=v_x} v_X. \tag{83}$$

Since the μ term depends on an arbitrary coupling g_{MSY}, one may obtain any desired value of μ for particular v_X and v_Y vevs by suitably adjusting g_{MSY}. However, if the required values of g_{MSY} are very different from unity, *i.e.* $g_{MSY} \gg 1$ or $g_{MSY} \ll 1$, we might need to introduce an additional physical scale to explain the μ term. To generate a value of $\mu = 150$ GeV, then values of g_{MSY} as shown in Fig. 13 are required depending

[15]For axion interactions, actual decay constant is f_a/N_{DW} where N_{DW} is the domain wall number.

on the values of $m_{3/2}$ and $h(M_P)$ which are assumed.

The virtues of this model then include:

- it is supersymmetric, thus stabilizing the Higgs sector and allowing for a gauge hierarchy,
- it solves the strong CP problem via a DFSZ-like axion a,
- it presents a unified treatment of the three intermediate mass scale where the PQ and Majorana neutrino scales arise as a consequence of SUSY breaking and
- it allows for a Little Hierarchy $\mu \ll m_{soft}$ for the case where $v_{PQ} \ll m_{hidden}$.

Detailed numerical calculations in the MSY model have been carried out in Ref. [55]. There, it is found that for generic W_{MSY} couplings $g_{MSY} \sim 0.1 - 1$, then a μ parameter $\mu \sim 100 - 200$ GeV can easily be generated from TeV-scale soft breaking terms. Furthermore, since the μ term sets the mass scale for the W, Z, h boson masses and is determined itself by the PQ vevs v_X and v_Y, then the axion mass $m_a \simeq 0.48 f_\pi m_\pi / f_a = 6.25 \times 10^{-3}$ GeV$/f_a$ is related to the Higgs mass m_h and the higgsino masses $m_{\tilde{w}_1, \tilde{z}_{1,2}} \sim \mu$. The required PQ charges for the MSY model are listed in Table 10.

Other closely related models make different choices for which fields enter into W_μ. We can also have:

$$\begin{aligned} W_\mu^{CCK} &= \frac{g_{CCK}}{m_P} X^2 H_u H_d \quad or \\ W_\mu^{SPM} &= \frac{g_{SPM}}{m_P} Y^2 H_u H_d. \end{aligned} \tag{84}$$

The above three possibilities for W_μ correspond to Ref's [53] (MSY), [52] (CCK) and [54] (SPM). The corresponding PQ charges for the three radiative PQ breaking models are listed in Table 10.

It has also been shown in Fig's 14 and 15 the values of g_{CCK} and g_{SPM} which are needed to generate a value of $\mu \simeq 150$ GeV. For a given value of $h(m_P)$ and $m_{3/2}$, then

multiplet	MSY	CCK	SPM
H_u	-1	-1	-1
H_d	-1	-1	-1
Q	$+1/2$	$3/2$	$+1/2$
L	$+1/2$	$3/2$	$+5/6$
U^c	$+1/2$	$-1/2$	$+1/2$
D^c	$+1/2$	$-1/2$	$+1/2$
E^c	$+1/2$	$-1/2$	$+1/6$
N^c	$+1/2$	$-1/2$	$+1/6$
X	-1	$+1$	$-1/3$
Y	$+3$	-3	$+1$

Table 10: PQ charge assignments for various superfields of the CCK, MSY and SPM models of radiative PQ breaking.

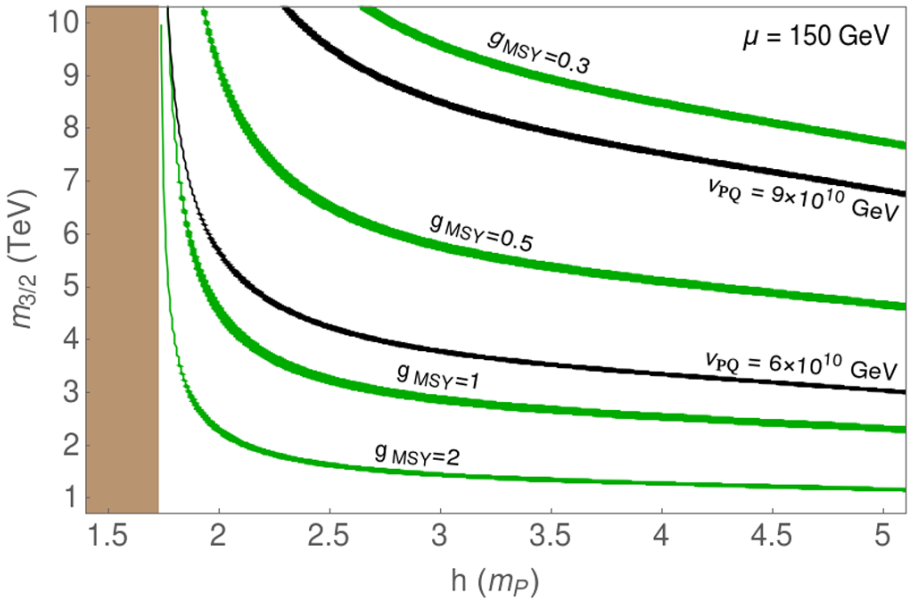

Figure 13: Value of g which is needed in the MSY to generate $\mu = 150$ GeV from a gravitino mass $m_{3/2}$ and a GUT coupling h. We also show some contours of v_{PQ}.

typically $g_{MSY} < g_{SPM}$ and $g_{CCK} < g_{MSY}$. The MSY model has the interesting feature that the PQ charge assignments are consistent with $SO(10)$ unification. We also remark that all three models can easily generate weak scale values of μ from multi-TeV values of $m_{3/2}$: *i.e.* $\mu \ll m_{3/2}$ so that a Little Hierarchy is naturally generated.

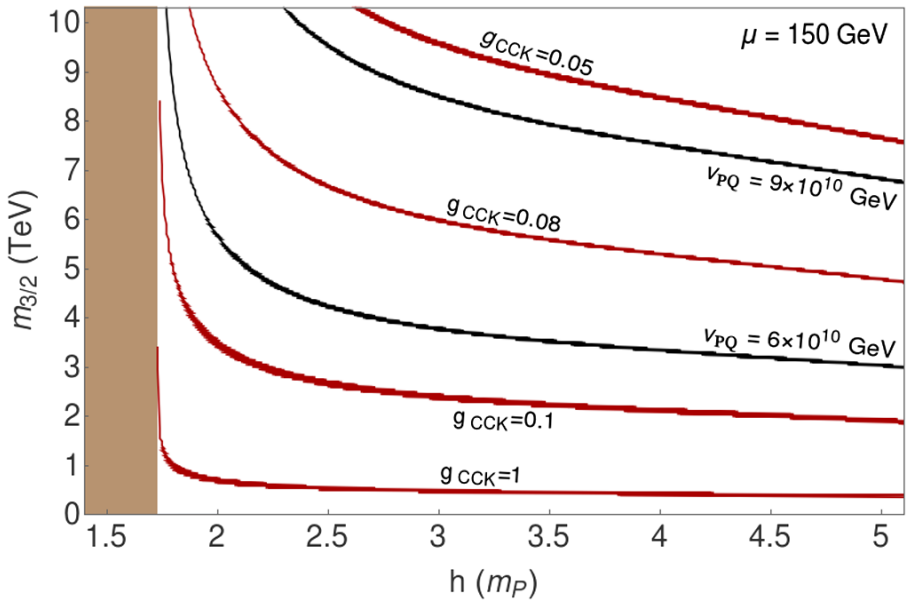

Figure 14: Value of g which is needed in the CCK to generate $\mu = 150$ GeV from a gravitino mass $m_{3/2}$ and a GUT coupling h. We also show some contours of v_{PQ}.

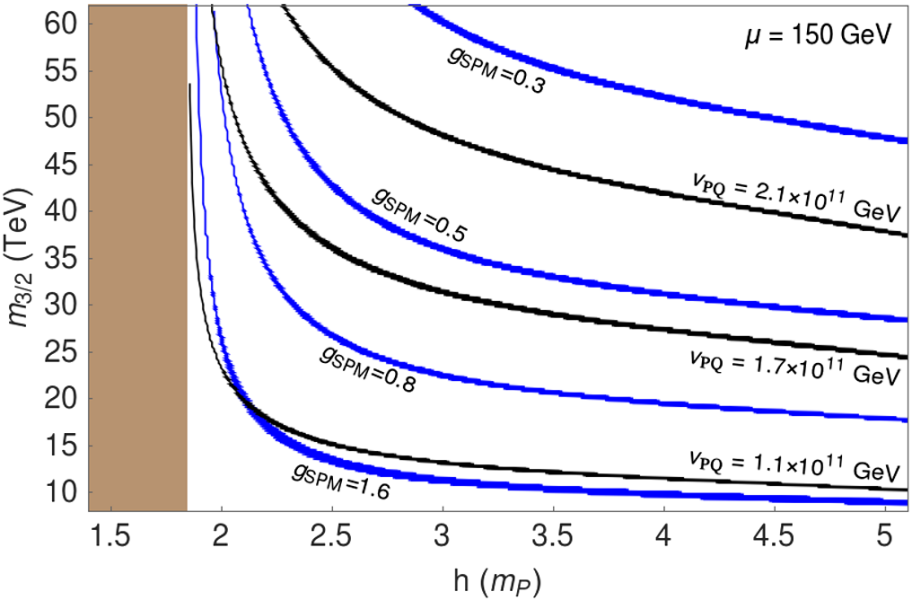

Figure 15: Value of g which is needed in the SPM model to generate $\mu = 150$ GeV from a gravitino mass $m_{3/2}$ and a GUT coupling h. We also show some contours of v_{PQ}.

CCL model from gauged $U(1)_R$ symmetry

In the model of Choi, Chun and Lee [191] (CCL), the μ term is generated in a manner similar to the SPM model [54], but with the difference that the fundamental symmetry

is a gauged $U(1)_R$ symmetry out of which the PQ symmetry arises to be an accidental approximate symmetry. The superpotential for CCL is

$$W_{CCL} = f_u Q H_u U^c + f_d Q H_d D^c + f_e L H_d E^c + f_\nu L H_u N^c + \\ + \lambda_\mu \frac{Y^2 H_u H_d}{m_p} + \kappa X^3 Y / m_P + \lambda_N X^n N^c N^c / 2 m_P^{n-1}, \tag{85}$$

with $U(1)_R$ and PQ charges for the $n = 2$ case given in Table 11.

multiplet	H_u	H_d	Q_i	L_i	U_i^c	D_i^c	E_i^c	N_i^c	X	Y
$U(1)_R$ charge	4	4	$-\frac{4}{3}$	$-\frac{4}{3}$	$-\frac{2}{3}$	$-\frac{2}{3}$	$-\frac{2}{3}$	$-\frac{2}{3}$	$\frac{5}{3}$	-3
PQ charge	3	3	-3	-2	0	0	-1	-1	1	-3

Table 11: $U(1)^R$ and PQ charge assignments for various superfields of the CCL model for $n = 2$.

The singlets X and Y get their VEVs at the intermediate scale when the PQ symmetry is broken via a large (relative to $m_{3/2}$) negative trilinear soft term contribution to the scalar potential, thereby giving rise to $\mu \sim m_{soft}$. The $U(1)_R$ gauge boson has mass of order the compactification scale so the low energy theory is that of the MSSM. Because the fundamental symmetry of CCL is a gauged $U(1)_R$ symmetry, the phenomenology of this model is dictated by a hierarchy of soft terms $m_{1/2} \gg m_{scalars} > m_{3/2}$ ($m_{1/2}$: gaugino mass). Scalar soft masses are fixed in terms of $U(1)_R$ D-terms and typically lead to large negative $m_{H_u}^2$ at the weak scale which then requires a large, unnatural μ term which would violate the $\mu \ll m_{soft}$ Little Hierarchy. The gravitino or the RH sneutrino turns out to be the LSP and hence end up as cold dark matter candidates. If the neutrino is Majorana type then the gravitino is the LSP and if the neutrino is Dirac type then the RH sneutrino is the LSP.

III.3. Gravity safe, electroweak natural axionic solution to strong CP and SUSY μ problems

It is well known that gravitational effects violate global symmetries, as has been considered via black hole "no hair" theorems [197] and wormhole effects [198]. In such cases, it has been questioned whether the PQ mechanism can be realistic once one includes gravity or embeds the SUSY PQ theory into a UV complete string framework [199, 201, 200]. As discussed in Sec. I.5.2., the aforementioned models which have $U(1)_{PQ}$ as the fundamental symmetry and hence simultaneously solve the strong CP and the SUSY μ problem, indeed suffer from the gravity spoliation problem as quantum gravity effects spoil the PQ solution to the strong CP problem. Kamionkowski and March-Russell [201] (KMR) considered the effect of gravitational operators such as

$$V(\phi) \ni \frac{g}{m_P^{2m+n-4}}|\phi|^{2m}\phi^n + h.c. + c \tag{86}$$

involving PQ charged fields ϕ in the scalar potential upon the axion potential. In the case of $2m+n=5$, *i.e.* a term suppressed by a single power of m_P, then these gravitational terms would displace the minimum of the PQ axion potential such that the QCD CP violating term $G_{\mu\nu A}\tilde{G}_A^{\mu\nu}$ settles to a non-zero minimum thus destroying the PQ solution to the strong CP problem. To maintain $\bar{\theta} \leq 10^{-10}$, KMR calculated that all gravitational operators contributing to the axion potential should be suppressed by at least powers of $(1/m_P)^8$. This is indeed a formidable constraint! To avoid such terms, additional symmetries are required [189]. In string theory, it is known that discrete symmetries arising from gauge symmetries are gravity-safe, as are other discrete symmetries or R-symmetries arising from string compactification. In Fig. 8 the Kim diagram is shown [188, 94]. The red/lavender column denotes an infinite set of Lagrangian terms in the model under consideration which obey some exact, gravity-safe,

discrete symmetry. Of this set of terms, the few lower order terms, denoted by the lavender region, obey an exact global symmetry, understood here to be the PQ symmetry whose breaking yields the QCD axion. The red-shaded terms obey the discrete symmetry but violate any global symmetry. The green/lavender row denotes the full, infinite set of global symmetry terms, of which the green-shaded terms are not gravity-safe. If the discrete symmetry is strong enough, then the gravity-unsafe terms will be sufficiently suppressed. The global PQ symmetry is expected to be approximate. The question then is: is it sufficiently strong so as to be gravity-safe? Some additional gravity-safe symmetry is required to ensure the PQ mechanism is robust. The lavender region represents gravity-safe terms which obey the global symmetry.

III.3.1. Gravity-safe symmetries : gauge symmetries or R-symmetries: continuous or discrete

Given that global symmetries are not gravity-safe (and hence not fundamental), it is common to turn to gauge symmetries as a means to forbid the μ term. Some models based on an extra local $U(1)'$ are examined in Sec. III.2.3. Some problems with this approach emerge in that one has to suitably hide any new gauge bosons associated with the extra gauge symmetry and one must also typically introduce (and hide) extra exotic matter which may be needed to ensure anomaly cancellation. In addition, such exotic matter may destroy the desireable feature of gauge coupling unification should the new exotica not appear in complete GUT multiplets.

An alternative approach is to introduce *discrete* gauge symmetries [189, 190]. Such $\mathbb{Z}_M$ symmetries may emerge from a local $U(1)'$ when a charge M object (charged under the new $U(1)'$) condenses at very high energy leaving a discrete $\mathbb{Z}_M$ gauge symmetry in the low energy effective theory. Since the $\mathbb{Z}_M$ emerges from a local gauge theory, it remains gravity-safe. In Sec. III.3.2, the MBGW model [57] which is based on a $\mathbb{Z}_{22}$ discrete gauge symmetry is examined. The model under $\mathbb{Z}_{22}$ is found to be anomaly-free

and is used to not only forbid the μ term but to generate a PQ symmetry needed to solve the strong CP problem. The lowest order PQ violating term allowed by the $\mathbb{Z}_{22}$ is sufficiently suppressed so that PQ arises as an accidental approximate global symmetry thereby rendering the model to be gravity-safe. The $\mathbb{Z}_{22}$ discrete gauge charges of the multiplets turn out to be not consistent with GUTs which should be manifested at some level in the high energy theory. Also, the presence of a charge 22 object which condenses at some high energy scale may not be very plausible and might be inconsistent with the UV completion of the theory (*i.e.* lie in the swampland).

Continuous or discrete R-symmetries offer a further choice for gravity-safe symmetries. A solution using a continuous $U(1)_R$ symmetry is examined in the third solution in Sec. III.2.1.[16] In the interest of minimality, it is noted that continuous R symmetries are not consistent with the particle content of just the MSSM [192]. Then it is also of interest to examine the possibility of discrete remnant R-symmetries $\mathbb{Z}_n^R$ which arise upon compactification of the full Lorentz symmetry of 10-d string theories. R-symmetries are characterized by the fact that superspace co-ordinates θ carry non-trivial R-charge: in the simplest case, $Q_R(\theta) = +1$ so that $Q_R(d^2\theta) = -2$. For the Lagrangian $\mathcal{L} \ni \int d^2\theta W$ to be invariant under $\mathbb{Z}_n^R$-symmetry, the superpotential W must carry $Q_R(W) = 2$+integer multiples of n.

These remnant discrete R-symmetries $\mathbb{Z}_n^R$– if sufficiently strong– can forbid lower order operators in powers of $1/m_P$ which would violate putative global symmetries such as PQ. Such a built-in mechanism from string theory may enable the PQ symmetry to be strong enough to support the axion solution to the strong CP problem. Since the R-symmetry is necessarily supersymmetric (it acts on superspace co-ordinates), this is another instance in how the implementation of the axion solution to the strong CP problem is enhanced and made more plausible by the presence of supersymmetry. However, not all possible R-symmetries are a suitable candidate for a fundamental

[16]See also Ref. [191].

multiplet	$\mathbb{Z}_4^R$	$\mathbb{Z}_6^R$	$\mathbb{Z}_8^R$	$\mathbb{Z}_{12}^R$	$\mathbb{Z}_{24}^R$
H_u	0	4	0	4	16
H_d	0	0	4	0	12
Q	1	5	1	5	5
U^c	1	5	1	5	5
E^c	1	5	1	5	5
L	1	3	5	9	9
D^c	1	3	5	9	9
N^c	1	1	5	1	1

Table 12: Derived MSSM field R charge assignments for various anomaly-free discrete $\mathbb{Z}_N^R$ symmetries which are consistent with $SU(5)$ or $SO(10)$ unification (from Lee *et al.* Ref. [137]).

symmetry. Table 12 (as derived in Ref's [136, 137]) shows the R-symmetries along with the R-charges of the multiplets which are consistent with either $SU(5)$ or $SO(10)$ unification, anomaly-free (allowing for a Green-Schwarz term), forbid the μ term and also forbid the R-parity violating and dimension-five proton decay operators and hence can serve the purpose of being a fundamental symmetry. In fact, the $\mathbb{Z}_N^R$ symmetries of Table 12 have been shown to be the *only* anomaly-free symmetries which allow for fermion masses and suppress the μ term while maintaining consistency with GUTs. As a bonus, they allow for neutrino masses while forbidding R-parity and dangerous proton decay operators. Implementation of the discrete R-symmetries is only possible in extra-dimensional GUTs, making their implementation in string compactifications very natural [193].

III.3.2. MBGW Model

The Martin-Babu-Gogoladze-Wang (MBGW) model [54, 57] begins with a superpotential

$$W = f_u Q H_u U^c + f_d Q H_d D^c + f_e L H_d E^c + f_\nu L H_u N^c$$
$$+ M_R N^c N^c + \lambda_\mu \frac{X^2 H_u H_d}{m_p} + \lambda_2 \frac{(XY)^2}{m_P}$$

which is augmented by soft SUSY breaking terms

$$V_{soft} \ni m_X^2 |\phi_X|^2 + m_Y^2 |\phi_Y|^2 + \left(\lambda_2 C \frac{(\phi_X \phi_Y)^2}{m_P} + h.c. \right) \tag{87}$$

so that the scalar potential is

$$V_{MBGW} = V_F + V_{soft} \tag{88}$$

with

$$V_F \ni 4 \frac{\lambda_2^2}{m_P} |\phi_X \phi_Y|^2 \left(|\phi_X|^2 + |\phi_Y|^2 \right). \tag{89}$$

The scalar potential admits non-zero minima in the fields ϕ_X and ϕ_Y for $C < 0$. The scalar potential for the case of $m_X = m_Y \equiv m_s = 10^4$ GeV and $C = -3.5 \times 10^4$ GeV is shown in Fig. 16.

It is found in Ref. [57] that the model admits a remnant $\mathbb{Z}_{22}$ discrete gauge symmetry which is anomaly free up to Green-Schwarz terms and forbids lower order operators which would lead to gravitational instability. Beside the terms in Eq. (87), the lowest order PQ-violating term in the superpotential is $\frac{(Y)^{11}}{m_P^8}$: thus this model is gravity safe according to the KMR criterion. An approximate PQ symmetry emerges as an accidental consequence of the discrete $\mathbb{Z}_{22}$ gauge symmetry. The $\mathbb{Z}_{22}$ and PQ charges are listed in Table 13.

By taking $\langle \phi_X \rangle \equiv v_x$ and $\langle \phi_Y \rangle \equiv v_Y$, then the scalar potential minimization condi-

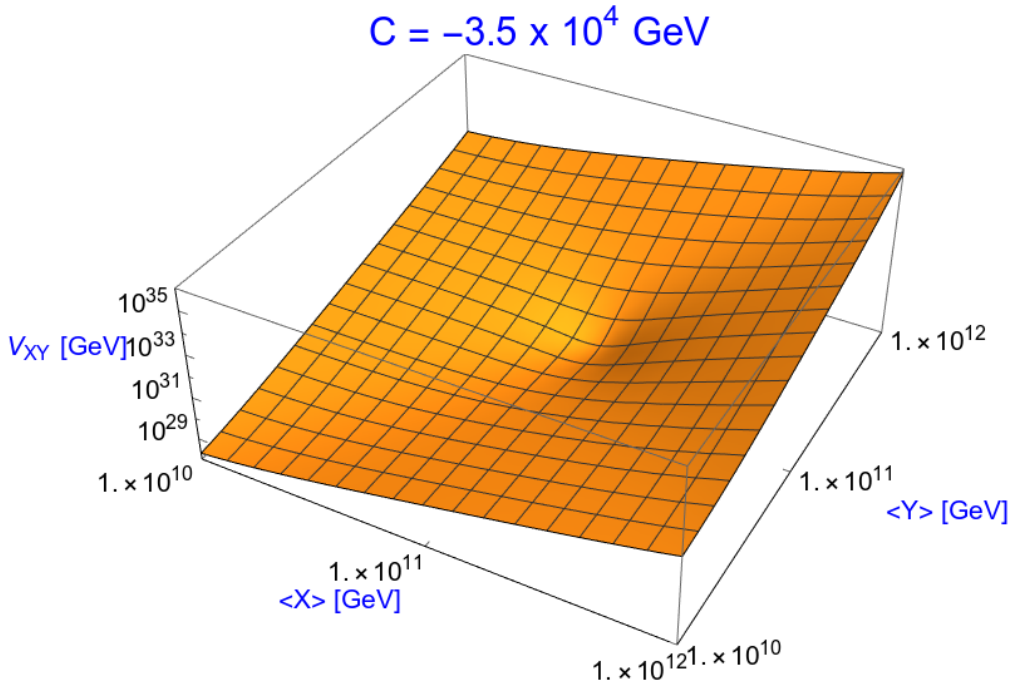

Figure 16: Scalar potential V_{MBGW} versus ϕ_X and ϕ_Y for $m_s = 10^4$ GeV and $C = -3.5 \times 10^4$ GeV.

multiplet	H_u	H_d	Q_i	L_i	U_i^c	D_i^c	E_i^c	N_i^c	X	Y
$\mathbb{Z}_{22}$ charge	22	18	3	11	19	1	15	11	13	20
PQ charge	-1	-1	$+1$	$+1$	0	0	0	0	$+1$	-1

Table 13: $\mathbb{Z}_{22}$ and PQ charge assignments for various superfields of the MBGW model.

tions read

$$\begin{aligned} 0 &= 2\frac{\lambda_2}{m_P}C^* v_x v_Y^2 + m_X^2 v_X + 4\frac{\lambda_2^2}{m_P^2}\left(v_X v_Y^2(v_X^2+v_Y^2) + v_X^3 v_Y^2\right) \\ 0 &= 2\frac{\lambda_2}{m_P}C^* v_x^2 v_Y + m_Y^2 v_Y + 4\frac{\lambda_2^2}{m_P^2}\left(v_X^2 v_Y(v_X^2+v_Y^2) + v_X^2 v_Y^3\right). \end{aligned} \tag{90}$$

A simplifying assumption of $m_X^2 = m_Y^2 \equiv m_s^2$ and $v_X = v_Y \equiv v_s$ leads to

$$v_s^2 = \frac{-C \pm \sqrt{C^2 - 12m_s^2}}{12\lambda_2} m_P \tag{91}$$

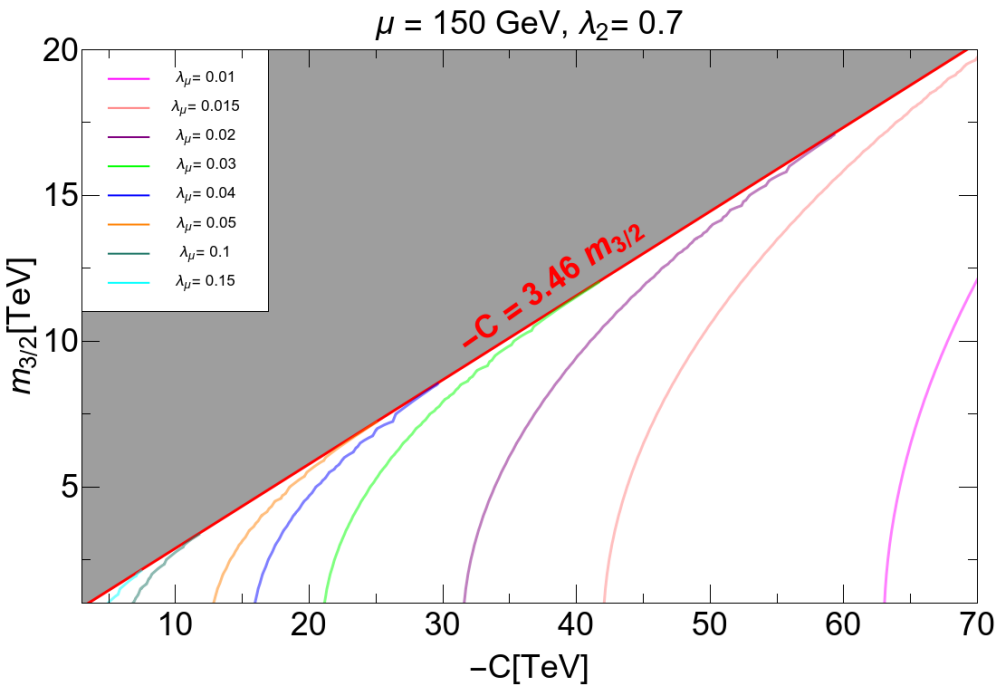

Figure 17: Value of λ_μ required for $\mu = 150$ Gev in the $m_{3/2}$ vs. $-C$ plane of the MBGW model.

so that the μ term is

$$\mu_{MBGW} \simeq \lambda_\mu \frac{v_s^2}{m_P} \tag{92}$$

with $v_s^2 \simeq \frac{|C|}{12\lambda_2} m_P$. Taking $m_s \simeq m_{3/2} = 10^4$ GeV with $\mu = 150$ GeV and $C = -3.5\times 10^4$ GeV leads to $v_s \simeq v_{PQ} \simeq 10^{11}$ GeV for $\lambda_2 = 0.7$ and $\lambda_\mu \simeq 0.036$. Thus, the MBGW model admits a Little Hierarchy $\mu \ll m_{3/2}$ whilst generating the PQ scale $v_{PQ} \sim 10^{11}$ (which generates mainly axion dark matter with a smaller portion of higgsino-like WIMPs [175, 176, 177, 181]). The allowed range of MBGW model parameter space is shown in Fig. 17 where we show contours of λ_μ values which lead to $\mu = 150$ GeV.

As mentioned previously, the MBGW model appears gravity-safe under the $\mathbb{Z}_{22}$ discrete gauge symmetry, The discrete gauge symmetry $\mathbb{Z}_M$ might arise if a charge M field condenses and is integrated out of the low energy theory while charge e fields survive (see Krauss and Wilczek, Ref. [195]). While the ensuing low energy theory should be gravity safe, for the case at hand one might wonder at the plausibility of a condensa-

tion of a charge 22 object and whether it might occupy the so-called *swampland* [202] of theories not consistent with a UV completion in string theory. In addition, the charge assignments [57] are not consistent with $SU(5)$ or $SO(10)$ grand unification which may be expected at some level in a more ultimate theory.

Alternatively, it is worth checking whether MBGW is gravity-safe under any of the discrete R-symmetries listed in Table 12. To check gravity safety, we note that additional superpotential terms of the form $\lambda_3 X^p Y^q$ may be allowed for given $\mathbb{Z}_N^R$ charge assignments and powers p and q. Such terms will typically break the PQ symmetry and render the model not gravity safe if scalar potential $V(\phi)$ include terms which are not suppressed by at least eight powers of $1/m_P$ [201]. The largest dangerous scalar potential terms develop from interference between $\lambda_2(XY)^2/m_P$ and $\lambda_3 X^p Y^q/m_P^{p+q-3}$ when constructing the scalar potential $V_F = \sum_{\hat{\phi}} |\partial W/\partial\hat{\phi}|^2_{\hat{\phi}\to\phi}$ (here, the $\hat{\phi}$ label chiral superfields with ϕ being their leading components). We find the MBGW model to be not gravity safe under any of the $\mathbb{Z}_N^R$ discrete R-symmetries of Table 12.

III.3.3. Gravity safety of radiative PQ breaking models

As discussed above, the radiative PQ breaking models are the most compelling simultaneous solution to the Strong CP problem and the SUSY μ problem owing to their large number of virtues. The only issue with this class of model is whether the required PQ symmetry is actually gravity-safe and whether it may emerge from any of the aforementioned $\mathbb{Z}_N^R$ symmetries. We have examined whether or not the three radiative PQ breaking models of Table 10 (CCK, MSY and SPM) can be derived from any of the more fundamental $\mathbb{Z}_N^R$ symmetries in Table 12 [195]. In almost all cases, the hXN^cN^c operator is disallowed: then there is no large Yukawa coupling present to drive the PQ soft term m_X^2 negative so that PQ symmetry is broken. And since the PQ symmetry does not allow for a Majorana mass term $M_N N^c N^c$, then no see-saw scale can be developed. One exception is the MSY model under $\mathbb{Z}_4^R$ symmetry with charge assignments

$Q_R(X) = 0$ and $Q_R(Y) = 2$: then a YH_uH_d term is allowed which would generate a μ term of order the intermediate scale. Also, without considering any specific R-charges for the fields X and Y, we can see that the R-charges for X and Y should be such that the term XYH_uH_d is allowed and since the R-charges of H_u and H_d are 0, then a term MXY would always be allowed: this term breaks PQ at high order and is not gravity safe. A second exception is SPM under the $\mathbb{Z}_6^R$ symmetry with charges $Q_R(X) = 0$ and $Q_R(Y) = 2$: then operators like Y^4/m_p are allowed which break PQ but are not sufficiently suppressed so as to be gravity-safe. Furthermore, we can see that in this model that the R-charge of Y is such that terms like M^2Y which break PQ are always allowed but are not gravity safe. Thus, we conclude that while the radiative PQ breaking models are indeed compelling and can address all three intermediate scales in a unified framework, the required PQ symmetry does not appear gravity-safe.

III.3.4. Hybrid Models

In this subsection, we review three models which combine approaches with PQ symmetry breaking triggered by SUSY breaking and gravity-safe construction of approximate PQ symmetry from discrete R-symmetry.

- These models are obtained by adopting a hybrid approach [195] between the radiative breaking models and the MBGW model.

- In the radiative breaking models, a Majorana neutrino scale is generated as the PQ field X gets VEV. However, in the hybrid models, the Majorana mass term MN^cN^c is allowed but it is not generated through PQ breaking– similar to MBGW model.

- In the radiative breaking models, intermediate PQ and Majorana neutrino scales develop as a consequence of intermediate scale SUSY breaking and the running of soft SUSY breaking mass term to negative squared values. In contrast, in

the MBGW model and in the hybrid models, PQ breaking is triggered by large negative soft terms instead of radiative breaking.

Three hybrid models as listed below :

Hybrid CCK Model

The superpotential for the hybrid CCK model (hyCCK) is given by [195]:

$$W_{hyCCK} \ni f_u Q H_u U^c + f_d Q H_d D^c + f_\ell L H_d E^c + f_\nu L H_u N^c + M_N N^c N^c/2 + f X^3 Y/m_P + \lambda_\mu X^2 H_u H_d/m_P. \tag{93}$$

Thus when the PQ symmetry breaks, the μ parameter is obtained as

$$\mu_{\rm eff} = \lambda_\mu \langle X \rangle^2/m_P. \tag{94}$$

We have checked that the hyCCK model is not gravity-safe under the $\mathbb{Z}_N^R$ symmetries for $N = 4, 6, 8$ or 12. However, it does turns out to be gravity-safe under $\mathbb{Z}_{24}^R$ symmetry with the $\mathbb{Z}_{24}^R$ charge and PQ charge assignments as shown in Table 14.

multiplet	H_u	H_d	Q_i	L_i	U_i^c	D_i^c	E_i^c	N_i^c	X	Y
$\mathbb{Z}_{24}^R$ charge	16	12	5	9	5	9	5	1	-1	5
PQ charge	-1	-1	1	1	0	0	0	0	1	-3

Table 14: $\mathbb{Z}_{24}^R$ and PQ charge assignments for various superfields of the hyCCK model.

The scalar potential for hyCCK is found to be

$$V = [f A_f \frac{\phi_X^3 \phi_Y}{m_P} + h.c.] + m_X^2 |\phi_X|^2 + m_Y^2 |\phi_Y|^2 + \frac{f^2}{m_P^2}[9|\phi_X|^4 |\phi_Y|^2 + |\phi_X|^6] \tag{95}$$

and is shown in Fig. 18 vs. scalar field values ϕ_X and ϕ_Y. For large negative values of soft term A_f, then a $\mathbb{Z}_{24}^R$ and PQ breaking minimum develops.

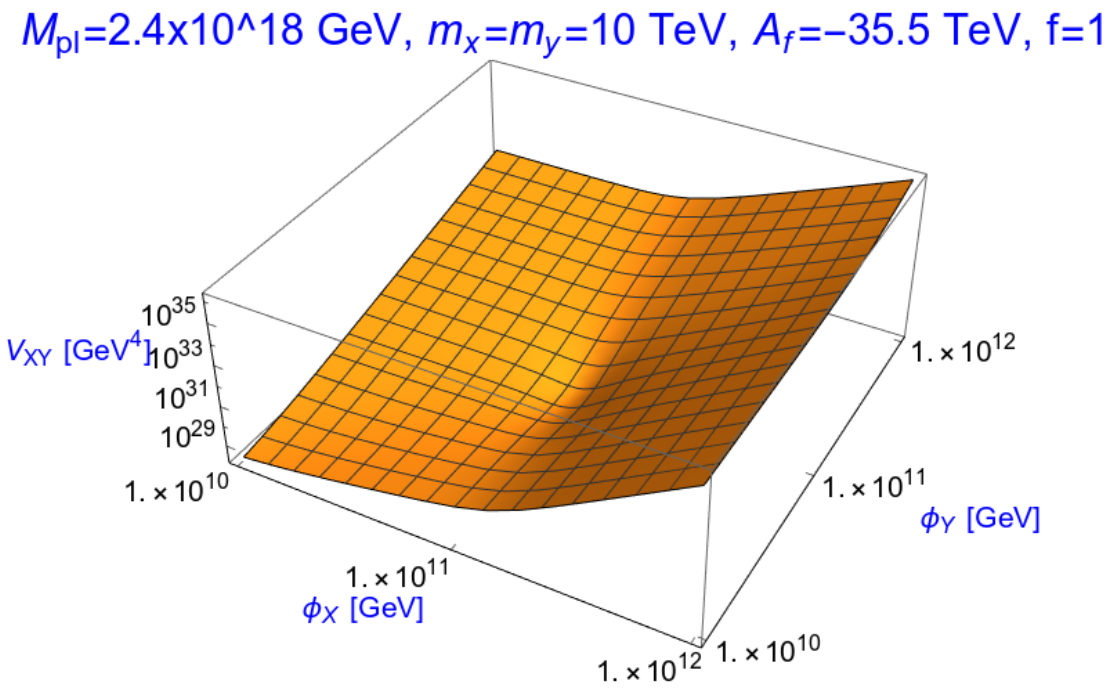

Figure 18: Scalar potential V_{hyCCK} versus ϕ_X and ϕ_Y for $m_X = m_Y \equiv m_{3/2} = 10$ TeV, $f = 1$ and $A_f = -35.5$ TeV.

The lowest order PQ violating terms in the superpotential are X^8Y^2/m_P^7, X^4Y^6/m_P^7 and Y^{10}/m_P^7 which implies that the lowest order PQ breaking term in the scalar potential is suppressed by $1/m_P^8$. Therefore, this model satisfies the KMR condition for being gravity-safe.

The allowed range of hyCCK model parameter space is shown in Fig. 19 where we show contours of λ_μ values which lead to $\mu = 150$ GeV in the $m_{3/2}$ vs. $-A_f$ plane for $f = 1$. We also show several representative contours of v_{PQ} values. Values of $\lambda_\mu \sim 0.015 - 0.2$ are generally sufficient for a natural μ term and are easily consistent with soft mass $m_{soft} \sim m_{3/2} \sim 2 - 30$ TeV as indicated by LHC searches. We also note that for $m_{3/2} \sim 5 - 20$ TeV, then $v_{PQ} \sim 10^{11}$ GeV which corresponds to the sweet spot for axion cold dark matter.

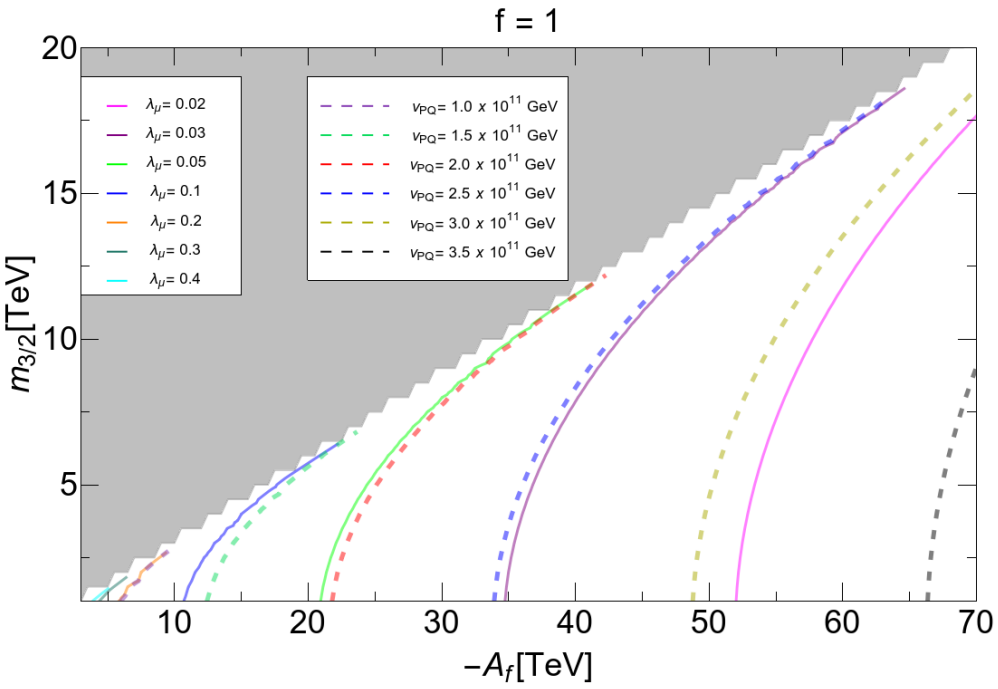

Figure 19: Representative values of λ_μ required for $\mu = 200$ GeV in the $m_{3/2}$ vs. $-A_f$ plane of the hyCCK model for $f = 1$. We also show several contours of v_{PQ}.

Hybrid SPM Model

The superpotential for the hybrid SPM model (hySPM) is given by [191, 195]

$$W_{hySPM} \ni f_u Q H_u U^c + f_d Q H_d D^c + f_\ell L H_d E^c + f_\nu L H_u N^c + M_N N^c N^c/2 + f X^3 Y/m_P + \lambda_\mu Y^2 H_u H_d/m_P.$$

In this case, when PQ symmetry breaks, the μ parameter is generated to be

$$\mu_{\rm eff} = \lambda_\mu \langle Y \rangle^2/m_P. \tag{96}$$

This model also turns out to be not gravity-safe under $\mathbb{Z}_N^R$ symmetries for $N = 4, 6, 8$ and 12 but is gravity-safe for $\mathbb{Z}_{24}^R$ symmetry. The gravity-safe $\mathbb{Z}_{24}^R$ charge and PQ charge assignments as shown in Table 15.

The scalar potential is obtained similar to that in the hyCCK model with the only

multiplet	H_u	H_d	Q_i	L_i	U_i^c	D_i^c	E_i^c	N_i^c	X	Y
$\mathbb{Z}_{24}^R$ charge	16	12	5	9	5	9	5	1	5	-13
PQ charge	-1	-1	1	1	0	0	0	0	-1/3	1

Table 15: $\mathbb{Z}_{24}^R$ and PQ charge assignments for various superfields of the hySPM model.

difference being that now the lowest order PQ violating terms in the superpotential are Y^8X^2/m_P^7, Y^4X^6/m_P^7 and X^{10}/m_P^7 which means that the lowest order PQ breaking terms in the scalar potential are suppressed by $1/m_P^8$ so that the hySPM model also satisfies the KMR condition for being gravity-safe.

The allowed range of hySPM model parameter space is shown in Fig. 20 where we show contours of λ_μ values which lead to $\mu = 150$ GeV in the $m_{3/2}$ vs. $-A_f$ plane for $f = 1$. We also show several representative contours of v_{PQ} values.

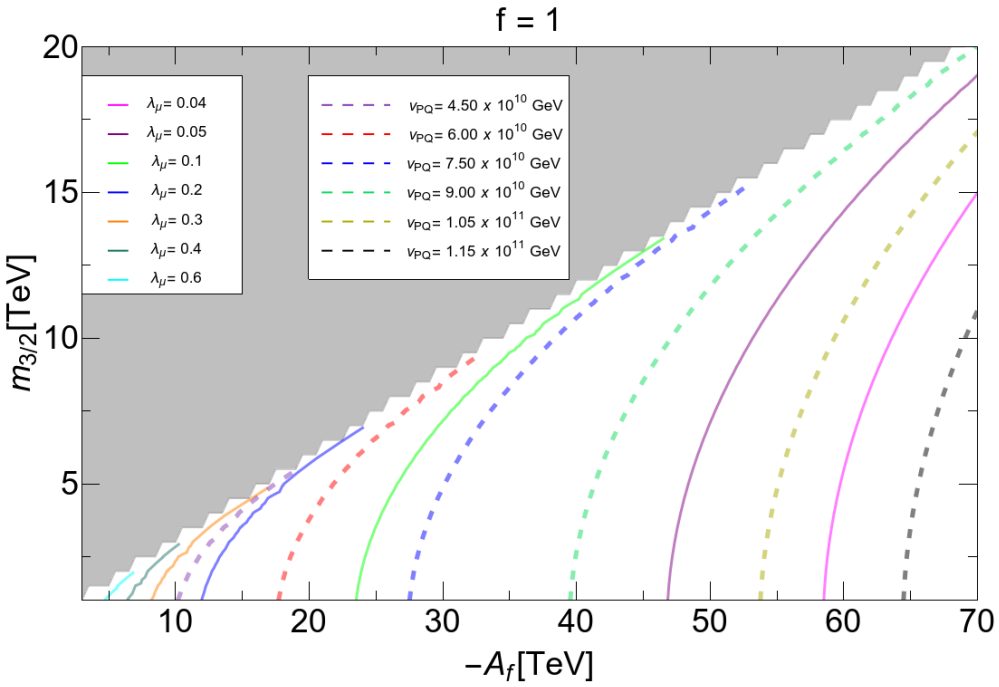

Figure 20: Representative values of λ_μ required for $\mu = 150$ GeV in the $m_{3/2}$ vs. $-A_f$ plane of the hySPM model for $f = 1$. We also show several contours of v_{PQ}.

Hybrid MSY model

The superpotential in the hybrid MSY model (hyMSY) is given as [195]:

$$W_{hyMSY} \ni f_u Q H_u U^c + f_d Q H_d D^c + f_\ell L H_d E^c + f_\nu L H_u N^c + M_N N^c N^c/2 + f X^3 Y/m_P + \lambda_\mu X Y H_u H_d/m_P.$$

However, it has been checked that the hyMSY model does not satisfy the KMR condition for being gravity-safe under any of the R-symmetries listed in Table 12.

Summary : Clearly, the SUSY μ problem has generated a rich panoply of solutions over the past 35 years. These solutions are summarized in Table 16 where we list each solution and how it may admit a LH, whether it also addresses the strong CP problem, whether it is gravity-safe and its relation to neutrino masses (Standard see-saw or other). If the naturalness edict is followed– which requires $|\mu|$ not too far from $m_{weak} \sim 100$ GeV– then one expects thermally-underproduced higgsino-like WIMPs as (part of) dark matter. As seen in Sec. II, if the natural WIMP abundance is enhanced by non-thermal processes to make up the entirety of dark matter, then they become excluded by a combination of direct and indirect WIMP detection experiments [203]. Thus, additional dark matter beyond WIMPs then seems to be required. The axion is a highly motivated candidate to make up the remaining bulk of dark matter. To gain accord with the requirements of cold dark matter, a gravity-safe solution to the strong CP problem and a solution to the SUSY μ problem (while also suppressing dangerous p-decay operators and allowing for see-saw neutrino masses), I came up with the hybrid models based on $\mathbb{Z}_{24}^R$ discrete R-symmetry which stand out as a rather complete answer. To begin the process of selecting amongst them or building others, it is of the essence to first discover SUSY and then to proceed with precision measurements of the SUSY spectra along with any exotica to gain insight into which if any of the solutions best

describes nature.

model	admit LH?	strong CP?	gravity safe?	see-saw?
GM	small λ_μ	$\times$	$--$	$SNSS$
CM	small λ_μ	$\times$	$--$	$SNSS$
R-sym	$(v_i/m_P)^{n_i} \ll 1$	$\times$	$--$	$SNSS$
$\mathbb{Z}_4^R$	small λ_μ	$\times$	$--$	$SNSS$
Instanton	small $e^{-S_{cl}}$	$\times$	$--$	$SNSS$
G_2MSSM	$\langle S_i \rangle / m_P \ll 1$	$\times$	$--$	$SNSS$
NMSSM	small λ_μ	$\times$	$--$	$SNSS$
nMSSM	small λ_μ	$\times$	$--$	$SNSS$
$\mu\nu$SSM	small λ_μ	$\times$	$--$	$bRPV$
$U(1)'$ (CDEEL)	small λ_μ	$\times$	$--$	$SNSS$
sMSSM	small λ_μ	$\times$	$--$	$SNSS$
$U(1)'$ (HPT)	small λ_μ	$\times$	$--$	$bRPV$
KN	$v_{PQ} < m_{hidden}$	$\surd$	?	$SNSS$
CKN	$\Lambda < \Lambda_h$	$\surd$	?	$SNSS$
BK/EWK	$\lambda_\mu \sim 10^{-10}$	$\surd$	?	$SNSS$
HFD	$v_{PQ} < m_{hidden}$	$\surd$	?	$SNSS$
MSY/CCK/SPM	$v_{PQ} < m_{hidden}$	$\surd$	$\times$	$RadSS$
CCL	small λ_μ	$\surd$	?	$several$
MBGW	small λ_μ	$\surd$	$\mathbb{Z}_{22}$	$SNSS$
Hybrid CCK/SPM	small λ_μ	$\surd$	$\mathbb{Z}_{24}^R$	$SNSS$

Table 16: Summary of twenty solutions to the SUSY μ problem and how they 1. admit a Little Hierarchy (LH), 2. solve the strong CP problem ($\surd$) or not ($\times$), 3. are expected gravity-safe and 4. Standard neutrino see-saw (SNSS) or other

IV. Stringy Naturalness and the Landscape

As seen in Sec. I.6, the string theory landscape supported by the multiverse argument has proven to be very successful in predicting the value of Cosmological Constant (Λ). Now the question is : Is it possible to predict the scale of SUSY breaking using a similar approach? In order to answer this question Douglas has suggested a power law statistical distribution for the overall soft SUSY breaking scale m_{soft} of the form m_{soft}^n where $n = 2n_F + n_D - 1$, and where n_F is the number of F-breaking fields and n_D is the number of D-breaking fields contributing to the overall SUSY breaking scale [68]. Since the values of n_D and n_F are not known, we assume several different values of n. For $n = 0$ we would expect a uniform distribution of the soft breaking terms which is the usual assumption while assuming $n = 1$, would give rise to a *linear* statistical draw towards large soft terms. It has been shown in Ref. [77] that in NUHM3 model (gravity-mediated SUSY breaking) mild statistical draw towards large soft SUSY breaking terms with $n = 1$(linear) or $n = 2$(quadratic) are preferred by LHC mass constaints over uniform distribution of the soft breaking terms (i.e., $n = 0$). Such mild statistical draw towards large soft SUSY breaking terms tempered by the requirement of $m_{weak} < 4$ m_{weak} (measured) [17] along with a natural value of μ results in the following features :

- A statistical peak was found at $m_h \simeq 125 \pm 2$ GeV. This is easy to understand: we are selecting for soft terms as large as possible subject to appropriate EWSB and a value of $m_Z^{PU} \leq 4 m_Z^{OU}$. This also selects for large (but not so large as to lead to CCB minima) A_0 terms which increase top squark mixing and lift m_h up to the vicinity of 125 GeV.

- The probability distribution $dP/dm_{\tilde{g}}$ yields a value $m_{\tilde{g}} \sim 4 \pm 2$ TeV, safely above

[17] Here, we assume a (natural) solution to μ problem so we can't tune μ to get m_z=91.2 GeV. In order to maintain the atomic principle as suggested in Ref. [76] we then require the value of $m_Z^{PU} <$ 4 m_Z^{OU} where m_Z^{PU} stands for the mass of Z boson in several pocket universes of the multiverse and m_Z^{OU} stands for the mass of Z boson in our Universe. This then translates to requiring $\Delta_{EW} < 30$.

LHC2 limits.

- The light top squark is lifted to $m_{\tilde{t}_1} \sim 1.5 \pm 0.5$ TeV, also safely above LHC Run 2 limits.

- Light higgsinos $\tilde{w}_1$ and $\tilde{z}_{1,2}$ with mass $\sim \mu \sim 200 \pm 100$ GeV. The mass gap is $m_{\tilde{z}_2} - m_{\tilde{z}_1} \sim 7 \pm 3$ GeV. Thus, higgsino pair production signals should ultimately show up at LHC14 via $pp \to \tilde{z}_1 \tilde{z}_2$ production followed by $\tilde{z}_2 \to \ell^+ \ell^- \tilde{z}_1$ decay with $m(\ell^+ \ell^-) < (7 \pm 3)$ GeV once sufficient luminosity is gained [221, 222].

- First and second generation matter scalars (squarks and sleptons) are pulled up to $m(\tilde{q}, \tilde{\ell}) \sim 20 \pm 10$ TeV.

In accord with the result obtained in Ref. [77] a SUSY benchmark point from the NUHM3 model, generated using Isajet, is given in table 17. This spectra, named landSUSY, lies well within the landscape SUSY predictions for an $n = 1$ mild draw to large soft terms [77].

In this section, we shall examine how such mild statistical draw towards large soft SUSY breaking terms would affect various aspects of Supersymmetry.

parameter	landSUSY
$m_0(1,2)$	16 TeV
$m_0(3)$	5 TeV
$m_{1/2}$	1.5 TeV
A_0	-7 TeV
$\tan\beta$	10
μ	0.2 TeV
m_A	3 TeV
$m_{\tilde{g}}$	3619 GeV
$m_{\tilde{u}_L}$	16211 GeV
$m_{\tilde{u}_R}$	16264 GeV
$m_{\tilde{e}_R}$	15956 GeV
$m_{\tilde{t}_1}$	1294 GeV
$m_{\tilde{t}_2}$	3561 GeV
$m_{\tilde{b}_1}$	3605 GeV
$m_{\tilde{b}_2}$	4999 GeV
$m_{\tilde{\tau}_1}$	4749 GeV
$m_{\tilde{\tau}_2}$	4982 GeV
$m_{\tilde{\nu}_\tau}$	4951 GeV
$m_{\tilde{w}_1}$	210 GeV
$m_{\tilde{w}_2}$	1312 GeV
$m_{\tilde{z}_1}$	200 GeV
$m_{\tilde{z}_2}$	207 GeV
$m_{\tilde{z}_3}$	688 GeV
$m_{\tilde{z}_4}$	1320 GeV
m_h	125 GeV
$\Omega^{std}_{\tilde{z}_1}h^2$	0.01
$BF(b\to s\gamma)\times 10^4$	3.0
$BF(B_s\to\mu^+\mu^-)\times 10^9$	3.8
$\sigma^{SI}(\tilde{z}_1,p)$ (pb)	1.0×10^{-9}
$\sigma^{SD}(\tilde{z}_1 p)$ (pb)	2.0×10^{-5}
$\langle\sigma v\rangle\vert_{v\to 0}$ (cm^3/sec)	2×10^{-25}
$\Delta_{\rm EW}$	23.3

Table 17: Input parameters (TeV) and masses (GeV) for a landscape SUSY benchmark point from the NUHM3 model with $m_t = 173.2$ GeV using Isajet 7.88[49].

IV.1. Is the magnitude of the Peccei–Quinn scale set by the landscape?

In Sec. III, we have seen that the most elegant solution to the strong CP problem involves the introduction of a global $U(1)_{PQ}$ symmetry[204]. When this PQ symmetry spontaneously breaks at some scale $f_a \sim 10^9 - 10^{16}$ GeV [18], it provides a dynamical solution to the strong CP problem through the emergence of a (pseudo-)Goldstone boson, the axion. While the PQ axion solution to the strong CP problem is indeed compelling, it is beset by two problems of its own.

- $U(1)_{PQ}$ being a global symmetry suffers from gravity-spoliation problem. This problem and its solution has been discussed in Sec. III
- In string theory, many candidate axions can emerge, but with a PQ scale $f_a \sim m_{\rm GUT}$ to $m_{\rm string}$[207, 208]. Meanwhile, cosmological (dark matter) constraints seem to require $f_a \sim 10^{11} - 10^{12}$ GeV[206]. A further problem then is: what accounts for the apparent suppression of the PQ breaking scale?

In this section, we shall address the second issue in the context of the string theory landscape: can the magnitude of the PQ breaking scale be understood from landscape considerations within a well-motivated model for axion (and WIMP) dark matter? [19]
A few related previous works discussed in Ref. [209, 210, 211, 212, 213] have also addressed this question.
As seen in Sec. III, among quite a few gravity-safe models which simultaneously solve the Strong CP problem and the SUSY μ problem, the hybrid models are the most plausible solutions owing to ultraviolet completion and their consistency with GUTs,

[18] In accord with the PDG[205], we take $f_A \equiv f_a/N_{\rm DW}$ where $N_{\rm DW}$ is the domain-wall number which is $N_{\rm DW} = 6$ for the DFSZ axion model assumed here.
[19] As seen in Sec. II, naturalness require higgsino-like WIMP which alone is unable to account for the entire dark matter content of the universe and so another particle is needed and axion, being a solution to the strong CP problem, is the most viable choice.

which at some point is expected to be true. Thus, these hybrid models can serve as well-motivated models for mixed axion-neutralino dark matter. However, here only the hybrid CCK model has been used for further calculation since hybrid SPM model will yield similar result because the relevant soft term that will affect the value of f_a is same in both of these models.

IV.1.1. Peccei-Quinn breaking scale in Hybrid CCK model

The scalar potential of the gravity-safe hybrid CCK model is given in Eqn. (95). Minimization conditions for the hyCCK model can be found in Ref. [55]. The scalar potential develops a non-zero minimum at $\langle\phi_X\rangle \equiv v_X$ and $\langle\phi_Y\rangle \equiv v_Y$ for a sufficiently large soft term $-A_f$, thus breaking the underlying $\mathbb{Z}_{24}^R$ and accidental, approximate PQ symmetries. The PQ breaking vev is given by $v_{PQ} = \sqrt{q_X^2 v_X^2 + q_Y^2 v_Y^2} = \sqrt{v_X^2 + 9v_Y^2}$ where q_X and q_Y are the PQ charges of X and Y field respectively as given in Table 14, and the Peccei-Quinn breaking scale f_a is defined as $f_a = \sqrt{2}v_{PQ}$. In accord with expectations from supergravity models, we will assume $m_X = m_Y = m_{\tilde{a}} = m_s \equiv m_{3/2}$ [95]. Thus, in this model, the PQ scale is a derived consequence of SUSY breaking.

The calculated value of f_a is given in Fig. 21 as a function of the $-A_f$ soft term assuming various values of $m_X = m_Y = m_0(1, 2) \equiv m_{3/2}$ and three different values of f. From Fig. 21, we see that f_a has a monotonically increasing value with increasing $-A_f$. For a particular value of $-A_f$ and $m_X = m_Y = m_0(1, 2) \equiv m_{3/2}$ if the value of f is reduced by a factor of 2, then f_a increases by approximately 41% and if the value of f is increased by a factor of 2, then f_a decreases by approximately 41%. Since $-A_f$ doesn't contribute directly to the determination of the weak scale, then there is no (anthropic) upper bound on its value and one might expect $-A_f$ and hence f_a to lie far beyond the well-known cosmological sweet spot where $f_a \sim 10^{11} - 10^{12}$ GeV[206].

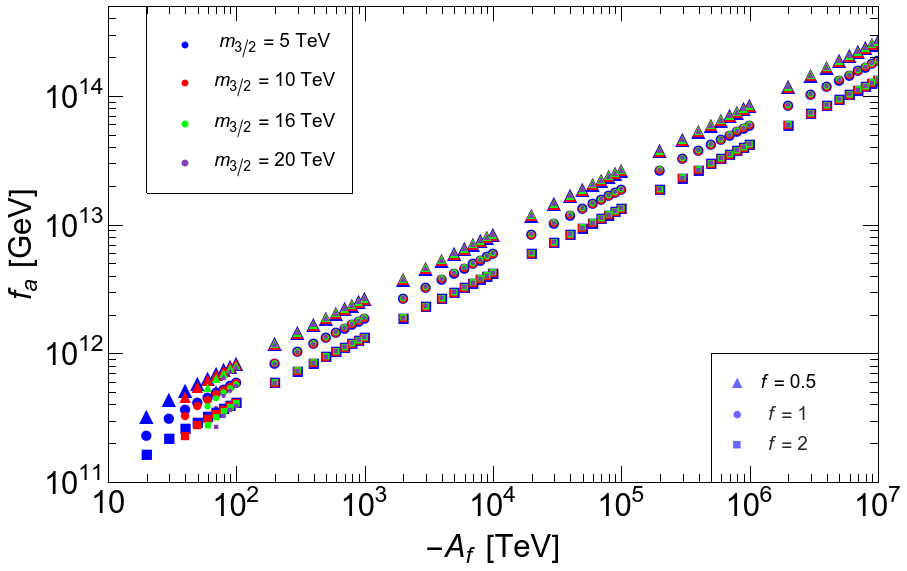

Figure 21: Value of Peccei-Quinn scale f_a vs. hyCCK soft parameter $-A_f$ for various values of $m_X = m_Y \equiv m_{3/2}$ and three different values of f.

IV.1.2. Relic density of mixed axion-WIMP dark matter

The evaluation of mixed axion-WIMP dark matter from SUSY axion models is more complicated than simply adding the WIMP thermal abundance to the coherent-oscillation-produced axions. The mixed neutralino-axion relic density is evaluated by applying the eight-coupled-Boltzmann equation computer code developed in Ref's [176, 177, 178]. For brevity, the eight coupled Boltzmann equations are not reproduced here. The code relies on the IsaReD [92] calculation of $\langle \sigma v \rangle (T)$ which is a crucial input to the coupled Boltzmann calculation. Starting from the time of re-heat with temperature T_R at the end of the inflationary epoch, the computer code tracks the coupled abundances of radiation (*i.e.* SM particles), neutralinos, axinos, gravitinos, saxions and axions (the latter two consists of both thermal/decay-produced and coherent oscillation-produced (CO) components).

The CO-produced abundance of axions is determined in part by the axion field initial

misalignment angle θ_i [206, 214]. For numerical analyses, a simple formula is adopted

$$\Omega_a^{\rm CO}h^2 \simeq 0.23 f(\theta_i)\theta_i^2 \left(\frac{f_a/N_{\rm DW}}{10^{12}\ {\rm GeV}}\right)^{7/6} \tag{97}$$

where $f(\theta_i) = \left[\log\left(e/(1-\theta_i^2/\pi^2)\right)\right]^{7/6}$ is the anharmonicity factor [214] and $N_{\rm DW}$ is the domain wall number (= 6 for the DFSZ model). In previous work the initial misalignment angle θ_i is adjusted to gain the measured value of the relic abundance. Here, a uniform distribution of $\theta_i : 0 - \pi$ values is allowed since we are scanning over many pocket universes which arise as subuniverses of the more vast multiverse.

In Fig. 22 we show the energy densities of various species vs. scale factor R/R_0 that influence the ultimate dark matter abundance for the landscape SUSY benchmark point landSUSY in Table 17. Here, R_0 is the reference scale factor at the beginning of re-heat and the corresponding temperature T is shown by the dashed green line (where instead the y-axis is interpreted as temperature in GeV). Here, $T_R = 10^7$ GeV [20] and $f_a = s_0 = 10^{12}$ GeV and where s_0 denotes the initial saxion field value. Also, it is assumed $m_{\tilde{a}} = m_s = m_{3/2} = 16$ TeV. The blue curve denotes the neutralino abundance which freezes out at $R \sim 10^6 R_0$ or $T \sim 10$ GeV. The saxion and axion contributions are split into their thermally- and decay-produced components and their coherent-oscillation (CO) produced components. Saxions decay around $R \sim 10^5 R_0$ ($T \sim 10$ GeV) whilst axinos decay around $R \sim 10^6 R_0$ (or $T \sim 1$ GeV). The saxion decays depend on a model dependent coupling ξ_s which governs the saxion decay rate $s \to aa$ and $s \to \tilde{a}\tilde{a}$ [177, 176]. It is assumed $\xi_s = 1$ so these decays are turned on. (Of course, for our case the $s \to \tilde{a}\tilde{a}$ decay is not kinematically open so s decays mainly to aa but also to other MSSM particles). CO-produced axions (brown curve) start to oscillate around $T \sim 1$ GeV and become the dominant component of dark matter as one enters the era of entropy conservation on the right-hand-side of the plot. Due to late decays of

[20] This value of T_R is in accord with well-motivated baryogenesis mechanisms such as non-thermal or Affleck-Dine leptogenesis [142].

axinos, which occur after neutralino freeze-out, the neutralino abundance increases to $\Omega_{\tilde{z}_1}h^2 \simeq 0.02$. To gain some perspective on the expected relative abundances of mixed

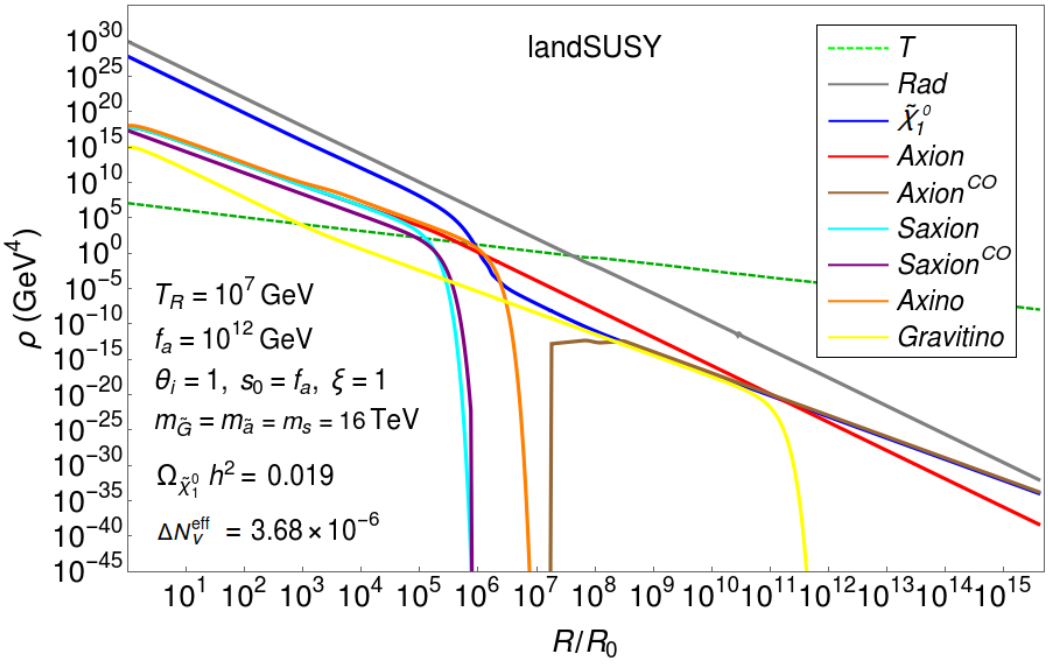

Figure 22: A plot of various energy densities ρ vs. scale factor R/R_0 starting from $T_R = 10^7$ GeV until the era of entropy conservation from our eight-coupled Boltzmann equation solution to the mixed axion-neutralino relic density in the SUSY DFSZ model for the landscape SUSY benchmark point. Here, $\xi_s = 1$. The corresponding temperature T is denoted by the dashed green line where in this case the y-axis is interpreted as T in GeV.

axion-WIMP dark matter, in Fig. 23 the relic density of mixed axion-WIMP dark matter vs. f_a for the landSUSY benchmark point is shown with $T_R = 10^7$ GeV and $m_s = m_{\tilde{a}} = m_{3/2} = 16$ TeV and where $\theta_i = \theta_s = 1$[21].

The green curve corresponds to the axion relic density while the blue curve corresponds to the WIMP relic density. The red curve shows the total relic density. We see that for low values of f_a, the axion relic density– arising here from coherent oscillations corresponding to Eq. (97)– is highly suppressed. Also, the thermally-produced WIMP dark matter is highly suppressed due to the higgsino-like nature of the LSP

[21]Here, the saxion field strength $s = \theta_s.f_a$.

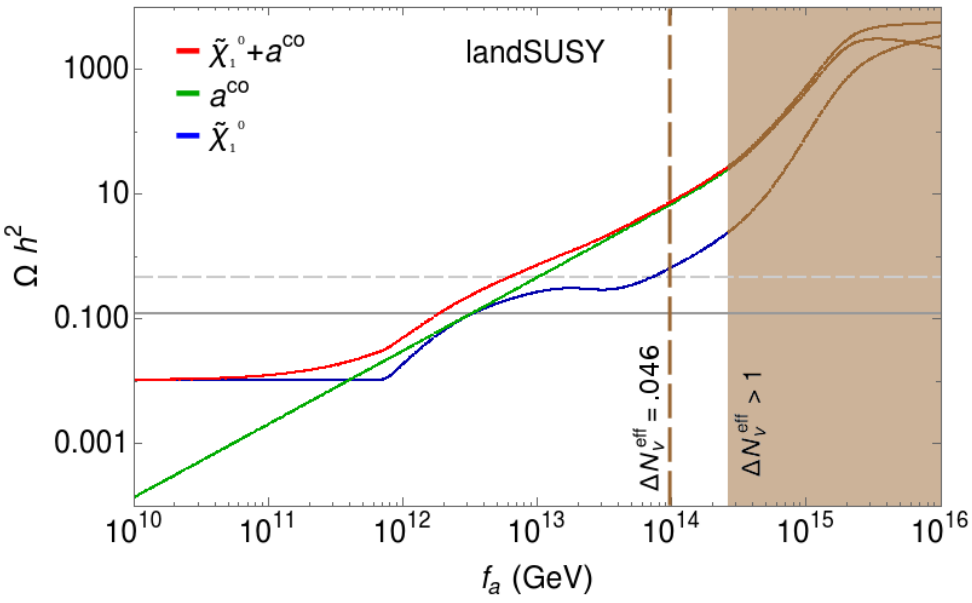

Figure 23: Relic density of axion and higgsino-like WIMP DM versus f_a for the landSUSY benchmark point with $\theta_i = 1$. The red curve denotes the sum of axion plus WIMP dark matter while green denotes the separate axion abundance and the blue curve denotes the separate WIMP abundance. The curves become brown when $\Delta N_\nu^{eff} > 1$.

which enhances its annihilation rate. The WIMP relic density is also highly suppressed by co-annihilations with the slightly heavier higgsinos $\tilde{w}_1$ and $\tilde{z}_2$. Thus, for $f_a \sim 10^{10} - 10^{12}$ GeV, we expect typically an under-production of mixed axion-higgsino DM. As f_a increases, the CO-produced axions steadily increase while WIMPs remain at their thermally-produced level. By $f_a \sim 10^{12}$ GeV, the axino and saxion decay rates are sufficiently suppressed (by $\Gamma_{\tilde{a},s} \sim 1/f_a^2$) that they begin decaying into higgsinos *after* WIMP freeze-out, thus augmenting the WIMP abundance with a non-thermal, decay-produced component. By $f_a \sim 3 \times 10^{12}$ GeV, then the mixed axion-WIMP abundance saturates the measured value $\Omega_{\rm CDM} h^2 \simeq 0.12$, and where at this point CDM consists nearly equally of axions along with a comparable thermal and non-thermal WIMP component. In this region, the non-thermal WIMP component arises mainly from thermal axino production followed by late $\tilde{a}$ decays in the early universe. As f_a increases fur-

ther, the thermal axino production rate falls off rapidly so that the WIMP abundance levels off. For even higher values of $f_a \geq 10^{14}$ GeV, saxion production via COs becomes large and so saxion-decay produced WIMP production rapidly rises. In addition, the $s \to aa$ decays sharply increase the already over-produced axions. These relativistic axions also lead to violation of limits on relativistic species present in the early universe characterized in terms of the effective number of neutrinos parameter ΔN_ν^{eff} which (very conservatively) is taken to be ≤ 1 (brown curve).[22] For $f_a \geq 2 \times 10^{15}$ GeV, then entropy dilution of all relics from CO-produced saxions can suppress the mixed axion-neutralino relic abundance.

In terms of the string theory landscape, we see that allowing values of $f_a \sim m_{\rm GUT}$ could lead to dark matter overproduction by a factor of $\sim 10^4$ compared to its measured value. As noted in previous works [209, 210, 211, 212, 213], it might be hard to visualize the existence of observers in a universe with such an overabundance of dark matter. Precisely how much of an overabundance of dark matter is anthropically too much is an open question. But clearly, if such a limit exists, then it would place an upper limit on the value of f_a. Even requiring a modest factor of four overabundance, indicated by the dashed gray horizontal line, would already require a value $f_a \leq 10^{13}$ GeV. This upper bound is well below the expected magnitude for f_a from string theory where instead $f_a \sim 10^{16} - 10^{18}$ GeV is typically expected [72]. The bound on f_a from the axion abundance may be considered a softer bound since it is possible to lower the axion abundance with a smaller value of $\theta_i \sim 0$ (although if θ_i scans on the landscape, then $\theta_i \sim 1$ is to be expected). However, we see that a bound on f_a still obtains from the WIMP contribution to $\Omega_{a\tilde{z}_1}h^2$, although this bound on WIMP overproduction occurs at over an order of magnitude higher values: in Fig. 23, $f_a \leq 10^{14}$ GeV occurs from just overproduction of the WIMP component of dark matter.

In Fig. 24, we see the total mixed WIMP plus axion dark matter abundance but

[22] In the Particle Data Book [205], it is tabulated that $N_{eff} = 3.13 \pm 0.32$.

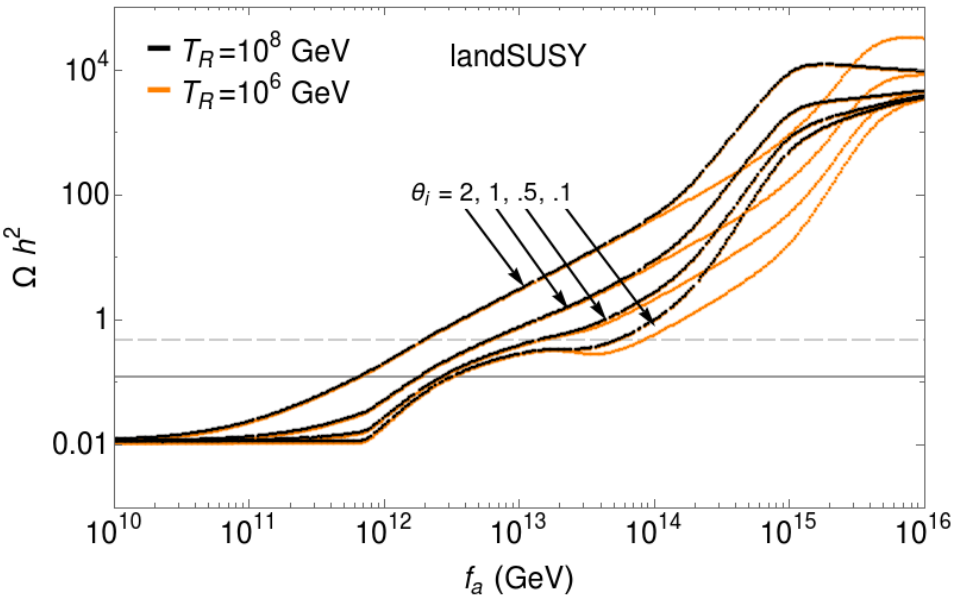

Figure 24: Relic density of total axion plus higgsino-like WIMP DM versus f_a. Results here are for $\theta_i = 0.1,\ 0.5,\ 1$ and 2 and for $\theta_i = 1$ but with $T_R = 10^6$ and 10^8 GeV.

this time assuming $T_R = 10^6$ GeV and 10^8 GeV with $\theta_i = 0.1,\ 0.5,\ 1$ and 2. For $T_R \geq 10^9$ GeV, thermal production and late decay of gravitinos can lead to conflict with bounds from late-decaying neutral particles in the early universe: in this case, the gravitino problem [215, 216]. We see that for different θ_i values the upper limit on f_a can move around by typically an order of magnitude: nonetheless, an upper bound on f_a from overproduction of dark matter should obtain which is still much less than the the string/GUT scale. We also show variation in the $a - \tilde{z}_1$ dark matter relic density versus varying T_R. For the DFSZ axion model, the axino and saxion production rates in the early universe hardly depend on T_R [217] (unlike the case of the KSVZ axion model [218]). Some variation in relic density is seen for $f_a \geq 10^{14}$ GeV where gravitino production, which does depend on T_R [219], becomes important and augments the non-thermal WIMP abundance.

IV.1.3. PQ scale from the landscape

Here, we investigate whether landscape considerations can determine the magnitude of the PQ scale f_a. We assume an $n = 1$ statistical draw towards large soft terms $-A_f$ which in turn leads to large PQ scales along the lines of Fig. 21 where the PQ scale is related to the breakdown of supersymmetry. For our landscape benchmark point landSUSY, the magnitude of f_a is determined by the quartic soft term A_f. However, since $-A_f$ is not connected with EWSB, then it need not be susceptible to the same bounds on MSSM soft terms that emerge from requiring an appropriate breakdown of electroweak symmetry with independent contributions to m_{weak} not more than a factor of a few from its value $m_{weak} \simeq 100$ GeV. Instead, the PQ scale f_a is intimately related to the production of both axion dark matter and (natural) higgsino-like WIMP dark matter.

Since we are working within a multiverse scenario wherein each pocket universe may have different laws of physics, and the multiverse is an expression of the universe emerging from a spacetime continuum characterized by eternal inflation, then of course inflationary cosmology is an essential component of our overall scheme. In inflationary cosmology, the universe has an early exponential expansion phase which drives the universe to flatness, which requires an overall energy density teetering on the boundary between an open or a closed universe. Such a universe is characterized by the overall energy density lying at its critical closure density:

$$\begin{aligned} \rho = \rho_c = 3H_0^2/8\pi G_N \quad \text{or} \quad \Omega \equiv \rho/\rho_c = 1 \\ \text{with} \quad \Omega \equiv \Omega_B + \Omega_{rad} + \Omega_{DM} + \Omega_\Lambda + \Omega_{curv} \end{aligned} \tag{98}$$

and where $\Omega_{curv} = 0$ for an inflationary universe which gives rise to a flat geometry. For our pocket universe, the measured value of the Hubble constant is $H_0 = 100h$ km/s/Mpc with $h = 0.678 \pm 0.009$ but for other pocket universes then H_0 will be

different depending on the various constituencies. We will adopt as usual ρ_B/ρ_γ equal to the value of our universe since we are assuming a "friendly" fertile patch of the multiverse where the SM remains as the low energy effective theory.[23] Thus, in the fertile patch of multiverse assumed here, only Λ, m_{soft} and θ_i are assumed to scan. The scanning of the soft term A_f sets the value of f_a for otherwise fixed values of scalar masses as expected for our landSUSY benchmark point: *i.e.* we assume a common value of all scalar masses $m_0(1,2) = m_X = m_Y \equiv m_{3/2}$. We allow smaller values of $m_0(3)$ as occurs in the mini-landscape picture wherein third generation fields lie on the bulk of the compactified orbifold whilst first/second generation fields lie near orbifold fixed points [220].

The generated probability distribution for $-A_f$ is shown in Fig. 25*a*), which is seen to rise linearly as expected. For a given value of A_f, then the value of f_a is determined by the minimization conditions arising from Eq. (95). In Fig. 25*b*), we show the derived distribution dP/df_a. Here, the probability distribution is seen to favor the highest values of f_a possible, which would be generated from very large values of $-A_f$.

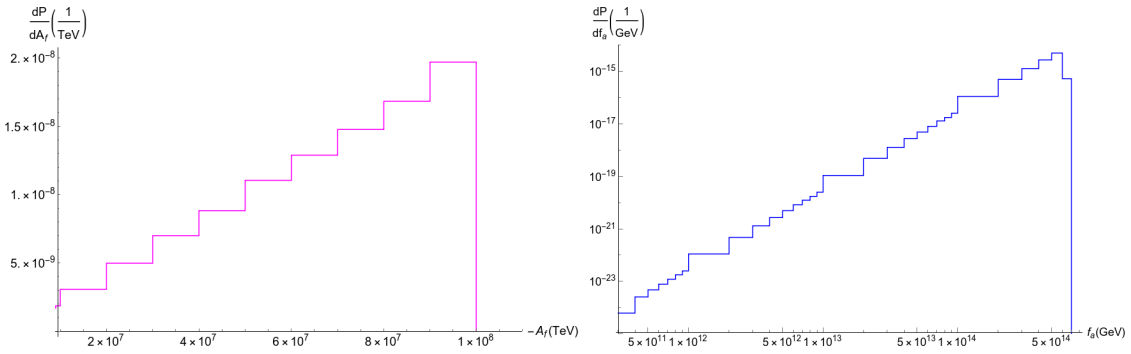

Figure 25: In *a*), we show the assumed distribution of soft SUSY breaking term $-A_f$ from an $n = 1$ statistical pull from the landscape. In *b*), we show the corresponding probability distribution in f_a.

[23] Anthropic arguments usually depend on a so-called "friendly" landscape wherein one focuses on most parameters asuming their SM values so as to retain predictivity [66]. Sometimes these are called *fertile patches* of the landscape of vacua since they should lead to the standard cosmological and particle physics models aside from just the few mass scales which may scan in the multiverse.

At this point, our prior distribution for f_a is set, but we will also need some selection criterion to avoid f_a exploding up to huge values, leading to perhaps a gross overproduction of dark matter. Thus, the question now is: how much dark matter is too much dark matter for our fertile patch of pocket universes within the greater multiverse? Some of the previous papers [209, 210, 211, 212, 213] have entertained values of ρ_{DM}/ρ_B as high as 25-100.

For illustrative purposes, we will consider the effect of limiting pocket universes to a modest bound of four times greater dark matter density than in our universe: suppose $\Omega_{\rm DM}h^2 \leq 0.48$. Such a bound would saturate the case where we maintain our measured value of ρ_c but allow the dark matter abundance to nearly saturate ρ_c at the expense of a dark energy component. Such models were commonly contemplated before the discovery of a non-zero dark energy component.

In Fig. 26a), the resulting probability distribution dP/df_a is shown which results from an $n = 1$ draw on $-A_f$ coupled to an anthropic/cosmological selection bound $\Omega_{a\tilde{z}_1}h^2 < 0.48$ (green curve). Even with our proposed modest selection bound, we see that the value of f_a is driven to its nearly maximal value such as to avoid overproduction of dark matter. From the plot, we would expect that a value of $f_a \sim 10^{14}$ GeV or only somewhat lower, with a rather sharp cutoff $f_a \leq 8 \times 10^{13}$ GeV. For comparison, we also show the black histogram where we instead require that the upper bound on dark matter abundance is only slightly beyond our measured value: $\Omega_{\rm DM} < 0.15$. This case would prefer $f_a \sim 5 \times 10^{12}$ GeV.

Let us compare the results of Fig. 26a) with those of Fig. 27 which shows the allowed mixed axion-WIMP dark matter abundance for our landSUSY benchmark point in the generic SUSY DFSZ axion model while scanning uniformly over θ_i and uniformly over $\log(f_a)$. From Fig. 27, we see that for $f_a \sim 10^{13} - 10^{14}$ GeV, we are already overproducing dark matter compared to our universe with $\Omega_{\rm DM}h^2 = 0.12$. There is only a miniscule probability to obtain from Fig. 26a) f_a values low enough to match

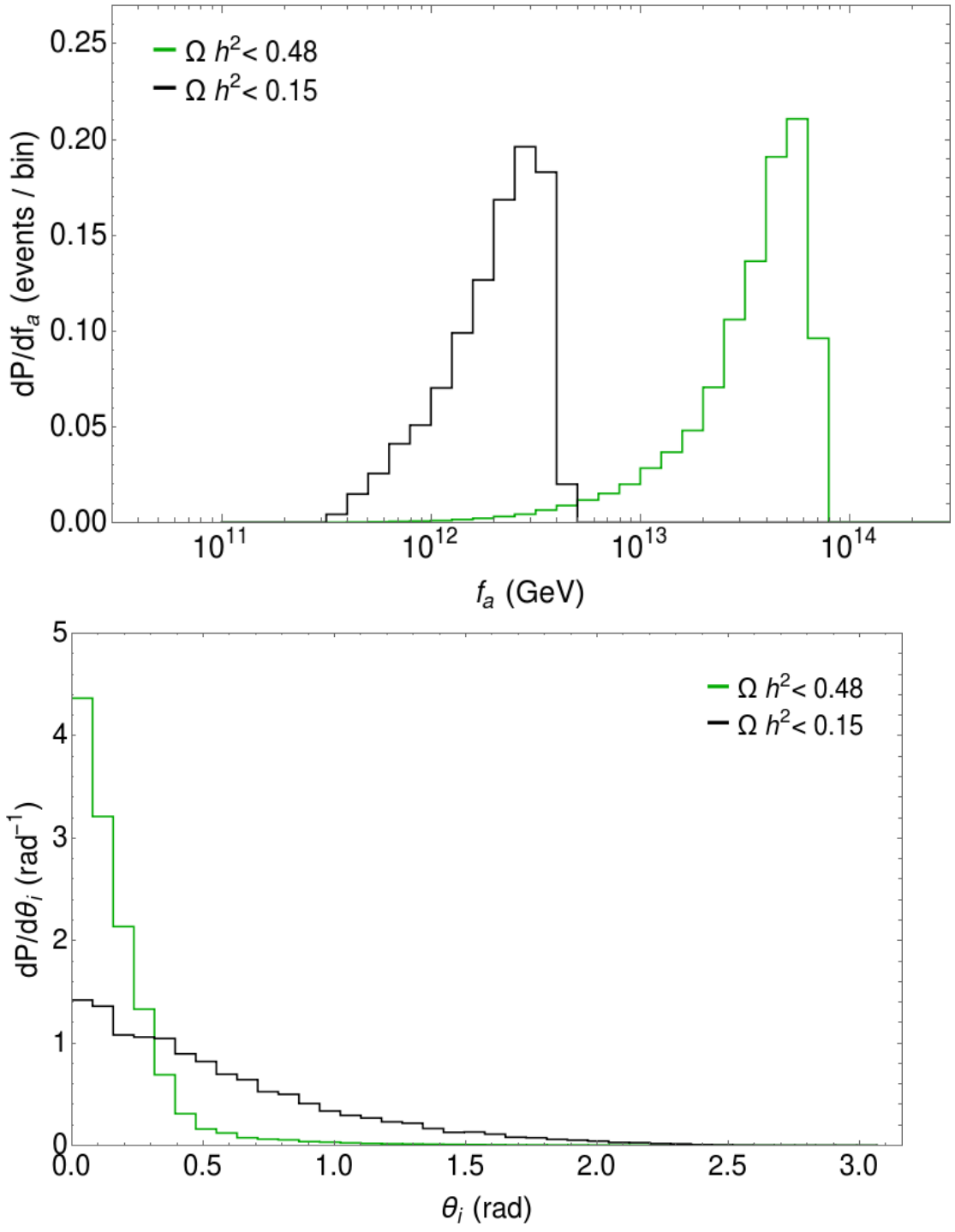

Figure 26: Probability distribution in *a*) f_a and *b*) θ_i assuming an $n = 1$ statistical pull on the soft SUSY breaking term $-A_f$ from the landscape and requiring no more than a factor four more DM (green) or else $\Omega_{\rm DM}h^2 \leq 0.15$ (black).

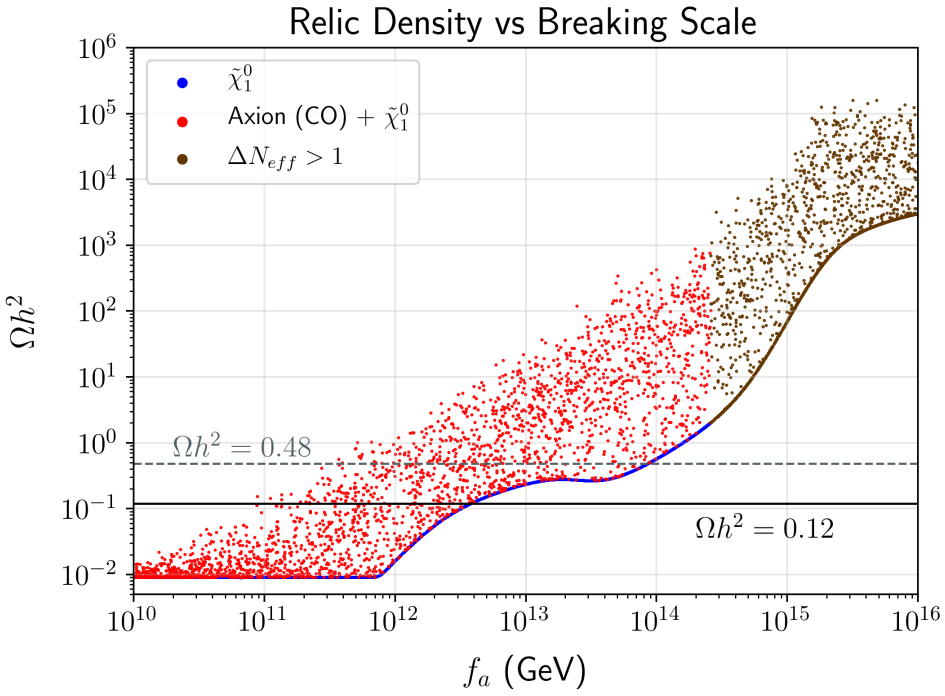

Figure 27: Range of relic density values for axion and higgsino-like WIMP dark matter versus f_a from uniform scan over θ_i with $m_{\tilde{a}} = m_s = 16$ TeV in the SUSY DFSZ axion model. (The blue points lie along the lower boundary of plotted points.)

the measured value, which occurs for $f_a \sim 10^{11} - \sim 4 \times 10^{12}$ GeV. In the previous works [209, 210, 211, 212, 213], large values of $f_a \sim 10^{14} - 10^{16}$ GeV could be compensated for by selecting on small values of θ_i. For our case of natural mixed axion-WIMP dark matter, this compensation is not permitted because large f_a also leads to large (non-thermal) overproduction of WIMP dark matter via delayed axino and saxion decays in the early universe. From Fig. 26*a*), we would expect that if the landscape is involved in determining the PQ scale f_a, then its value should be very near the maximally allowed abundance of DM in pocket universes such as to allow observers to exist. But it is hard to believe that our pocket universe's value of dark matter abundance is nearly anthropically maximal (as depicted by the black curve of Fig. 26*a*).

In Fig. 26*b*), we show the corresponding distribution $dP/d\theta_i$ from the $n = 1$ pull on soft terms coupled with our modest anthropic veto that $\Omega_{\rm DM}h^2 < 0.48$. The plot

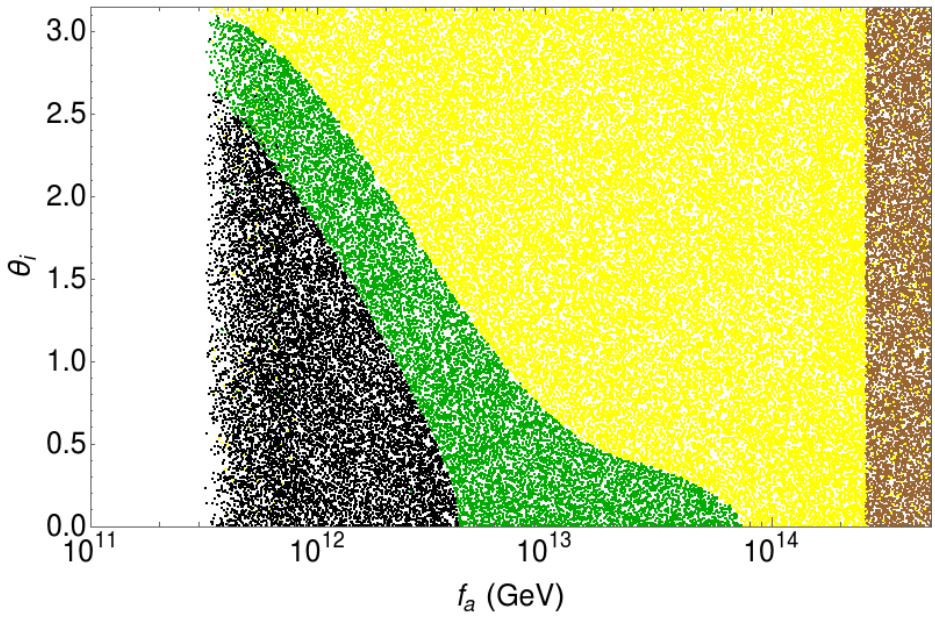

Figure 28: Allowed and disallowed (yellow) points in the f_a vs. θ_i plane assuming a modest selection bound of $\Omega_{\rm DM}h^2 < 0.48$ (green) and $\Omega_{\rm DM}h^2 < 0.15$ (black).

shows a probability that θ_i is peaked around its smallest allowed values. This is easy to understand in that while the landscape prior strongly favors large values of f_a, from Eq. 97 we see that overproduction of axions can be avoided by selecting only those vacua with correspondingly tiny values of θ_i. This effect is easily understood from Fig. 28 where we show regions of the θ_i vs. f_a plane for our landSUSY benchmark point which lead to $\Omega_{\rm DM}h^2 < 0.48$ (green points) or $\Omega_{\rm DM}h^2 > 0.48$ (yellow points). The brown points denote where also $\Delta N_{eff} > 1$. From the figure, we see that for large $f_a \sim 8 \times 10^{13}$ GeV, only a small range of θ_i allows for non-overproduction of dark matter. And once $f_a \geq 8 \times 10^{13}$ GeV, then no value of θ_i is possible which allows one to avoid DM overproduction.

IV.1.4. Prediction of PQ scale from generic SUSY DFSZ axion model with uniform scan on θ_i

In Sec. IV.1.1, we adopted a particular gravity-safe SUSY axion model based on a $\mathbb{Z}_{24}^R$ discrete R-symmetry. The hyCCK superpotential in Eq. (93) shows that a statistical draw towards large soft terms also yields a draw to large PQ breaking scale f_a. The value of f_a gains an upper bound by requiring no overproduction of dark matter. For the modest assumption of less than a factor four times the measured abundance of dark matter, then we found $f_a \sim 10^{14}$ GeV which is well below the values expected from pre-landscape string theory but which typically leads to much more dark matter production than we observe in our universe.

In this section, we try to be more general by eschewing a particular SUSY axion model and instead assume a generic SUSY DFSZ axion model[177, 176] where f_a is an input instead of an output parameter. In this case, we will adopt a uniform distribution in θ_i in accord with expectations from the landscape, but then require that the dark matter abundance lie at its measured value: $\Omega_{a\tilde{z}_1}h^2 = 0.12$. From this, we can then determine the necessary value of f_a such that, for scanned values of $m_{\tilde{a}}$, m_s and $m_{3/2}$, the measured abundance of mixed axion-neutralino dark matter is obtained. We will scan uniformly over each of $m_{\tilde{a}},\ m_s$ and $m_{3/2} : 1 - 50$ TeV.

For a SUSY benchmark point within a two-component dark matter framework, direct and indirect WIMP dark matter searches can put a stringent upper limits upon the neutralino density which are more severe than the measured value, $\Omega_{\rm DM}h^2 = 0.12$. In many cases, indirect DM detection (IDD) offers the most contraining limits on the non-thermal, decay-produced neutralinos for models with thermally underproduced higgsino-like neutralinos. In natural SUSY models from the $n = 1$ landscape, thermally produced neutralinos typically make up 5-20% of the total CDM density which renders them safe from Fermi-LAT+MAGIC[85] limits on overproduction of gamma

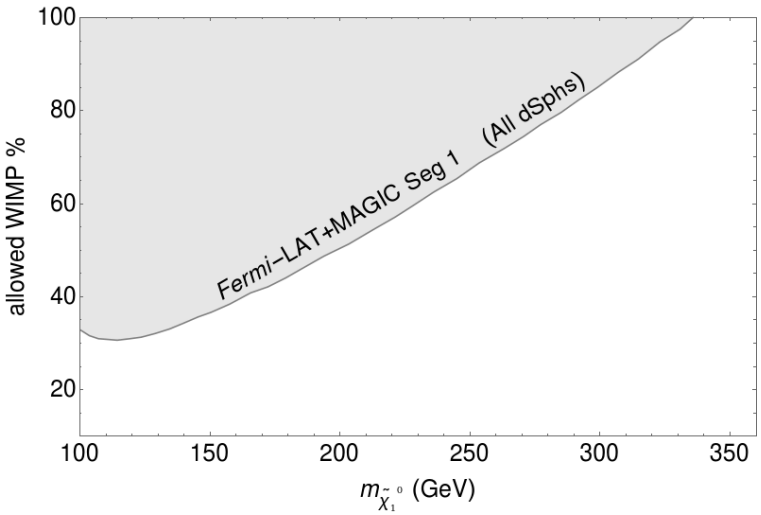

Figure 29: Percent of neutralino dark matter contributing to total dark matter vs. $m_{\tilde{z}_1} \simeq \mu$ compared to recent limits from Fermi-LAT+MAGIC bounds on gamma rays from dwarf spheroidal galaxies.

rays in dwarf spheroidal galaxies[119]. In Fig. 29, we show the allowed percentage of WIMP dark matter compared to $m_{\tilde{z}_1}$ along with the Fermi-LAT+MAGIC IDD limit for our landSUSY benchmark point. If we increase $\mu \sim 340$ GeV, then $m_{\tilde{z}_1} \sim 340$ GeV and all generated points would be Fermi-LAT+MAGIC allowed. The gray-shaded region shows the excluded WIMP composition for all landSUSY points within a good approximation.

In Fig. 30, we work within the SUSY DFSZ axion model using again our landSUSY benchmark point but with input parameters $m_s,\ \theta_s,\ \theta_i,\ f_a,\ T_R$ and $m_{3/2}$. Here, we fix $T_R = 10^7$ GeV and $\theta_s = 1$ but allow m_s, $m_{\tilde{a}}$ and $m_{3/2}$ to scan over the range given above with a uniform scan on θ_i and a log prior scan on f_a. We only accept solutions with $\Omega_{a\tilde{z}_1}h^2 = 0.12$. We show the parameter space with augmented neutralino densities $\Omega_{\tilde{z}_1}h^2 < 0.12, 0.06$ and 0.03 with black, orange and purple colors respectively. We impose an upper limit on θ_i ($\theta_i < 3.14$) so that the highly fine-tuned region $\theta_i \simeq \pi$ is not present in our analysis.

In Fig. 30 frame *a*), the resulting abundance of neutralino dark matter is shown while

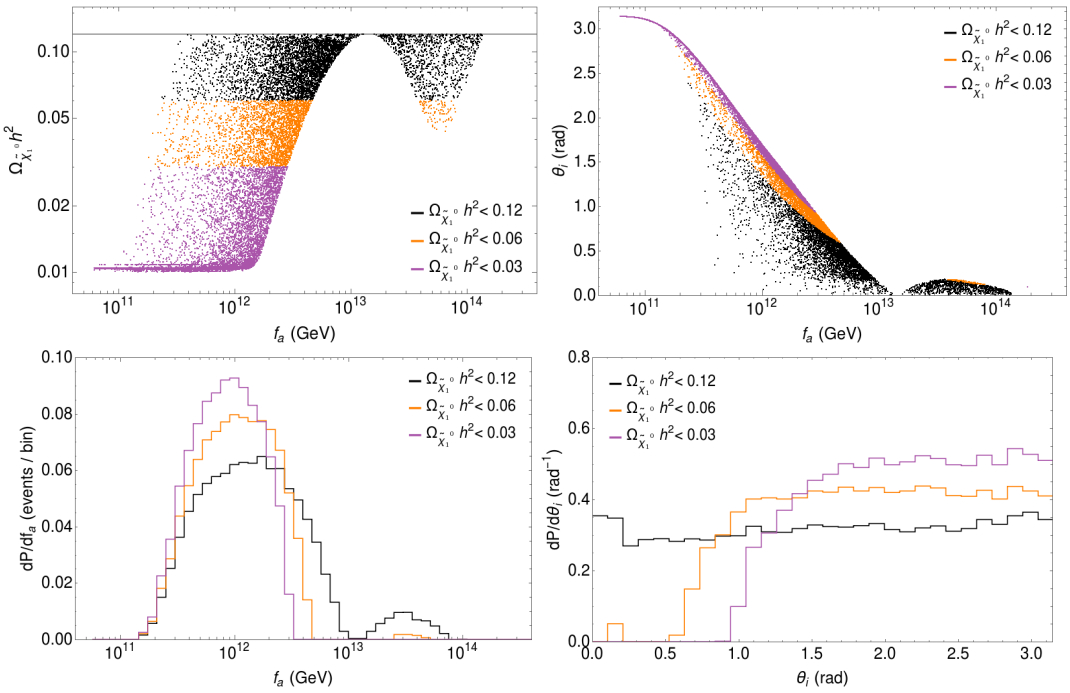

Figure 30: In *a*), we plot the value of $\Omega_{\tilde{z}_1}h^2$ versus f_a from a uniform scan over θ_i : $0 \to 3.14$ (and $m_{\tilde{a}}$, m_s and $m_{3/2}$). In *b*), we show the corresponding correlation of θ_i vs. f_a. In *c*), we show the ensuing probability distribution for f_a. In *d*), we show the probability distribution in θ_i after selection effects. In all the frames, we require the total abundance of DM to equal its measured value: $\Omega_{a\tilde{z}_1}h^2 = 0.12$.

the remainder of DM is made of DFSZ axions. The horizontal line around $f_a \lesssim 10^{11}$ GeV is just the expected thermal abundance of 200 GeV higgsino-like WIMP dark matter. For higher $f_a > 10^{11}$ GeV, then non-thermal LSP production begins to occur where axinos can be produced in the early universe and decay to LSPs after neutralino freeze-out. There is a gap around $f_a \sim 10^{13}$ GeV where axino decays are still contributing to the neutralino density. For $f_a \sim 10^{14}$ GeV, points again become allowed due to diminished thermal production of axinos in the early universe. The WIMP abundance increases for $f_a \geq 10^{14}$ GeV due to increasing CO-production of saxions which then decay (in part) to WIMPs[177, 176]. An upper limit of $f_a \leq 2 \times 10^{14}$ GeV ensues in this case since for large f_a, the DM is always overproduced. There is no conflict here with Fig. 27 since in this case with random values of m_s and $m_{\tilde{a}}$, then relative axino and

saxion production and decay rates can vary which leads to allowed points for $f_a \sim 10^{14}$ GeV.

The corresponding correlation of θ_i with the required value of f_a to make $\Omega_{a\tilde{z}_1} = 0.12$ is shown in frame *b*). Here, large values of θ_i are correlated with low values of f_a to boost the axion production to gain accord with the measured relic abundance. For very large f_a, then consequently small values of θ_i are required to allow for $\Omega_{a\tilde{z}_1}h^2 = 0.12$.

In frame *c*), we show the resulting probability distribution dP/df_a versus f_a. Including all points with the measured abundance, then one obtains the black histogram which peaks around $f_a \sim 2\times 10^{12}$ GeV but with a tail extending to over 10^{14} GeV. For the cases in which neutralino makes less than half of the measured DM density, the peak shifts to lower values of f_a (orange and purple histograms) with a small probability at high f_a.

In frame *d*), we show the probability distribution $dP/d\theta_i$ for the three cases considered. Here, the black histogram is almost uniform across its range whilst the orange histogram displays a gap at small θ_i where no allowed solutions occur. The high f_a region does not show up for $\Omega_{\tilde{z}_1}h^2 \lesssim 0.04$ and θ_i can only take values greater than $\sim$1 when the neutralino makes less than 25% of the total DM abundance (purple).

Summary : In this section, we have sought to answer the question: is the magnitude of the PQ scale f_a set by the landscape, or by something else? To address this question, we have adopted the scenario advocated by Douglas wherein the soft terms are statistically favored by a prior distribution $m_{soft}^{2n_F+n_D-1}$ and where we take the value $n = 2n_F + n_D - 1 = 1$ (*i.e.* a linear distribution favoring large soft SUSY breaking terms). Along with this prior distribution, we invoke a selection criteria that vetos models with inappropriate EW breaking (CCB minima or no EWSB) and vetos models with contributions to the weak scale ≥ 4 (corresponding to $\Delta_{\rm EW} > 30$) in accord with nuclear physics constraints derived by Agrawal *et al.* on anthropically allowed values

for the weak scale. We implement this approach within a highly motivated SUSY axion model labeled as hyCCK. By choosing a MSSM benchmark point in accord with $n = 1$ landscape predictions and allowing for the PQ soft term $-A_f$ to scan linearly and to set the magnitude of the PQ scale f_a, then we find that as large as possible values of f_a are statistically preferred. In this approach, typically both WIMP and axion dark matter are overproduced. Though Axion overproduction at large f_a can be compensated by a small misalignment angle θ_i, since WIMPs are also overproduced at large f_a, due to axino and saxion production coupled with delayed decays to SUSY LSPs after neutralino freeze-out (*i.e.* non-thermal WIMP production), then even with small θ_i one cannot avoid overproduction of mixed axion-WIMP dark matter. Thus, the answer to the question posed in the title is: No, in our well-motivated landscape SUSY model based upon gravity-safe, electroweak natural hyCCK SUSY axion model, the magnitude of the PQ scale is highly unlikely to be set by the landscape.

Instead, an alternative but perhaps underappreciated mechanism is available to set the magnitude of the PQ scale. This is that in generic supergravity models with hidden sector SUGRA breaking via the superHiggs mechanism, then soft terms arise from SUGRA breaking with magnitudes of order the gravitino mass $m_{3/2}$. For a well-specified hidden sector, then the soft terms are all calculable and correlated. For our landscape SUSY model with $m_0(1,2) \sim m_{3/2}$, we would also expect $-A_f \sim m_{3/2} \sim 10 - 100$ TeV. This places us from Fig. 21 into the zone where $f_a \sim 10^{11} - 10^{12}$ GeV which is the sweet spot for generating a thermal underabundance of higgsino-like WIMP dark matter but with mainly SUSY DFSZ axion dark matter.

IV.2. A landscape solution to the SUSY flavor and CP problems

As mentioned in the beginning of Sec. IV, mild statistical draw towards large soft SUSY breaking terms with $n = 1$(linear) or $n = 2$(quadratic), augmented with atomic principle $m_Z^{PU} < 4\, m_Z^{OU}$ along with a natural value of μ (that translates into naturalness

condition $\Delta_{EW} < 30$), in NUHM3 model has proven to be preferred over uniform distribution of the soft breaking terms (i.e., $n = 0$) by LHC Higgs and sparticles mass constraints. However, beside satisfying the LHC Higgs and sparticles mass constraints, it also pulls the first and second generation matter scalars (squarks and sleptons) up to $m(\tilde{q}, \tilde{\ell}) \sim 20 \pm 10$ TeV. It must be noted here that the first and second generation matter scalars are drawn independently to the multi-TeV regime where the upper cutoff arises from two-loop RGE terms which drive third generation soft masses towards tachyonic values. Since the upper bounds on $m_0(1, 2)$ are the same for each generation, and flavor independent, then these will be drawn toward quasi-degenerate values. In this section, we shall see how the presence of such heavy sfermions are advantageous for a SUSY model in that they provide a mixed decoupling/quasi-degeneracy solution to the SUSY flavor problem and a decoupling solution to the SUSY CP problem.

IV.2.1. Living dangerously with heavy sfermions

In Sec I.6 it has been emphasized that Douglas' general stringy considerations imply a statistical draw towards large soft terms. It has also been mentioned earlier that the soft terms cannot become arbitrarily large without leading to non-standard EW vacua or else too large of a value of pocket universe weak scale m_Z^{PU}: such vacua must be anthropically vetoed. Here, we concern ourselves with the upper bound on matter sfermion masses for the first two generations, which we label according to high-scale soft term values $m_0(1)$ and $m_0(2)$. For simplicity, we will assume all high scale matter sfermion masses within a single generation are degenerate (as is expected in models containing some remnant $SO(10)$ GUT symmetry). These could be placed for context within the i-extra parameter non-universal Higgs models [40] (NUHMi, $i = 2 - 4$). In NUHM2 $m_0(1) = m_0(2) = m_0(3)$ while in NUHM3 $m_0(1) = m_0(2) \neq m_0(3)$. Here, NUHM4 is considered since we are allowing for splittings between first and second generation masses (as well as the third) *i.e.* $m_0(1) \neq m_0(2) \neq m_0(3)$. But we will also

allow for the presence of off-diagonal soft term masses. To make contact with general constraints from SUSY flavor and CP violating processes, as presented for instance in Ref's [223], [224], [225] and [226]. we will work within the superCKM mass basis wherein the quark and lepton mass matrices are diagonal but the squark and slepton mass matrices are not yet diagonalized.

From a scan over NUHM3 parameter space in Ref. [77], it was found that the statistical distribution of first/second generation sfermion masses for $n = 1$ or 2 was peaked around $m_{\tilde{f}} \sim 20$ TeV but with tails extending as far as 40 TeV. What sets the upper bound for such sfermion masses?

At first sight, the Σ_u^u and Σ_d^d terms contain first/second generation D-term contributions to the EW scale. For first/second generation sfermions, neglecting the small Yukawa couplings, we find the contributions

$$\Sigma_{u,d}^{u,d}(\tilde{f}_{L,R}) = \mp \frac{c_{col}}{16\pi^2} F(m^2_{\tilde{f}_{L,R}}) \left(-4g_Z^2(T_3 - Q_{em}x_W)\right), \tag{99}$$

where T_3 is the weak isospin, Q_{em} is the electric charge assignment (taking care to flip the sign of Q_{em} for right-sfermions), $c_{col} = 1(3)$ for color singlet (triplet) states, $x_W \equiv \sin^2\theta_W$ and where

$$F(m^2) = m^2\left(\log\frac{m^2}{Q^2} - 1\right). \tag{100}$$

We adopt an optimized scale choice $Q^2 = m^2_{\rm SUSY} \equiv m_{\tilde{t}_1} m_{\tilde{t}_2}$.[24] The explicit first generation squark contributions to Σ_u^u (neglecting the tiny Yukawa couplings) are given by

$$\Sigma_u^u(\tilde{u}_L) = \frac{3}{16\pi^2} F(m^2_{\tilde{u}_L}) \left(-4g_Z^2(\frac{1}{2} - \frac{2}{3}x_W)\right)$$
$$\Sigma_u^u(\tilde{u}_R) = \frac{3}{16\pi^2} F(m^2_{\tilde{u}_R}) \left(-4g_Z^2(\frac{2}{3}x_W)\right)$$

[24]The optimized scale choice is chosen to minimize the log contributions to $\Sigma_u^u(\tilde{t}_{1,2})$ which occur to all orders in perturbation theory.

$$\Sigma_u^u(\tilde{d}_L) = \frac{3}{16\pi^2} F(m^2_{\tilde{d}_L}) \left(-4g_Z^2(-\frac{1}{2} + \frac{1}{3}x_W) \right)$$
$$\Sigma_u^u(\tilde{d}_R) = \frac{3}{16\pi^2} F(m^2_{\tilde{d}_R}) \left(-4g_Z^2(-\frac{1}{3}x_W) \right).$$

These contributions, arising from electroweak D-term contributions to masses, are frequently neglected since the various contributions cancel amongst themselves in the limit of mass degeneracy due to the fact that weak isospins and electric charges (or weak hypercharges) sum to zero in each generation. However, if squark and slepton masses are in the multi-TeV regime but are *non-degenerate* within each generation, then the contributions may be large and non-cancelling. In this case, they may render a theory which is otherwise considered to be natural, in fact, unnatural.

The first generation slepton contributions to Σ_u^u are given by

$$\Sigma_u^u(\tilde{e}_L) = \frac{1}{16\pi^2} F(m^2_{\tilde{e}_L}) \left(-4g_Z^2(-\frac{1}{2} + x_W) \right)$$
$$\Sigma_u^u(\tilde{e}_R) = \frac{1}{16\pi^2} F(m^2_{\tilde{e}_R}) \left(-4g_Z^2(-x_W) \right)$$
$$\Sigma_u^u(\tilde{\nu}_L) = \frac{1}{16\pi^2} F(m^2_{\tilde{\nu}_{eL}}) \left(-4g_Z^2(\frac{1}{2}) \right);$$

these may also be large for large $m^2_{\tilde{\ell}}$ although again they cancel amongst themselves in the limit of slepton mass degeneracy.

In our evaluation of Δ_{EW}, in fact we sum all contributions from a complete generation before including them into Δ_{EW}. This allows for complete D-term cancellations in the limits of weak scale sfermion degeneracy. Of course, the sfermions are not completely degenerate at the weak scale even if they begin as degenerate at the high scale $Q \equiv m_{GUT}$ due at least to weak scale D-term contributions to their masses. We have evaluated these contributions and find they lead to upper bounds on $m_0(1,2) \leq 5000$ TeV for $\Delta_{EW} < 30$, so that these D-terms do not set the upper limits on first/second generation sfermion masses.

A stricter constraint on first/second generation sfermion masses from the landscape

comes from 2-loop RGE contributions to the running of sfermion masses. The form of the two loop RGEs for sfermion masses is given by

$$\frac{dm_i^2}{dt} = \frac{1}{16\pi^2}\beta_{m_i^2}^{(1)} + \frac{1}{(16\pi^2)^2}\beta_{m_i^2}^{(2)}, \tag{101}$$

where $t = \ln Q$, $i = Q_j,\ U_j,\ D_j,\ L_j$ and E_j, and $j = 1-3$ is a generation index. The one loop β-function for the evolution of *third* generation scalar masses depends only on third generation and Higgs scalar masses and on the gaugino masses. The two loop terms are formally suppressed relative to one loop terms by the square of a coupling constant as well as an additional loop factor of $16\pi^2$. However, these two loop terms include contributions from *all* scalars. Specifically, the two loop β functions include [228]

$$\beta_{m_i^2}^{(2)} \ni a_i g_3^2\sigma_3 + b_i g_2^2\sigma_2 + c_i g_1^2\sigma_1, \tag{102}$$

where

$$\begin{aligned}
\sigma_1 &= \frac{1}{5}g_1^2\{3(m_{H_u}^2 + m_{H_d}^2) + Tr[\mathbf{m}_Q^2 + 3\mathbf{m}_L^2 + 8\mathbf{m}_U^2 + 2\mathbf{m}_D^2 + 6\mathbf{m}_E^2]\},\\
\sigma_2 &= g_2^2\{m_{H_u}^2 + m_{H_d}^2 + Tr[3\mathbf{m}_Q^2 + \mathbf{m}_L^2]\}, \quad \text{and}\\
\sigma_3 &= g_3^2 Tr[2\mathbf{m}_Q^2 + \mathbf{m}_U^2 + \mathbf{m}_D^2],
\end{aligned}$$

and the $\mathbf{m}_i^2$ are squared mass matrices in generation space. The numerical coefficients a_i, b_i and c_i are related to the quantum numbers of the scalar fields, but are all positive quantities.

Thus, incorporation of multi-TeV masses for the first and second generation scalars leads to an overall positive, *possibly dominant*, contribution to the slope of third generation soft mass trajectories versus energy scale. Although formally a two loop effect, the smallness of the couplings is compensated by the much larger values of masses of the first two generations of scalars. In running from $m_{\rm GUT}$ to $m_{\rm weak}$, this results in

an overall *reduction* in third generation scalar masses. In fact, this effect was argued in Ref. [229] to lead to violation of naturalness constraints from a decoupling solution to the SUSY flavor problem. It was also used in Ref's [230] and [231] to generate SUSY models with an inverted scalar mass hierarchy to reconcile naturalness with a decoupling solution to the SUSY flavor and CP problems along the lines of "effective supersymmetry"[232]. For values of sfermion masses which fall short of tachyonic, a sort of see-saw effect amongst scalar masses occurs: the higher the value of first and second generation scalar masses, the larger will be the two loop suppression of third generation and Higgs scalar masses. In this class of models, first and second generation scalars with masses of order $10-40$ TeV may co-exist with TeV-scale third generation scalars, thus giving a very large suppression to both FCNC and CP violating processes while driving third generation sfermions to natural values.

In the context of our string landscape picture, this is yet another example of living dangerously[25], wherein soft terms are pulled to large values which actually *increases the naturalness of the theory* so long as we stop short of impending disaster: which in this case would be that huge first/second generation sfermion masses might drive third generation masses tachyonic leading to CCB vacua.

The situation is illustrated in Fig. 31 where we adopt the NUHM3 model to plot the value of Δ_{EW} versus $m_0(1,2)$ for $m_{1/2}=1200$ GeV, $A_0=-1.6m_0(3)$ and $\tan\beta=10$ with $\mu=200$ GeV and $m_A=2000$ GeV. We also take $m_0(3)=5$, 7.5 and 10 TeV (blue/orange, green and red curves, respectively). From the plot we see that as $m_0(1,2)$ increases, the models are driven to greater naturalness in that third generation soft terms are driven to smaller values by large two-loop RGE contributions. As $m_0(1,2)$ increases even further, then cancellations with the $\Sigma_u^u(\tilde{t}_{1,2})$ terms are disrupted and the models again become more unnatural, leading to too large of contributions to the

[25]Arkani-Hamed and Dimopoulos [66] state: "anthropic reasoning leads to the conclusion that we live dangerously close to violating an important but fragile feature of the low-energy world...", in this case, appropriate electroweak symmetry breaking.

pocket universe weak scale m_Z^{PU}. For even higher $m_0(1,2)$ values, then top squark soft terms are driven tachyonic leading to CCB vacua.

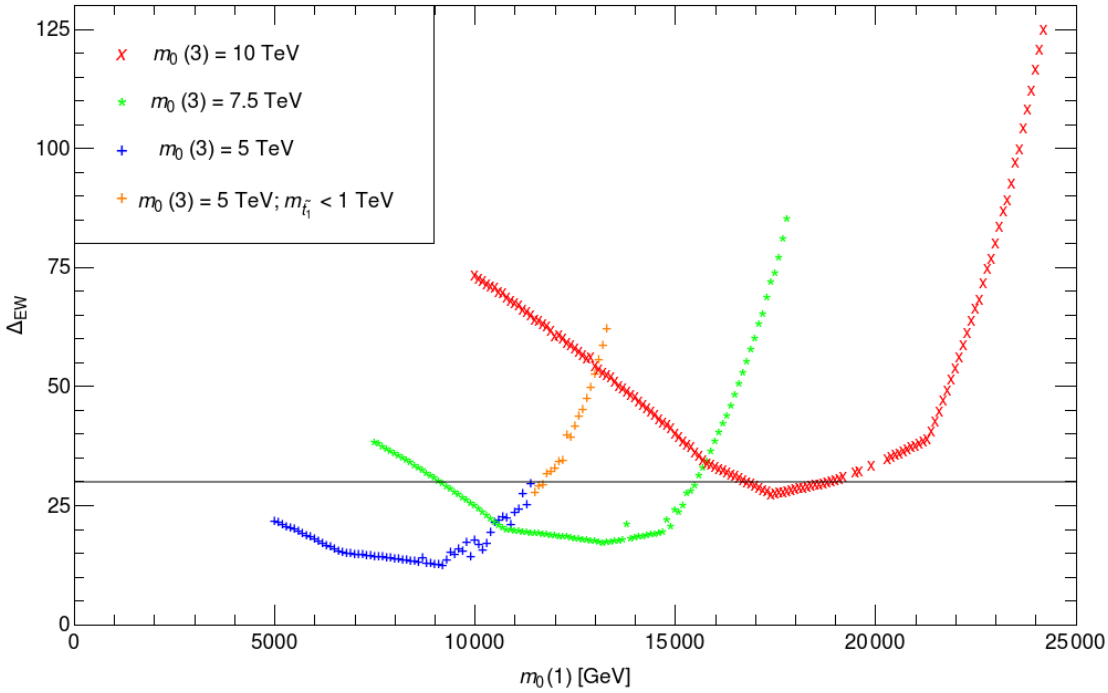

Figure 31: We plot the value of Δ_{EW} vs. $m_0(1,2)$ for $m_0(3) = 5$, 7.5 and 10 TeV and $m_{1/2} = 1200$ GeV, $A_0 = -1.6m_0(3)$ and $\tan\beta = 10$ with $\mu = 200$ GeV and $m_A = 2000$ GeV.

An important point is that for particular parameter values, we do gain an upper bound on first/second generation soft terms. The upper bound changes within parameter space variation, but depends only on gauge quantum numbers, so it is the same for both generations one and two. Thus, the first and second generation soft masses are pulled to large values by the landscape, but with the same upper bounds. This means that for strong enough pull, then $m_0(1)$ and $m_0(2)$ will be pulled to similar upper limits. If the pull is strong enough, they will be pulled towards quasi-degeneracy, which helps, along with decoupling, to solve the SUSY flavor problem.

IV.2.2. SUSY flavor problem

In the SM, a fourth quark, charm, was posited in order to suppress flavor changing neutral current (FCNC) processes, for which there were strict limits [233]. In a successful application of practical naturalness, Gaillard and Lee [234] required the charm-quark box diagram contribution to the $m_{K_L} - m_{K_S} \equiv \Delta m_K$ mass difference to be less than the measured value of Δm_K itself: this lead to the successful prediction that 1 GeV $< m_c <$ 2 GeV shortly before the charm quark discovery.

By supersymmetrizing the SM into the MSSM, then many new parameters are introduced, mainly in the soft SUSY breaking sector [235]. These include sfermion mass matrices

$$\mathcal{L}_{soft} \ni -\tilde{f}_i^\dagger (\mathbf{m_f^2})_{ij} \tilde{f}_j \tag{103}$$

where i and j are generation indices $i, j = 1 - 3$ and the sfermion index $\tilde{f}$ runs over the various matter superfields $\hat{Q}$, $\hat{U}^c$, $\hat{D}^c$, $\hat{L}^c$ and $\hat{E}^c$ in the notation of Ref. [13]. There are also trilinear soft terms that can contribute to flavor violation:

$$\mathcal{L}_{soft} \ni (\mathbf{a}_u)_{ij} \epsilon_{ab} \tilde{Q}_i^a H_u^b \tilde{u}_{Rj}^\dagger + (\mathbf{a}_d)_{ij} \tilde{Q}_i^a H_{da} \tilde{d}_{Rj}^\dagger + + (\mathbf{a}_e)_{ij} \tilde{L}_i^a H_{da} \tilde{e}_{Rj}^\dagger + h.c. \tag{104}$$

In gravity mediation, the trilinears are expected to be proportional to the corresponding Yukawa couplings so that these terms are small for first/second generation values. We will thus focus mainly on the mass matrices in Eq. (103).

In the superCKM basis, the 6×6 sfermion mass matrices are built out of 3×3 LL, RR, LR and RL sub-matrices which have the form *e.g.*[26]

$$(\mathbf{m}_{\tilde{f}}^2)_{LL} = \begin{pmatrix} (m_{f1}^2)_{LL} & (\Delta_{12}^f)_{LL} & (\Delta_{13}^f)_{LL} \\ (\Delta_{21}^f)_{LL} & (m_{f2}^2)_{LL} & (\Delta_{23}^f)_{LL} \\ (\Delta_{31}^f)_{LL} & (\Delta_{32}^f)_{LL} & (m_{f3}^2)_{LL} \end{pmatrix} \tag{105}$$

[26]For a more detailed review, see Ref. [226].

with $(m^2_{\tilde{U}})_{LL} = V^u_L \mathbf{m}^2_Q V^{u\dagger}_L$, $(m^2_{\tilde{U}})_{RR} = V^u_R \mathbf{m}^{2T}_U V^{u\dagger}_R$ and $(m^2_{\tilde{U}})_{LR} = -\frac{v \sin\beta}{\sqrt{2}} V^u_L \mathbf{a}^*_U V^{u\dagger}_R$ *etc.* and where the CKM matrix is given by $V_{KM} = V^u_L V^{d\dagger}_L$. For mass matrices proportional to the unit matrix $\mathbf{m}^2_{\tilde{f}} = m^2_{\tilde{f}} \mathbf{1}$ (flavor universality), then no flavor-changing transitions are allowed and the SUSY flavor problem is solved. But for gravity-mediation, no known principles enforce flavor universality because the transformation that diagonalizes the quark mass matrices does not simultaneously diagonalize the corresponding squark mass squared matrices. In that case, then the off-diagonal mass matrix contributions Δ^f_{ij} may contribute to FCNC processes via mass insertions, and furthermore, non-degenerate diagonal terms can also lead to FCNC effects [236]. Constraints on the off-diagonal terms are typically listed in terms of dimensionless quantities $(\delta^f_{ij})_{LL,RR,LR,RL} \equiv \frac{(\Delta^f_{ij})_{LL,RR,LR,RL}}{\tilde{m}^2}$ where the $\tilde{m}$ represent an averaged sfermion mass for the corresponding mass matrix.

First we concentrate on limits for flavor-changing off-diagional mass matrix elements as they vary from the weak scale on into the decoupling regime. In Fig. 32, we list the most restrictive limits on several Δ_{ij} quantities arising from Δm_K constraint [237, 238, 239] and also from updated branching fraction limits on $\mu \to e\gamma$ decay: $BF(\mu \to e\gamma) < 4.2 \times 10^{-13}$ at 90% CL [240]. We plot Fig. 32 for $m^2_{\tilde{g}} \sim .3 m^2_{\tilde{q}}$ for Δm_K constraints and $m^2_{\tilde{z}_1} = 0.3 m^2_{\tilde{\ell}}$ although the constraints only depend weakly on these mass ratios [225, 224]. From Fig. 32, we see that for sfermion masses of order the weak scale ~ 100 GeV, then the updated $\mu \to e\gamma$ branching fraction now slightly pre-empts the Δm_K constraints although all require off-diagonal mass terms less than $1 - 10$ GeV. These limits exemplify the SUSY flavor problem from days gone by when sparticles were expected to occur around the weak scale. As $m_{\tilde{f}}$ increases, then the restrictions on off-diagonal masses become increasingly mild, thus illustrating the onset of the decoupling solution to the SUSY flavor problem. For large sfermion masses, then the Δm_K constraint is again most confining. For $m_{\tilde{f}} \sim 10$ TeV, the off-diagonal masses are constrained to be $\leq 1 - 10$ TeV while for landscape SUSY masses, where first/second generation sfermions are expected in the $20 - 30$ TeV range, then the off-diagonal limits

are $\leq 5 - 50$ TeV. Such values are only mildly suppressed compared to the average squark/slepton masses although one must proceed into the $m_{\tilde{f}} \sim 100$ TeV range for unfettered flavor violation [229].

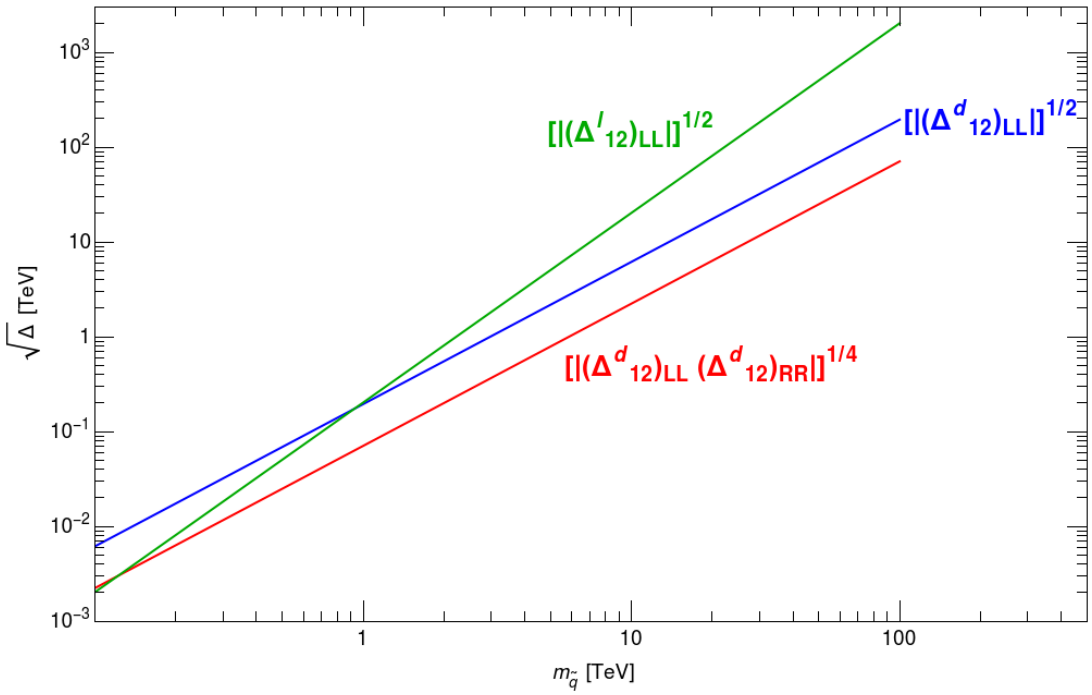

Figure 32: Upper limits on off-diagonal squark mass terms from Δm_K constraints (blue and red) and off-diagonal slepton masses from $BF(\mu \to e\gamma)$ (green).

Along with limits on off-diagonal mass matrix terms, to achieve flavor universality one needs degeneracy on the diagonal. Limits on degeneracy have been computed in Misiak *et al.* [226]. From the Δm_K constraint, for the first two generations of squarks these amount to

$$|m_{\tilde{q}1} - m_{\tilde{q}2}| \leq 2m_c m_{\tilde{q}}^2/m_W^2 \tag{106}$$

for both up and down squarks. Thus, for sparticle masses of order m_W, splittings of only a few GeV are allowed and we must be in a state of near degeneracy. As $m_{\tilde{q}}$ increases, then these bounds become much weaker.

The situation is shown in Fig. 33 where we plot the GUT scale values of the first

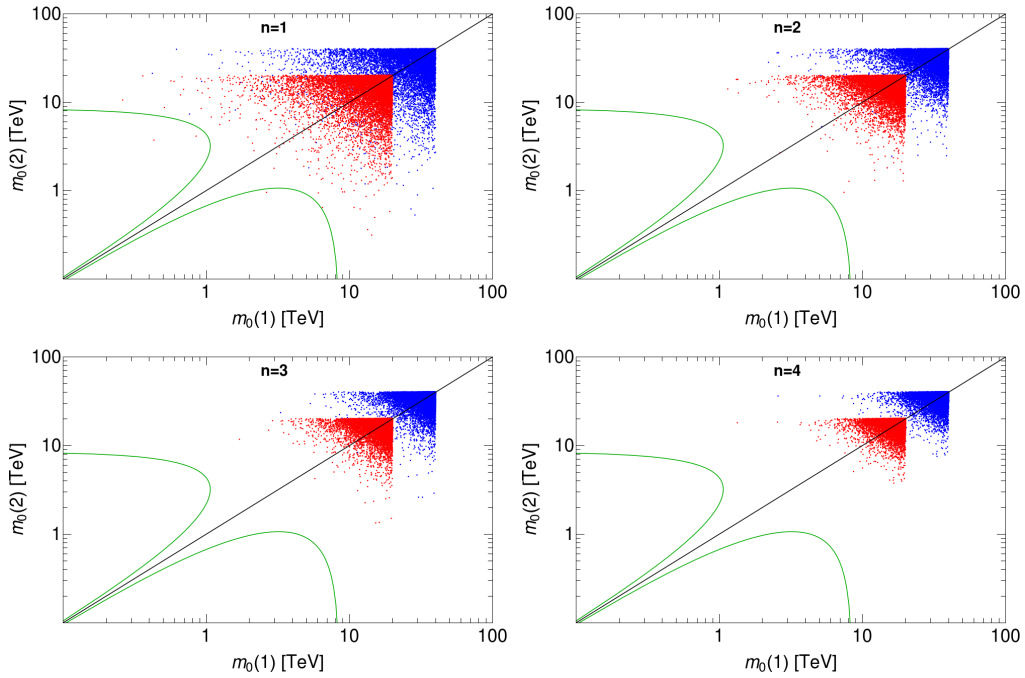

Figure 33: The values of $m_0(2)$ vs. $m_0(1)$ from an *a*) $n = 1$, *b*) $n = 2$, *c*) $n = 3$ and *d*) $n = 4$, statistical selection of first and second generation matter scalar soft terms. The lower-left of green curves is excluded while red points denote soft terms scanned up to 20 TeV while blue points show points scanned up to 40 TeV.

two generation sfermion masses $m_0(2)$ vs. $m_0(1)$ (as $m_0(1,2)$ increase, then weak scale sfermion masses are nearly equal to high scale sfermion masses). The line of degeneracy is solid black, while the bounds from Misiak *et al.* are labeled in green. Here, we see that for sparticle masses of order the weak scale, then rather strict degeneracy is required. However, as $m_0(1,2)$ increase, then degeneracy is gradually relaxed until by $m_0(1,2) \sim 10$ TeV the bounds essentially disappear, showing again the decoupling solution. In each of the four frames, we also show the predicted landscape distribution of sfermion masses for a statistical draw of *a*) $n = 1$, *b*) $n = 2$, *c*) $n = 3$ and *d*) $n = 4$. We adopt particular, flavor-independent upper bounds of $m_0(1,2) < 20$ and 40 TeV since the true upper bound is parameter dependent. In frame *a*) with $n = 1$, just a few landscape points lie in the excluded region. As n increases, then there is a stronger statistical draw towards large soft terms and the sfermion masses are drawn to

flavor independent upper bounds. Thus, there is also increasing degeneracy of diagonal soft breaking terms. In this sense, the landscape provides a mixed decoupling, quasi-degeneracy solution to the SUSY flavor problem. For higher n values, then none of the landscape points lie in the excluded region.

IV.2.3. SUSY CP problem

Limits can also be placed on complex valued soft terms due to their inducement of CP violating effects on ϵ and ϵ'/ϵ in the kaon system and also from neutron (d_n) and electron (d_e) electric dipole moments (EDMs) [227, 225]. The latter contribute only to LR mixing terms and are suppressed by Yukawa couplings for the first two generations so we concentrate on the former kaon constraints.

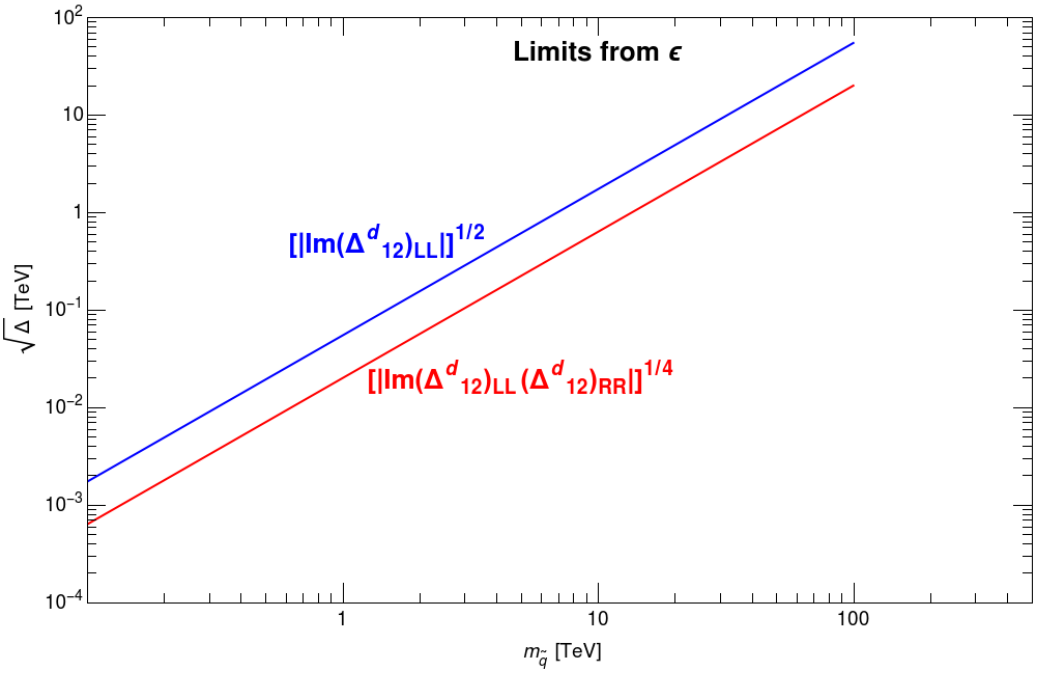

Figure 34: Upper limits on $\left[Im|(\Delta^d_{12})_{LL}|\right]^{1/2}$ (blue) and $\left[Im|(\Delta^d_{12})_{LL}(\Delta^d_{12})_{RR}|\right]^{1/4}$ (red) from kaon system ϵ constraints.

In Fig. 34, we show the constraints on the Imaginary part $[|Im(\Delta^d_{12})_{LL}|]^{1/2}$ and $[|Im(\Delta^d_{12})_{LL}(\Delta^d_{12})_{RR}|]^{1/4}$ from requiring contributions to the ϵ parameter to be below its

measured value. The contributions are plotted against average first/second generation squark mass for $m_{\tilde{g}}^2/m_{\tilde{q}}^2 = 0.3$. From the plot, we see that for weak scale sparticle masses $m_{\tilde{q}} \sim 100$ GeV, then the CP violating mass terms are required to be below about $0.5 - 2$ GeV. However, as $m_{\tilde{q}}$ is pulled towards the landscape expected values in the tens of TeV range, then the CP-violating masses are only constrained to be $\leq 4 - 10$ TeV (assuming 30 TeV squark masses). For unfettered CP-violating soft masses, then squark masses are required as high as 100 TeV.

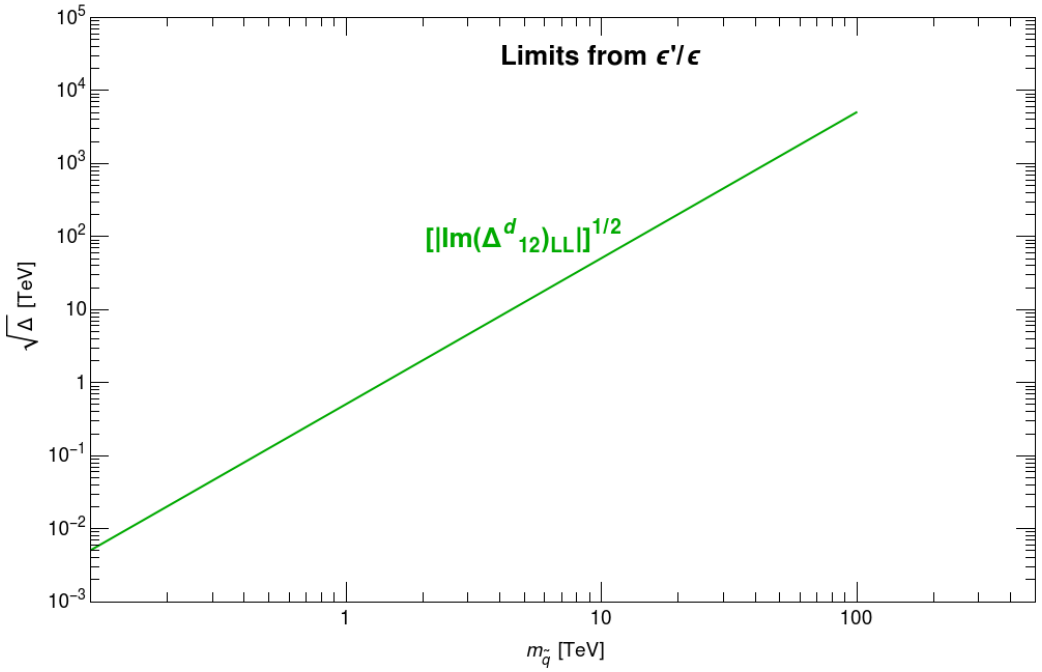

Figure 35: Upper limits on Imaginary part of off-diagonal squark mass terms from Kaon system ϵ'/ϵ constraints.

From the measured value of ϵ'/ϵ, we can also constrain $[|Im(\Delta_{12}^d)_{LL}|]^{1/2}$. These results are shown in Fig. 35 versus the average first/second generation squark mass for $m_{\tilde{g}}^2/m_{\tilde{q}}^2 = 0.3$. For weak scale squark masses, then the CP-violating mass term is required to be ≤ 5 GeV. As $m_{\tilde{q}}$ increases into the expected landscape range of $20 - 40$ TeV, then the CP-violating masses can lie in the 100 TeV range, thus solving the SUSY CP constraint at least in this channel.

Summary : In this section, the focus has been on the landscape pull on first/second generation sfermion masses. Their upper bound doesn't arise from EW D-term contributions (which allow sfermions up to 1000 TeV due to large, nearly perfect cancellations). Instead, their upper bound arises from two-loop RG contributions to third generation soft masses which actually push these values to small, even tachyonic values. As shown in Fig. 31, this is yet another example of the landscape pull toward *living dangerously*: increasing first/second generation soft masses make the theory increasingly natural until they move it towards disallowed too large weak scale values and ultimately to CCB minima in the Higgs potential. First/second generation soft masses are thus pulled into the tens of TeV range towards a flavor-independent upper bound. After evaluating FCNC and CP-violating constraints, it can be safely concluded that the string landscape picture offers a compelling picture of at best only mild constraints on off-diagonal flavor changing soft terms and CP-violating masses via a mixed decoupling/quasi-degeneracy solution to the SUSY flavor problem and a decoupling solution to the SUSY CP problem.

IV.3. Mirage mediation from the landscape

It has been shown in Ref. [77] and also in the beginning of Sec IV the effect of String Landscape [Sec. I.6] in the NUHM3 model (gravity-mediated SUSY breaking). In this section, we extend this methodology to mixed gravity/moduli plus anomaly-mediated soft SUSY breaking (SSB) terms [245] in the context of the natural generalized mirage mediation model (nGMM) [42] (discussed in Sec. I.3.3). Since the draw to large soft terms is related to a draw to large gravitino masses in supergravity, then we would expect a gravitino mass $m_{3/2}$ in the tens of TeV regime from SUSY on the landscape. But gaugino, third generation and Higgs soft terms contribute to the weak scale either directly or via 1-loop terms and so must instead lie in the TeV, not tens of TeV, regime. In such circumstances, then one would expect comparable anomaly-

mediated and moduli-mediated contributions to soft terms– a situation which requires mirage mediated rather then gravity-mediated only values for soft terms [245].

IV.3. 1. Methodology

In our approach, we will adopt the form of soft SUSY breaking terms expected from general mirage mediation [42] with a parameter space given by

$$\alpha,\ m_{3/2},\ c_m,\ c_{m3},\ a_3,\ \tan\beta,\ \mu,\ m_A \quad (GMM'). \tag{107}$$

This procedure allows for more direct exploration of stringy natural SUSY parameter space where most landscape solutions require $\mu \sim 100 - 300$ GeV in anthropically-allowed pocket universes[71].

Then the final formulae for the soft terms are given by Eqn : (38).
This natural GMM model, depicted as GMM′, is incorporated in Isajet [49] which is used here for spectra generation. To begin our scan over GMM′ parameter points, we proceed as follows.

- We select a particular value of $m_{3/2}$ which then fixes the AMSB contributions to SSB terms.
- We also fix $\mu = 200$ GeV for a natural solution to the SUSY μ problem. This then allows for arbitrary values of m_Z^{PU} to be generated but disallows any possibility of fine-tuning μ to gain m_Z^{OU}.

Next, we will invoke Douglas' power law selection of moduli-mediated soft terms relative to AMSB contributions within the GMM model. Thus, for an assumed value of $n = 2n_F + n_D - 1$, we will generate

- α^n with $\alpha : 3 - 25$, a power law statistical selection for moduli-mediated gaugino masses M_a, $(a = 1 - 3)$ over the gauge groups.

- $(a_3\alpha)^n$, a power-law statistical selection of moduli-mediated A-terms, with $(a_3\alpha) : 3 - 75$,
- $m_0(1,2) \sim m_{3/2}$ so that $c_m = (16\pi^2/\alpha)^2$ so that first/second generation scalars are set maximally at $m_{3/2}$,
- $(\sqrt{c_{m3}\alpha^2})^n$ to gain a power-law statistical selection on third generation scalar masses $m_0(3)$, with $(\sqrt{c_{m3}\alpha^2}) : 3 - 80$
- a power-law statistical selection on $m^2_{H_d}$ via m^n_A with $m_A : 300 - 7000$ GeV.
- a uniform selection on $\tan\beta : 3 - 40$.

Our first informative scan allows us to narrow the range of α and $\sqrt{c_{m3}\alpha^2}$ while expanding the range of $a_3\alpha$, m_A and $\tan\beta$. Our second scan proceeds with

- α^n with $\alpha : 5 - 20$, a power law statistical selection for moduli-mediated gaugino masses M_a, $(a = 1 - 3)$ over the gauge groups.
- $(a_3\alpha)^n$, a power-law statistical selection of moduli-mediated A-terms, with $(a_3\alpha) : 3 - 100$,
- $m_0(1,2) \sim m_{3/2}$ so that $c_m = (16\pi^2/\alpha)^2$ so that first/second generation scalars are set maximally at $m_{3/2}$,
- $(\sqrt{c_{m3}\alpha^2})^n$ to gain a power-law statistical selection on third generation scalar masses $m_0(3)$, with $(\sqrt{c_{m3}\alpha^2}) : 30 - 60$
- a power-law statistical selection on $m^2_{H_d}$ via m^n_A with $m_A : 300 - 10000$ GeV.
- a uniform selection on $\tan\beta : 3 - 50$.

followed by a focused scan by generating

- α^n with $\alpha : 5 - 20$, a power law statistical selection for moduli-mediated gaugino masses M_a, $(a = 1 - 3)$ over the gauge groups.
- $(a_3\alpha)^n$, a power-law statistical selection of moduli-mediated A-terms, with $(a_3\alpha) : 3 - 75$,
- $m_0(1,2) \sim m_{3/2}$ so that $c_m = (16\pi^2/\alpha)^2$ so that first/second generation scalars are set maximally at $m_{3/2}$,
- $(\sqrt{c_{m3}\alpha^2})^n$ to gain a power-law statistical selection on third generation scalar masses $m_0(3)$, with $(\sqrt{c_{m3}\alpha^2}) : 30 - 60$
- a power-law statistical selection on $m_{H_d}^2$ via m_A^n with $m_A : 1000 - 7000$ GeV.
- a uniform selection on $\tan\beta : 3 - 40$.

We adopt a uniform selection on $\tan\beta$ since this parameter is not a soft term. Note that with this procedure– while arbitrarily large soft terms are statistically favored– in fact they are all bounded from above since once they get too big, they will lead either to non-standard EW vacua or else too large a value of m_Z^{PU}. To avoid such anthropically disallowed vacua we augment the above scans with the constraint $\Delta_{EW} < 30$ [Sec. 1.6]. In this way, models such as split SUSY or high scale SUSY would be ruled out since for a natural value of μ, then they would necessarily lead to $m_Z^{PU} \gg (2-5)m_Z^{OU}$.

IV.3. 2. Results

In the following figures, we scan the soft terms of the GMM′ model according to the power law m_{soft}^n for $n = 1$ and 2 with a fixed gravitino mass $m_{3/2} = 20$ TeV. Proceeding with much higher values of $m_{3/2} \geq 25$ TeV always results in too-large of contributions to the weak scale when we take $m_0(1,2) \simeq m_{3/2}$ (see Fig. 10 of Ref. [246]). We keep μ fixed at 200 GeV according to a natural solution to the SUSY μ problem. We also veto non-standard EW vacua while for vacua with appropriate EWSB we require

$f_{EWSB} = \Theta(30 - \Delta_{EW})$ which corresponds to $m_Z^{PU} \leq 4m_Z^{OU}$. This latter anthropic selection imposes an upper bound on most GMM′ parameters and sparticle masses which would otherwise increase without limit according to f_{SUSY}.

Parameters

In Fig. 36, we first show the normalized probability histogram $dP/d\alpha$ as a function of α. The histogram is normalized to unit area. We also show for convenience on the upper scale various corresponding values of the gaugino mirage unification scale μ_{mir}. From the figure, for a simple linear draw ($n = 1$ corresponding to SUSY breaking from a single F-term), we see that the blue histogram has a rather broad peak spanning between $\alpha \sim 6{-}16$ which then corresponds to a predicted mirage scale $\mu_{mir} \sim 10^{10}{-}10^{14}$ GeV. There is relatively little probability for $\mu_{mir} \leq 10^9$ Gev or for $\mu_{mir} \geq 2 \times 10^{14}$ GeV. The mirage scale is actually testable in the GMM model since if we measure any two of the three gaugino masses at the weak scale, then using the known RGEs [228] we can extrapolate up in energy to see where they intersect. An intersection of all three gaugino masses at some intermediate mass scale would be strong supporting evidence for mirage mediation and would pick off the requisite value of α.

If instead we hypothesize an $n = 2$ draw on soft terms, then we arrive at the red histogram. Here we see that the stronger statistical draw on moduli-mediated soft terms results in a preference for higher α values peaked now at $\alpha \sim 15$ corresponding to $\mu_{mir} \sim 10^{14}$ GeV. Substantial probability remains for μ_{mir} as low as 10^{11} GeV.

In Fig. 37, we show histograms of probability for the other remaining parameters. In frame *a*), we show dP/dc_m which peaks for values of $c_m \sim 100 - 150$ for both $n = 1$ and $n = 2$. Since we have required $c_m = (16\pi^2/\alpha)^2$, this distribution just reflects the inverse-square distribution of α already shown in Fig. 36. In frame *b*), we show the distribution in c_{m3}. In this case, we find values of c_{m3} peaking at $c_{m3} \sim 5 - 15$ which sets the third generation matter scalar masses. These are more tightly restricted by

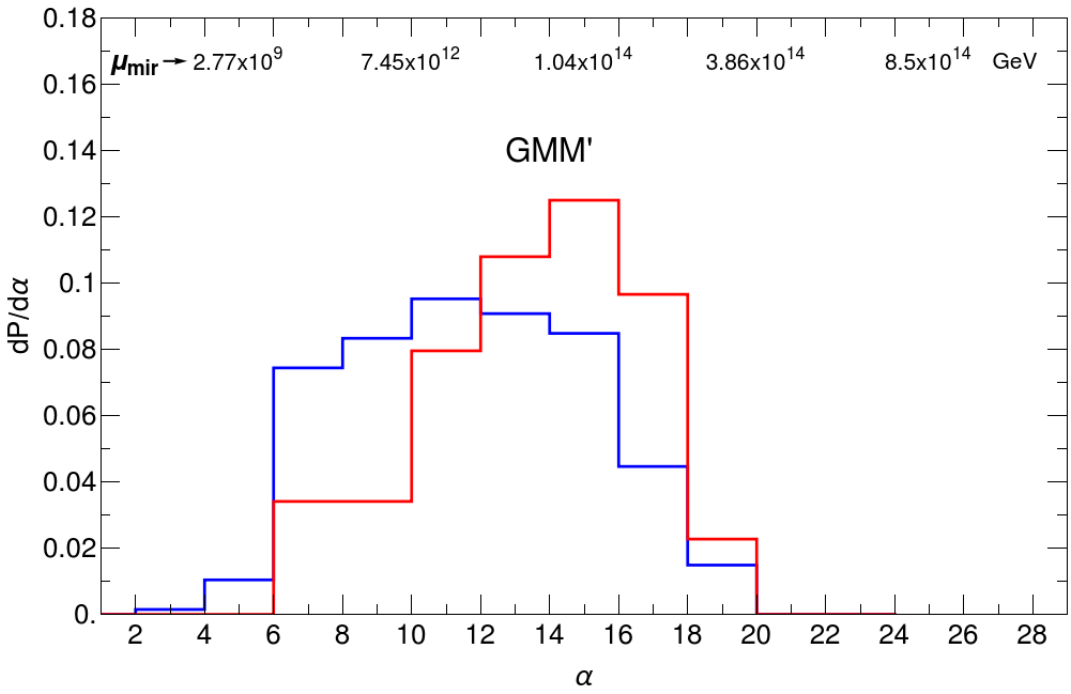

Figure 36: Probability distribution for mixed moduli-anomaly mixing parameter α from $n = 1$ (blue) and $n = 2$ (red) statistical scans over the GMM′ model with $m_{3/2} = 20$ TeV.

the landscape since they largely determine the $\Sigma_u^u(\tilde{t}_{1,2})$ contributions to the weak scale. Since we cannot tune these away, then if they are too large we would have $m_Z^{PU} \geq 4m_Z^{OU}$ and we would violate the nuclear physics results of Ref. [76].

In frame *c*), we show the distribution in a_3 which sets the magnitude of the moduli-mediated contribution to the trilinear soft term A_0. Here, we find a statistical draw to large $-A_0$ terms with a_3 peaking around $3-6$. Such large A_t terms actually *reduce* the weak scale contributions $\Sigma_u^u(\tilde{t}_{1,2})$ [16, 71]. At the same time, large A_t terms yield maximal mixing in the stop sector leading to an uplift of m_h to ~ 125 GeV [20, 21]. If the a_3 parameter gets too big, then again large $\Sigma_u^u(\tilde{t}_{1,2})$ terms result while if even large values of a_3 occur then we are pushed into CCB vacua (which must be vetoed).

In frame *d*), we plot the distribution in $\tan\beta$, which was scanned uniformly. Here, we see the most probable value is $\tan\beta \sim 8-20$. For larger values of $\tan\beta \sim 20-50$,

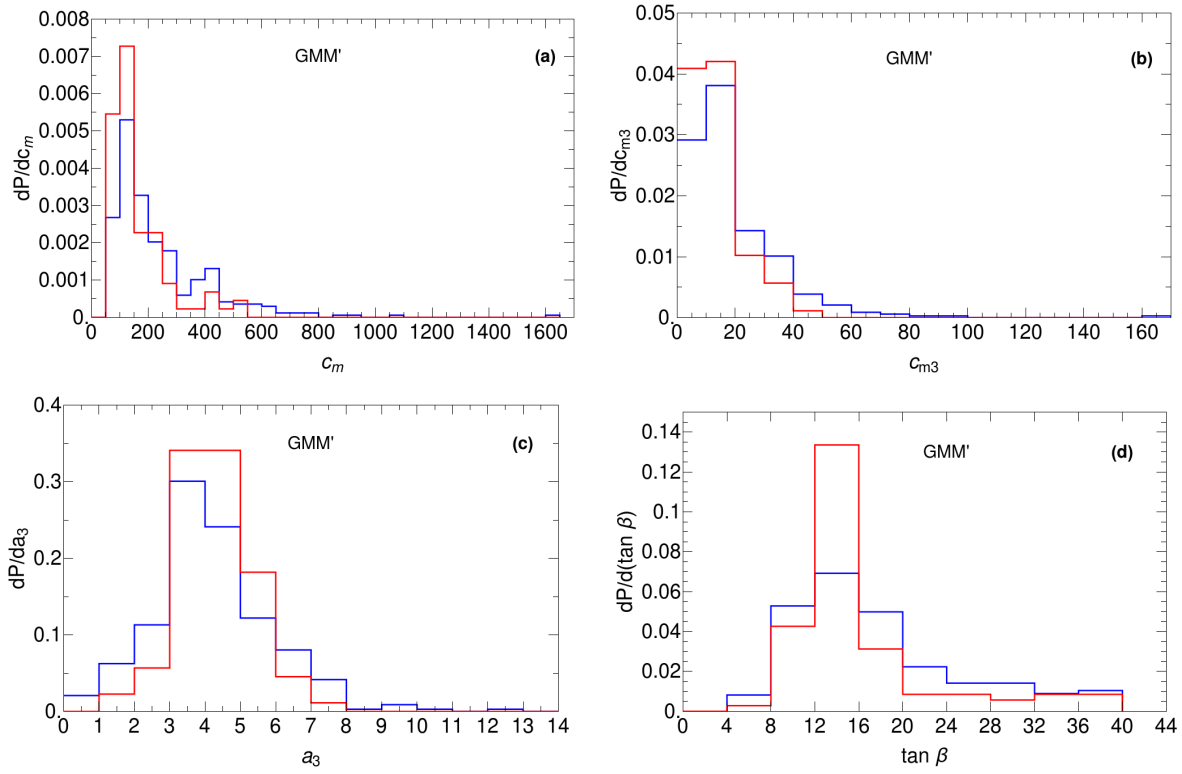

Figure 37: Distributions in (a) c_m, (b) c_{m3}, (c) a_3 and (d) $\tan\beta$. Here, $n = 1$ (blue) and $n = 2$ (red) are from statistical scans over the nGMM model with $m_{3/2} = 20$ TeV.

then the τ and b-Yukawa couplings become large leading to large $\Sigma_u^u(\tilde{b}_{1,2})$ contributions to the weak scale.

Higgs and sparticle mass predictions

In Fig. 38, we show the Higgs mass m_h probability distribution from the GMM model in the landscape for $m_{3/2} = 20$ TeV with $n = 1$ (blue) and $n = 2$ (red). From the plot, we see that the most probable value of m_h is 125 GeV for both cases. The value of m_h reaches maximally 127 GeV but much higher values of m_h always require $m_Z^{PU} > 4m_Z^{OU}$ from the $\Sigma_u^u(\tilde{t}_{1,2})$ contributions to the weak scale. These distributions are highly encouraging *post-dictions* of the Higgs mass from general considerations of the string landscape!

In Fig. 39a), we show the probability distribution for $m_{\tilde{g}}$ from the landscape within

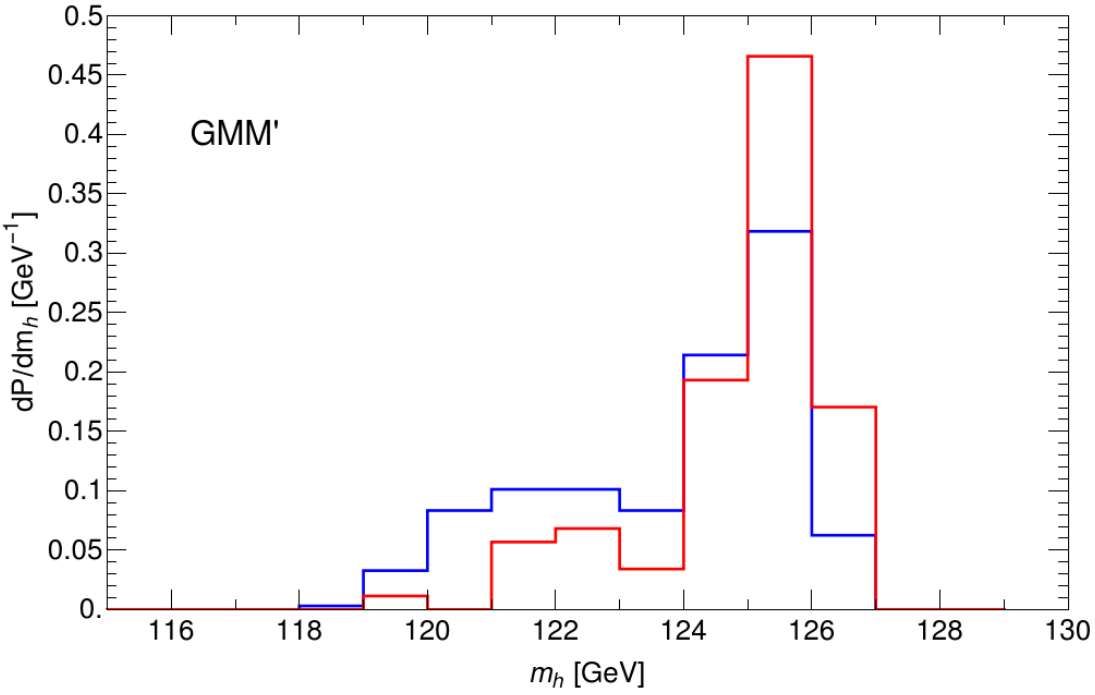

Figure 38: Probability distribution for mass of light Higgs boson m_h from $n = 1$ (blue) and $n = 2$ (red) statistical scans over nGMM model with $m_{3/2} = 20$ TeV.

generalized mirage-mediation. Here, we see that for $n = 1$ with $m_{3/2} = 20$ TeV, then $m_{\tilde{g}} \sim 2 - 5$ TeV, almost always safely beyond LHC Run 2 limits. For the $n = 2$ case, then the distribution in $m_{\tilde{g}}$ becomes somewhat harder with $m_{\tilde{g}} \sim 2.5 - 5$ TeV with a most-probable value of $m_{\tilde{g}} \sim 4$ TeV. From these distributions, it seems reasonable that LHC has not yet discovered SUSY via gluino pair production. The HL-LHC reach extends to $m_{\tilde{g}} \sim 2.7$ TeV[247] while HE-LHC with $\sqrt{s} = 27$ TeV will have a reach in $m_{\tilde{g}}$ to about 6 TeV[248]. Thus, discovery of SUSY via gluino pair production may have to await a higher energy upgrade of LHC[249].

In Fig. 39*b*), we show the probability distribution for $m_{\tilde{t}_1}$. Here, we see for both $n = 1$ and $n = 2$ statistical draw, then $m_{\tilde{t}_1} \sim 1{-}2$ TeV. These values of $m_{\tilde{t}_1}$ are generally beyond current LHC top squark mass limits and so again it may be no surprise that LHC has not yet seen a signal via top-squark pair production. While HL-LHC should

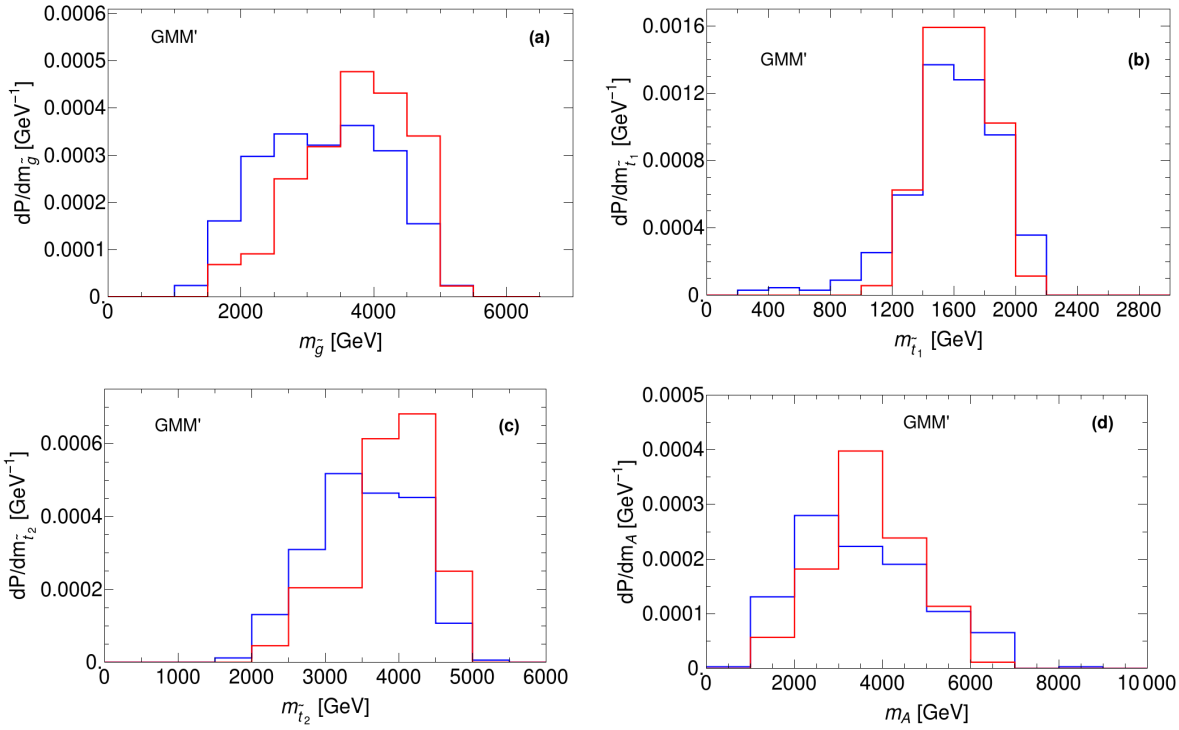

Figure 39: Distributions in (a) $m_{\tilde{g}}$, (b) $m_{\tilde{t}_1}$, (c) $m_{\tilde{t}_2}$ and (d) m_A. Here, $n = 1$ (blue) and $n = 2$ (red) are from a statistical scans over the nGMM model with $m_{3/2} = 20$ TeV.

have a reach in $m_{\tilde{t}_1}$ to about 1.5 TeV, the reach of HE-LHC extends to about $m_{\tilde{t}_1} \sim 3$ TeV[248]. Thus, it may well require an energy upgrade of LHC to discover SUSY via top-squark pair production.

In Fig. 39c), we show the distribution in $m_{\tilde{t}_2}$. In this case, we expect the landscape with GMM to yield a value $m_{\tilde{t}_2} \sim 2.5 - 5$ TeV. Typically, we expect the higher range of these values to be beyond the reach of even HE-LHC.

In Fig. 39d), we show the expected probability for the pseudoscalar Higgs mass m_A. We find that $m_A \sim 2 - 6$ TeV. Such values are typically beyond the reach of HL-LHC [250].

One of the features of mirage-mediation is the expected compressed spectra of gauginos as compared to models with unified gaugino masses. For unified gauginos, we expect weak scale gaugino masses in the ratio $M_1 : M_2 : M_3 \sim 1 : 2 : 6 - 7$. For the

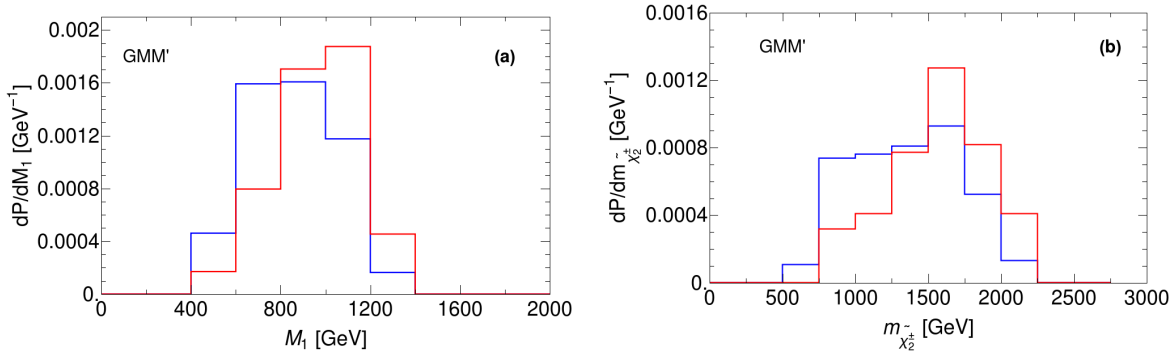

Figure 40: Distributions in (a) M_1 and (b) M_2. Here, $n = 1$ (blue) and $n = 2$ (red) are from statistical scans over the nGMM model with $m_{3/2} = 20$ TeV.

GMM model, these ratios can be quite different. The $SU(3)$ gaugino mass $M_3 \sim m_{\tilde{g}}$ (up to loop corrections) so that the approximate value of M_3 is given in Fig. 39*a*). In Fig. 40, we show the expected electroweak gaugino masses. In frame *a*), the predicted bino mass $M_1 \sim 0.5 - 1.3$ TeV. This value is well above the expected value of $\mu \sim 100 - 350$ GeV and so we would expect the lightest-SUSY-particle (LSP) to be higgsino-like. The bino will be difficult to extract at LHC. However, a linear e^+e^- collider with $\sqrt{s} > 2m(higgsino)$ should be able to pair produce higgsinos via reactions such as $e^+e^- \to \tilde{\chi}_1^0\tilde{\chi}_2^0$ and measure the mass splitting $m_{\tilde{\chi}_2^0} - m_{\tilde{\chi}_1^0}$ which is sensitive to the bino mass [251]. Such a machine should be able to extract M_1 to test the distribution in Fig. 40*a*. In Fig. 40*b*), we show the wino mass M_2 probability distribution. It is expected that $M_2 \sim 0.8 - 2.2$ TeV. The LHC can access wino pair production $\tilde{\chi}_2^\pm\tilde{\chi}_4^0$ via the same-sign diboson signature [252, 253] (SSdB) which is unique to SUSY models with light higgsinos: $pp \to \tilde{\chi}_2^\pm\tilde{\chi}_4^0 \to W^\pm W^\pm + \not{E}_T$. The clean signature and signal production rate may allow one to extract a measurement of M_2 at HL- or HE-LHC via the total SSdB production rate. Otherwise, again an e^+e^- collider should be able to extract M_2 via the higgsino mass splittings which are measureable in higgsino pair production reactions [251].

In Fig. 41 we show the expected weak scale gaugino mass ratios *a*) M_2/M_1 and *b*)

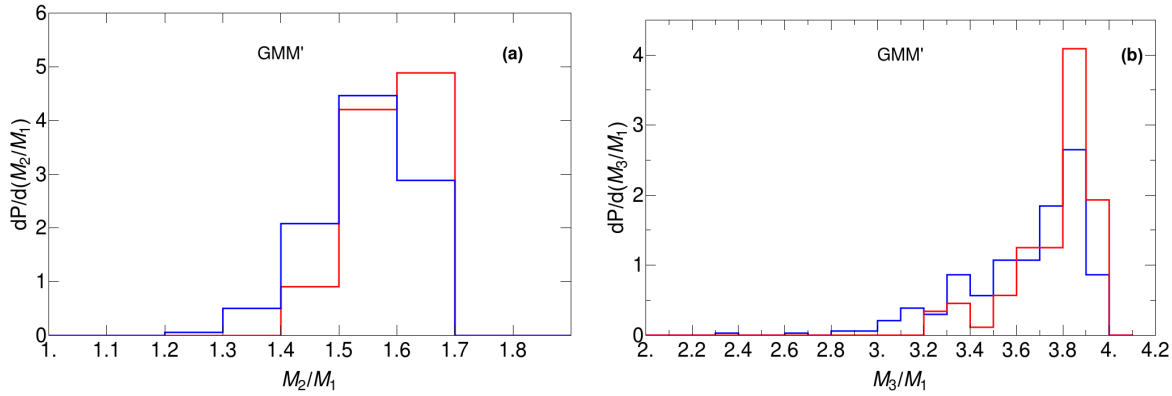

Figure 41: Distributions in (a) M_2/M_1 and (b) M_3/M_1. Here, $n = 1$ (blue) and $n = 2$ (red) are from statistical scans over the nGMM model with $m_{3/2} = 20$ TeV.

M_3/M_1 which are expected from the landscape with mirage mediation. From frame a), we see that M_2/M_1 is expected to occur with ratio $\sim 1.4 - 1.7$ so that indeed the electroweakinos are compressed, but not highly compressed. Such a compressed gaugino mass spectrum would be solid evidence for mirage-mediation [254]. In frame b), we find that $M_3/M_1 \sim 3 - 4$ rather than the expectation from gaugino-unified models where $M_3/M_1 \sim 6 - 7$. While the gaugino mass spectrum is compressed, the gap $m_{\tilde{g}} - m_{LSP}$ is actually greater than in gaugino-unified models since the LSP is higgsino-like and close to the weak scale whilst gluinos are pulled statistically to large values.

We also plot in Fig. 42 the expected $m_{\tilde{\chi}_2^0} - m_{\tilde{\chi}_1^0}$ mass gap. This gap is expected to be directly measurable at LHC via the higgsino pair production reaction $pp \to \tilde{\chi}_1^0 \tilde{\chi}_2^0$ followed by $\tilde{\chi}_2^0 \to \tilde{\chi}_1^0 \ell^+ \ell^-$ [221]. (Indeed, there appears already some excess in this channel at Atlas with 139 fb^{-1}; see Fig. 10a) of Ref. [255].) From the plot, we see the mass gap is typically $m_{\tilde{\chi}_2^0} - m_{\tilde{\chi}_1^0} \sim 4 - 12$ GeV so the opposite-sign (OS) dileptons will likely be quite soft. This discovery channel for SUSY appears to be the *most propitious one* for HL-LHC [256].

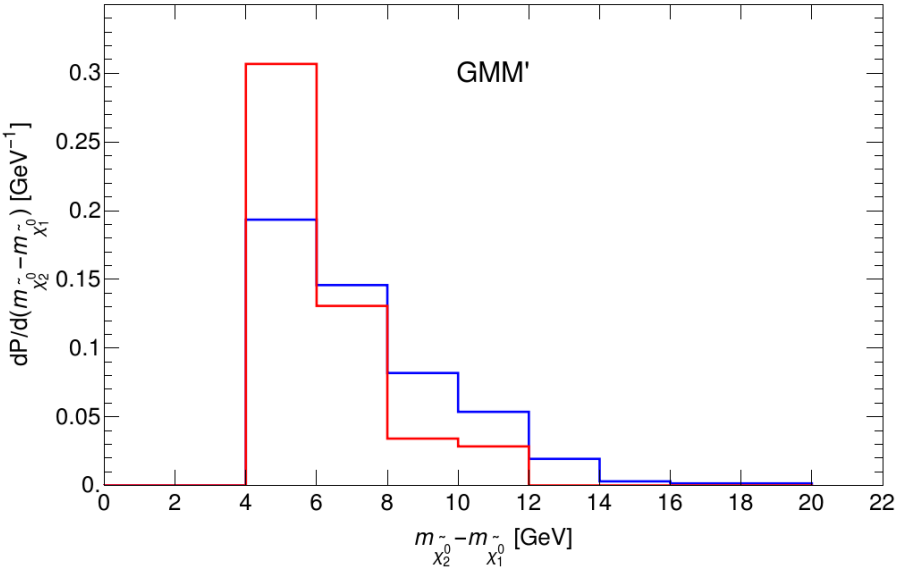

Figure 42: Probability distribution for light neutral higgsino mass difference $m_{\tilde{z}_2} - m_{\tilde{z}_1}$ from $n = 1$ (blue) and $n = 2$ (red) statistical scans over the nGMM model with $m_{3/2} = 20$ TeV.

m_0^{MM} vs. $m_{1/2}^{MM}$ parameter space for $m_{3/2} = 20$ TeV

A panoramic view of some of our essential conclusions may be displayed in the m_0^{MM} vs. $m_{1/2}^{MM}$ plane which is then analogous to the m_0 vs. $m_{1/2}$ plane of the mSUGRA/CMSSM or NUHM2,3 models. Here, we define $m_0^{MM} = \sqrt{c_m}\alpha(m_{3/2}/16\pi^2)$ which is the pure moduli-mediated contribution to scalar masses. The moduli-mediated contribution to gaugino masses is correspondingly given by $m_{1/2}^{MM} \equiv \alpha m_{3/2}/(16\pi^2)$.

In Fig. 43a), we show the m_0^{MM} vs. $m_{1/2}^{MM}$ plane for an $n = 1$ landscape draw but with $a_3 = 1.6\sqrt{c_m}$, with $c_m = c_{m3}$ and with $\tan\beta = 10$, $m_A = 2$ TeV and $\mu = 200$ GeV. The lower-left yellow region shows where $m_{\tilde{w}_1} < 103.5$ GeV in violation of LEP2 constraints. Also, the lower-left orange box shows where $\Delta_{BG} < 30$ (old naturalness calculation). The bulk of the low $m_{1/2}$ region here leads to tachyonic top-squark soft terms owing to the large trilinear terms $A_0^{MM} \equiv -a_3\alpha(m_{3/2}/16\pi^2)$. This region is nearly flat with increasing m_0 mainly because the larger we make the GUT scale top-squark squared

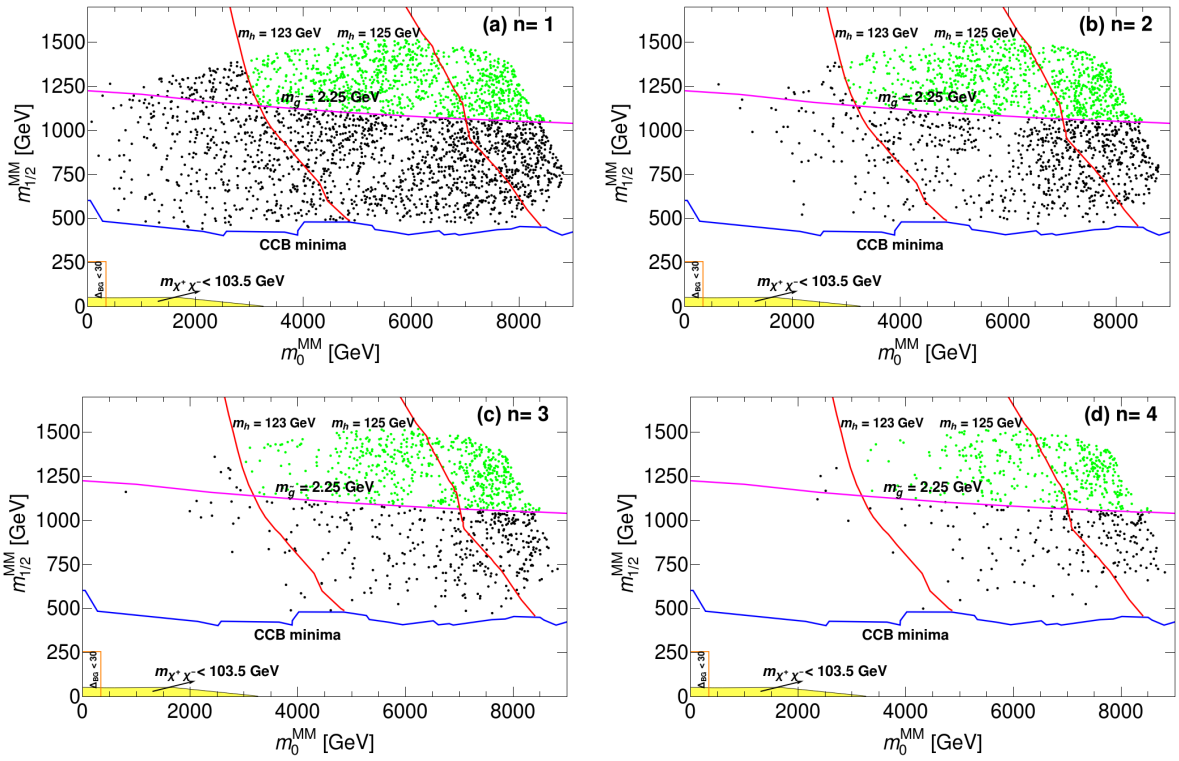

Figure 43: For $m_{3/2} = 20$ TeV, we plot the GMM parameter space in the m_0^{MM} vs. $m_{1/2}^{MM}$ parameter space for $a_3 = 1.6\sqrt{c_m}$ with $c_{m3} = c_m$ and $\tan\beta = 10$ with $m_A = 2$ TeV. We plot for a landscape draw of (a) $n = 1$, (b) $n = 2$, (c) $n = 3$ and (d) $n = 4$ with $m_Z^{PU} < 4m_Z^{OU}$.

mass soft terms, the larger is the cancelling correction from RG running. For larger $m_{1/2}$ values, then we obtain viable EW vacua since large values of M_3 help to enhance top squark squared mass running to large positive values (see *e.g.* Eq. 9.16h of Ref. [13]). The dots show the expected statistical result of scanning the landscape, and the larger density of dots on the plot corresponds to greater *stringy naturalness*. We also show the magenta contour of $m_{\tilde{g}} = 2.25$ TeV, below which is excluded by LHC gluino pair searches. We also show contours of $m_h = 123$ and 125 GeV. The green points are consistent with LHC sparticle search limits and Higgs mass measurement. From the plot, we see that the region of high stringy naturalness tends to lie safely beyond LHC sparticle search limits while at the same time yielding a Higgs mass $m_h \simeq 125$ GeV.

In Fig's 43b), c) and d), we increase the power law statistical selection of soft terms

to $n = 2$, 3 and 4, respectively.[27] As n increases, then large soft terms are increasingly favored until one hits the region for very large $m_{1/2}^{MM}$ and m_0^{MM} where contributions to the weak scale exceed a factor of 4 above our measured value. The density of dots increasingly moves out towards large values of m_0^{MM} and $m_{1/2}^{MM}$ as n increases. This is an example of *living dangerously* in the landscape as noted by Arkani-Hamed, Dimopoulos and Kachru [66]. Then we see that the region beyond LHC gluino mass limits becomes increasingly stringy natural! This is in sharp contrast to expectations from conventional naturalness which favors sparticle masses close to the weak scale [71]. For stringy naturalness, a value $m_{\tilde{g}} = 3$ TeV is more natural than a value of $m_{\tilde{g}} = 300$ GeV! Thus, we see that the predictions from mirage-mediated landscape SUSY are in close accord with what LHC is currently seeing: a Higgs mass of $m_h \simeq 125$ GeV but as yet no sign of sparticles.

Finally, to compare and contrast the GMM model to the NUHM2 model with universal gaugino masses, we list in Table 18 two benchmark models computed using Isajet 7.88 [49].

Here, we have selected a GMM$'$ model with α chosen so that $m_{1/2}^{MM} = m_{1/2} = 1250$ GeV, $m_0^{MM} = m_0 = 5000$ GeV and $A_0^{MM} = A_0 = -1.6m_0 = -8000$ GeV. Both cases contain $\tan\beta = 10$, $\mu = 200$ and $m_A = 2$ TeV. The AMSB contribution to soft terms is fixed for GMM$'$ by choosing $m_{3/2} = 20$ TeV. From Table 18, we see that the scalar mass spectrum is heavy and rather similar for the two cases. For the gaugino spectrum, we see that while $m_{\tilde{w}_2} \sim m_{\tilde{z}_4} \sim M_2 \sim 1100$ GeV for both models, the gluino mass $m_{\tilde{g}} \sim 2556$ GeV for GMM$'$ which is rather less than the value $m_{\tilde{g}} \sim 2931$ GeV for NUHM2. Also, we see that $m_{\tilde{z}_3} \sim M_1 \sim 748$ GeV for GMM$'$ while $m_{\tilde{z}_3} \sim 562$ GeV for NUHM2. Thus, the gaugino masses are *compressed* in GMM$'$ compared to the gauginos from NUHM2 with a universal value of $m_{1/2}$ at m_{GUT}. Both models have a cluster of higgsinos around $\mu \sim 200$ GeV so these models may be difficult to distinguish at

[27] The relative density of dots between different frames in Fig. 43 has no meaning.

parameter	$NUHM2$	GMM'
m_0	5000	
$m_{1/2}$	1250	
A_0	-8000	
$\tan\beta$	10	10
$m_{3/2}$		20000
α		9.9
c_m		16
c_{m3}		16
a_3		6.4
μ	200	200
m_A	2000	2000
$m_{\tilde{g}}$	2931.4	2556.5
$m_{\tilde{u}_L}$	5479.6	5305.3
$m_{\tilde{u}_R}$	5598.3	5432.8
$m_{\tilde{e}_R}$	4822.6	4827.9
$m_{\tilde{t}_1}$	1750.2	1646.2
$m_{\tilde{t}_2}$	3953.6	3803.6
$m_{\tilde{b}_1}$	3987.4	3836.7
$m_{\tilde{b}_2}$	5322.1	5169.5
$m_{t\tilde{a}u_1}$	4745.2	4752.2
$m_{t\tilde{a}u_2}$	5116.3	5094.0
$m_{\tilde{\nu}_\tau}$	5122.8	5101.0
$m_{\tilde{w}_2}$	-1061.2	-1116.9
$m_{\tilde{w}_1}$	-210.0	-210.1
$m_{\tilde{z}_4}$	-1074.7	-1129.9
$m_{\tilde{z}_3}$	-562.3	-748.5
$m_{\tilde{z}_2}$	208.2	207.8
$m_{\tilde{z}_1}$	-198.3	-199.7
m_h	124.8	124.2
$\Omega^{std}_{\tilde{z}_1}h^2$	0.011	0.010
$BF(b\to s\gamma)\times 10^4$	3.1	3.1
$BF(B_s\to\mu^+\mu^-)\times 10^9$	3.8	3.8
$\sigma^{SI}(\tilde{z}_1,p)$ (pb)	0.16×10^{-8}	0.11×10^{-8}
$\sigma^{SD}(\tilde{z}_1 p)$ (pb)	0.33×10^{-4}	0.21×10^{-4}
$\langle\sigma v\rangle\vert_{v\to 0}$ (cm^3/sec)	0.2×10^{-24}	0.2×10^{-24}
$\Delta_{\rm EW}$	24.4	18.2

Table 18: Input parameters and masses in GeV units for a natural mirage mediation SUSY benchmark point as compared to a similar point from the NUHM2 model with $m_t = 173.2$ GeV. The input parameters for the natural mirage mediation model such as α and c_m have been calculated from m_0^{MM} and $m_{1/2}^{MM}$ which are taken equal to m_0 and $m_{1/2}$ respectively as in NUHM2 model. The c_m and c_{m3} have been taken equal to each other so that masses of first/second and third generation sfermions are equal at the GUT scale so as to match the NUHM2 model.

LHC upgrades. It may require an e^+e^- collider operating with $\sqrt{s} > 2m(higgsino)$ to measure the gaugino masses indirectly via their contribution to higgsino mass splitting. Such a collider could then distinguish mirage unification of gauginos compared to GUT scale unified gaugino masses [251].

Summary : In this section, we see the effect of string landscape on natural mirage-mediation model (nGMM$'$). The string landscape scenario is apt to lift the gravitino mass $m_{3/2}$ into the tens of TeV range such that AMSB SSB terms are comparable to the weak scale. In such a case, then one expects moduli-mediated and anomaly-mediated soft terms to be comparable and in such a setting the appropriate $N = 1$ SUGRA framework is that of generalized mirage-mediation.

So, though similar analysis has been done for a pure gravity-mediation model (NUHM3) in [77], nGMM$'$ being a more realistic model is examined under string landscape scenario.

Within the nGMM$'$ model and including a natural solution to the SUSY μ problem, we have made statistical predictions for model parameters and sparticle and Higgs boson mass values for the cases of $n = 1$ and 2 with $m_{3/2} = 20$ TeV. For $n = 1$ with $m_{3/2} = 20$ TeV we find the mirage mediation scale $\mu_{mir} \sim 10^{10} - 2 \times 10^{14}$ GeV while for $n = 2$ then $\mu_{mir} \sim 8 \times 10^{12} - 3 \times 10^{14}$ GeV. These predictions can be somewhat falsified by measuring the gaugino masses at LHC or a high energy e^+e^- collider and extrapolating their masses via renormalization group running to find their intersection point μ_{mir}, which then determines the mixing parameter α. In this happy event, then one could also *directly extract the gravitino mass* $m_{3/2}$. The mirage-mediation scenario would be rather implausible if no mirage mediation scale was found (the three gaugino masses did not unify at a point) or if μ_{mir} was found to lie outside these ranges.

Regarding Higgs and sparticle mass predictions, the light Higgs boson mass is found to peak rather sharply around $m_h \simeq 125$ GeV. Meanwhile, the gluino is pulled up to

$m_{\tilde{g}} \sim 3.5 \pm 1.5$ TeV and the light top squark is pulled to $m_{\tilde{t}_1} \sim 1.5 \pm 0.5$ TeV. With such large values of $m_{\tilde{g}}$ and $m_{\tilde{t}_1}$, an energy upgrade of LHC may be needed to realize SUSY discovery via gluino and/or top-squark pair production. The pseudoscalar Higgs boson $m_A \sim 3.5 \pm 1.5$ TeV so it seems typically beyond the projected reach of LHC luminosity upgrades. The most likely avenue for SUSY discovery at LHC would be via direct Higgsino pair production $pp \to \tilde{\chi}_1^0 \tilde{\chi}_2^0 \to \ell^+\ell^- + \not{E}_T$ where the presence of an initial state jet radiation may help to trigger on the expected soft dilepton signature[221]. The soft dilepton invariant mass is expected to be bounded by $m_{\tilde{z}_2} - m_{\tilde{z}_1} \sim 5 - 10$ GeV. In fact, such a soft opposite-sign dilepton excess seems to be building in Atlas data.

V. Collider Phenomenology of RNS models

In Sec. I.3, we have discussed a few Radiatively-Driven Natural Supersymmetric (RNS) Models. In this section, collider phenomenology of these RNS models will be discussed.

The four most important search channels for RNS models at the LHC or its upgrades are the following.

- Gluino pair production $pp \to \tilde{g}\tilde{g}X$ followed by either two-body gluino decay to top squarks $\tilde{g} \to \tilde{t}_1^* t,\ \tilde{t}_1 \bar{t}$ or, if these are closed, then gluino three-body decays to mainly third generation quarks [278]: $\tilde{g} \to t\bar{t}\tilde{z}_i,\ b\bar{b}\tilde{z}_i$ or $t\bar{b}\tilde{w}_j^+ + c.c.$. This signature has been discussed in detail in Sec. V.1.

- Top squark pair production $pp \to \tilde{t}_1\tilde{t}_1^* X$ followed by $\tilde{t}_1 \to t\tilde{z}_i$ or $b\tilde{w}_j^+$ [279].

- Higgsino pair production via $pp \to \tilde{z}_i\tilde{z}_j j, \tilde{w}_1\tilde{z}_i j, \tilde{w}_1\tilde{w}_1 j$ channels is unlikely to be visible above SM Zj background in $j + \not{E}_T$ channel because the signal to background ratio is just 1-2% [280]. However, the $pp \to \tilde{z}_1\tilde{z}_2 j$ channel (with contributions from $pp \to \tilde{w}_1\tilde{z}_2 j$) , where $\tilde{z}_2 \to \ell\bar{\ell}\tilde{z}_1$ with a soft OS dilepton pair and where the hard initial state radiated jet supplies a trigger, offers a promising search channel for low mass higgsinos with $m_{\tilde{z}_{1,2}} \sim 100 - 300$ GeV [281]. Indeed, the LHC collaborations have presented their first results for this search [282, 283], and it is especially encouraging that the ATLAS collaboration is able to access a $\tilde{z}_2 - \tilde{z}_1$ mass gap as small as 2.5 GeV.

- Wino pair production $pp \to \tilde{w}_2^\pm \tilde{z}_{3\text{ or }4} X$ followed by $\tilde{w}_2 \to W\tilde{z}_{1,2}$ and $\tilde{z}_{3\text{ or }4} \to W^\pm \tilde{w}_1^\mp$. Half the time, this final state leads to a *same-sign diboson* (SSdB) final state which, when followed by leptonic W decays, leads to same-sign dileptons $+MET$ with very little accompanying jet activity [284] (as opposed to SS dileptons arising from gluino cascade decays). The SSdB signature has very low SM background rates arising mainly from $t\bar{t}W$ production as will be seen in Sec V.2.

V.1. Gluino reach and mass extraction at the LHC in radiatively-driven natural SUSY

In this section, gluino pair production signatures are examined within the RNS framework. The goal is first, to delineate the gluino reach of LHC14 and its high-luminosity upgrade, and second, to study the extent to which the gluino mass may be extracted at the LHC. For integrated luminosities in excess of 100 fb^{-1} that should be accumulated within the next few years, we show that judicious cuts can be found so that the gluino pair production signal emerges with very little SM background in the data sample, allowing for a gluino reach well beyond the expectation within the mSUGRA/CMSSM framework. Moreover, assuming decoupled first and second generation squarks, the measured event rate from the gluino signal depends *only* on the value of $m_{\tilde{g}}$. The rate for gluino events after cuts that eliminate most of the SM background can, therefore, be used to extract the gluino mass, assuming that gluino events as well as the experimental detector can be reliably modeled. This "counting rate" method of extracting $m_{\tilde{g}}$ [295] has several advantages over the kinematic methods which have been advocated [296]. It remains viable even if a variety of complicated cascade decay topologies are expected to be present. In addition, it is unaffected by ambiguities over which jets or leptons are to be associated with which of the two gluinos that are produced. We explore the counting rate extraction of $m_{\tilde{g}}$ in RNS model and find it typically leads to extraction of $m_{\tilde{g}}$ with a statistical precision of 2-5%, depending on the value of $m_{\tilde{g}}$ and the assumed integrated luminosity, ranging between 300-3000 fb^{-1}.

This analysis is done within the framework of the two extra parameter non-universal Higgs model (NUHM2) [40] with parameter inputs,

$$m_0,\ m_{1/2},\ A_0,\ \tan\beta,\ \mu,\ m_A \quad (NUHM2)\ . \tag{108}$$

Isajet/Isasugra 7.85 spectrum generator [49] has been used to obtain sparticle masses. Below we shall see the RNS model line that is adopted for the analysis. The event topologies expected from gluino pair production within the RNS framework using a benchmark point with $m_{\tilde{g}} = 2$ TeV are briefly described followed by a detailed discussion on simulation of the SUSY signal and the relevant SM backgrounds and the cuts selected to eliminate the backgrounds efficiently. Finally, we shall see the projections for the mass reach for gluinos in the RNS framework and the precision with which $m_{\tilde{g}}$ may be extracted at the LHC.

V.1.1. A RNS model line

To facilitate the examination of gluino signals in models with natural SUSY spectra, the RNS model-line adopted here is $m_0 = 5000$ GeV, $A_0 = -8000$ GeV, $\tan\beta = 10$, $\mu = 150$ GeV and $m_A = 1000$ GeV, while $m_{1/2}$ varies across the range $600 - 1200$ GeV corresponding to a gluino mass range of $m_{\tilde{g}} \sim 1600 - 2800$ GeV, *i.e.*, starting just below present LHC bounds on $m_{\tilde{g}}$ and extending just beyond the projected reach for HL-LHC. The spectrum, together with some low energy observables, is illustrated for a benchmark point with $m_{\tilde{g}} \simeq 2000$ GeV in Table 19. Along this model line, the computed value of the light Higgs mass is quite stable and varies over $m_h : 124.1 - 124.7$ GeV. (A couple GeV theory error in the RG-improved one loop effective potential calculation of m_h which includes leading two-loop effects is expected.) The value of $\Delta_{\rm EW}$ varies between $8.3 - 24$ along the model line so the model is very natural with electroweak fine-tuning at the $12\% - 4\%$ level. The cross section for $pp \to \tilde{g}\tilde{g}X$, calculated using Prospino [297] with NLL-FAST [298], is shown in Fig. 44 vs. $m_{\tilde{g}}$ for $m_{\tilde{q}} \simeq 5$ TeV and for $\sqrt{s} = 13$ and 14 TeV. For $m_{\tilde{g}} \sim 2$ TeV and $\sqrt{s} = 14$ TeV – the benchmark point adopted here for devising the analysis cuts – $\sigma(\tilde{g}\tilde{g}) \sim 1.7$ fb; the cross section drops to about $\sigma \sim 0.02$ fb for $m_{\tilde{g}} \sim 3$ TeV.

Once the gluinos are produced, all across the model line they decay dominantly via

parameter	value
m_0	5000
$m_{1/2}$	800
A_0	-8000
$\tan\beta$	10
μ	150
m_A	1000
$m_{\tilde{g}}$	2007.8
$m_{\tilde{u}_L}$	5169.3
$m_{\tilde{u}_R}$	5322.7
$m_{\tilde{e}_R}$	4808.0
$m_{\tilde{t}_1}$	1479.3
$m_{\tilde{t}_2}$	3650.1
$m_{\tilde{b}_1}$	3678.3
$m_{\tilde{b}_2}$	5049.3
$m_{\tilde{\tau}_1}$	4734.4
$m_{\tilde{\tau}_2}$	5079.7
$m_{\tilde{\nu}_\tau}$	5087.0
$m_{\tilde{w}_2}$	691.3
$m_{\tilde{w}_1}$	155.3
$m_{\tilde{z}_4}$	702.2
$m_{\tilde{z}_3}$	362.8
$m_{\tilde{z}_2}$	158.2
$m_{\tilde{z}_1}$	142.4
m_h	124.4
$\Omega^{std}_{\tilde{z}_1}h^2$	0.008
$BF(b\to s\gamma)\times 10^4$	3.3
$BF(B_s\to\mu^+\mu^-)\times 10^9$	3.8
$\sigma^{SI}(\tilde{z}_1 p)$ (pb)	4.3×10^{-9}
$\Delta_{\rm EW}$	10.3

Table 19: NUHM2 input parameters and masses in GeV units for a *radiatively-driven natural SUSY* benchmark points introduced in the text. We take $m_t = 173.2$ GeV

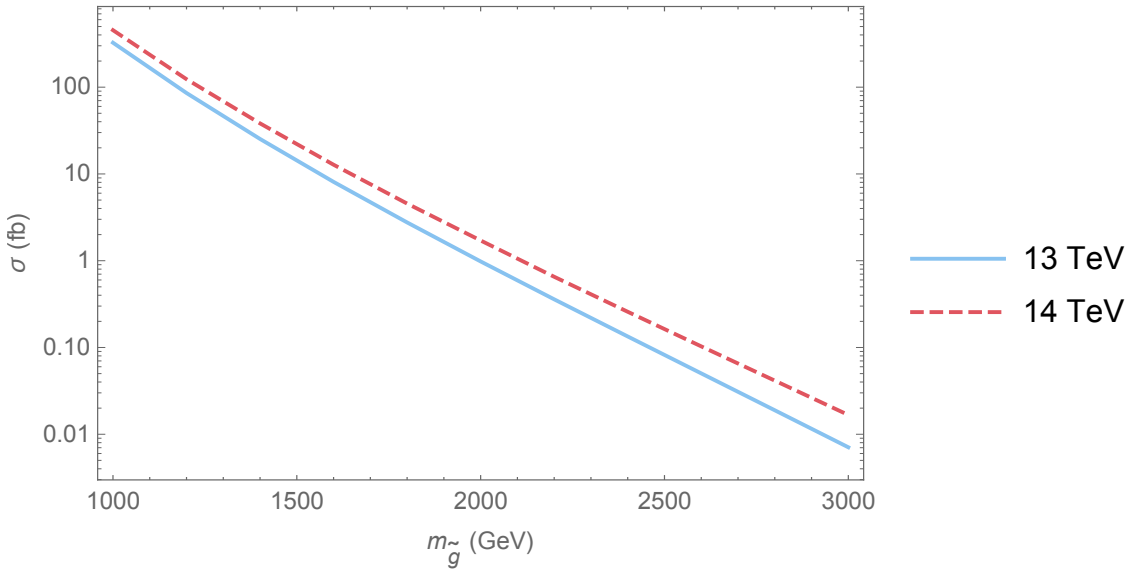

Figure 44: Total NLO+NLL cross section for $pp \to \tilde{g}\tilde{g}X$ at LHC with $\sqrt{s} = 13$ and 14 TeV, versus $m_{\tilde{g}}$ for $m_{\tilde{q}} \simeq 5$ TeV.

the 2-body mode $\tilde{g} \to \tilde{t}_1\bar{t}$ or $\tilde{t}_1^* t$. For the benchmark point in Table 19, the daughter top-squarks rapidly decay via $\tilde{t}_1 \to b\tilde{w}_1$ at $\sim 50\%$, $t\tilde{z}_1$ at $\sim 20\%$, $t\tilde{z}_2$ at $\sim 24\%$ and $t\tilde{z}_3$ at $\sim 6\%$. Stop decays into $b\tilde{w}_2$ and $t\tilde{z}_4$ are suppressed since in this model with stop soft masses unified at m_0 at the GUT scale, then the $\tilde{t}_1$ is mainly a right-stop eigenstate with suppressed decays to winos. The stop branching fractions vary hardly at all as $m_{1/2}$ varies along the model line. The higgsino-like $\tilde{z}_1$ state is expected to comprise a portion of the dark matter in the universe (the remaining portion might consist of, *e.g.*, axions [299]) while the higgsino-like $\tilde{z}_2$ and $\tilde{w}_1$ decay via 3-body modes to rather soft visible debris because the mass gaps $m_{\tilde{z}_2} - m_{\tilde{z}_1}$ and $m_{\tilde{w}_1} - m_{\tilde{z}_1}$ are typically only 10-20 GeV and hence essentially invisible for the purposes of this paper.

Putting together production and decay processes, gluino pair production final states consist of $t\bar{t}t\bar{t} + \not{E}_T$, $t\bar{t}t\bar{b} + \not{E}_T$ and $t\bar{t}b\bar{b} + \not{E}_T$ parton configurations. In the case where $\tilde{z}_2$ is produced via the gluino cascade decays, then the boosted decay products from $\tilde{z}_2 \to \ell^+\ell^-\tilde{z}_1$ decay may display an invariant mass edge $m(\ell^+\ell^-) < m_{\tilde{z}_2} - m_{\tilde{z}_1} \sim 10 - 20$ GeV. The existence of such an edge in gluino cascade decay events containing an OS/SF

dilepton pair would herald the presence of light higgsinos [258, 300] though the cross sections for these events are very small. In this section, we shall focus on the observation of the signal and prospects for gluino mass reconstruction using the inclusive sample with $t\bar{t}t\bar{t} + \not{E}_T$, $t\bar{t}t\bar{b} + \not{E}_T$ and $t\bar{t}b\bar{b} + \not{E}_T$ final states, with no attention to how the final state higgsinos (which are produced in the bulk of the cascade decays) decay.

V.1.2. Event generation

Two procedures have been employed for event generation, one using ISAJET 7.85 [49], which is referred to as our "Isajet" simulation and one using MADGRAPH 2.3.3 [261] interfaced to PYTHIA 6.4.14 [262] with detector simulation by DELPHES 3.3.0 [263], which is referred to as our "MadGraph" simulation.

Isajet Simulation

Our Isajet simulation includes detector simulation by the Isajet toy detector, with calorimeter cell size $\Delta\eta \times \Delta\phi = 0.05 \times 0.05$ and $-5 < \eta < 5$. The HCAL energy resolution is taken to be $80\%/\sqrt{E} + 3\%$ for $|\eta| < 2.6$ and $100\%/\sqrt{E} + 5\%$ for $|\eta| > 2.6$, where the plus denotes combination in quadrature. The ECAL energy resolution is assumed to be $3\%/\sqrt{E} + 0.5\%$. A UA1-like jet finding algorithm with jet cone size $R = 0.4$ is used and it is required that $E_T(jet) > 50$ GeV and $|\eta(jet)| < 3.0$. Leptons are considered isolated if they have $p_T(e \text{ or } \mu) > 20$ GeV and $|\eta| < 2.5$ with visible activity within a cone of $\Delta R < 0.2$ of $\sum E_T^{cells} < 5$ GeV. The strict isolation criterion helps reduce multi-lepton backgrounds from heavy quark ($c\bar{c}$ and $b\bar{b}$) production.

A hadronic cluster with $E_T > 50$ GeV and $|\eta(jet)| < 1.5$ is identified as a b-jet if it contains a B hadron with $p_T(B) > 15$ GeV and $|\eta(B)| < 3$ within a cone of $\Delta R < 0.5$ around the jet axis. A b-jet tagging efficiency of 60% is adopted and it is assumed that light quark and gluon jets can be mistagged as b-jets with a probability of 1/150 for $E_T < 100$ GeV, 1/50 for $E_T > 250$ GeV and a linear interpolation for 100

GeV $< E_T <$ 250 GeV.[28] These values are referred as our "Isajet" parameterization of b-tagging efficiencies.

MadGraph Simulation

In our MadGraph simulation, the events are showered and hadronized using the default MadGraph/PYTHIA interface with default parameters. Detector simulation is performed by Delphes using the default Delphes 3.3.0 "CMS" parameter card with several changes, which are enumerated here.

1. The HCAL and ECAL resolution formulae are set to be those used in the aforementioned Isajet simulation.

2. The jet energy scale correction is turned off.

3. An anti-k_T jet algorithm [271] is used with $R = 0.4$ rather than the default $R = 0.5$ for jet finding in Delphes (which is implemented via FastJet [272]). As in our Isajet simulation, only jets with $E_T(jet) > 50$ GeV and $|\eta(jet)| < 3.0$ are considered in the analysis. The choice of $R = 0.4$ in the jet algorithm is made both to make our MadGraph simulation conform to our Isajet simulation and to allow comparison with CMS b-tagging efficiencies [273]: see Table 21 below.

4. A jet flavor association module based on the "ghost hadron" procedure [274] is used, which allows decayed hadrons to be unambiguously assigned to jets. With this functionality a jet with $|\eta| < 1.5$ can be identified as a b-jet if it contains a B hadron (in which the b quark decays at the next step of the decay) with $|\eta| < 3.0$ and $p_T > 15$ GeV. These values are in accordance with our Isajet simulation.

5. Tau tagging is turned off, as the tagging of hadronic taus is not used in these analyses. Sometimes Delphes will wrongly tag a true b-jet as a tau, if the B

[28] These values are based on ATLAS studies of b-tagging efficiencies and rejection factors in $t\bar{t}H$ and WH production processes [275].

hadron in the jet decays to a tau. As we are trying to perform a cross section measurement in a regime where the overall signal cross section is small, we do not want to "lose" these b-jets.

Processes Simulated

Our Isajet simulation was used to generate the signal from gluino pair production at our benchmark point, as well as for other parameter points along our model line. Our Isajet simulation was also used to simulate backgrounds from $t\bar{t}$, W + jets, Z + jets, WW, WZ, and ZZ production. The W + jets and Z + jets backgrounds use exact matrix elements for one parton emission, but rely on the parton shower for subsequent emissions. In addition, background events for QCD jet production (jet-types including g, u, d, s, c, and b quarks) over five p_T ranges are also generated with our Isajet simulation procedure, as shown in Table II of Ref. [295]. Additional jets are generated via parton showering from the initial and final hard scattering subprocesses.

Our MadGraph simulation was used to generate the signal from gluino pair production at our benchmark point, as well as for other parameter points along our model line. It was also used to generate backgrounds from $t\bar{t}$, $t\bar{t}b\bar{b}$, $b\bar{b}Z$, and $t\bar{t}t\bar{t}$ production as well as from single top production. To avoid the double counting that would ensue from simulating $t\bar{t}$ as well as $t\bar{t}b\bar{b}$, events with more than two truth b-jets in the $t\bar{t}$ sample were vetoed.

In our MadGraph simulation, we normalize the overall cross section for our signal to NLL values obtained from NLL-FAST [298]. For $t\bar{t}$ we used an overall cross section of 953.6 pb, following Ref. [265]. As MadGraph chooses the scale dynamically event-by-event, we follow Ref. [305] and use a K-factor of 1.3 for our $t\bar{t}b\bar{b}$ backgrounds; the authors of this work find larger K-factors when a dynamic scale choice is not employed [301]. For the evaluation of the background from $b\bar{b}Z$ production we use a K-factor of 1.5, following Ref. [302], while for the $t\bar{t}t\bar{t}$ backgrounds we use a K-factor of 1.27, following Ref. [303].

For our single-top cross sections we use the ATLAS-CMS recommended predictions [304] which are based on the Hathor v2.1 program [306]. Following this reference we take the total NLO cross section for single-top production processes ($qb \to q't$ mediated by the t-channel W-exchange for which the NLO cross section is 248.1 pb and $gb \to Wt$ production for which the NLO cross section is 84.4 pb, together with the electroweak s-channel process, $ud \to tb$, for which the NLO cross section is 11.4 pb) to be 343.9 pb.

We found very similar results when using signal events from our Isajet simulation procedure as when using signal events from our MadGraph simulation procedure. We found significantly more $t\bar{t}$ events with high values of missing $\not{E}_T$ from our MadGraph simulation procedure than we did from our Isjaet procedure, presumably due to differences in showering algorithms. To be conservative, we use the larger $t\bar{t}$ backgrounds generated from MadGraph in our analyses. The hard $\not{E}_T$ cuts described below together with the requirement of at least two tagged b-jets, very efficiently remove the backgrounds from $W, Z+$ jets and from VV production simulated with Isajet. In the interest of presenting a clear and concise description of our analysis, we will not include these backgrounds in the figures and tables in the remainder of this work. For consistency with the most relevant SM backgrounds from $t\bar{t}$, $Zb\bar{b}$, $t\bar{t}b\bar{b}$, $t\bar{t}t\bar{t}$ and single top production, we likewise utilize our signal samples generated using the MadGraph simulation procedure.

V.1.3. Gluino event selection

To separate the gluino events from SM backgrounds, we begin by applying a set of precuts to our event samples, which we call **C1** (for "cut set 1"). These are very similar to a set of cuts found in the literature [295, 307]. However, since our focus is on the signal from very heavy gluinos ($m_{\tilde{g}} \geq 1.6$ TeV), we have raised the cut on jet p_T to 100 GeV from 50 GeV and included a cut on the transverse mass of the lepton and $\not{E}_T$ in events with only one isolated lepton (to reduce backgrounds from events with W bosons).

C1 Cuts:

$$\begin{aligned} \not{E}_T &> \max(100 \text{ GeV}, 0.2M_{eff}), \\ n(jets) &\geq 4, \\ E_T(j_1, j_2, j_3, j_4) &> 100 \text{ GeV}, \\ S_T &> 0.2, \\ m_T(\ell, \not{E}_T) &> 150 \text{ GeV}, \text{ if } n_{lep} = 1. \end{aligned}$$

Here, M_{eff} is defined as in Hinchliffe *et al.* [307] as $M_{eff} = \not{E}_T + E_T(j_1) + E_T(j_2) + E_T(j_3) + E_T(j_4)$, where $j_1 - j_4$ refer to the four highest E_T jets ordered from highest to lowest E_T, $\not{E}_T$ is missing transverse energy, S_T is transverse sphericity[29], and m_T is the transverse mass of the lepton and the $\not{E}_T$.

Since the signal naturally contains a high multiplicity of hard b-partons from the decay of the gluinos because third generation squarks tend to be lighter than other squarks, in addition to the basic **C1** cuts, we also require the presence of two tagged b-jets,

***b*-jet multiplicity Cut:**

$$n_b \geq 2. \tag{109}$$

using the "Isajet" parameterization of b-tagging efficiencies and light jet mistagging. Even after these cuts, we must still contend with sizable backgrounds, as can be seen from Fig. 45 where we show the $\not{E}_T$ distribution from the $t\bar{t}$, $t\bar{t}b\bar{b}$, $b\bar{b}Z$, $t\bar{t}t\bar{t}$ and single

[29]Sphericity is defined, *e.g.*, in *Collider Physics*, V. Barger and R. J. N. Phillips (Addison Wesley, 1987). Here, we restrict its construction to using only transverse quantities, as is appropriate for a hadron collider.

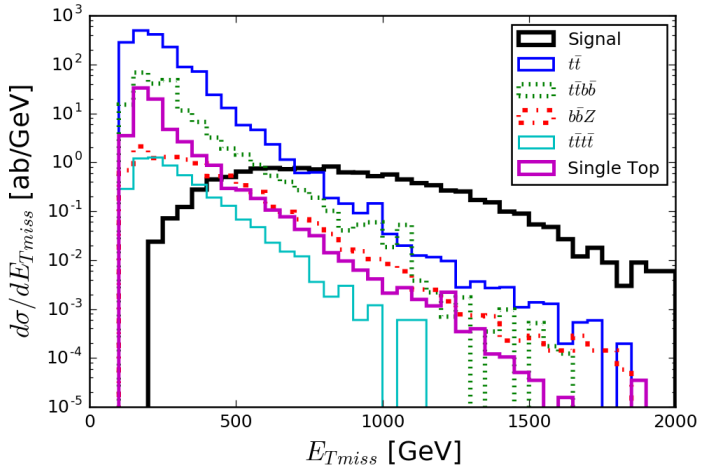

Figure 45: Distribution of $\not{E}_T$ after C1 cuts (109) with the requirement of two b-tagged jets for the gluino pair production signal, as well as the most relevant backgrounds ($t\bar{t}$, $t\bar{t}b\bar{b}$, $b\bar{b}Z$, $t\bar{t}t\bar{t}$ and single top).

top backgrounds, as well as from the gluino pair production for the benchmark point in Table 19. We see that the backgrounds fall more quickly with $\not{E}_T$ than the signal leading us to impose a $\not{E}_T$ cut,

$\not{E}_T$ Cut:

$$\not{E}_T > 750 \text{ GeV}. \tag{110}$$

After this cut, we are left with comparable backgrounds from $t\bar{t}$ and $t\bar{t}b\bar{b}$ production with a somewhat smaller contribution from $b\bar{b}Z$ production. The $t\bar{t}t\bar{t}$ and single top background rates are much smaller.

Once we have made the $\not{E}_T$ cut (110), we examine the distribution of the multiplicity of b-tagged jets, with the goal of further improving the signal to background ratio. This distribution is shown in Fig. 46. This figure suggests two roads to selection criteria that will leave a robust signal and negligible backgrounds. Obviously, we can require three

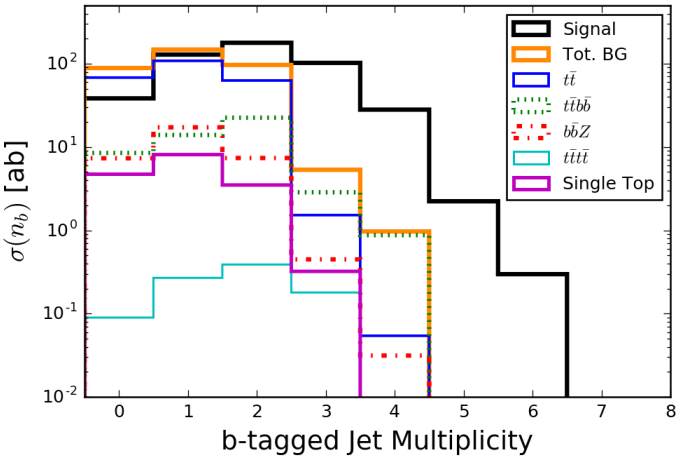

Figure 46: The number of b-tagged jets, using our Isajet parameterization of the b-tagging efficiency, after C1 cuts (109) and the requirement that $\not{E}_T > 750$ GeV.

b-tags, which decimates the backgrounds (especially $t\bar{t}$) at the cost of some signal. Our goal is to devise a strategy that will allow mass measurements even with integrated luminosities of 100-200 fb^{-1} that will be available by the end of the 2018 LHC shutdown for which significant loss of event rate rapidly becomes a problem. With this in mind, we also examine the possibility that we can only require two b-tags. While this saves some signal, we clearly need to impose additional cuts to obtain a clean signal sample. We pursue both of these approaches: the larger cross section from the "2b" analysis will certainly be useful in early LHC running, but the greater reduction of backgrounds provided by the "3b" analysis would be expected to yield cleaner data samples at the high luminosity LHC.

To further clean up the $n_b \geq 2$ signal sample, we first note that that the bulk of the background comes from $t\bar{t}$ production. It is reasonable to expect that $t\bar{t}$ production leads to $\not{E}_T > 750$ GeV only if a semi-leptonically decaying top is produced with a very high transverse momentum, with the daughter neutrino "thrown forward" in the top rest frame, while the other top decays hadronically (so the $\not{E}_T$ is not cancelled). In this case, the b-jet from the decay of the semi-leptonically decaying top would tend to

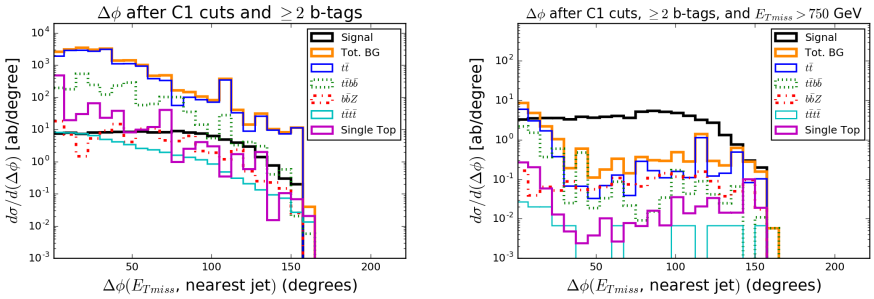

Figure 47: The distribution of $\Delta\phi(\not{E}_T,$ nearest jet). Explicitly this quantity is the minimum angle between the $\not{E}_T$ vector and the transverse momentum of one of the leading four jets. This quantity is shown (left) after C1 cuts (109) with the requirement of two b-tagged jets and (right) after these cuts, and a cut of $\not{E}_T > 750$ GeV.

be collimated with the neutrino; *i.e.*, to the direction of $\not{E}_T$. We do not expect such a correlation in the signal since the heavy gluinos need not be particularly boosted to yield $\not{E}_T > 750$ GeV. This motivated us to examine the distribution of the minimum value of $\Delta\phi$, the angle between the transverse momenta of a jet and the $\not{E}_T$ vector, for each of the four leading jets. We show this distribution in Fig. 47, after the **C1** and the two tagged b-jet cuts, both with (right frame) and without (left frame) the $\not{E}_T > 750$ GeV cut. Without this hard $\not{E}_T$ cut, we see that the distribution of $\Delta\phi$ is very slowly falling for the $t\bar{t}$ background, and roughly flat for the signal as for the other backgrounds, until all the distributions cut-off at about 150°. The expected peaking of the $t\bar{t}$ background at low values of $\Delta\phi$ is, however, clearly visible in the right frame, while the signal is quite flat. The next largest backgrounds from $t\bar{t}b\bar{b}$ and single top also show a similar peaking (for the same reason) at low $\Delta\phi$ values. We are thus led to impose the cut,

$\Delta\phi$ Cut:

$$\Delta\phi(\not{E}_T, \text{nearest of four leading jets}) > 30°, \tag{111}$$

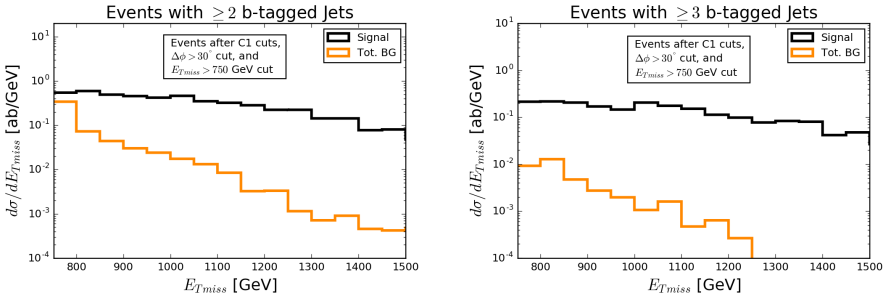

Figure 48: The distribution of $\not{E}_T$ after **C1** cuts (109), the $\not{E}_T > 750$ cut (110), and the $\Delta\phi > 30^\circ$ cut (111) with the additional requirement of (left) at least two b-tagged jets (right) at least three b-tagged jets. The background distribution represents the sum of the contributions from the $t\bar{t}$, $t\bar{t}b\bar{b}$, $b\bar{b}Z$, $t\bar{t}t\bar{t}$ and single top backgrounds.

which greatly diminishes the dominant backgrounds in the two tagged b-jet channel with only a very modest loss of signal. Indeed, because the signal-to-background ratio is so vastly improved with only a slight reduction of the signal, we have retained this cut in both our $2b$ and $3b$ analyses.

Having made this cut, we return to the $\not{E}_T$ distribution, to see whether further optimization might be possible. Toward this end, we show the distribution after the **C1** cuts (109), the $\not{E}_T > 750$ GeV cut (110), and the $\Delta\phi > 30^\circ$ cut (111) in Fig. 48, requiring at least two b-tagged jets (left panel) or three b-tagged jets (right panel). We see that an additional cut on $\not{E}_T$ will be helpful in the $2b$ analysis, but not as helpful in the $3b$ analysis. Therefore, our final cut choices are:

$2b$ **Analysis:**

$$\begin{aligned} &\text{C1 cuts,} \\ n_b &\geq 2, \\ \Delta\phi(\not{E}_T, \text{nearest of four leading jets}) &> 30^\circ, \\ \not{E}_T &> 900 \text{ GeV}, \end{aligned}$$

and

$3b$ **Analysis:**

$$\begin{aligned} &\text{C1 cuts,} \\ &n_b \geq 3, \\ \Delta\phi(\not{E}_T, &\text{nearest of four leading jets}) > 30^\circ, \\ &\not{E}_T > 750 \text{ GeV}, \end{aligned}$$

The cross section including acceptance after each of the cuts, for the signal benchmark point, as well as for the sum of the $t\bar{t}$, $t\bar{t}b\bar{b}$, $b\bar{b}Z$, $t\bar{t}t\bar{t}$ and single top backgrounds, is given in Table 20, for both the $2b$ and the $3b$ analyses.

Cut	$2b$ Sig.	$2b$ BG	$3b$ Sig.	$3b$ BG
C1	872	5.14×10^5	872	5.14×10^5
$\not{E}_T > 750$ GeV	479	340	479	340
b-tagging	311	103	133	6.31
$\Delta\phi > 30^\circ$	249	28.1	105	1.78
Final $\not{E}_T$ cut	167	5.31	105	1.78

Table 20: Cross section times acceptance in attobarns (1000 ab= 1 fb) after various cuts are applied. The "b-tagging" cut refers to the requirement of ≥ 2 b-tagged jets in the $2b$ analysis and ≥ 3 b-tagged jets in the $3b$ analysis. For the $2b$ analysis, the "final $\not{E}_T$ cut" refers to the additional requirement that $\not{E}_T > 900$ GeV; there is no additional cut in the $3b$ analysis.

Gluino Event Characteristics

Now that we have finalized our analysis cuts, we display the characteristic features of gluino signal events satisfying our selection criteria for our natural SUSY benchmark point with $m_{\tilde{g}} \simeq 2$ TeV and $m_{\tilde{t}_1} \sim 1500$ TeV. Figure 49 shows the transverse energy distribution of the four hardest jets from the two-tagged b-jet signal as well as from the backgrounds, after the cut set (112). We see that the two hardest jets typically have $E_T \sim 700$ GeV and 400 GeV, respectively, while the third and fourth jet E_T

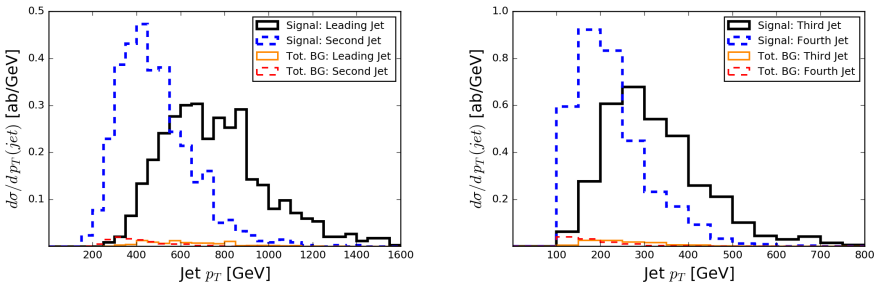

Figure 49: Transverse momenta of the leading jet and second-leading jet in p_T (left) and for the third and fourth-leading jets (right) for signal and background events after $2b$ analysis cuts. The distribution of these quantities after $3b$ analysis cuts is similar.

distributions peak just below 300 GeV and 200 GeV. The distributions for the signal with three tagged b-jets are very similar and not shown for brevity. While the actual peak positions in the distributions depend on the gluino and stop masses, the fact that the events contain four hard jets is rather generic. We also see that the SM background after these cuts is negligibly small, and that we do indeed have a pure sample of gluino events.

In Fig. 50, we show the jet multiplicity for the benchmark point signal and background events after our selection cuts for both the two tagged b-jet (solid) and the three-tagged b-jet (dashed) samples. Recall that jets are defined to be hadronic clusters with $E_T > 50$ GeV. We see that the signal indeed has very high jet multiplicity relative to the background. Since the exact jet multiplicity may be sensitive to details of jet definition, and because our simulation of the background with very high jet multiplicity is less reliable due to the use of the shower approximation rather than exact matrix elements, we have *not used* jet multiplicity cuts to further enhance the signal over background. (Note: the sum of cross-sections above a minimum jet-multiplicity, as implemented in the **C1** cuts, is not expected to depend much on the implementation of the jet multiplicity cut.)

In Fig. 51 we show the transverse momentum of b-tagged jets in signal and back-

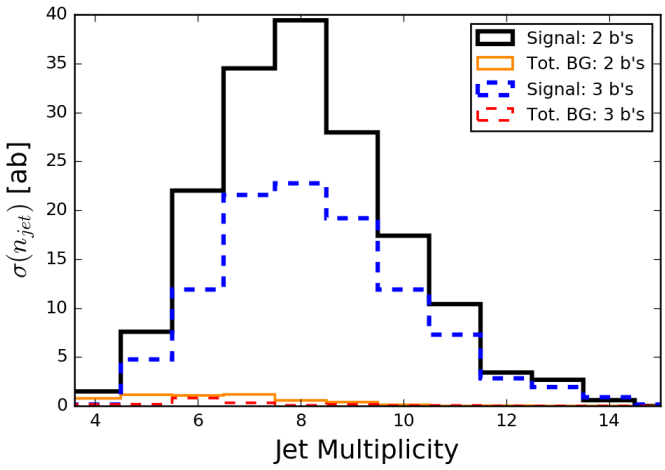

Figure 50: Jet multiplicity for signal and background events satisfying our $2b$ and $3b$ analysis cuts. Recall that we require jets to have $p_T > 50$ GeV and $|\eta| < 3.0$.

ground events satisfying the final cuts for ≥ 2 tagged b-jet events (left frame) and for ≥ 3 tagged b-jet events (right frame). We see that the hardest b-jet E_T ranges up to ~ 1 TeV, while the second b-jet, for the most part, has $E_T \sim 100 - 600$ GeV. Again, we stress that the b-jet spectrum shape will be somewhat sensitive to the gluino-stop as well as stop-higgsino mass differences, but the hardness of the b-jets is quite general. We expect that the b-jets would remain hard (though the E_T distributions would have different shapes) even in the case when the stop is heavier than the gluino, and the gluino instead dominantly decays via the three body modes, $\tilde{g} \to t\bar{t}\tilde{z}_{1,2}$ and $\tilde{g} \to tb\tilde{w}_1$.

Before turning to a discussion of our results for the mass reach and of the feasibility of the extraction of $m_{\tilde{g}}$ using the very pure sample of signal events, we address the sensitivity of our cross section calculations to the Isajet b-tagging efficiency and purity algorithm that we have used. This algorithm was based on early ATLAS studies [275] of WH and $t\bar{t}H$ processes where the transverse momentum of the b-jets is limited to several hundred GeV. More recently, the CMS Collaboration [273] has provided loose, medium and tight b-tagging algorithms with corresponding charm and light parton mis-tags whose validity extends out to a TeV. We show a comparison of the SUSY signal

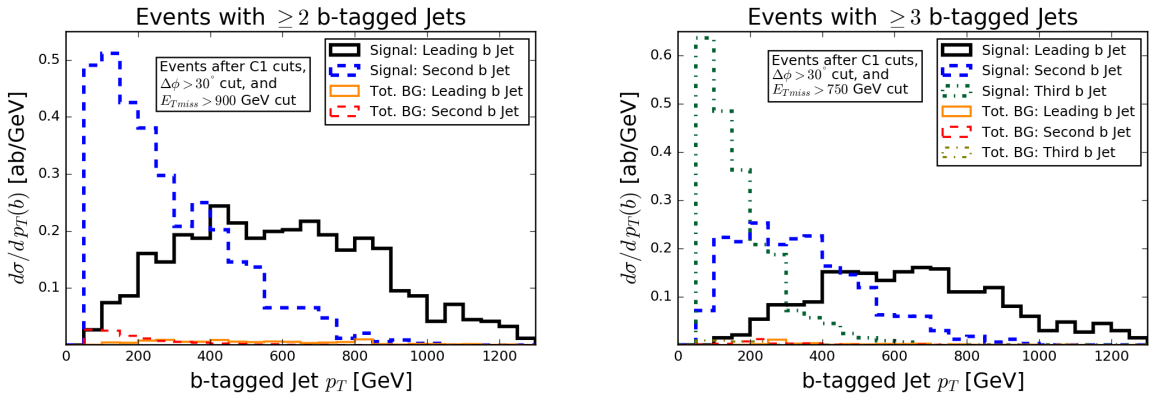

Figure 51: The distribution of the transverse momenta of the leading and second leading b-tagged jet after (left) the $2b$ analysis cuts and (right) the $3b$ analysis cuts.

	Isajet	CMS Medium	CMS Tight
≥ 2 tagged b jets, $\not{E}_T > 900$ GeV	167 (32)	207 (25)	121 (39)
≥ 3 tagged b jets, $\not{E}_T > 750$ GeV	105 (59)	182 (47)	61.1 (78)

Table 21: The LHC signal cross section in ab for our SUSY benchmark point for ≥ 2 tagged b-jet events, and for ≥ 3 tagged b-jet events after all the analysis cuts in (112) and (112), respectively. The numbers in parenthesis are the corresponding signal-to-background ratios. We show results for the Isajet parametrization of b-tagging efficiency as well as for the medium and tight b-tagging efficiencies in Ref. [273].

rate for our SUSY benchmark point for the sample with at least two/three tagged b-jets after the selection cuts (112)/(112) in Table 21. We illustrate results for the medium and tight algorithms in Ref. [273]. Also shown, in parenthesis are the corresponding signal-to-background ratios, after these cuts. We see that the cross sections for the Isajet parametrization of the b-tagging efficiency, as well as the corresponding values of S/B lie between those obtained using the medium and tight algorithms in the recent CMS study. Although it is difficult to project just how well b-tagging will perform in the high luminosity environment, we are encouraged to see that our simple algorithm gives comparable answers to those obtained using the more recent tagging algorithms in Ref. [273] even though we have very hard b-jets in the signal.

V.1.4. Results

In this section, we show that the pure sample of gluino events that we have obtained can be used to make projections for both the gluino mass reach as well as for the extraction of the gluino mass, along the RNS model line introduced in the beginning of Sec. V.1.1. We consider several values of integrated luminosities at LHC14 ranging from 150 fb^{-1} to the 3000 fb^{-1} projected to be accumulated at the high luminosity LHC.

Gluino mass reach

We begin by showing in Fig. 52 the gluino signal cross section after all analysis cuts via both the ≥ 2 tagged b-jets (left frame) and the ≥ 3 tagged b-jets (right frame) channels. The total SM backgrounds in these channels are 5.3 ab and 1.8 ab, respectively. The various horizontal lines show the minimum cross section for which a Poisson fluctuation of the expected background occurs with a Gaussian probability corresponding to 5σ, for several values of integrated luminosities at LHC14, starting with 150 fb^{-1} expected (per experiment) before the scheduled 2018 LHC shutdown, 300 fb^{-1} the anticipated design integrated luminosity of LHC14, as well as 1 ab^{-1} and 3 ab^{-1} that are expected to be accumulated after the high luminosity upgrade of the LHC. We have checked that for an observable signal we always have a minimum of five events and a sizable signal-to-background ratio. (The lowest value for signal-to-background ratio we consider, *i.e.*, the value at the maximum gluino mass for which we have 5σ discovery with at least five events is for 3000 fb^{-1} in our $2b$ analysis, for which $S/B = 1.6$.) We see from Fig. 52 that, with 150 fb^{-1}, LHC experiments would be probing $m_{\tilde{g}}$ values up to 2300 GeV (actually somewhat smaller since the machine energy is still 13 TeV) via the $2b$ analysis, with only a slightly smaller reach via the $3b$ analysis. Even for the decoupled squark scenario, we project a 3000 fb^{-1} LHC14 5σ gluino reach to ~ 2400 GeV; this will extend to about 2800 GeV in both the $2b$ and $3b$ channels at the HL-LHC. These projections are significantly greater than the corresponding reach from the mSUGRA

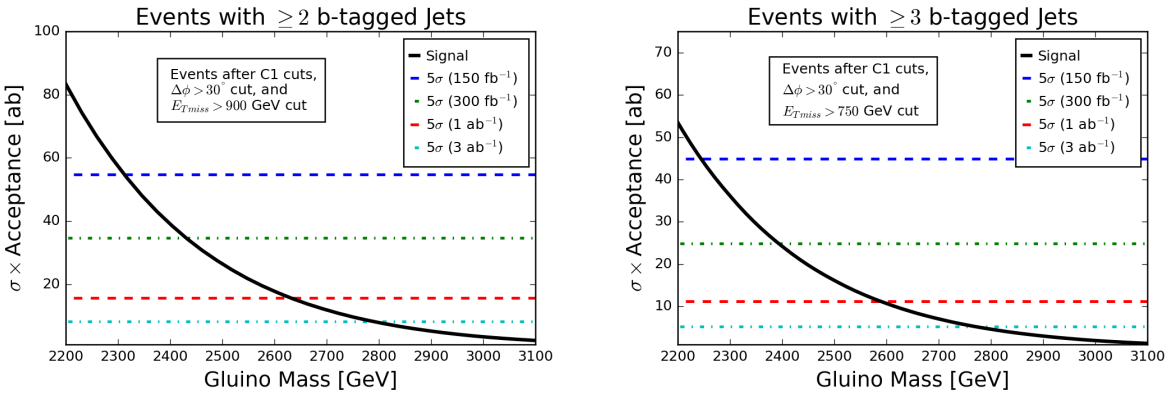

Figure 52: The gluino signal cross section for the ≥ 2 tagged b-jet (left) and the ≥ 3 tagged b-jet channels (right) after all the analysis cuts described in the text. The horizontal lines show the minimum cross section for which the Poisson fluctuation of the corresponding SM background levels, 5.3 ab for $2b$ events and 1.8 ab for $3b$ events, occurs with a Gaussian probability corresponding to 5σ for several values of integrated luminosities at LHC14.

model [308] because (1) the presence of hard b-jets in the signal serves as an additional handle to reduce SM backgrounds, especially those from W, Z+jet production processes [309], and (2) the larger $m_{\tilde{g}} - m_{\tilde{z}_1}$ mass gap expected from RNS leads to harder jets and harder $\not{E}_T$ as compared to mSUGRA. A further improvement in reach may of course be gained by combining ATLAS and CMS data sets.

Gluino mass measurement

We now turn to the examination of whether the clean sample of gluino events that we have obtained allows us to extract the mass of the gluino. For decoupled first/second generation squarks, these events can only originate via gluino pair production. Assuming that the background is small, or can be reliably subtracted, the event rate is completely determined by $m_{\tilde{g}}$. A determination of this event rate after the analysis cuts in (112) or (112) should, in principle, yield a measure of the gluino mass.

Our procedure for the extraction of the gluino mass (for our benchmark point) is illustrated in the left frame of Fig. 53, where we show a blow-up of the SUSY signal cross section versus $m_{\tilde{g}}$ for ≥ 2 tagged b-jet events after all our analysis cuts. The

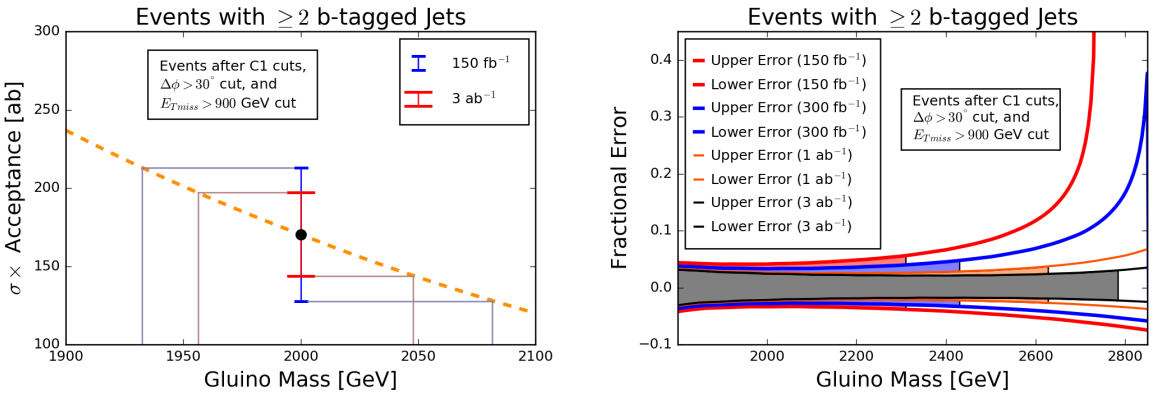

Figure 53: Illustration of our method to extract the precision with which the gluino mass may be extracted at the LHC for the $2b$ sample (left frame) and the statistical precision that may be attained as a function of $m_{\tilde{g}}$ for integrated luminosities of 150 fb^{-1}, 300 fb^{-1}, 1 ab^{-1} and 3 ab^{-1} (right frame). The left frame shows a blow-up of the gluino signal cross section versus $m_{\tilde{g}}$ for the $\geq$ 2 tagged b-jets after all the analysis cuts described in the text. Also shown are the "1σ" error bars for a determination of this cross section (where the 1σ statistical error on the observed number of signal events and a 15% uncertainty on the gluino production cross section have been combined in quadrature) for an integrated luminosity of 150 fb^{-1} (blue) and 3 ab^{-1} (red). The other lines show how we obtain the precision with which the gluino mass may be extracted for our benchmark gluino point for these two values of integrated luminosities. The bands in the right frame illustrate the statistical precision on the extracted value of $m_{\tilde{g}}$ that may be attained at the LHC for four different values of integrated luminosity. We terminate the shading at the 5σ discovery reach shown in Fig 52.

signal cross section can be inferred from the observed number of events in the sample and subtracting the expected background. The error bar shown in the figure is obtained by combining in quadrature the 1σ statistical error on the cross section based on the expected total number of (signal plus background) events expected in the sample, with a 15% theoretical error on the gluino production cross section[30]. This error bar is used to project "the 1σ" uncertainty in the measurement of $m_{\tilde{g}}$. From the figure, $m_{\tilde{g}} = 2000^{+80}_{-70}$ GeV with 150 fb^{-1}, and $m_{\tilde{g}} = (2000^{+50}_{-45})$ GeV with 3 ab^{-1}. The right frame of Fig. 53 shows the precision with which the gluino mass may be extracted via

[30]The LHC SUSY Cross Section Working Group [310] currently cites a theoretical error of $\sim 30\%$. We project that this error will be reduced by a factor of 2 by the time the high luminosity LHC is operational. We have checked that the precision on the gluino mass changes by only $\gtrsim 1\%$ if we use a 30% theory error instead of 15%. As an example the larger 1σ error bar changes from 4.8% to 6.2% for the maximum discoverable gluino mass ($\sim$ 2400 GeV) with 300 fb^{-1} of integrated luminosity.

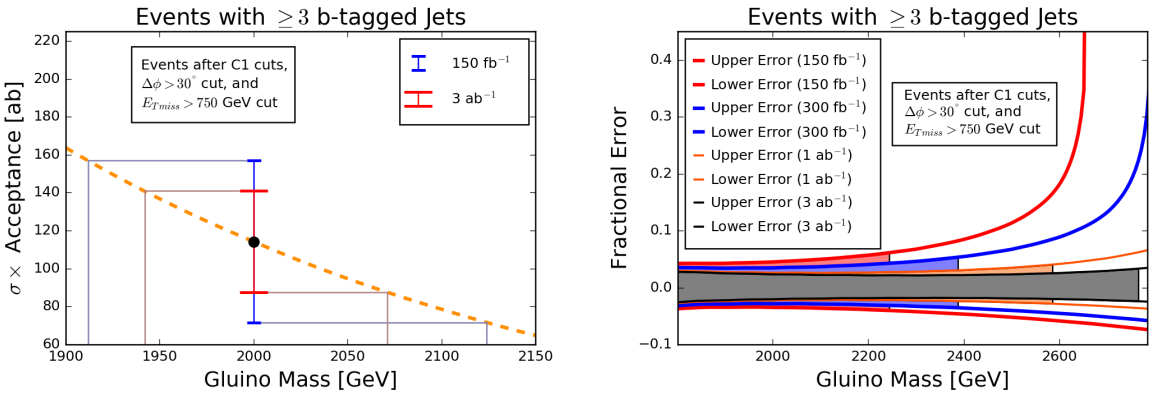

Figure 54: The same as Fig. 53, but for the clean SUSY sample with ≥ 3 tagged b-jets.

the clean events in the ≥ 2 tagged b-jets channel versus the gluino mass for four different values of integrated luminosity ranging from 150 fb^{-1} to 3 ab^{-1}. The shading on the various bands extends out to the 5σ reach projection in Fig. 52. We see that gluino mass extraction with a sub-ten percent precision is possible with even 150 fb^{-1} of integrated luminosity if gluinos are lighter than 2.5 TeV and cascade decay via stops into light higgsinos as in the RNS framework. It should be noted though that the 5σ reach of the LHC extends to just ~ 2.3 TeV so that the determination, $m_{\tilde{g}} = 2.5$ TeV would be a mass measurement for a discovery with a significance smaller than the customary 5σ. At the high luminosity LHC, the gluino mass may be extracted with a statistical precision better than 2-5% (depending on their mass) all the way up to $m_{\tilde{g}} \sim 2.8$ TeV, *i.e*, if gluinos are within the 5σ discovery range of the HL-LHC! Gluino mass determination would also be possible for the range of gluino masses for which the discovery significance was smaller than 5σ.

Prospects for gluino mass measurement via the ≥ 3 tagged b-jet sample are shown in Fig. 54. We see that the statistical precision on the mass measurement that may be attained is somewhat worse than that via the $\geq 2b$ channel shown in Fig. 53, though not qualitatively different except at the high mass end. The difference is, of course, due to the lower event rate in this channel.

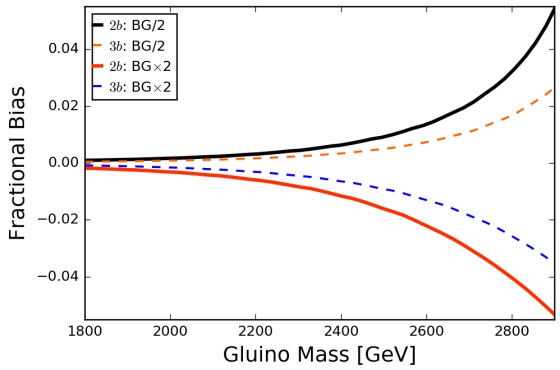

Figure 55: The systematic bias, discussed in the text, in the measurement of the gluino mass resulting from a mis-estimate of the SM background by a factor of 2 in either direction. The solid lines are for the signal in the $2b$ channel while the dashed lines are for the signal in the $3b$ channel.

Before proceeding further, we point out that in order to extract the gluino mass, we have assumed that our estimate of the background is indeed reliable. Since the expected background has to be subtracted from the observed event rate to obtain the signal cross section, and via this the value of $m_{\tilde{g}}$, any error in the estimation of the expected background will result in a *systematic shift* in the extracted gluino mass. For instance, an over-estimation of the background expectation compared to its true value, will result in too small a signal and a corresponding overestimate of the mass of the gluino. We expect that by the time a precise mass measurement becomes feasible, it will be possible to extract the SM background to a good precision by extrapolating the backgrounds normalized in the "background region" (that are expected to have low signal contamination) to the "signal region" using the accumulated data. We show in Fig. 55 the systematic bias on the gluino mass that could result because the background estimate differs from the true value by a factor of 2. We see that this (asymmetric) systematic bias is below 2% for $m_{\tilde{g}} \leq 2.6$ TeV, but becomes as large as 4% for the largest masses for which there is a 5σ signal at the high luminosity LHC in the two tagged b-jets sample. This bias is smaller for the three tagged b-jets sample because

the corresponding background is smaller.

Our conclusions for the precision with which LHC measurements might extract the gluino mass are very striking, and we should temper these with some cautionary remarks. The most important thing is that any extraction of the mass from the absolute event rate assumes an excellent understanding of the detector in today's environment as well as in the high luminosity environment of future experiments. While we are well aware that our theorists' simulation does not include many important effects, *e.g.*, particle detection efficiencies, jet energy scales, full understanding of b-tagging efficiencies particularly for very high E_T b-jets, to name a few, we are optimistic that these will all be very well understood (given that there will be a lot of data) by the time gluino mass measurements become feasible. The fact that our proposal relies on an inclusive cross section with ≥ 4 jets (of which 2 or 3 are b-jets) and does not entail very high jet multiplicities suggests that our procedure should be relatively robust. An excellent understanding of the $\not{E}_T$ tail from SM sources, as well as of the tagging efficiency (and associated purity) for very high E_T b-jets are crucial elements for this analysis.

In Fig. 56 we compare the approximate reach for various present and future hadron collider options for gluino pair production. The region to the right of the dashed line yields large electroweak fine-tuning and is considered unnatural. The green bar shows the present LHC 95% CL limit on $m_{\tilde{g}}$ as derived in several simplified models which should be applicable to the present RNS case. The dark and light blue bars show our projected LHC14 300 and 3000 fb^{-1} 5σ reaches for RNS. These cover only a portion of natural SUSY parameter space. The lavendar bar shows the reach of HE-LHC with $\sqrt{s} = 33$ TeV as abstracted from Ref. [311] where it is assumed that the gluino directly decays to a light LSP via $\tilde{g} \to q\bar{q}\tilde{z}_1$ (presumably with no enhancement of decays to third generation quarks). The 5σ HE-LHC for 3000 fb^{-1} extends to $m_{\tilde{g}} \sim 5$ TeV and thus covers *all* of natural SUSY parameter space. The red bar shows the corresponding gluino reach of a 100 TeV pp collider at 5σ and 3000 fb^{-1}, as taken also from Ref. [311].

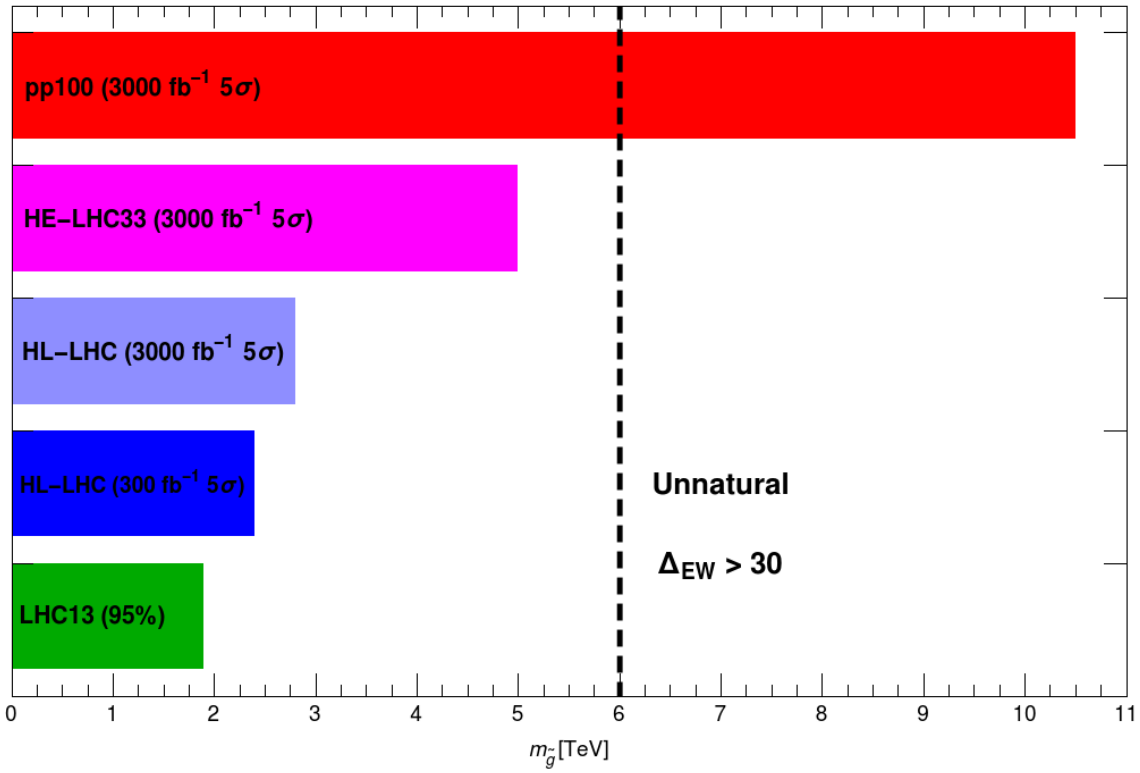

Figure 56: The approximate reach for various present and future hadron collider options for gluino pair production. The region to the right of the dashed line yields large electroweak fine-tuning and is considered unnatural.

Here, the reach extends just beyond $m_{\tilde{g}} \sim 10$ TeV. It probes only more deeply into unnatural SUSY parameter space beyond the complete coverage of the gluino offered by HE-LHC, but does offer the possibility of a squark discovery.

V.2. Aspects of the same-sign diboson signature from wino pair production with light higgsinos at the high luminosity LHC

One very special feature of the RNS models is that they have higgsino-like LSP with non-negligible gaugino component owing to the small value of μ as compared to Bino, Wino and Gluino required by naturalness constraint. This situation is shown in Fig. 3 which specifically shows the evolution of masses of Bino, Wino, Gluino and higgsino

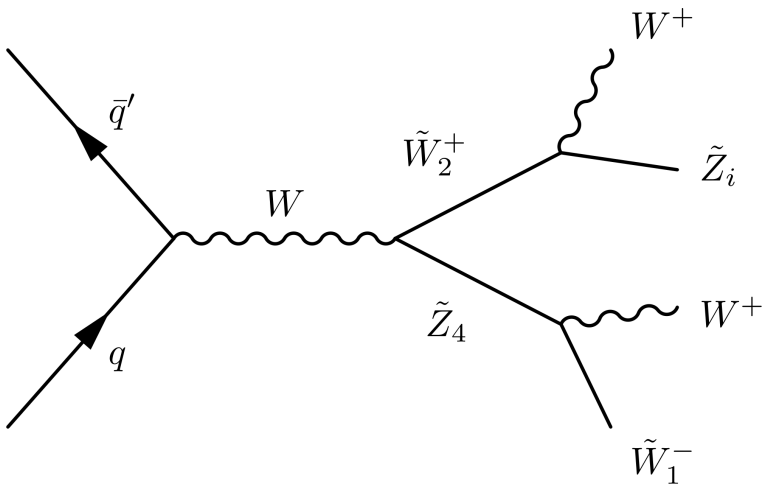

Figure 57: A Feynman diagram for same-sign diboson production at LHC in SUSY models with light higgsinos.

with energy for the NUHM2 model. Other RNS models will differ in the relative masses of Bino and Wino at the weak scale, as shown in Fig. 6 but higgsinos still have the lowest mass. This hierarchy leads to a novel, rather clean, same-sign diboson signature from wino pair production at hadron colliders. This is a distinctive signature to search for *natural* SUSY in hadron colliders. In this section, this signature has been examined in the context of the NUHM2 model. The Feynman diagram for this signature is shown in Fig. 57: $pp \to \tilde{w}_2^{\pm}\tilde{z}_4$ followed by $\tilde{w}_2^{\pm} \to W^{\pm}\tilde{z}_{1,2}$ and $\tilde{z}_4 \to W^{\pm}\tilde{w}_1^{\mp}$ decays. Half of the time, the daughter Ws will have the same sign, leading to distinctive same sign di-boson (SSdB) plus $\not{E}_T$ events with no additional jet activity other than from QCD radiation. The subsequent leptonic decays of the Ws lead to *clean same-sign dilepton* + $\not{E}_T$ events for which the SM backgrounds are very small. We stress that this class of same-sign dilepton events are easily distinguished from those arising from gluino/squark pair production [257] because they are relatively free of accompanying hard jet activity.

This SSdB signature has been previously examined in Ref. [258, 252]. In these studies, the main SM backgrounds considered were $t\bar{t}$, WZ, and $t\bar{t}W$ production (though

$t\bar{t}Z$ and inclusive $W^{\pm}W^{\pm}$ production from $qq \to q'q'W^{\pm}W^{\pm}$ processes are also mentioned). After a set of cuts to help distinguish the natural SUSY SSdB signal from SM backgrounds, it was found that the background dominantly arose from $t\bar{t}W$ production, and the LHC14 reach was obtained in the NUHM2 model[31]. It was emphasized that in models with gaugino mass unification (such as the NUHM2 model), the SUSY reach via the SSdB channel would (for integrated luminosities larger than ~ 100 fb^{-1}) exceed the reach via gluino pair production because the winos are only a third as light as gluinos. This assumes that gluinos decay democratically to all generations. In natural SUSY, where gluinos preferentially decay to the third generation, it has been shown that b-tagging [259] could be used to further enhance the gluino reach [247] in the $\not{E}_T$ channel. In Ref. [260], it was emphasized that for natural SUSY models with gaugino mass unification, the $pp \to \tilde{z}_1\tilde{z}_2 j$ reaction followed by $\tilde{z}_2 \to \ell^+\ell^-\tilde{z}_1$ decay, combined with the SSdB channel, would cover the majority of natural SUSY parameter space with $\Delta_{EW} < 30$ at the high luminosity LHC. This conclusion no longer obtains in string-motivated models such as natural generalized mirage mediation [42] or the mini-landscape [246] where the compressed spectrum of gauginos may allow for both wino and gluino masses beyond HL-LHC reach even while maintaining naturalness.

In this section, we revisit the SSdB signature from wino pair production in SUSY models with light higgsinos, making a number of important improvements. First, we expand upon earlier calculations by explicitly including several additional SM background processes: (1) $WWjj$ production, (2) $t\bar{t}Z$ production, (3) $t\bar{t}t\bar{t}$ production and (4) WWW production.[32] Second, we focus on the updated integrated luminosity target for the HL-LHC, namely 3000 fb^{-1} = 3 ab^{-1}. Third, we emphasize that the SSdB signature

[31]Since the NUHM2 model allows the soft terms $m_{H_u}^2$ and $m_{H_d}^2$ to be traded for weak scale inputs μ and m_A, it is easy to generate natural SUSY models by inputting low values of $|\mu| \sim 100 - 300$ GeV.

[32]In addition, our current calculations adopt MadGraph [261] and Pythia [262] for signal/background calculations and Delphes [263] for our LHC detector simulation. While it is not obvious that Delphes/PYTHIA is an improvement over the previous use of the Isajet detector simulation, the relative consistency of our new results with the previous results (when direct comparisons can be made) does provide a check on possible systematic errors.

from wino pair production offers an *independent discovery channel* for natural SUSY models, whether gaugino masses are unified or not. For instance, in anomaly-mediated SUSY breaking (AMSB) models, the gaugino masses are expected to occur in the weak scale ratio of $M_1 : M_2 : M_3 \sim 3.3 : 1 : -7$. For natural AMSB with $|\mu| \ll M_2$, it could be that gluino masses are well above LHC reach while wino masses are quite light: $M_2 \geq 300$ GeV. In such a case, the SSdB signature might be a robust discovery channel even if gluinos are too heavy to be detected. Since we do not assume gaugino mass unification, we present results in terms of the physical wino mass rather than *e.g.* in terms of $m_{1/2}$.

In addition to presenting projections for the 5σ reaches for the discovery of winos in this channel for various values of the wino mass $m_{\tilde{w}_2}$ and the values of $m_{\tilde{w}_2}$ that can be expected to be excluded at 95% confidence level, we also analyze the prospects for wino mass measurement. We point out that using rate information, we can measure the wino mass at better than the 10% level over its entire discovery range. It has been shown that if there is an excess in the clean SS dilepton sample, a determination of the charge asymmetry would provide an important consistency check. Various kinematic distributions have also been examined that may reveal characteristic features of the SSdB events. We find that although these distributions in themselves are not strongly sensitive to the wino mass, they may still be useful in a multivariate approach for extracting M_2.

V.2.1. Evaluation of signal and background cross sections

Signal production cross sections

Since the SSdB signature from pair production of winos is the subject of this study, we begin by showing in Fig. 58 the leading order (LO) and next-to-leading order (NLO) production cross sections for various wino pair production processes– as solid and dashed curves respectively. These cross sections are calculated for the $\sqrt{s} = 14$

TeV LHC using the PROSPINO computer code [264] and are plotted with respect to the charged wino mass, $m_{\tilde{w}_2}$. Since we will also be interested in examining the lepton charge asymmetry, we also show separately the cross sections for $pp \to \tilde{w}_2^+ \tilde{z}_4$ (red curves) and for $pp \to \tilde{w}_2^- \tilde{z}_4$ (green curves).

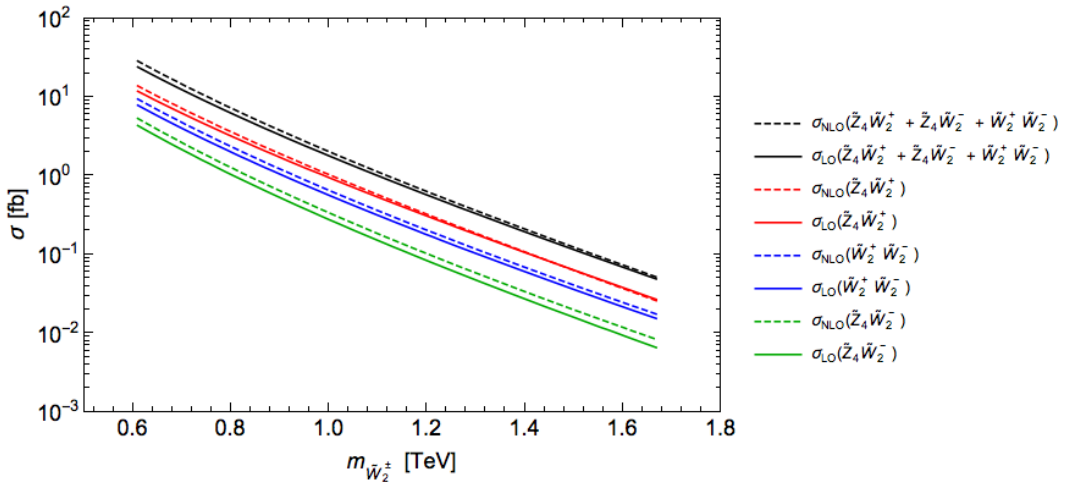

Figure 58: Leading order (solid) and next-to-leading order (dashed) cross sections for various wino pair production processes at the LHC with $\sqrt{s} = 14$ TeV versus charged wino mass $m_{\tilde{w}_2}$. The neutral wino mass $m_{\tilde{z}_4} \simeq m_{\tilde{w}_2}^{\pm} \sim M_2$.

Note that the $\tilde{w}_2^+ \tilde{z}_4$ cross section typically exceeds the cross section for $\tilde{w}_2^- \tilde{z}_4$ by a factor $\sim 3-4$. This charge asymmetry in production cross section arises from the preponderance of valence u quarks in the proton versus valence d quarks and increases with $m_{\tilde{w}_2}$ due to the growing importance of valence quark over sea quark annihilation as the sampled parton fractional momentum, x_F, increases. This results in a preponderance of $++$ over $--$ dilepton events as we shall see below.

The charged wino pair production cross section $pp \to \tilde{w}_2^+ \tilde{w}_2^-$ (blue curves) lies in between the $\tilde{w}_2^+ \tilde{z}_4$ and $\tilde{w}_2^- \tilde{z}_4$ curves. The black curves denote the cross sections for the summed wino pair production channels, which vary from the tens of fb level for $m_{\tilde{w}_2} \sim 600$ GeV to $\sim 10^{-2}$ fb for $m_{\tilde{w}_2} \sim 1.6$ TeV. These wino pair production cross sections hardly vary with respect to μ (or $\tan\beta$ or $m_{\tilde{q}}$) as can be seen from Figs. 4 and

5 of Ref. [258], since the winos couple directly to $W^{\pm}$ via the large $SU(2)_L$ coupling, g, according to the interactions described in eq. (8.102) of Ref. [13], and since the higgsino admixture in the wino-like state is small.

Wino branching fractions

The $\tilde{w}_2$ and $\tilde{z}_4$ branching fractions are calculated using ISAJET 7.85 [49] and have been shown in Ref. [258, 252]. It must be noted that for natural SUSY with light higgsinos, the branching ratios for $\tilde{w}_2^+ \to \tilde{z}_{1,2}W^+,\ \tilde{w}_1^+Z$ and $\tilde{w}_1^+h$ decays each rapidly asymptote to $\sim 25\%$ for heavy winos with only small branching fractions to the bino-like $\tilde{z}_3$. Likewise, the branching fractions for $\tilde{z}_4 \to \tilde{w}_1^+W^-$, $\tilde{w}_1^-W^+$, $\tilde{z}_{1,2}Z$ and $\tilde{z}_{1,2}h$ are also each $\sim 25\%$ for $|\mu| \ll |M_2|$.

These simple decay patterns can be analytically understood in the limit that the $\tilde{w}_1$ and $\tilde{z}_{1,2}$ are mostly higgsino-like, and $\tilde{w}_2$ and one of $\tilde{z}_3$ or $\tilde{z}_4$ is mostly a wino (with the other neutralino being dominantly a bino). As already mentioned, the bino-like neutralino couples to the wino only via its small higgsino component, so decays to it are dynamically suppressed even if they are kinematically allowed. In natural SUSY, we are interested in the case $\mu^2 \ll M_2^2$, and medium to large $\tan\beta$ values, typically with $\tan\beta > |M_2/\mu|$. In this case, it is straightforward to check that the chargino mixing angle $\gamma_L \sim -\gamma_R \frac{\mu}{M_2}$ (we use the notation of Ref. [13]) so that γ_L can be ignored compared to γ_R. The small gaugino components of the higgsino-like states and the higgsino components of the wino-like states can be evaluated to lowest order in the gaugino-higgsino mixing angles, and the relevant couplings and partial widths for the various decays obtained from the expressions in Appendix B of Ref. [13]. We then find

$$\Gamma(\tilde{w}_2 \to \tilde{z}_1 W) \simeq \Gamma(\tilde{w}_2 \to \tilde{z}_2 W) \simeq \Gamma(\tilde{w}_2 \to \tilde{w}_1 Z) \simeq \Gamma(\tilde{w}_2 \to \tilde{w}_1 h) \simeq \frac{g^2}{64\pi} m_{\tilde{w}_2}, \quad (112)$$

$$\Gamma(\tilde{z}_4 \to \tilde{w}_1^- W^+) \simeq \Gamma(\tilde{z}_4 \to \tilde{w}_1^+ W^-) \simeq \Gamma(\tilde{z}_4 \to \tilde{z}_{1,2} Z) \simeq \Gamma(\tilde{z}_4 \to \tilde{z}_{1,2} h) \simeq \frac{g^2}{64\pi} m_{\tilde{z}_4}, \tag{113}$$

where, to illustrate our point, we have retained only the largest mass terms in the expressions for the partial widths. This is a good approximation when higgsinos are much lighter than the winos. In our numerical calculation, we retain the full expressions, of course. In the last of these equations we have assumed that $\tilde{z}_4$ is the wino-like state. Also, the neutral wino decay widths to Z or h are the summed widths to both higgsino-like states.[33] If other decay modes of the wino (*e.g.*, to the bino, to sfermions, or to the heavy Higgs bosons) are kinematically or dynamically suppressed, we obtain the approximately equal branching fractions of 25% mentioned above. We have checked by a numerical scan that when $|\mu| = 150 - 300$ GeV, as favored by naturalness, the branching ratios for these modes are *well within* the 0.23-0.27 range if the wino is heavier than 500 GeV and the bino is not quasi-degenerate with the wino.

Combining decay channels, we find that typically $\sim 1/8$ of $\tilde{w}_2^\pm \tilde{z}_4$ production events lead to final states with same-sign dibosons W^+W^+ or W^-W^-. To identify SSdB events, we require leptonic decays of the final state Ws to e or μ which reduces our overall branching fraction to $\sim 6 \times 10^{-3}$. Thus, although the wino pair production cross sections may be as large as 10 fb, the combined signal channel branching fractions lead to relatively small signal rates. Therefore, the SSdB signal channel really becomes the signal of choice only for the very high integrated luminosities projected to be accumulated at the high-luminosity LHC.

[33]The reader may wonder why the decay rates to Higgs bosons which go via the *unsuppressed* wino-higgsino-Higgs boson coupling are comparable to the decay rates to vector bosons which can only occur via small mixing angles. The reason is that this suppression is compensated by the enhancement of the amplitude for decays to longitudinal W or Z bosons by a factor $m_{\tilde{w}_2,\tilde{z}_4}/M_{W,Z}$, an example of the Goldstone boson equivalence theorem.

Signal benchmark model line

To make specific predictions for the expected SSdB signal rate, we will adopt a natural SUSY model line using the two-extra-parameter non-universal Higgs model NUHM2 [40]. This model allows for direct input of a low μ parameter as required by naturalness. The model line we adopt is adapted from Ref. [258] and has $m_0 = 5$ TeV, $A_0 = -8$ TeV, $\tan\beta = 10$, $m_A = 1.5$ TeV, and $\mu = 150$ GeV. We will allow the unified gaugino mass parameter $m_{1/2}$ to vary from 700 to 1375 GeV which corresponds to $m_{\tilde{g}} \sim 1.8 - 3.2$ TeV or $m_{\tilde{w}_2} \sim 610 - 1200$ GeV. The value of m_h is ~ 125 GeV along the entire model line, while Δ_{EW} is $\sim 10 - 30$, corresponding to 10% - 3% EW fine-tuning. Although the NUHM2 model assumes a unification of gaugino mass parameters, this is unimportant for the analysis of the wino signal that we are focusing upon, in the sense that essentially identical results would be obtained in any model with the same value of the wino mass M_2. While there may be some sensitivity to the bino mass parameter, we remind the reader that the bino-like state couples to the wino-vector boson system only via its small higgsino components, so any decays into this state typically have small branching fractions.

In Table 22, we show a listing of various sparticle masses and observables associated with our model line for the benchmark model with $m_{1/2} = 800$ GeV, labeled as `Point B`.[34] Within the NUHM2 framework, the model point with the 692 GeV wino state $\tilde{w}_2$ has $m_{\tilde{g}} \approx 2000$ GeV and so is just beyond the current gluino mass limit (from 13 TeV LHC running with ~ 35 fb^{-1}). Though the details of most of the SUSY spectrum are unimportant for our present purposes, we note that our sample case (indeed the entire model line) has very heavy first/second generation sfermions, with stops and gluinos in between these and the EW gauginos, while higgsinos are very light. This qualitative pattern is a generic feature of natural SUSY models. We emphasize that

[34] We refer to this as `Point B` because we consider three signal benchmark points, labeled A, B, and C, in order of increasing wino mass.

parameter	Point B
m_0	5000
$m_{1/2}$	800
A_0	-8000
$\tan\beta$	10
μ	150
m_A	1500
$m_{\tilde{g}}$	2007.4
$m_{\tilde{u}_L}$	5170.2
$m_{\tilde{u}_R}$	5318.4
$m_{\tilde{e}_R}$	4815.2
$m_{\tilde{t}_1}$	1470.3
$m_{\tilde{t}_2}$	3651.2
$m_{\tilde{b}_1}$	3682.7
$m_{\tilde{b}_2}$	5051.2
$m_{t\tilde{a}u_1}$	4740.2
$m_{t\tilde{a}u_2}$	5075.6
$m_{n\tilde{u}_\tau}$	5082.8
$m_{\tilde{w}_2}$	692.2
$m_{\tilde{w}_1}$	155.2
$m_{\tilde{z}_4}$	703.1
$m_{\tilde{z}_3}$	363.1
$m_{\tilde{z}_2}$	158.2
$m_{\tilde{z}_1}$	142.4
m_h	124.4
$\Omega_{\tilde{z}_1}^{std}h^2$	0.008
$BF(b\to s\gamma)\times 10^4$	3.1
$BF(B_s\to\mu^+\mu^-)\times 10^9$	3.8
$\sigma^{SI}(\tilde{z}_1,p)$ (pb)	4.1×10^{-9}
$\sigma^{SD}(\tilde{z}_1 p)$ (pb)	1.5×10^{-4}
$\langle\sigma v\rangle\vert_{v\to 0}$ (cm^3/sec)	2.9×10^{-25}
$\Delta_{\rm EW}$	9.3

Table 22: Input parameters and masses in GeV units for an NUHM2 model SUSY benchmark point labeled Point B with $m_t = 173.2$ GeV and $m_{1/2} = 800$ GeV.

while our benchmark model line is in a model with gauge coupling unification, this will have very little (if any) effect on any conclusions we draw about the prospects for discovery, exclusion, or mass measurement of the parent wino. In other words, for the purposes of analysis of the wino signal alone, we can disregard the LHC gluino limit and model cases with lighter winos that may arise in natural models without gaugino mass unification using $m_{1/2}$ as a surrogate for the wino mass, M_2.

SM background cross sections

In order to assess prospects for observability of the signal, we must have a good understanding of various SM backgrounds that could also lead to the clean same sign dilepton plus $\not{E}_T$ signature. We have considered backgrounds from $t\bar{t}$, WZ, $t\bar{t}W$, $t\bar{t}Z$, $t\bar{t}t\bar{t}$, WWW, and $W^{\pm}W^{\pm}jj$ production processes in the SM. Top pair production yields (non-instrumental) backgrounds only if a secondary lepton from top decay is accidently isolated. We use LO event generation from MadGraph in our simulation of both signals and backgrounds, but rescale the LO total cross sections to be in accordance with NLO values found in the literature.

Specifically, we use 953.6 pb as the total NLO cross section for $t\bar{t}$, following Ref. [265]. Ref. [303] gives us a K factor of 1.27 for four-top production. We use 1.88 as the K factor for associated WZ production following Ref. [266] and 1.24 for the K factor for $t\bar{t}W$ production following Ref. [267][35]. We obtain the K factor 1.39 for $t\bar{t}Z$ from Ref. [268]; Ref. [269] gives us a K factor of 1.04 for $WWjj$[36]. Finally, for the WWW process we use the cross sections in Ref. [270]. In our analyses we use a common K factor of 2.45 for both WWW processes, which is not appreciably different than the

[35]While in Ref. [266], K factors differ slightly for W^+Z and W^-Z, and in Ref. [267] the K factors differ slightly for $t\bar{t}W^+$ and $t\bar{t}W^-$, these are very close (1.86 and 1.92 respectively for W^+Z and W^-Z and 1.22 and 1.27 for $t\bar{t}W^+$ and $t\bar{t}W^-$ respectively), especially when compared with likely theory errors, so we use 1.88 (1.24) as the K factor for both WZ ($t\bar{t}W$) processes.

[36]This is the value in Ref. [269] for the two-jet inclusive cross section with factorization and renormalization scales set to 150 GeV. If we were to further restrict to one-jet and zero-jet bins (see our analysis cuts, below), the K factor would move closer to 1; we have chosen the larger K factor to be conservative.

$W^+W^+W^-$ K factor of 2.38 or the $W^+W^-W^-$ K factor of 2.59. We note that these are K factors for inclusive WWW production; if one imposes a jet veto the K factor is significantly reduced (to 1.29 for the combined WWW K factor). While we do impose a jet multiplicity cut of $n_{jet} \leq 1$, we choose to be conservative and use the larger value for the K factor in our calculation of the background.

These K factors and NLO cross sections for the underlying fundamental SM processes are shown in columns 2 and 3 of Table 23, together with the corresponding information for the signal benchmark `Point B`. These are, of course, the raw production cross sections for the various final states; various branching fractions and detection efficiencies have to be folded in to obtain the signal and background cross sections. We see that even the various $2 \to 3$ and $2 \to 4$ SM processes have potentially larger rates than the signal, so we may anticipate that we will require relatively stringent selection cuts to make the signal observable.

Event simulation

To simulate SSdB signal events, we first generate the SUSY spectrum as a Les Houches Accord (LHA) file using Isajet 7.85 [49]. We then feed the LHA information to MadGraph/ MadEvent 2.3.3 [261] which is interfaced with Pythia 6.4 [262] for parton showering and hadronization. The generated events are passed to Delphes 3.3.0 [263] for fast detector simulation, where we utilize the default "CMS" parameter card for version 3.3.0 with the modifications listed below.

- We require jets to have transverse energy $E_T(jet) > 50$ GeV and pseudorapidity $|\eta(jet)| < 3.0$.
- The electromagnetic calorimeter (ECAL) energy resolution is set to $3\%/\sqrt{E} \oplus 0.5\%$, while the hadronic calorimeter (HCAL) energy resolution is taken to be $80\%/\sqrt{E} \oplus 3\%$ for $|\eta| < 2.6$ and $100\%/\sqrt{E} \oplus 5\%$ for $|\eta| > 2.6$, where $\oplus$ denotes combination in quadrature.

- The jet energy scale correction is turned off.

- The anti-k_T jet algorithm [271] is utilized, but using $R = 0.4$ rather than the default $R = 0.5$. (Jet finding in Delphes is implemented via FastJet [272].) One motivation for choosing $R = 0.4$ in the jet algorithm is to facilitate comparison with CMS b-tagging efficiencies [273].

- We performed jet flavor association using our own module which implements the "ghost hadron" procedure [274] which allows the assignment of decayed hadrons to jets in an unambiguous manner. We use this module to aid in b-tagging, specifically in determining whether jets contain B hadrons. When a jet contains a B hadron in which the b quark will decay at the next step of the decay, then if this B hadron lies within $|\eta| < 3.0$ and $E_T > 15$ GeV, we identify this b-jet as a "truth b-jet". We b-tag truth b-jets with $|\eta| < 1.5$ with an efficiency of 60%. We also b-tag jets which are not truth b-jets with $|\eta| < 1.5$ with an efficiency of $1/X$ where $X = 150$ for $E_T < 100$ GeV, $X = 50$ for $E_T > 250$ GeV and X is found from a linear interpolation for 100 GeV $< E_T <$ 250 GeV[37]. We have checked [247] that our b-jet tagging algorithm yields good agreement with the b-tagging efficiencies and mistag rates in Ref. [273]; specifically it gives results intermediate between the CMS "medium" and "tight" b-tagging algorithms.

- "Tau tagging", *i.e.*, identifying objects as taus, is not used.

- The lepton isolation modules were modified to allow us to adopt the isolation criterion that the sum of E_T of physics objects in a cone with $\Delta R < 0.2$ about the lepton direction is less than $\min(5 \text{ GeV}, 0.15 E_T(\ell))$, where $E_T(\ell)$ is the transverse energy of the lepton. (Delphes 3.3.0 did not allow the minimum of these two

[37]The parameters for this b-tagging procedure are based on ATLAS studies of b-tagging efficiencies and rejection factors in $t\bar{t}H$ and WH production processes [275].

thresholds to be used rather than using either a fixed value of E_T or a fraction of the lepton E_T.)

V.2.2. Analysis cuts to enhance SUSY SSdB signal

Initial selection cuts (C1)

We begin by imposing the selection cuts, listed below, that were suggested in Ref's. [252, 258] to enhance same sign dilepton events originating in wino production over those coming from SM processes.

- Exactly two isolated same-sign leptons with $p_T(\ell_1) > 20$ GeV and $p_T(\ell_2) > 10$ GeV. (ℓ_1 denotes the higher p_T lepton, while ℓ_2 is the lower p_T lepton.)
- $n(b-\text{jets}) = 0$
- $\not{E}_T > 200$ GeV, and
- $m_T^{min} > 175$ GeV,

where $m_T^{min} = min[m_T(\ell_1, \not{E}_T, m_T(\ell_2, \not{E}_T)]$. We denote these initial cuts as cut set **C1**.

The cross sections after these cuts– after folding in various branching fractions and detection efficiencies– for the `Point B` signal benchmark point and from various SM processes (in ab) are listed in column 4 of Table 23. The combined same-sign dilepton cut, large $\not{E}_T$ cut, and b-jet veto serve to severely reduce the $t\bar{t}$ background. Indeed, after these cuts, the analysis of Ref. [258, 252] found the dominant background to come from $t\bar{t}$ and WZ production. Any $t\bar{t}$ background events which survive these cuts will likely have one lepton arising from real $W \to \ell\nu$ decay with the other lepton arising from a semi-leptonic b decay, which will hence be soft. In such a case, at least to the extent that the $\not{E}_T$ dominantly arises from the leptonic decay of a single W, the transverse mass, $m_T(\ell, \nu_\ell)$, is mostly bounded by m_W (up to small contamination from off-shell

Ws, $\not{E}_T$ smearing, and any additional $\not{E}_T$ from leptonic decays of the B-hadron). Thus, the further requirement of $m_T^{min} \gg m_W$ should serve to greatly reduce the $t\bar{t}$ and also WZ backgrounds. Here, in accord with Refs. [258, 252], we require $m_T^{min} > 175$ GeV; after imposing this cut we are indeed left with no $t\bar{t}$ or WZ backgrounds in our samples. Among the largest backgrounds is $t\bar{t}W$ production, which we find to be a factor of two larger than in Ref. [258]. Unlike the earlier studies, we also find sizable contributions from $t\bar{t}Z$ production as well as from WWW production and $W^{\pm}W^{\pm}jj$ production. Summing these sources, we find a total background cross section after **C1** cuts of 34 ab in contrast to just 6 ab after the same cuts in Ref. [258]. The cross section for the signal at the benchmark `Point B` is 29 ab, or a little under 5σ statistical significance for an integrated luminosity of 1 ab^{-1}, and over 8.5σ significance with 3 ab^{-1}.

Optimizing the reach of HL-LHC: selection cuts C2

The cut set **C1** was suggested in Ref. [258, 252] to determine the reach of LHC14 in the SSdB channel for 100-1000 fb^{-1}. Since one of our goals is to project the maximum reach of the HL-LHC for SUSY in the SSdB channel, we attempt to further optimize our cuts.

We begin by noting that the various background processes in Table 23 with significant cross sections after **C1** cuts are all expected to contain additional hard jets, while jet activity in the signal process arises only from initial state QCD radiation (and very soft jets from decay of the heavier higgsinos). We thus anticipate that jet multiplicity will be a useful discriminating variable.[38] With this motivation we show the expected jet multiplicity, $n(j)$, from signal and background events after the **C1** cuts in Fig. 59. From the solid (red) signal histogram, we see that signal events indeed mainly have $n(j) = 0$ or 1. In contrast, background events, the sum of which is shown by the shaded histogram, generally have $n(j) \geq 2$. Thus, we apply the additional cut,

[38] In this vein, the scalar sum of jet E_T or the ratio of this to the scalar sum of leptonic E_T may prove to be even more robust and equally discriminating variables.

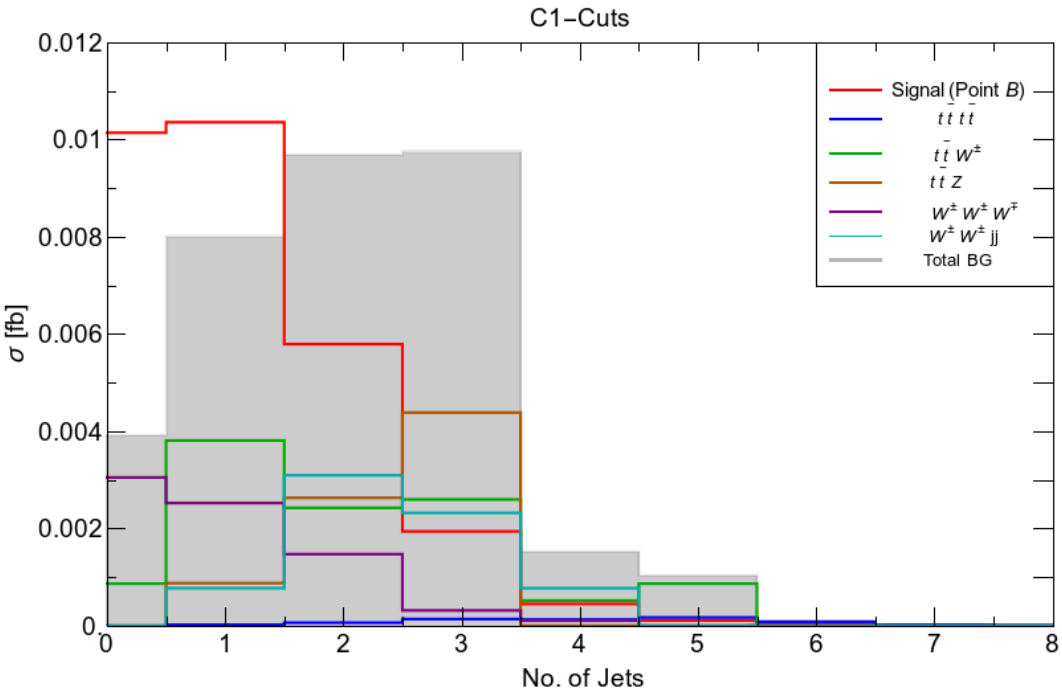

Figure 59: Distribution of jet multiplicity, $n(j)$, for SSdB events from the `Point B` signal benchmark point and various SM backgrounds after **C1** cuts.

- $n(j) \leq 1$.

The cross sections after cut set **C1** and $n(j) \leq 1$ are listed in column 5 of Table 23.[39] We see that the main background contributions now come from $t\bar{t}W$ and WWW production processes. To further reduce these, we examined several other kinematic distributions including $\not{E}_T$, $m_T(\ell_1\ell_2, \not{E}_T)$ (the dilepton-plus-$\not{E}_T$ cluster transverse mass) [276], m_T^{min} and m_{T2} [277]. The most useful of these turned out to be the $\not{E}_T$ distribution shown in Fig. 60. From this figure, we see that in the $\not{E}_T = 200 - 250$ GeV bin, the summed background exceeds the signal for `Point B`, while in higher $\not{E}_T$ bins, signal clearly emerges above background. However, care must be taken since our signal rate is already rather small. We elect to make one final cut

[39]The $t\bar{t}W$, $t\bar{t}Z$ and WWW cross sections have been normalized to their NLO values. Since jet production from these backgrounds occurs already at LO, and initial state shower radiation is already included in our event generation, we expect additional NLO QCD corrections to these backgrounds to be unimportant.

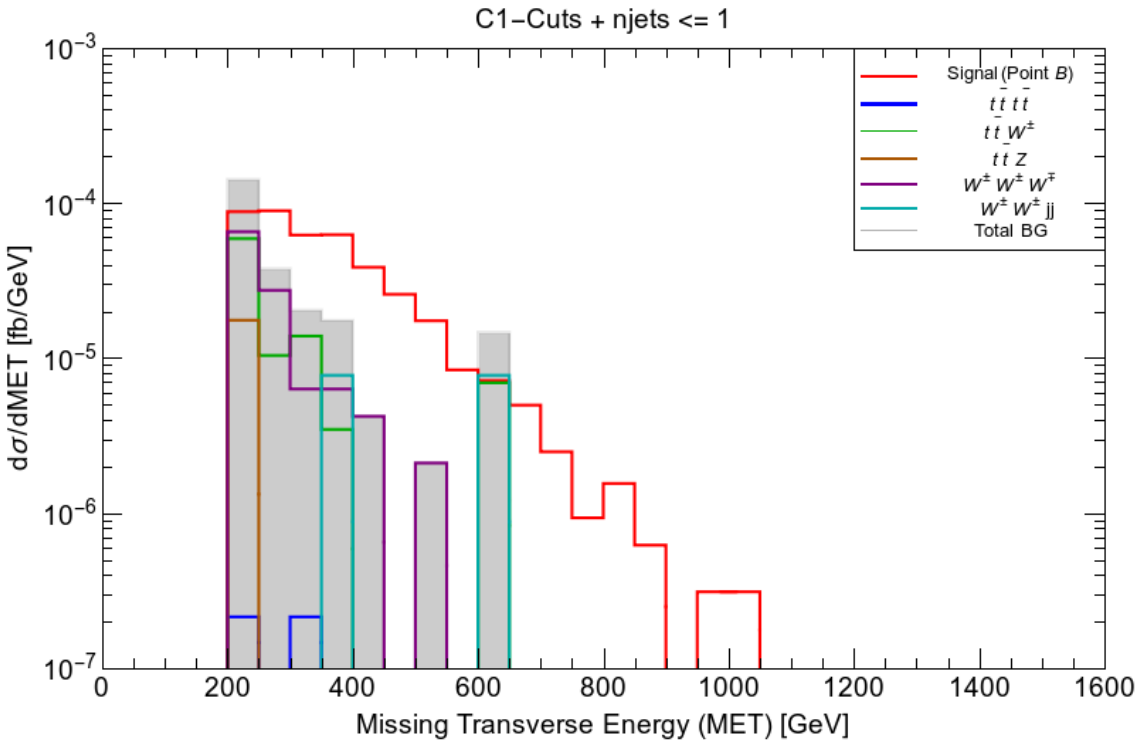

Figure 60: Distribution of $\not{E}_T$ for the signal benchmark `Point B` and various SM backgrounds in SSdB production after **C1** cuts plus the $n(j) \leq 1$ cut.

- $\not{E}_T > 250$ GeV,

and label this set of cuts (**C1** cuts plus $n(j) \leq 1$, plus $\not{E}_T > 250$ GeV) as the cut set **C2**.

We show the expected p_T distributions of the leptons after the **C2** cuts in Fig. 61 for three signal benchmark points along the model line, as well as for the summed SM background. The points have $m_{\tilde{w}_2} = 530$ GeV (`Point A`), 692 GeV (`Point B`, already introduced above), and 886 GeV (`Point C`). We see that the distributions are qualitatively similar, and while the S/B ratio may be slightly improved by requiring harder cuts on the leptons, this would only be at the cost of reducing an already rate-limited signal. We choose, therefore, not to impose any further cuts.

The total background after these cuts is shown in the last column of Table 23. We see that almost half this background comes from SM WWW production. Earlier we

process	$K-$factor	σ(NLO) (ab)	**C1**	**C1** + $n_{jet} \leq 1$	**C2**
SUSY (`Point B`)	1.25	$1.55 \cdot 10^4$	28.8	20.5	16.1
$t\bar{t}$	1.72	$9.5 \cdot 10^8$	0	0	0
WZ	1.88	$5.2 \cdot 10^7$	0	0	0
$t\bar{t}W$	1.24	$5.2 \cdot 10^5$	11.1	4.7	1.7
$t\bar{t}Z$	1.39	$8.8 \cdot 10^5$	7.9	0.9	0
$t\bar{t}t\bar{t}$	1.27	$1.1 \cdot 10^4$	0.6	0.	0.
WWW	2.45	$3.2 \cdot 10^5$	7.4	5.6	2.3
$WWjj$	1.04	$3.9 \cdot 10^5$	7.0	0.8	0.8
total BG	–	$1.0065 \cdot 10^9$	34.1	11.9	4.8

Table 23: Component background and signal cross sections in ab before any cuts, after **C1** cuts, after **C1** cuts plus a jet veto, and after **C2** at LHC14. Also shown is the K-factor that we use.

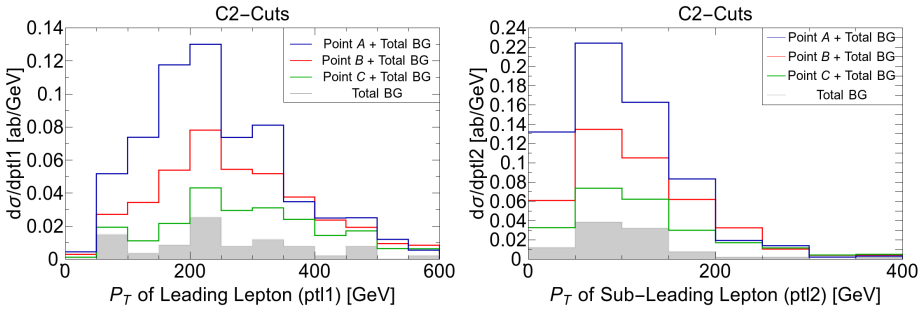

Figure 61: Distribution of $p_T(\ell_1)$ (left frame) and $p_T(\ell_2)$ (right frame) for the `Point A`, `Point B`, and `Point C` benchmarks, which are points along our NUHM2 model line with $m_{\tilde{w}_2} = 530$, 692 and 886 GeV, respectively, together with the total SM background after **C2** cuts.

have mentioned that we have used $K_{WWW} = 2.45$, *i.e*, the value obtained for inclusive WWW production, instead of the much smaller value $K_{WWW} = 1.29$ one obtains for WWW production with a jet veto. It is very possible that we may have over-estimated this background, but we choose to err on the conservative side in our assessment of the discovery prospects of the HL-LHC, the subject of the next section.

V.2.3. Discovery prospects at the HL-LHC

In Fig. 62, we show the total same sign dilepton signal rate after our final analysis cuts, **C2**, as a function of the wino mass, $m_{\tilde{w}_2}$, (solid blue curve) along with the total SM background (denoted by the dotted red line). We also compute the reach for 5σ discovery and 95% CL exclusion for the HL-LHC (using Poisson statistics) with a data sample of 3 ab^{-1}. We find that the 5σ discovery reach extends to $m_{\tilde{w}_2} \sim 860$ GeV, while the 95% CL exclusion reach extends to $m_{\tilde{w}_2} \sim 1080$ GeV. As stressed previously, although the model line we have used includes the assumption of gaugino mass unification, our projected reach does not depend on this assumption, but only on $M_2 \gg |\mu|$, as expected in natural SUSY. In models with gaugino mass unification, the 5σ (95% CL) reach in $m_{\tilde{w}_2}$ correspond to a reach (exclusion) in terms of the unified gaugino mass $m_{1/2}$ of ~ 1010 (1280) GeV. In terms of the comparable reach in terms of $m_{\tilde{g}}$, these correspond to $m_{\tilde{g}} \sim 2430$ (3000) GeV. These values may be compared to the 5σ 3 ab^{-1} HL-LHC for direct gluino pair production of $m_{\tilde{g}} \sim 2800$ GeV obtained in Ref. [247]. Although we do not show it on the figure, we mention that with the hard **C2** cuts, the discovery reach of the LHC extends to 500 GeV (720 GeV) for an integrated luminosity of 300 fb^{-1} (1 ab^{-1}), while the corresponding 95%CL exclusion extends to 780 GeV (980 GeV). It is worth keeping in mind that especially for the 300 fb^{-1} case, somewhat softer analysis cuts [258, 252] may be better suited for optimizing the LHC reach.

The key mass relation for the SSdB signature is that $|\mu| \ll M_2$. It is therefore inter-

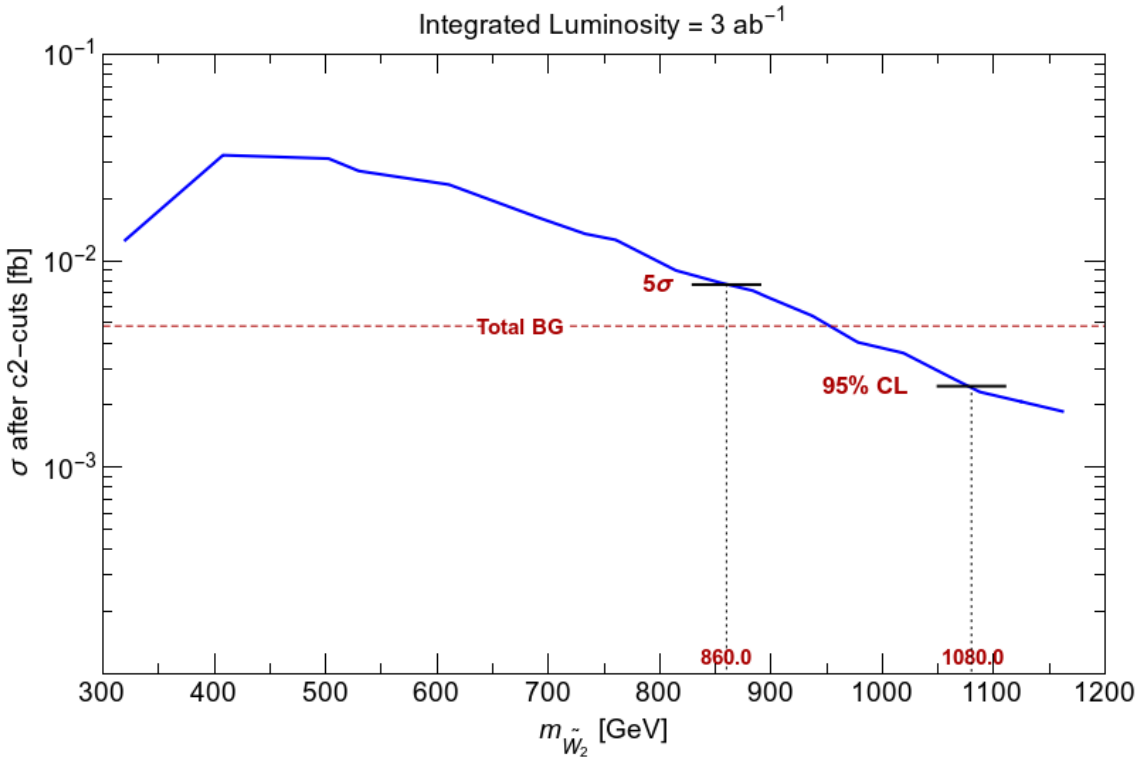

Figure 62: Cross section for SSdB production after **C2** cuts versus $m(wino)$ at the LHC with $\sqrt{s} = 14$ TeV. We show the 5σ and 95% CL reach assuming a HL-LHC integrated luminosity of 3 ab^{-1}.

esting to explore our discovery reach beyond our benchmark assumption of $|\mu| = 150$ GeV. In Fig. 63, we denote the (3 ab^{-1}) HL-LHC (5σ) discovery reach in the μ-M_2 plane by the green solid line in the vicinity of $m_{\tilde{w}_2} \simeq 800 - 900$ GeV. As expected the reach is only weakly sensitive to the higgsino mass. The red diagonal line in Fig. 63 shows where $\mu = m_{\tilde{w}_2}$. Above this line the SSdB signature arises from higgsino pair production and subsequent decays to winos; but it would have a much smaller rate because (1) the higgsino cross section is smaller than the wino cross section, and (2) dilution of the signal from higgsino decays to binos (if these are accessible). Below the blue diagonal line in Fig. 63 denotes the region where $\tilde{w}_2 \to \tilde{z}_{1,2} + W$ or $\tilde{z}_4 \to \tilde{w}_1 + W$ decays can occur, leading the the SSdB final state, with on-shell Ws. Close to this line and for not-too-large $m_{\tilde{w}_2}$, though, the same sign dilepton events would not necessarily

be clean as the large wino-higgsino mixings would lead to sizeable mass gaps and concomitant harder debris from the decay of the lighter inos. As μ increases, the model becomes increasingly unnatural, with a value $\mu > 350$ (indicated by a magenta dashed line) corresponding to electroweak fine-tuning measure $\Delta_{EW} > 30$. The natural SUSY region is the region below this horizontal line.

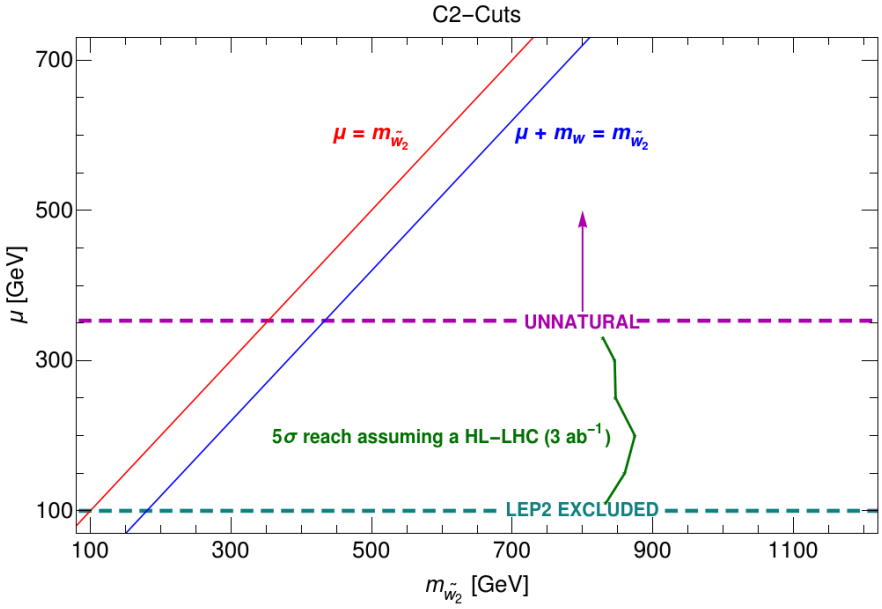

Figure 63: Discovery reach in the SSdB channel at the HL-LHC in the $m_{\tilde{w}_2}$ vs. μ plane.

V.2.4. SSdB SUSY event characteristics

We have already illustrated the $\not{E}_T$ and lepton transverse momentum distributions after all cuts in Fig. 60 and Fig. 61, respectively. We saw that while the $\not{E}_T$ distribution from signal emerges from the background for $\not{E}_T > 250$ GeV, this distribution is typically backed up against the cut. Although the distribution may harden somewhat with increasing wino mass, we saw that the observability of the signal becomes rate limited by the time we reach $m_{\tilde{w}_2} = 860$ GeV, so wino events would typically have $\not{E}_T \sim 250 - 500$ GeV. The lepton p_T distributions peak at 200-250 GeV for the hard lepton

and 50-100 GeV for the second lepton, independent of the wino mass. This should not be very surprising because the leptons are produced at the end of a cascade decay chain, so the $p_{T\ell}$ distributions are only altered by the changes in the boost of the daughter W bosons which share the parent wino energy with the (nearly invisible) higgsinos.

To further characterize the nature of the SSdB events from SUSY, and to see if we can gain some sensitivity to the wino mass from the kinematic properties of these events, we have examined several kinematic variables: A_{eff}, m_T^{min} (which entered the **C1** cuts), its sibling m_T^{max}, m_{T2}, m_{CT} and $m_{\ell\ell}$, where

$$A_{eff} = \not{E}_T + \sum_i^{n(j)} p_T(j_i) + p_T(\ell_1) + p_T(\ell_2),$$

and m_{CT} is the cluster transverse mass given by

$$m_{CT}^2 = m_{CT}^2 = \left(\not{E}_T + \sqrt{\vec{p}_{T\ell\ell}^{\,2} + m_{\ell\ell}^2}\right)^2 - (\vec{\not{E}}_T + \vec{p}_{T\ell\ell})^2.$$

In Fig. 64, we show the normalized distributions of m_T^{min} (because it enters our analysis cuts) together with those of A_{eff}, m_{CT}, and m_T^{max}, the larger of the transverse masses of the lepton and $\not{E}_T$. These are the distributions whose *shapes* show the most sensitivity to the wino mass for the three benchmark SUSY cases introduced above. We see that even for these three cases with a fairly wide separation of wino masses, the shapes of the distributions are qualitatively quite similar, with perhaps the m_T^{max} distribution showing the greatest sensitivity to the parent wino mass. As we noted in the discussion of Fig. 61, the wino mass has a relatively small effect on the kinematics of signal events, affecting only the boost of the W bosons. While these (quite correlated) distributions show some differences, especially in the tails of the distributions which correspond to relatively low numbers of signal events, we will see below that because the signal rate can be predicted with good precision, the event rate for the SSdB signal offers a much

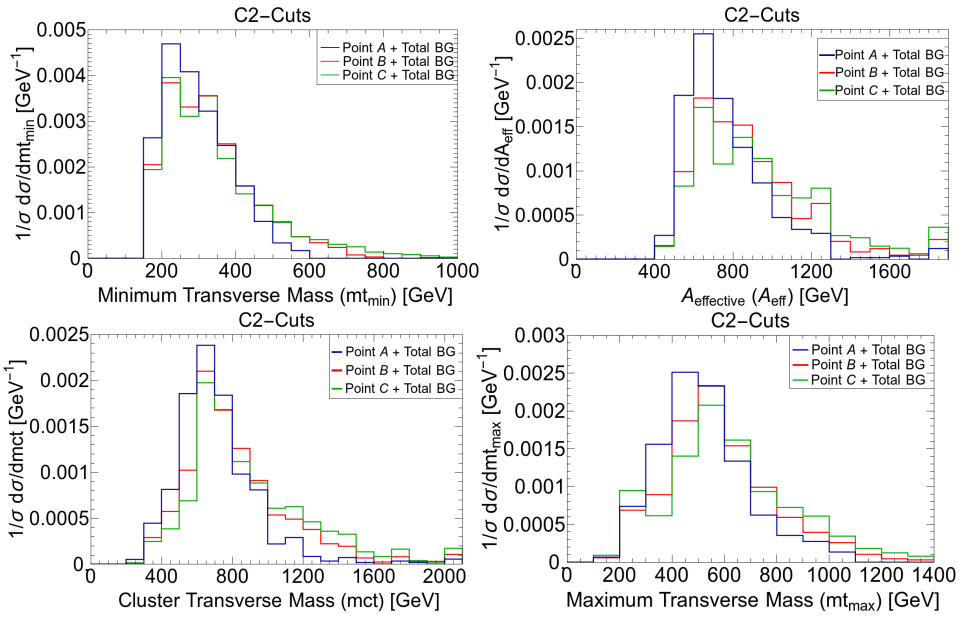

Figure 64: Distributions of m_T^{min} (top left), A_{eff} (top right), m_{CT} (bottom left) and m_T^{max} (bottom right) from the SUSY SSdB signal plus SM backgrounds after **C2** cuts for the three benchmark cases `Point A`, `Point B`, and `Point C` introduced earlier in the text. We have normalized these distributions to all have the same area.

better handle on the wino mass. We stress, though, that the kinematic properties of these events are nonetheless useful for validating the signal origin, and could potentially serve as ingredients in an artificial neural network stew.

The charge asymmetry

$$A = \frac{n(++) - n(--)}{n(++) + n(--)}$$

of clean same sign dilepton events (which, of course, includes both signal and background events) provides yet another handle for validating the wino origin of any signal. We show a fit to the expected A values (our simulated sample had considerable statistical fluctuations) for signal-plus-background events versus $m_{\tilde{w}_2}$ in Fig. 65, together with the expected background value. The total BG horizontal line is determined by

$$A_{TotalBG} = \frac{n_{TotalBG}(++) - n_{TotalBG}(--)}{n_{TotalBG}(++) + n_{TotalBG}(--)}$$

where $n_{TotalBG}(++)$ and $n_{TotalBG}(--)$ are the total number of background events with two positive leptons and two negative leptons respectively. Since $n_{TotalBG}(++)$ and $n_{TotalBG}(--)$ originate from SM background, hence do not depend on $m_{\tilde{w}_2}$ and hence is a horizontal line. The charge asymmetry arises because there are more up-type than

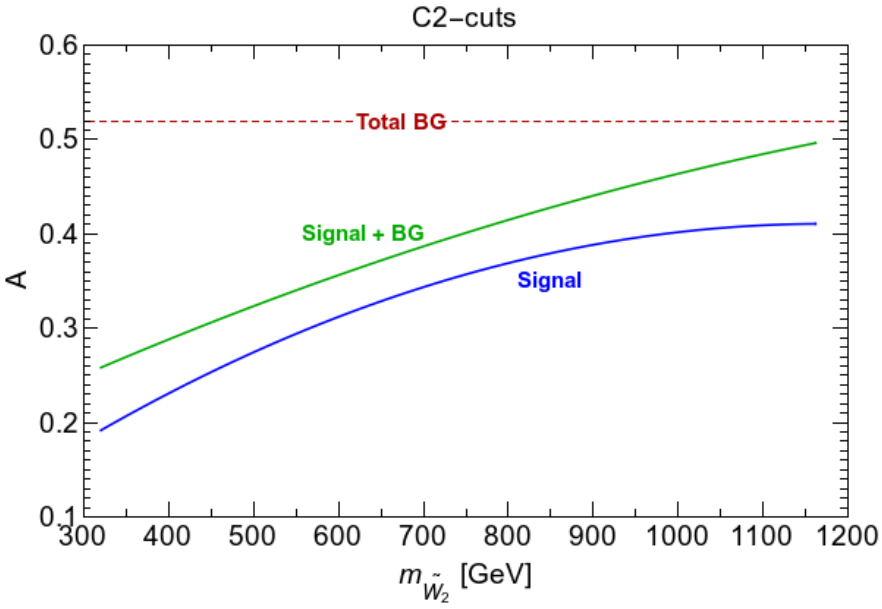

Figure 65: Same-sign dilepton charge asymmetry from signal-plus-background vs. $m_{\tilde{w}_2}$ from SUSY same-sign diboson production after **C2** cuts versus $m_{\tilde{w}_2}$ at LHC with $\sqrt{s} =$ 14 TeV. The statistical error with which the charge asymmetry can be determined is $\sim \pm 0.1$ is $m_{\tilde{w}_2} \leq 800$ GeV.

down-type valence quarks in a proton. The importance of valence quark collisions for wino pair production processes increases with wino mass, so we expect the asymmetry to also increase with $m_{\tilde{w}_2}$. This is indeed borne out in the figure where we see that the expected asymmetry ranges from 0.2 for $m_{\tilde{w}_2}$ as low as ~ 300 GeV to 0.4 for $m_{\tilde{w}_2} \sim 1000$ GeV.[40] Unfortunately, the measured charge asymmetry does not provide as good of a wino mass determination as one might naively suppose from looking at the figure. The reason is that because of the relatively low total event rate, even with 3 ab^{-1}, the statistical error on its measurement is $\sim \pm 0.1$ for $m_{\tilde{w}_2} < 800$ GeV, which corresponds

[40]The asymmetry of the background is even larger because the $W^{\pm}W^{\pm}jj$ component of the background, though subdominant, has contributions from collisions of *two* valence quarks.

to a wino mass uncertainty of ~ 300 GeV. We nevertheless stress that a determination of the charge asymmetry provides a consistency check of wino origin of the SSdB signal if $m_{\tilde{w}_2}$ can be extracted from the total event rate. An examination of this extraction is the subject of the next section.

V.2.5. Measurement of the wino mass in the SSdB channel

We saw that while experiments at the HL-LHC would be able to discover winos with masses up to 860 GeV and to exclude these out to 1100 GeV if no excess is seen, the determination of its mass from the kinematic properties of the signal event proved rather difficult. We traced this to the fact that the leptons were produced only at the end of a cascade so that the sensitivity to the mass of the parent winos is correspondingly reduced.

In principle, it should also be possible to determine the wino mass from the *rate* with which the signal events are produced. This is particularly true in this case because the cross section for wino production can be rather precisely computed for the case of natural SUSY (for which the heavier inos are expected to be nearly pure gauginos) and depends on just the wino mass. We also saw that, at least for $m_{\tilde{w}_2} > 500$ GeV, the natural SUSY branching fraction for wino decays to W is 0.25 ± 0.02 with conservative error bars.[41] The determination of the SSdB signal rate after **C2** cuts shown in Fig. 62 thus provides a plausible mass measurement strategy, because, to a good approximation, the observed number of events depends only on the wino mass.

For example, for our assumed benchmark point, `Point B`, and using **C2** cuts, with 3 ab^{-1} we expect a total of 63 ± 8 events (see Table 23), where the error bar is purely statistical. Since we would estimate the signal cross section by taking the observed

[41] As we have already noted, the observation of a signal in the clean, same sign dilepton channel already points to light higgsinos and much heavier EW gauginos. Additional circumstantial evidence for light higgsinos could, for instance, come from the observation of monojet plus soft dilepton events, which must be present at observable rates if $m_{\tilde{z}_2} - m_{\tilde{z}_1} \geq 10$ GeV and higgsinos are not much heavier than 220-240 GeV.

number of events and subtracting the expected number of background events, this $\pm$ 8 events corresponds to a $\approx 16\%$ measurement of the cross section, which, as one can find by examining the cross section after **C2** cuts (as in Fig. 62) corresponds to a measurement of $m_{\tilde{w}_2} \sim 690 \pm 35$ GeV, which represents a better than 5% measurement of the wino mass.

This precision is possible when we consider statistical errors alone. There is also a systematic error arising from the theory uncertainty on the cross section, uncertainties on the wino decay branching ratios, uncertainties on the efficiencies for events passing cuts, uncertainties on the reconstruction efficiencies, etc. Since the current uncertainty ($\sim$ 10% in the production cross section) mostly arises from the uncertainties in the parton distributions which will undoubtedly be well-measured by the time this analysis is done, and the lepton detection efficiencies will also be well understood, we expect the main systematic will arise from the squared wino branching fraction, which as we have already noted is $\leq 16\%$. Conservatively taking the total systematic to be $\sim 20\%$, then our error on the wino mass for `Point B` increases to ≈ 50 GeV. Even if the total systematic error on the cross section is 30%, then the combined statistical and systematic error on the mass is ≈ 70 GeV, which is about a 10% measurement of the wino mass. If our background is underestimated by a factor of two, our measurement of the wino mass will be biased by ≈ 70 GeV toward lower values; if it is over-estimated by a factor of two, then our measurement will be biased by ≈ 35 GeV toward higher values.

We can still make a good mass measurement for large values of the wino mass; for instance, the purely statistical error on the mass measurement is still only $\approx 10\%$ for a 1 TeV wino (although there is no 5σ signal). However for these larger mass values with their correspondingly smaller signal cross sections, very precise determinations of the background cross section become increasingly important. Presumably, these will be experimentally determined by an extrapolation into the signal region by the time the

HL-LHC accumulates 3 ab^{-1} of data. Our point is that better than 10% determination of the wino mass will be possible if the SSdB signal from natural SUSY is detected at the HL-LHC

V.3. LHC luminosity and energy upgrades confront natural supersymmetry models

As discussed in Sec. I.2.4, The electroweak fine-tuning measure $\Delta_{\rm EW}$ allows for correlated SUSY soft terms as are expected in any ultra-violet complete theory. Requiring no less than 3% electroweak fine-tuning implies upper bounds of about 360 GeV on all higgsinos, while top squarks are lighter than ~ 3 TeV and gluinos are bounded by $\sim 6-9$ TeV (depending on the details of the model).

These sparticle mass bounds derived from the $\Delta_{\rm EW}$ measure lie well beyond current LHC search limits and allow for the possibility that SUSY is still natural and still awaiting discovery. The question then is: how far along are LHC SUSY searches on their way to discovering or falsifying supersymmetry? And what sort of LHC upgrade is needed to either discover or falsify natural SUSY? Indeed, recently the European Strategy Study has begun to assess what sort of accelerator (or other experiments) are needed beyond high-luminosity LHC (HL-LHC). One option is to double the field strength of the dipole steering magnets to 16 Tesla. This would allow for an energy upgrade of LHC to $\sqrt{s} = 27$ TeV with an assumed 15 ab^{-1} of integrated luminosity (HE-LHC). The goal of this section is to re-examine the SUSY theory/experiment confrontation with a view to informing these questions about future experiments and to examine what collider options are needed to completely probe the natural SUSY parameter space. In doing so, we will confront four different natural SUSY models with updated LHC limits from four SUSY search channels which are deemed most important for discovering/falsifying natural supersymmetry.

nNUHM2	nNUHM3	nAMSB	nGMM
$m_0 : 0.1 - 15$ TeV	$m_0(1,2) : 0.1 - 40$ TeV	$m_0 1,2 : 0.1 - 40$ TeV	$\alpha : 0 - 40$ TeV
	$m_0(3) : 0.1 - 15$ TeV	$m_0(3) : 0.1 - 15$ TeV	$c_{m3} < c_m/4$
$m_{1/2} : 0.5 - 3$ TeV	$m_{1/2} : 0.5 - 3$ TeV	$m_{3/2} : 60 - 500$ TeV	$m_{3/2} : 1 - 35$ TeV
$A_0 : -30 \to +30$ TeV	$A_0 : -30 \to +30$ TeV	$A_0 : -35 \to +15$ TeV	$a_3 : -20 \to +20$
			$c_m = (16\pi^2/\alpha)^2$

Table 24: Scan limits for various parameters in the natural SUSY models considered here. Parameter definitions for nNUHM2,3, nAMSB and nGMM can be found in Sec. I.3. For each model, we also allow $\tan\beta : 3 - 60$, $\mu : 100 - 360$ GeV and $m_A : 0.3 - 10$ TeV.

The four natural SUSY models we examine here include the following:

- Natural gravity-mediation as exhibited in the two- and three-extra parameter non-universal Higgs model (nNUHM2 and nNUHM3) [40].
- Natural (generalized) anomaly-mediation (nAMSB) model [47]
- Natural generalized mirage mediation (nGMM) model [42]

These four models have been discussed in Sec. I.3 and are encoded in Isajet v7.88 [49] which has been used for spectra generation and the $\Delta_{\rm EW}$ calculation. For each of the four models, we scan over the whole parameter space (with $\tan\beta : 3 - 60$) and accept solutions which are consistent with current LHC sparticle mass constraints, with $m_h = 125 \pm 2$ GeV (adopting $\sim \pm 2$ GeV theory error in our Higgs mass calculation). The parameter scan limits for each model are shown in Table 24. We also require that solutions have $\Delta_{\rm EW} < 30$ in order to satisfy naturalness– which amounts to a reasonable SUSY model prediction for the magnitude of the weak scale. For the nGMM parameter space, we require α to be positive (real mirage unification) and $\alpha < 40$ so that anomaly mediation is not highly suppressed.

In this section, updated reach projections for revised HE-LHC specifications with $\sqrt{s} = 27$ TeV and a projected integrated luminosity (IL) of 15 ab^{-1} is presented followed

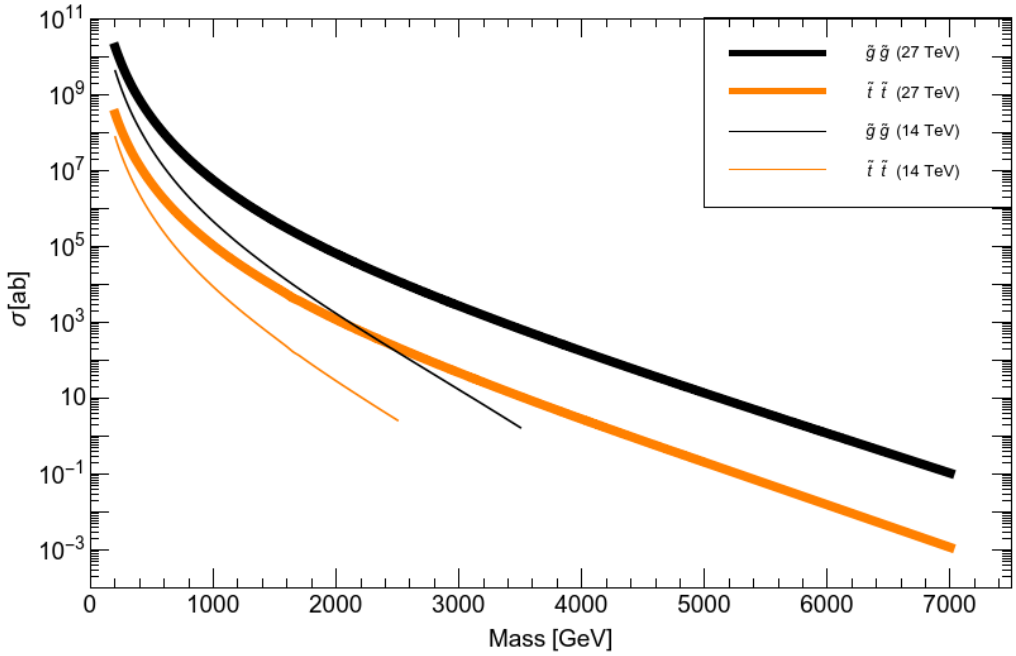

Figure 66: Plot of NLL+NLO predictions [286] of $\sigma(pp \to \tilde{g}\tilde{g}X)$ and $\sigma(pp \to \tilde{t}_1\tilde{t}_1^*X)$ production at LHC for $\sqrt{s} = 14$ and 27 TeV.

by confrontation of the four natural SUSY models introduced earlier with present LHC bounds in each of these search channels, and reach projections for HL- and HE-LHC which are obtained using various detector simulation tools . It has been found that while HL-LHC can probe a portion of natural SUSY parameter space, it will take an energy upgrade to the HE-LHC option for a definitive search for natural weak scale SUSY.

V.3.1. Updated reach projections of HE-LHC for gluinos and top-squarks

Previously HE-LHC reach analyses for top-squark pair production [114] and gluino pair production [285, 114] in natural SUSY were performed assuming $\sqrt{s} = 33$ TeV and IL$= 0.3 - 3$ ab^{-1}. Here, these analyses are updated to values assigned for the European Strategy report, namely $\sqrt{s} = 27$ TeV and IL$= 15$ ab^{-1}. Along these lines, the first step is to generate updated total production cross sections for our signal processes.

Fig. 66 shows the total production cross section for $pp \to \tilde{g}\tilde{g}X$ (black) and $pp \to \tilde{t}_1\tilde{t}_1^* X$ (orange) at both $\sqrt{s} = 14$ TeV (thin solid) and 27 TeV (thick solid). The results are computed at NLL+NLO and the 14 TeV results are taken from the study of Ref. [286] where the gluino pair production results for decoupled squarks have been used. Since Ref. [286] presents results for $\sqrt{s} = 13$, 14, 33 and 100 TeV, total cross sections for $\sqrt{s} = 27$ TeV is obatined via interpolation of the 14 and 33 TeV results. Specifically, $\log\sqrt{s}$ versus $\log\sigma_{tot}$ is fitted to a quadratic and the resulting function is used to obtain $\sqrt{s} = 27$ TeV cross sections.

From the results shown in Fig. 66, we see that for $m_{\tilde{g}} = 2$ TeV, then the gluino pair production cross section ratio $\sigma(27)/\sigma(14) = 38$ while for $m_{\tilde{g}} = 3.5$ TeV this ratio increases to ~ 394. For $m_{\tilde{t}} = 1$ TeV, then we find a total top squark pair production ratio $\sigma(27)/\sigma(14) = 12$ while for $m_{\tilde{t}_1} = 2.5$ TeV then $\sigma(27)/\sigma(14)$ increases to 83. These ratios clearly reflect the advantage of moving to higher LHC energies in order to probe more massive strongly interacting sparticles.

Updated top squark analysis for $\sqrt{s} = 27$ TeV

In Ref. [114], the reach of a 33 TeV LHC upgrade for top-squark pair production was investigated. Here, the analysis is repeated but for updated LHC energy upgrade $\sqrt{s} = 27$ TeV. We use Madgraph [261] to generate top-squark pair production events within a simplified model where $\tilde{t}_1 \to b\tilde{w}_1^+$ at 50%, and $\tilde{t}_1 \to t\tilde{z}_{1,2}$ each at 25% branching fraction, which are typical of most natural SUSY models [279]. The higgsino-like electroweakino masses are $m_{\tilde{z}_{1,2},\tilde{w}_1^\pm} \simeq 150$ GeV. We interface Madgraph with Pythia [262] for initial/final state showering, hadronization and underlying event simulation. The Delphes toy detector simulation [263] is used with specifications as listed in Ref. [114] (which we will not repeat here). We also used Madgraph-Pythia-Delphes for a variety of SM background processes which are listed in Table 25.

In Ref. [114], an optimized set of cuts was found for extracting the signal from a

process	σ (ab)
$b\bar{b}Z$	1.87
$t\bar{t}Z$	1.1
t	4.4×10^{-2}
$t\bar{t}$	3.3×10^{-2}
$t\bar{t}b\bar{b}$	2.3×10^{-2}
$t\bar{t}t\bar{t}$	1.7×10^{-3}
$t\bar{t}h$	6.8×10^{-4}
total	3.07

Table 25: Cross sections in ab after cuts from SM background processes for the top-squark pair production analysis at $\sqrt{s} = 27$ TeV.

2.75 TeV top squark over SM backgrounds at $\sqrt{s} = 33$ TeV LHC upgrade. The cuts that were settled upon were

- $n(b-jets) \geq 2$,
- $n(isol.\ leptons) = 0$,
- $E_T^{miss} > max(1500\ \text{GeV}, 0.2M_{eff})$,
- $E_T(j_1) > 1000$ GeV,
- $E_T(j_2) > 600$ GeV,
- $S_T > 0.1$ and
- $\Delta\phi(\vec{E}_T^{miss}, \text{jet close}) > 30$ deg.

In the above, M_{eff} is the usual effective mass variable, S_T is transverse sphericity and the $\Delta\phi$ cut is on the transverse opening angle between the missing E_T vector and the closest jet (which helps reduce background from boosted tops in $t\bar{t}$ production). The surviving background rates in ab are listed in Table 25. We use the same K-factors as listed in Ref. [114] to bring our total background cross sections into accord with various beyond-leading-order calculations. In the present analysis, we have also included the $t\bar{t}Z$ background calculation which was not present in Ref. [114].

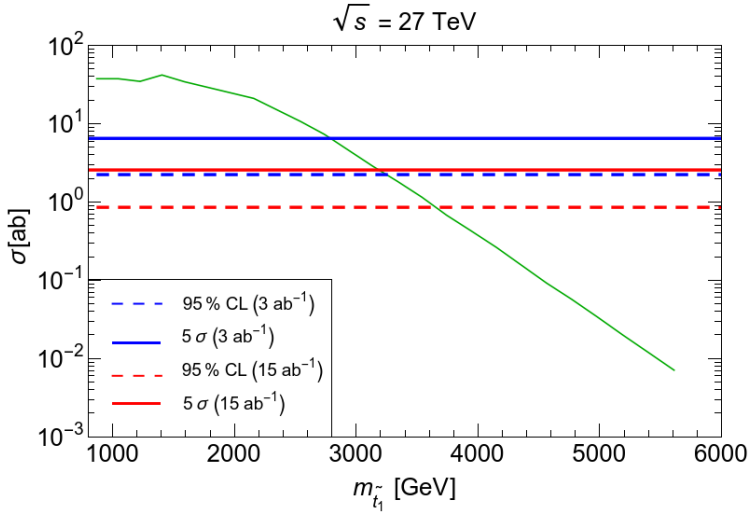

Figure 67: Plot of top-squark pair production cross section vs. $m_{\tilde{t}_1}$ after cuts at HE-LHC with $\sqrt{s} = 27$ TeV (green curve). We also show the 5σ and 95% CL reach lines assuming 3 and 15 ab^{-1} of integrated luminosity (for a single detector).

Using these background rates for LHC at $\sqrt{s} = 27$ TeV, we compute the 5σ and 95% CL reach of HE-LHC for 3 and 15 ab^{-1} of integrated luminosity using Poisson statistics. These results are plotted in Fig. 67 along with the top-squark pair production cross section after cuts versus $m_{\tilde{t}_1}$.

From the Fig. 67, we see the 5σ discovery reach of LHC27 extends to $m_{\tilde{t}_1} = 2800$ GeV for 3 ab^{-1} and to 3160 GeV for 15 ab^{-1}. The 95% CL exclusion limits extend to $m_{\tilde{t}_1} = 3250$ GeV for 3 ab^{-1} and to $m_{\tilde{t}_1} = 3650$ GeV for 15 ab^{-1}. We see that S/B exceeds 0.8 whenever we deem the signal to be observable. Of course, somewhat increased reach limits can be obtained in the event of a combined ATLAS/CMS analysis.

Updated gluino analysis for $\sqrt{s} = 27$ TeV

In Ref. [114], optimized cuts were investigated for extracting the signal from a 5.4 TeV gluino over SM backgrounds at a $\sqrt{s} = 33$ TeV LHC upgrade. The optimized cuts were found to be

- $n(b-jets) \geq 2$,

- $n(isol.\ leptons) = 0$,
- $E_T^{miss} > max(1900\ \text{GeV}, 0.2M_{eff})$,
- $E_T(j_1) > 1300$ GeV,
- $E_T(j_2) > 900$ GeV,
- $E_T(j_3) > 200$ GeV,
- $E_T(j_4) > 200$ GeV,
- $S_T > 0.1$ and
- $\Delta\phi(\vec{E}_T^{miss}, \text{jet close}) > 10$ deg.

The corresponding backgrounds in ab after cuts are listed in Table 26. The backgrounds are again normalized to recent beyond-leading-order results as detailed in Ref. [114]. We again compute the 5σ reach and 95% CL exclusion lines using Poisson statistics for 3 and 15 ab^{-1} of integrated luminosity.

process	σ (ab)
bbZ	0.061
$t\bar{t}Z$	0.037
t	0.003
$t\bar{t}$	0.026
$t\bar{t}b\bar{b}$	0.0046
$t\bar{t}t\bar{t}$	0.0
$t\bar{t}h$	8.1×10^{-4}
total	0.132

Table 26: Cross sections in *ab* after cuts, from SM background processes for the gluino pair production analysis at $\sqrt{s} = 27$ TeV.

Our results are shown in Fig. 68 where we plot the gluino pair production signal versus $m_{\tilde{g}}$ for a nNUHM2 model line with parameter choice $m_0 = 5m_{1/2}$, $A_0 = -1.6m_0$, $m_A = m_{1/2}$, $\tan\beta = 10$ and $\mu = 150$ GeV with varying $m_{1/2}$. We do not expect the results to be sensitive to this precise choice as long as first generation squarks are heavy.

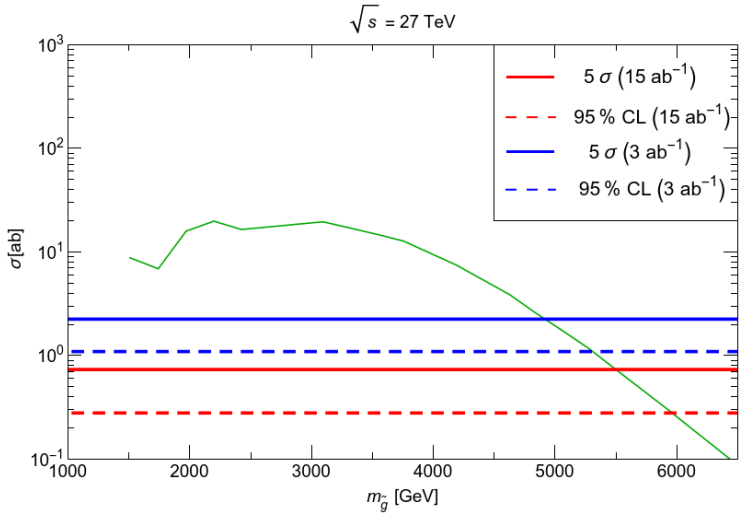

Figure 68: Plot of gluino pair production cross section vs. $m_{\tilde{g}}$ after cuts at HE-LHC with $\sqrt{s} = 27$ TeV (green curve). We also show the 5σ and 95% CL reach lines assuming 3 and 15 ab^{-1} of integrated luminosity.

From the Figure, we see that the 5σ discovery reach of LHC27 extends to $m_{\tilde{g}} = 4900$ GeV for 3 ab^{-1} and to $m_{\tilde{g}} = 5500$ GeV for 15 ab^{-1} of integrated luminosity. The corresponding 95% CL exclusion reaches extend to $m_{\tilde{g}} = 5300$ GeV for 3 ab^{-1} and to $m_{\tilde{g}} = 5900$ GeV for 15 ab^{-1} of integrated luminosity.

V.3.2. Confronting natural SUSY models at the LHC and its upgrades

Gluino pair production

Fig.69 shows the results of the scans over parameter space of the nNUMH2, nNUHM3, nAMSB and nGMM models with $\Delta_{\rm EW} < 30$ and with $m_h : 123 - 127$ GeV in the $m_{\tilde{g}}$ vs. $m_{\tilde{z}_1}$ plane. We also require $m_{\tilde{g}} > 2$ TeV and $m_{\tilde{t}_1} > 1.1$ TeV in accord with recent simplified model mass limits from ATLAS and CMS. The density of points is not to be taken as meaningful. As argued in Sec. IV, there should exist a power law draw to large soft terms which would not be reflected here but which would then favor larger sparticle masses beyond current LHC reach and $m_h \simeq 125$ GeV. The available natural parameter space can be construed as some boundary enclosing all the natural SUSY

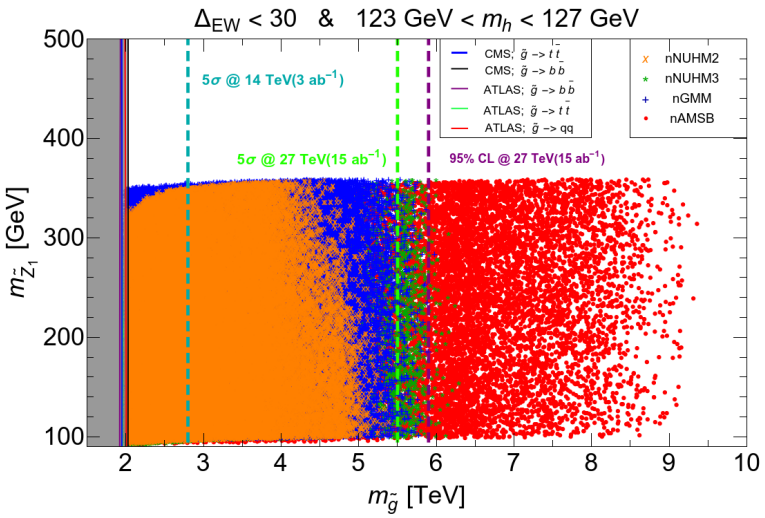

Figure 69: Plot of points in the $m_{\tilde{g}}$ vs. $m_{\tilde{z}_1}$ plane from a scan over nNUHM2, nNUHM3, nGMM and nAMSB model parameter space. We compare to recent search limits from the ATLAS/CMS experiments (solid vertical lines) and future LHC upgrade options (dashed vertical lines).

scan points in accord with the measured Higgs mass and current LHC sparticle mass constraints.

From Fig. 69, we see that the range of $m_{\tilde{g}}$ extends from about 2 TeV to around $m_{\tilde{g}} \sim 6$ TeV for NUHM2,3 and nGMM models but to significantly higher values for nAMSB. The upper limit on $m_{\tilde{g}}$ occurs because the gluino mass drives top squark soft mass terms to such large values that $\Sigma_u^u(\tilde{t}_{1,2}) > 30$, leading to a violation of our naturalness criterion. To understand why higher gluino masses are allowed in the nAMSB model, we first note that $m_{\tilde{g}} \geq 6$ TeV occurs only for *negative* values of A_0. In this case, in order to obtain m_h consistent with its observed value very large negative magnitudes of A_0 are required (compared to the positive A_0 case). The resulting very large contribution of A_t to their RG evolution then strongly suppresses the weak scale soft top squark mass parameters, allowing correspondingly larger values of $m_{\tilde{g}}$ (*vis à vis* the other models). The fact that $|M_2|$ is smaller than $|M_3|$ in the nAMSB case also helps. The range of $m_{\tilde{z}_1}$ varies from 100-350 GeV in accord with the range of μ which

is bounded from below by LEP2 searches for chargino pair production and bounded from above by naturalness in Eq. (12). We also show by the solid vertical lines around $m_{\tilde{g}} \sim 2$ TeV the results of several ATLAS and CMS simplified model search limits for gluino pair production [287] [288]. It is apparent from the plot that a large range of parameter space remains to be explored. The blue dashed line around $m_{\tilde{g}} \sim 2800$ GeV shows the computed 5σ reach of high luminosity LHC (HL-LHC) with $\sqrt{s} = 14$ TeV and 3 ab^{-1} of integrated luminosity as seen in Sec. V.1 [247]. While the HL-LHC will somewhat extend the SUSY search via the gluino pair production channel, much of the allowed gluino mass range will remain beyond its reach. We also show with the green (purple) dashed lines the HE-LHC 5σ reach (95% CL exclusion region) for gluino pair production as computed above for $\sqrt{s} = 27$ TeV and 15 ab^{-1} of IL. We see that HE-LHC should probe nearly all of parameter space for the nNUHM2, nNUHM3 and nGMM models while evidently a considerable fraction of nAMSB parameter space would be beyond HE-LHC reach in the gluino pair production channel.

Top squark pair production

Fig. 70 shows the locus of scan points from the four natural SUSY models in the $m_{\tilde{t}_1}$ vs. $m_{\tilde{z}_1}$ plane. The $m_{\tilde{z}_1}$ value is bounded by ~ 350 GeV so almost no points occupy the near degeneracy region $m_{\tilde{t}_1} \sim m_{\tilde{z}_1}$ where much LHC search effort has focussed. The current search limits from ATLAS [289] and CMS [290] are shown as solid red and black contours respectively. These LHC search limits exclude some of natural SUSY parameter space but evidently a large swath of natural SUSY parameter space remains to be explored since top-squark masses may extend up to $m_{\tilde{t}_1} \sim 3.5$ TeV without compromising naturalness.

The ATLAS collaboration projected 95% CL exclusion region for top squarks at HL-LHC [291] is also shown by the black dashed line at $m_{\tilde{t}_1} \sim 1.4$ TeV. While HL-LHC will probe additional parameter space, much of the top squark mass range will lie beyond

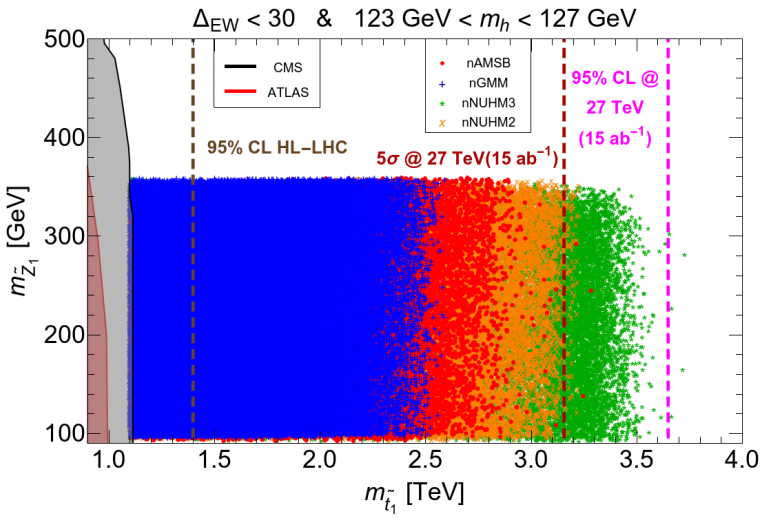

Figure 70: Plot of points in the $m_{\tilde{t}_1}$ vs. $m_{\tilde{z}_1}$ plane from a scan over nNUHM2, nNUHM3, nGMM and nAMSB model parameter space. We compare to recent search limits from the ATLAS/CMS experiments (solid contours) and to projected future limits (dashed lines).

its reach. The reach of HE-LHC with $\sqrt{s} = 27$ TeV and IL of 15 ab^{-1} was computed in Sec. V.3.1. We show the 5σ reach contour as a red dashed line extending out to $m_{\tilde{t}_1} \sim 3.1$ TeV while the 95% CL exclusion region extends to $m_{\tilde{t}_1} \sim 3650$ GeV. The HE-LHC apparently will be able to probe essentially the entire natural SUSY parameter space in the top-squark pair production channel.

In Fig. 71 we show the gluino and top-squark reach values in the $m_{\tilde{t}_1}$ vs. $m_{\tilde{g}}$ plane. The gray shaded region is excluded by the current search limits from CMS[288, 290]. In this plane, it is important to note that in the nNUHM2, nNUHM3 and nGMM models, the highest values of $m_{\tilde{g}}$ correspond to the lowest values of $m_{\tilde{t}_1}$ while the highest $m_{\tilde{t}_1}$ values correspond to the lowest $m_{\tilde{g}}$ values. Thus, a marginal signal in one of these channels (due to sparticle masses being near their upper limit) should correspond to a robust signal in the complementary channel. In particular, for nNUHM3 where gluinos might be slightly beyond HE-LHC reach, the top squarks should be readily detectable. The nAMSB model case is different, because as we saw in Sec. V.3.1, the very large

negative values of A_0 needed to obtain the correct value of m_h allow gluino masses in the $6-9$ TeV range with modest values of $m_{\tilde{t}_1}$. (The top squark and gluino mass values in the nAMSB model with $A_0 > 0$ are in line with those in the other models.) We see that while gluino pair production might escape detection at the HE-LHC in the nAMSB framework, the top squark signal should be easily visible since $m_{\tilde{t}_1} \leq 3$ TeV in this case.

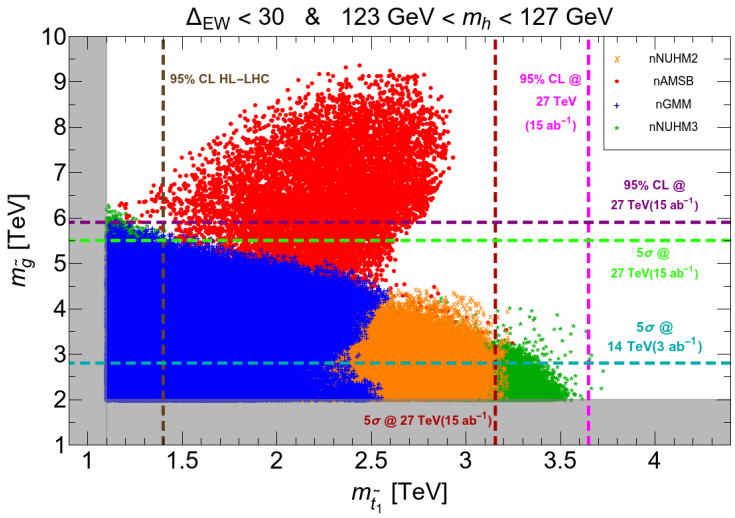

Figure 71: Plot of points in the $m_{\tilde{t}_1}$ vs. $m_{\tilde{g}}$ plane from a scan over nNUHM2, nNUHM3, nGMM and nAMSB model parameter space. We compare to projected future search limits from the LHC experiments.

Higgsino pair production

The four higgsino-like neutralinos $\tilde{w}_1^{\pm}$ and $\tilde{z}_{1,2}$ are the only SUSY particles required by naturalness to lie not too far above the weak scale, $m_{weak} \sim 100$ GeV. In spite of their lightness, they are very challenging to detect at LHC. The lightest neutralino evidently comprises only a subdominant part of dark matter[292] and if produced at LHC via $pp \to \tilde{z}_1\tilde{z}_1$ would escape detection. In fact, signals from electroweak higgsino pair production $pp \to \tilde{z}_i\tilde{z}_j, \tilde{w}_1\tilde{z}_i, \tilde{w}_1\tilde{w}_1 + X$ $(i,j = 1,2)$ are undetectable above SM backgrounds such as vector boson and top quark pair pruduction because the decay

products of the heavier higgsinos $\tilde{w}_1$ and $\tilde{z}_2$ are expected to be soft. The monojet signal arising from initial state QCD radiation in higgsino pair production events has been evaluated in Ref. [280] and was found to have similar shape distributions to the dominant $pp \to Zj$ background but with background levels about 100 times larger than signal. See, however, Ref. [293].

A way forward has been proposed via the $pp \to \tilde{z}_1\tilde{z}_2 j$ channel where $\tilde{z}_2 \to \ell^+\ell^-\tilde{z}_1$: a soft opposite-sign (OS) dilepton pair recoils against a hard initial state jet radiation which serves as a trigger[281]. Recent searches in this $\ell^+\ell^- j + \not{E}_T$ channel have been performed by CMS[282] and by ATLAS[283]. Their resultant reach contours are shown as solid black and blue contours respectively in the $m_{\tilde{z}_2}$ vs. $m_{\tilde{z}_2} - m_{\tilde{z}_1}$ plane in Fig. 72. These searches have indeed begun to probe the most promising portion of the parameter space, since the lighter range of $m_{\tilde{z}_2}$ masses have some preference from naturalness. The CMS experiment has also presented projected exclusion contours for LHC14 with 300 fb^{-1} and HL-LHC with 3 ab^{-1} shown as the green and purple dashed contours[294]. We see that while these contours can probe considerably more parameter space, much of natural SUSY parameter space lies beyond these projected reaches. So far, reach contours for HE-LHC in this search channel have not been computed but it may be anticipated that HE-LHC will not be greatly beneficial here since $pp \to \tilde{z}_1\tilde{z}_2 j + X$ is primarily an electroweak production process so the signal cross section will increase only marginally while QCD background processes like $t\bar{t}$ production will increase substantially: harder cuts may, however, be possible. The nAMSB model inhabits typically a larger mass gap region of the plane since in this model winos are much lighter than in nNUHM2 or nGMM for a given gluino mass. It is imperative that future LHC searches try to squeeze their reach to the lowest $m_{\tilde{z}_2} - m_{\tilde{z}_1}$ mass gaps which are favored to lie in the 3-5 GeV region for string landscape projections as seen in Sec IV.

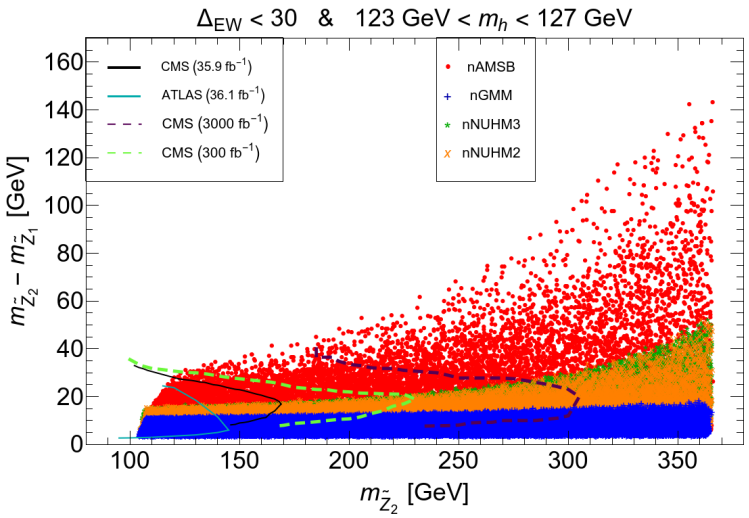

Figure 72: Plot of points in the $m_{\tilde{z}_2}$ vs. $m_{\tilde{z}_2} - m_{\tilde{z}_1}$ plane from a scan over nNUHM2, nNUHM3, nGMM and nAMSB model parameter space. We compare to recent search limits from the ATLAS/CMS experiments and some projected luminosity upgrades as computed by CMS.

Wino pair production

As seen in Sec. V.2, the wino pair production reaction $pp \to \tilde{w}_2^{\pm}\tilde{z}_4 X$ (in nNUHM2,3 and nGMM) or $pp \to \tilde{w}_2^{\pm}\tilde{z}_3 X$ (in nAMSB) offers a new and lucrative search channel which is not present in unnatural models where $|\mu| \gg M_{gauginos}$. The decay modes $\tilde{w}_2^{\pm} \to W^{\pm}\tilde{z}_{1,2}$ and $\tilde{z}_{3 \text{ or } 4} \to W^{\pm}\tilde{w}_1^{\mp}$ lead to a same sign diboson (SSdB) plus $\not{E}_T$ final states accompanied by minimal jet activity- just that arising from initial state radiation[284]. Thus, the ensuing same-sign dilepton+$\not{E}_T$ signature is quite different from that which arises from gluino and squark pair production where multiple hard jets are expected to be present. The SSdB signature from wino pair production has very low SM backgrounds which might arise from processes like $t\bar{t}W$ production.

Fig. 73 shows the location of natural SUSY model points in the $m_{\tilde{w}_2}$ vs. μ plane. The region with large μ is increasingly unnatural as indicated in the plot. From Fig. 73, we see that the nAMSB model points tend to populate the lower $m_{\tilde{w}_2}$ region, $m_{\tilde{w}_2} \leq 1400$ GeV. This is because $M_2 \sim m_{\tilde{g}}/7$ in AMSB models with $m_{\tilde{g}} \leq 6 - 9$ TeV

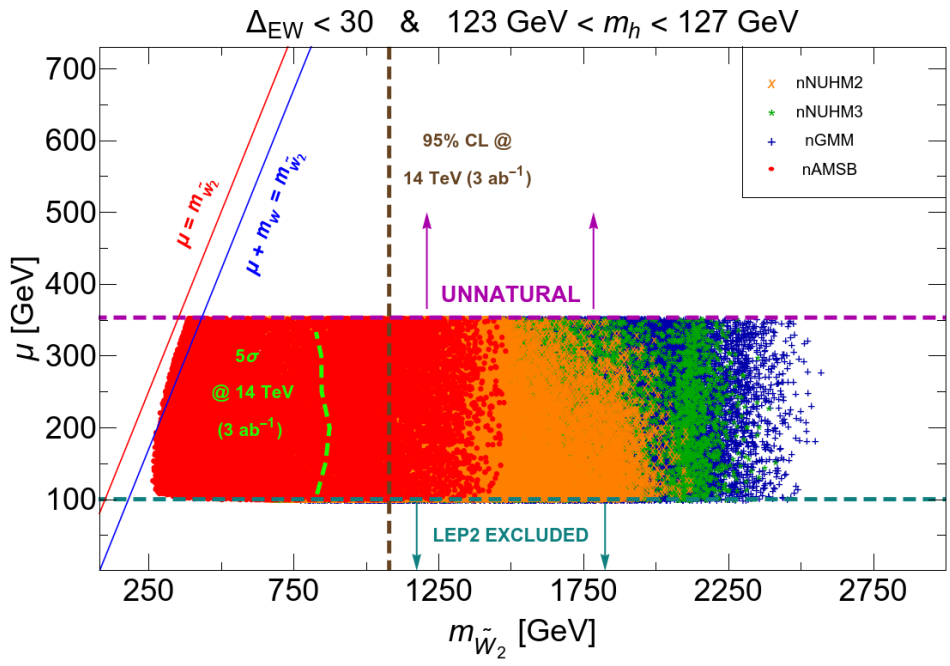

Figure 73: Plot of points in the $m_{\tilde{w}_2^-}$ vs. μ plane from a scan over nNUHM2, nNUHM3, nGMM and nAMSB model parameter space. We compare to projected search limits for the ATLAS/CMS experiments at HL-LHC.

from naturalness considerations.

We are unaware of any LHC search limits via the SSdB channel, though this signature should begin to be competitive with the conventional $\not{E}_T$ searches for an integrated luminosity of ~ 100 fb^{-1} expected to be accumulated by the end of LHC Run 2. The projected HL-LHC reach has been evaluated in Sec. V.2 where the 5σ discovery and 95% CL exclusion dashed contours are shown in Fig. 63. Evidently HL-LHC will be able to probe a large part of parameter space for the nAMSB model while only a lesser portion of natural parameter space of nNUHM2, nNUHM3 and nGMM models can be probed. The corresponding reach of HE-LHC has not been computed for the SSdB channel. But again, since this is an EW production channel, the signal rates are expected to rise by a factor of a few by moving from $\sqrt{s} = 14$ TeV to $\sqrt{s} = 27$ TeV while some of the QCD backgrounds like $t\bar{t}$ production will rise by much larger factors. We also note that because the heavy winos are expected to decay to higgsinos plus a

$W^{\pm}, Z$ or h in the ratio 2:1:1[284], VV, Vh and hh plus $\not{E}_T$ signals may be present, possibly with additional soft leptons from higgsino decays. A study of these signals is beyond the scope of the present analysis.

VI. Summary

Requirement of natural SUSY models : As stated in the Introduction, though the SM is the most celebrated theory of fundamental particles and forces, till date, it is not sufficient to explain all aspects of nature. That is why we need BSM theories. Out of several BSM theories, Supersymmetry is perhaps most promising because it solves several problems with the SM, for example: the instability of Higgs mass within SM, namely, the Big Hierarchy problem. However, since there is no experimental evidence of supersymmetric particles or *sparticles* yet, it may lead one to conclude that these *sparticles* are much heavier than their corresponding SM particles. Current experimental constraints pushes the *sparticles* in the multi-TeV regime except the higgsinos which are allowed to be within few GeV. The mass difference between *sparticles* and their corresponding SM particles implies that SUSY is a broken symmetry. Since the SUSY breaking mechanism is not known yet, there are several hypothesis describing different methods in which SUSY can be broken. These heavy *sparticles* can render a SUSY model *unnatural/finetuned* depending on how naturalness in defined. In the pre-LHC era, naturalness was defined using Δ_{BG} [25, 26] or Δ_{HS} [22, 23, 24]. These naturalness measures require light *sparticles* which do not satisfy the LHC *sparticles* mass constraints. These measures were shown to be flawed. Δ_{BG} does not account for parameter correlations as in top down string models or parameter selection as bottom up landscape models. Δ_{HS} splits m_{higgs} into dependent terms which is not allowed in practical naturalness. In the LHC era, naturalness measure was improved to electroweak naturalness Δ_{EW} to which Δ_{BG} and Δ_{HS} collapse considering string theory. With Δ_{EW} to be the naturalness measure, SUSY continues to be natural while still satisfying the LHC *sparticles* and Higgs mass constraints.

Problems with natural SUSY models : However, natural SUSY models also suffer from few problems. Firstly, such natural models require the superpotential μ parameter

$\mu \approx 100$ - 350 GeV and trouble to explain the origin of such low value of μ is called the μ-problem which, in the LHC era, gets redefined as the Little Hierarchy problem. Secondly, the LSP in natural SUSY which serves as a viable DM candidate, alone cannot account for the entire DM content of the universe. So, a second candidate is needed and axion, being a solution to the strong CP problem, is the most promising candidate for this purpose. However, solution to strong CP problem requires implementation of $U(1)_{PQ}$ symmetry as the fundamental symmetry, which being a global symmetry, make the model suffer from the gravity-spoliation problem. Thirdly, can we predict the energy scale at which SUSY or $U(1)_{PQ}$ symmetry breaks? Finally, is there a way to justify the high mass of *sparticles* and why would nature prefer massive *sparticles* over lighter ones ? The goal of this dissertation is to address all of these above mentioned problems or questions.

Dark Matter in natural SUSY models : In Sec.II, dark matter content of three natural SUSY models : nNUHM2 [40], nAMSB [47] and nGMM$'$ [42] have been confronted with various observable properties of DM and it was seen that the LSPs in these models, all of which are higgsino-like neutralinos with non-negligible gaugino component and are suitable DM candidates, are underproduced or excluded by various experiments. Therefore, the case of natural higgsino-like-WIMP-only dark matter is indeed excluded. This implies that a second candidate is needed to form the rest of the DM of the universe and the axion is a very well motivated candidate.

Simultaneous solution to SUSY μ problem and the strong CP problem : The axion is a pseudoscalar particle which arises when PQ symmetry is broken to solve the strong CP problem. Another side effect of breaking PQ symmetry is that it can solve the SUSY μ problem and accommodate the Little Hierarchy (LH), as shown in Sec. III. Although, there are several other methods to solve the SUSY μ problem and accommodate Little Hierarchy, the solutions related to PQ symmetry breaking are most promising because they, only by breaking PQ symmetry, solve a number of problems

: 1. The SUSY μ problem (LH), 2. The strong CP problem, 3. generates axion to complete the DM content of our Universe. The class of models which generate PQ breaking radiatively as a consequence of SUSY breaking have an additional advantage that they provide a mechanism for generating neutrino mass as well. This class of models are simple DFSZ axionic extensions of the MSSM, namely : the MSY model, the CCK model and the SPM model. However, these solutions, in spite of having so many advantages, suffer from the gravity-spoliation problem because the fundamental symmetry in these models, namely $U(1)_{PQ}$, is a global symmetry.

Gravity-spoliation problem and its solution : The most promising way to solve the gravity-spoliation problem is to impose a discrete symmetry as the fundamental symmetry out of which the PQ symmetry will emerge as an accidental approximate symmetry. The MBGW model turns out to be a gravity-safe model under $\mathbb{Z}_{22}$ discrete symmetry and also solves the SUSY μ problem (LH), the strong CP problem and generates axion but unlike the radiative PQ breaking models, it does not generate neutrino mass, though it allows a Majorana mass term for neutrinos. But, the fundamental $\mathbb{Z}_{22}$ discrete symmetry is inconsistent with GUTs and this symmetry would arise in nature when a charge $22e$ object will condense and presence of an object with such high charge is not very plausible with a UV completion of a theory. So, two gravity-safe hybrid type models have been found here with PQ superpotential as in the radiative models, but with an explicit see-saw neutrino sector which is unrelated to SUSY or PQ breaking. Instead, the PQ breaking results as a consequence of a large quartic (Planck-suppressed) soft term so that it generates an axionic solution to the strong CP problem along with a natural value of the MSSM μ term. These hybrid models have a fundamental $\mathbb{Z}_{24}^R$ discrete symmetry and it has been shown in Ref. [136, 137] that $\mathbb{Z}_N^R$ discrete symmetries with $N = 4, 6, 8, 12$ and 24 are consistent with GUTs and emerge from compactification of 10-d Lorentzian spacetime in string theory and hence provide a more plausible UV completion of the theory. The $\mathbb{Z}_{24}^R$ discrete symmetry also forbids

the dangerous dimension-four R-parity violating terms and the dimension-five proton decay operators. Thus, R-parity is no longer an ad-hoc symmetry which ensures the stability of LSP and makes it a viable DM if it is electrically and color neutral. Hence, both the components of mixed axion-neutralino dark matter have a common origin : the $\mathbb{Z}_{24}^R$ discrete symmetry. It has been shown in Refs. [206] that for mixed axion-neutralino dark matter, cosmological (dark matter) constraints require the PQ breaking scale $f_a \sim 10^{11} - 10^{12}$ GeV but from string theory f_a could arise as high as $f_a \sim m_{\rm GUT}$ to $m_{\rm string}$[207, 208].

PQ breaking scale from string landscape : In Sec. IV, we have tried to find a theoretical explanation behind suppression of f_a. Since, the string theory landscape arising from the multiverse argument has successfully explained the smallness of the Cosmological Constant (Λ), the same argument has been used to predict the value of f_a. For this, we adopt Douglas's power law for statistical selection of soft SUSY breaking terms (m_{soft}^n) where we take the value $n = 2n_F + n_D - 1 = 1$ (*i.e.* a linear distribution favoring large soft SUSY breaking terms) and veto models with inappropriate EW breaking (CCB minima or no EWSB) and models with contributions to the weak scale ≥ 4 (corresponding to $\Delta_{\rm EW} > 30$) in accord with nuclear physics constraints derived by Agrawal *et al.* on anthropically allowed values for the weak scale. Such an approach receives support in that previously it has been shown that $n = 1$ (or 2) has a most probable Higgs mass of $m_h \simeq 125$ GeV whilst lifting sparticle masses beyond the reach of Run 2 of the LHC. But, here it has been found that, since the relevant soft term $-A_f$, responsible for generation of f_a, does not enter the calculation of $\Delta_{\rm EW}$, hence requiring $\Delta_{\rm EW} < 30$ does not impose any upper cut on f_a and higher values of f_a become more and more probable owing to statistical pull on all soft terms according to Douglas's power law. Instead, if $-A_f$ is made correlated to $m_{3/2}$, which is usually the case for a well-specified hidden sector, then, as can be seen in Fig 21, f_a falls within the cosmological sweet spot $10^{11} - 10^{12}$ GeV.

Solution to SUSY flavor and CP problem from string landscape : We further proceed to see that the statistical pull on SSB terms according to Douglas's power law makes the first and second generation sfermions as massive as 20-40 TeV. This flavor-independent upper bound on the first/second generation soft masses arises from two-loop RG contributions to third generation soft masses which actually push these values to small, even tachyonic values. The effect of these highly massive first and second generation sfermions on the SUSY flavor and CP problems was calculated and confronted with their respective constraints obtained experimentally. It was found that this approach leads to a mixed decoupling/quasi-degeneracy solution to the SUSY flavor problem and a decoupling solution to the SUSY CP problem.

Mirage mediation from string landscape : Previously this landscape approach has been tested with a pure gravity-mediation model (NUHM2) [77] and it resulted in most probable Higgs mass of $m_h \simeq 125$ GeV whilst lifting sparticle masses beyond the reach of Run 2 of the LHC. Since, mirage-mediated models are more realistic because they contain both gravity-mediation and anomaly-mediation contributions (which are expected to be always present), hence here we test this landscape approach with a natural mirage-mediation model (nGMM$'$). Within this model and including a natural solution to the SUSY μ problem, it has been shown that the light Higgs boson mass is found to peak rather sharply around $m_h \simeq 125$ GeV, while other sparticles are still beyond LHC reach. The gluino and squarks were found to be in the multi-TeV regime while higgsinos were found to have masses around few hundreds of GeV. The mass difference between the NLSP and the LSP were found to be most probable around $5-10$ GeV which is the most lucrative channel to search for SUSY particles.

Collider phenomenology of natural SUSY models : The most likely avenue for SUSY discovery at LHC would be via direct Higgsino pair production $pp \to \tilde{\chi}_1^0 \tilde{\chi}_2^0 \to \ell^+\ell^- + \not{E}_T$ where the presence of an initial state jet radiation may help to trigger on the expected soft dilepton signature[221]. The soft dilepton invariant mass is expected

to be bounded by $m_{\tilde{z}_2} - m_{\tilde{z}_1} \sim 5 - 10$ GeV. In fact, such a soft opposite-sign dilepton excess seems to be building in Atlas data.

Several other lucrative channels for SUSY search in hadron colliders like LHC have been investigated in Sec. V. One such promising channel is gluino pair production assuming gluinos decay via $\tilde{g} \to t\tilde{t}_1$, followed by stop decays, $\tilde{t}_1 \to b\tilde{w}_1, t\tilde{z}_{1,2}$, to higgsinos, where the visible decay products of the higgsinos are very soft. This is the dominant gluino decay chain expected within the radiatively-driven natural SUSY framework that has been suggested for phenomenological analysis of simple natural SUSY GUT models. The RNS model used here for this analysis is the NUHM2 model. The result obtained is that in the RNS model, signals from gluino pair production should be observable at the 5σ level out to $m_{\tilde{g}} < 2.4$ (2.8) TeV for an integrated luminosity of 300 fb^{-1} (3000 fb^{-1}) in the $\geq$ 4-jet sample with very hard $\not{E}_T$ and two or three tagged b-jets. The clean sample of gluino events that we obtain should also allow a measurement of $m_{\tilde{g}}$ with a statistical precision ranging from 2-5% depending on the gluino mass and the assumed integrated luminosity, ranging between 300-3000 fb^{-1}, along with a smaller but non-negligible systematic uncertainty of 1-4% mentioned in the previous paragraph. The precision of gluino mass extraction should be even greater using the combined ATLAS/CMS data set.

Another promising channel for SUSY search is from wino pair production, $pp \to \tilde{w}_2\tilde{z}_4$, followed by wino decays to W bosons plus quasi-visible higgsinos. Thus, the signal consists of $\ell^{\pm}\ell'^{\pm} + \not{E}_T$ events which are distinct from same-sign dilepton events from gluino/squark production in that they are relatively free of hard jet activity. Here also the model used is the NUHM2 model. Several cuts were applied to efficiently remove the SM backgrounds. After all cuts the HL-LHC 5σ reach (95%CL exclusion) was found to extend out to $m_{\tilde{w}_2} = 860$ GeV (1080 GeV). We recommend to extract the wino mass through three different channels : Event Counting, Charge Asymmetry, Fits to Distribution. Thus we can have a better measurement and consistency check of the

Wino mass.

LHC upgradation required to discover or falsify natural supersymmetry : Finally, we see what sort of LHC upgrades might be sufficient to either discover or falsify natural supersymmetry. Four SUSY search channels : 1. Gluino pair production, 2. Top squark pair production, 3. Higgsino pair production and 4. Wino pair production have been investigated within the context of Four RNS models : nNUHM2,3, nGMM and nAMSB and confronted with current LHC constraints and upgraded HL-LHC and HE-LHC projected constraints and it was found that the current LHC did not cover most of the parameter space of natural SUSY. The final assessment is that the search for natural SUSY will, and should, continue on at LHC and HL-LHC, where more extensive regions of parameter space may be explored. The envisioned HE-LHC upgrade to $\sqrt{s} = 27$ TeV and IL= 15 ab^{-1} seems sufficient to either discover or falsify natural SUSY in the top-squark pair production signal channel, very possibly with an additional signal in the gluino-pair production channel. On the other hand, HL-LHC will be sufficient to explore neutralino mass gaps $m_{\tilde{z}_2} - m_{\tilde{z}_1}$ down to ~ 3 GeV and higgsino masses up to ~ 350 GeV for complete coverage. For this channel HE-LHC might not be beneficial since QCD backgrounds are expected to rise more rapidly with energy than the EW higgsino pair production signal channel. For the wino pair production channel, the HL-LHC may explore a portion of – but not all of – natural SUSY parameter space in this channel. It is again unclear whether an energy upgrade will help much in this channel since QCD backgrounds are expected to increase more rapidly than the EW-produced signal channel.

Papers upon which this Thesis is based

1. "Midi-review: Status of weak scale supersymmetry after LHC Run 2 and ton-scale noble liquid WIMP searches",
   H. Baer, D. Sengupta, S. Salam, K. Sinha and V. Barger,
   arXiv:2002.03013 [hep-ph].

2. "Mirage mediation from the landscape",
   H. Baer, V. Barger and D. Sengupta,
   Phys. Rev. Res. **2** (2020), 013346
   doi:10.1103/PhysRevResearch.2.013346
   arXiv:1912.01672 [hep-ph].

3. "A landscape solution to the SUSY flavor and CP problems",
   H. Baer, V. Barger and D. Sengupta,
   Phys. Rev. Res. **1** (2019) no.3, 033179
   doi:10.1103/PhysRevResearch.1.033179
   arXiv:1910.00090 [hep-ph].

4. "Is the magnitude of the Peccei-Quinn scale set by the landscape?",
   H. Baer, V. Barger, D. Sengupta, H. Serce, K. Sinha and R. W. Deal
   Eur. Phys. J. C **79** (2019) no. 11, 897
   doi:10.1140/epjc/s10052-019-7408-x
   arXiv:1905.00443 [hep-ph].

5. "Revisiting the SUSY μ problem and its solutions in the LHC era",
   K. J. Bae, H. Baer, V. Barger and D. Sengupta,
   Phys. Rev. D **99** (2019) no.11, 115027
   doi:10.1103/PhysRevD.99.115027
   arXiv:1902.10748 [hep-ph].

6. "Beyond the Standard Model Physics at the HL-LHC and HE-LHC",
X. Cid Vidal (Santiago de Compostela U., IGFAE) et al.
CERN-LPCC-2018-05
doi:10.23731/CYRM-2019-007.585
arXiv:1812.07831 [hep-ph].

7. "Gravity safe, electroweak natural axionic solution to strong CP and SUSY μ problems",
H. Baer, V. Barger and D. Sengupta,
Phys. Lett. B **790** (2019) 58-63
doi:10.1016/j.physletb.2019.01.007
arXiv:1810.03713 [hep-ph].

8. "LHC luminosity and energy upgrades confront natural supersymmetry models",
H. Baer, V. Barger, J. S. Gainer, D. Sengupta, H. Serce and X. Tata,
Phys. Rev. D **98** (2018) no.7, 075010
doi:10.1103/PhysRevD.98.075010
arXiv:1808.04844 [hep-ph].

9. "Is natural higgsino-only dark matter excluded?",
H. Baer, V. Barger, D. Sengupta and X. Tata,
Eur. Phys. J. C **78** (2018) no.10, 838.
doi:10.1140/epjc/s10052-018-6306-y
arXiv:1803.11210 [hep-ph].

10. "Anomaly mediated SUSY breaking model retrofitted for naturalness",
H. Baer, V. Barger and D. Sengupta,
Phys. Rev. D **98** (2018) no.1, 015039
doi:10.1103/PhysRevD.98.015039

arXiv:1801.09730 [hep-ph].

11. "Aspects of the same-sign diboson signature from wino pair production with light higgsinos at the high luminosity LHC",
H. Baer, V. Barger, J. S. Gainer, M. Savoy, D. Sengupta and X. Tata,
Phys. Rev. D **97** (2018) no.3, 035012
doi:10.1103/PhysRevD.97.035012
arXiv:1710.09103 [hep-ph].

12. "Gluino reach and mass extraction at the LHC in radiatively-driven natural SUSY",
H. Baer, V. Barger, J. S. Gainer, P. Huang, M. Savoy, D. Sengupta and X. Tata,
Eur. Phys. J. C **77** (2017) no.7, 499
doi:10.1140/epjc/s10052-017-5067-3
arXiv:1612.00795 [hep-ph].

References

[1] G. Aad *et al.* [ATLAS Collaboration], "Observation of a new particle in the search for the Standard Model Higgs boson with the ATLAS detector at the LHC," Phys. Lett. **B716** (2012) 1.

[2] S. Chatrchyan *et al.* [CMS Collaboration], "Observation of a new boson at a mass of 125 GeV with the CMS experiment at the LHC," Phys. Lett. **B716** (2012) 30.

[3] S.L. Glashow, "Partial Symmetries of Weak Interactions," Nucl. Phys. 22, 579 (1961)

[4] A. Salam, "Weak and Electromagnetic Interactions," Conf. Proc. C 680519, 367 (1968)

[5] S. Weinberg, "A Model of Leptons," Phys. Rev. Lett. 19, 1264 (1967)

[6] P. W. Higgs, "Broken symmetries, massless particles and gauge fields," Phys. Lett.12, 132 (1964); P. W. Higgs, "Broken Symmetries and the Masses of Gauge Bosons," Phys. Rev. Lett.13, 508 (1964); F. Englert and R. Brout, "Broken Symmetry and the Mass of Gauge Vector Mesons," Phys. Rev. Lett.13, 321 (1964).

[7] G. S. Guralnik, C. R. Hagen and T. W. B. Kibble, "Global Conservation Laws and Massless Particles", Phys. Rev. Lett.13, 585 (1964).

[8] G. Aad et al. [ATLAS and CMS Collaborations], Phys. Rev. Lett. 114, 191803 (2015) doi:10.1103/PhysRevLett.114.191803 [arXiv:1503.07589 [hepex]].

[9] G. Hinshaw et al. [WMAP Collaboration], Astrophys. J. Suppl. 208, 19 (2013) doi:10.1088/0067-0049/208/2/19 [arXiv:1212.5226 [astro-ph.CO]].

[10] P. A. R. Ade et al. [Planck Collaboration], arXiv:1502.01589 [astro-ph.CO].

[11] K. A. Olive et al. [Particle Data Group Collaboration], Chin. Phys. C 38, 090001 (2014). doi:10.1088/1674-1137/38/9/090001.

[12] R. D. Peccei, Lect. Notes Phys. 741, 3 (2008) doi:10.1007/978-3-540-73518-2 [hep-ph/0607268].

[13] H. Baer and X. Tata, "Weak scale supersymmetry: From superfields to scattering events," Cambridge, UK: Univ. Pr. (2006) 537 p.

[14] T. Hemmick *et al.*, Phys. Rev. D **41**, 2074 (1990)

[15] For a review, see *e.g.* R. Arnowitt and P. Nath, "Developments in Supergravity Unified Models," In *Kane, G.L. (ed.): Perspectives on supersymmetry II* 222-243 [arXiv:0912.2273 [hep-ph]] and references therein; V. D. Barger, M. S. Berger and P. Ohmann, "Supersymmetric grand unified theories: Two loop evolution of gauge and Yukawa couplings," Phys. Rev. D **47**, 1093 (1993) and Phys. Rev. D **49**, 4908 (1994); G. L. Kane, C. F. Kolda, L. Roszkowski and J. D. Wells, "Study of constrained minimal supersymmetry," Phys. Rev. D **49**, 6173 (1994).

[16] H. Baer, V. Barger, P. Huang, A. Mustafayev and X. Tata, "Radiative natural SUSY with a 125 GeV Higgs boson," Phys. Rev. Lett. **109** (2012) 161802.

[17] H. Baer, V. Barger, P. Huang, D. Mickelson, A. Mustafayev and X. Tata, "Radiative natural supersymmetry: Reconciling electroweak fine-tuning and the Higgs boson mass," Phys. Rev. D **87** (2013) 115028.

[18] M. Papucci, J. T. Ruderman and A. Weiler, "Natural SUSY Endures," JHEP **1209** (2012) 035 doi:10.1007/JHEP09(2012)035 [arXiv:1110.6926 [hep-ph]].

[19] C. Brust, A. Katz, S. Lawrence and R. Sundrum, "SUSY, the Third Generation and the LHC," JHEP **1203** (2012) 103 doi:10.1007/JHEP03(2012)103 [arXiv:1110.6670 [hep-ph]].

[20] M. Carena and H. E. Haber, "Higgs boson theory and phenomenology," Prog. Part. Nucl. Phys. **50**, 63 (2003); P. Draper and H. Rzehak, "A Review of Higgs Mass Calculations in Supersymmetric Models," Phys. Rept. **619**, 1 (2016).

[21] H. Baer, V. Barger and A. Mustafayev, "Implications of a 125 GeV Higgs scalar for LHC SUSY and neutralino dark matter searches," Phys. Rev. D **85** (2012) 075010.

[22] H. Baer, V. Barger and D. Mickelson, "How conventional measures overestimate electroweak fine-tuning in supersymmetric theory," Phys. Rev. D **88** (2013) no.9, 095013 doi:10.1103/PhysRevD.88.095013 [arXiv:1309.2984 [hep-ph]].

[23] H. Baer, V. Barger, D. Mickelson and M. Padeffke-Kirkland, "SUSY models under siege: LHC constraints and electroweak fine-tuning," Phys. Rev. D **89** (2014) no.11, 115019 doi:10.1103/PhysRevD.89.115019 [arXiv:1404.2277 [hep-ph]].

[24] H. Baer, V. Barger and M. Savoy, "Supergravity gauge theories strike back: There is no crisis for SUSY but a new collider may be required for discovery," Phys. Scripta **90** (2015) 068003 doi:10.1088/0031-8949/90/6/068003 [arXiv:1502.04127 [hep-ph]].

[25] J. R. Ellis, K. Enqvist, D. V. Nanopoulos and F. Zwirner, "Observables in Low-Energy Superstring Models," Mod. Phys. Lett. A **1**, 57 (1986).

[26] R. Barbieri and G. F. Giudice, "Upper Bounds on Supersymmetric Particle Masses," Nucl. Phys. B **306** (1988) 63. doi:10.1016/0550-3213(88)90171-X

[27] L. E. Ibanez, C. Lopez and C. Munoz, "The Low-Energy Supersymmetric Spectrum According to N=1 Supergravity Guts," Nucl. Phys. **B256** (1985) 218; A. Lleyda and C. Munoz, "Nonuniversal soft scalar masses in supersymmetric theories," Phys. Lett. **B317** (1993) 82.

[28] H. Abe, T. Kobayashi and Y. Omura, "Relaxed fine-tuning in models with non-universal gaugino masses," Phys. Rev. **D76** (2007) 015002.

[29] S. P. Martin, "Compressed supersymmetry and natural neutralino dark matter from top squark-mediated annihilation to top quarks," Phys. Rev. **D75** (2007) 115005.

[30] For a recent review, see *e.g.* J. L. Feng, "Naturalness and the Status of Supersymmetry," Ann. Rev. Nucl. Part. Sci. **63** (2013) 351.

[31] M. Schumann " Direct Detection of WIMP Dark Matter: Concepts and Status" **J.Phys. G46 (2019) no.10, 103003**

[32] H. Baer, V. Barger and M. Savoy, "Upper bounds on sparticle masses from naturalness or how to disprove weak scale supersymmetry," Phys. Rev. D **93** (2016) no.3, 035016 doi:10.1103/PhysRevD.93.035016 [arXiv:1509.02929 [hep-ph]].

[33] K. L. Chan, U. Chattopadhyay and P. Nath, "Naturalness, weak scale supersymmetry and the prospect for the observation of supersymmetry at the Tevatron and at the CERN LHC," Phys. Rev. D **58** (1998) 096004 doi:10.1103/PhysRevD.58.096004 [hep-ph/9710473]; S. Akula, M. Liu, P. Nath and G. Peim, "Naturalness, Supersymmetry and Implications for LHC and Dark Matter," Phys. Lett. B **709** (2012) 192; M. Liu and P. Nath, "Higgs boson mass, proton decay, naturalness, and constraints of the LHC and Planck data," Phys. Rev. D **87** (2013) 095012.

[34] H. Baer, V. Barger and P. Huang, "Hidden SUSY at the LHC: the light higgsino-world scenario and the role of a lepton collider," JHEP **1111** (2011) 031 doi:10.1007/JHEP11(2011)031 [arXiv:1107.5581 [hep-ph]].

[35] H. Baer, V. Barger, J. S. Gainer, D. Sengupta, H. Serce and X. Tata, "LHC luminosity and energy upgrades confront natural supersymmetry models," Phys. Rev. D **98** (2018) no.7, 075010 doi:10.1103/PhysRevD.98.075010 [arXiv:1808.04844 [hep-ph]].

[36] H. Baer, V. Barger, M. Padeffke-Kirkland and X. Tata, "Naturalness implies intra-generational degeneracy for decoupled squarks and sleptons," Phys. Rev. D **89** (2014) no.3, 037701 doi:10.1103/PhysRevD.89.037701 [arXiv:1311.4587 [hep-ph]].

[37] H. Baer, V. Barger and D. Sengupta, "A landscape solution to the SUSY flavor and CP problems," Phys. Rev. Res. **1** (2019) no.3, 033179 doi:10.1103/PhysRevResearch.1.033179 [arXiv:1910.00090 [hep-ph]].

[38] K. J. Bae, H. Baer, V. Barger and D. Sengupta, "Revisiting the SUSY μ problem and its solutions in the LHC era," Phys. Rev. D **99** (2019) no.11, 115027 doi:10.1103/PhysRevD.99.115027 [arXiv:1902.10748 [hep-ph]].

[39] H. Baer, V. Barger, M. Savoy and H. Serce, "The Higgs mass and natural supersymmetric spectrum from the landscape," Phys.Lett. B **758** (2016) 113-117 doi:10.1016/j.physletb.2016.05.010 [arXiv:1602.07697 [hep-ph]].

[40] D. Matalliotakis and H. P. Nilles, "Implications of nonuniversality of soft terms in supersymmetric grand unified theories," Nucl. Phys. B **435** (1995) 115; M. Olechowski and S. Pokorski, "Electroweak symmetry breaking with nonuniversal scalar soft terms and large tan beta solutions," Phys. Lett. B **344** (1995) 201; P. Nath and R. L. Arnowitt, "Nonuniversal soft SUSY breaking and dark matter," Phys. Rev. D **56** (1997) 2820; J. Ellis, K. Olive and Y. Santoso, Phys. Lett. **B539** (2002) 107; J. Ellis, T. Falk, K. Olive and Y. Santoso, Nucl. Phys. **B652** (2003) 259; H. Baer, A. Mustafayev, S. Profumo, A. Belyaev and X. Tata, JHEP**0507** (2005) 065.

[41] K. Choi, A. Falkowski, H. P. Nilles, M. Olechowski and S. Pokorski, J. High Energy Phy**0411**, 076 (2004); K. Choi, A. Falkowski, H. P. Nilles and M. Olechowski, Nucl. Phys. **B718**, 113 (2005). J. P. Conlon, F. Quevedo and K. Suruliz, JHEP **0508**, 007 (2005) [arXiv:hep-th/0505076]; A. Pierce and J. Thaler, "Prospects for Mirage Mediation," JHEP **0609** (2006) 017; B. L. Kaufman, B. D. Nelson and M. K. Gaillard, "Mirage models confront the LHC: Kähler-stabilized heterotic string theory," Phys. Rev. D **88** (2013) no.2, 025003.

[42] H. Baer, V. Barger, H. Serce and X. Tata, "Natural generalized mirage mediation," Phys. Rev. D **94** (2016) no.11, 115017 doi:10.1103/PhysRevD.94.115017 [arXiv:1610.06205 [hep-ph]].

[43] L. Randall and R. Sundrum, Nucl. Phys. **B557**, 79 (1999); G. F. Giudice, M. Luty, H. Murayama and R. Rattazzi, J. High Energy Phys.**9812**, 027 (1998); J. Bagger, T. Moroi and E. Poppitz, J. High Energy Phys. **0004**, 009 (2000); P. Binetruy, M. K. Gaillard and B. Nelson, Nucl. Phys. **B604**, 32 (2001).

[44] T. Cohen, M. Lisanti, A. Pierce and T. R. Slatyer, "Wino Dark Matter Under Siege," JCAP **1310** (2013) 061 doi:10.1088/1475-7516/2013/10/061 [arXiv:1307.4082 [hep-ph]].

[45] J. Fan and M. Reece, "In Wino Veritas? Indirect Searches Shed Light on Neutralino Dark Matter," JHEP **1310** (2013) 124 doi:10.1007/JHEP10(2013)124 [arXiv:1307.4400 [hep-ph]].

[46] H. Baer, V. Barger and H. Serce, "SUSY under siege from direct and indirect WIMP detection experiments," Phys. Rev. D **94** (2016) no.11, 115019 doi:10.1103/PhysRevD.94.115019 [arXiv:1609.06735 [hep-ph]].

[47] H. Baer, V. Barger and D. Sengupta, "Anomaly mediated SUSY breaking model retrofitted for naturalness," Phys. Rev. D **98** (2018) no.1, 015039 doi:10.1103/PhysRevD.98.015039 [arXiv:1801.09730 [hep-ph]].

[48] K. J. Bae, H. Baer, A. Lessa and H. Serce, "Mixed axion-wino dark matter," Front. in Phys. **3** (2015) 49 doi:10.3389/fphy.2015.00049 [arXiv:1502.07198 [hep-ph]].

[49] ISAJET, by H. Baer, F. Paige, S. Protopopescu and X. Tata, hep-ph/0312045.

[50] S. Weinberg, "The U(1) Problem," Phys. Rev. D **11** (1975) 3583.

[51] G. 't Hooft, "Symmetry Breaking Through Bell-Jackiw Anomalies," Phys. Rev. Lett. **37** (1976) 8.

[52] K. Choi, E. J. Chun and J. E. Kim, "Cosmological implications of radiatively generated axion scale," Phys. Lett. B **403** (1997) 209.

[53] H. Murayama, H. Suzuki and T. Yanagida, "Radiative breaking of Peccei-Quinn symmetry at the intermediate mass scale," Phys. Lett. B **291** (1992) 418.

[54] S. P. Martin, "Implications of supersymmetric models with natural R-parity conservation," Phys. Rev. D **54** (1996) 2340; S. P. Martin, "Dimensionless supersymmetry breaking couplings, flat directions, and the origin of intermediate mass scales," Phys. Rev. D **61** (2000) 035004; S. P. Martin, "Collider signals from slow decays in supersymmetric models with an intermediate scale solution to the mu problem," Phys. Rev. D **62** (2000) 095008.

[55] K. J. Bae, H. Baer and H. Serce, "Natural little hierarchy for SUSY from radiative breaking of the Peccei-Quinn symmetry," Phys. Rev. D **91** (2015) 015003.

[56] J. E. Kim and H. P. Nilles, "The mu Problem and the Strong CP Problem," Phys. Lett. B **138** (1984) 150.

[57] K. S. Babu, I. Gogoladze and K. Wang, "Stabilizing the axion by discrete gauge symmetries," Phys. Lett. B **560** (2003) 214.

[58] M. Kamionkowski and J. March-Russell, "Planck scale physics and the Peccei-Quinn mechanism," Phys. Lett. B **282** (1992) 137; see also S. M. Barr and D. Seckel, "Planck scale corrections to axion models," Phys. Rev. D **46** (1992) 539; R. Holman, S. D. H. Hsu, T. W. Kephart, E. W. Kolb, R. Watkins and L. M. Widrow, "Solutions to the strong CP problem in a world with gravity," Phys. Lett. B **282** (1992) 132.

[59] M. B. Green and J. H. Schwarz, "Anomaly Cancellation in Supersymmetric D=10 Gauge Theory and Superstring Theory," Phys. Lett. **149B** (1984) 117.

[60] L. M. Krauss and F. Wilczek, "Discrete Gauge Symmetry in Continuum Theories," Phys. Rev. Lett. **62** (1989) 1221; M. Dine, "Problems of naturalness: Some lessons from string theory," hep-th/9207045; R. Kallosh, A. D. Linde, D. A. Linde and L. Susskind, "Gravity and global symmetries," Phys. Rev. D **52** (1995) 912.

[61] A. Linde, "A brief history of the multiverse," Rept. Prog. Phys. **80** (2017) no.2, 022001 doi:10.1088/1361-6633/aa50e4 [arXiv:1512.01203 [hep-th]].

[62] F. Denef and M. R. Douglas, "Distributions of flux vacua," JHEP **0405** (2004) 072 doi:10.1088/1126-6708/2004/05/072 [hep-th/0404116].

[63] W. Taylor and Y. N. Wang, JHEP **1512** (2015) 164 doi:10.1007/JHEP12(2015)164 [arXiv:1511.03209 [hep-th]].

[64] S. Weinberg, "Anthropic Bound on the Cosmological Constant," Phys. Rev. Lett. **59** (1987) 2607. doi:10.1103/PhysRevLett.59.2607

[65] S. Weinberg, "The Cosmological Constant Problem," Rev. Mod. Phys. **61** (1989) 1. doi:10.1103/RevModPhys.61.1

[66] N. Arkani-Hamed, S. Dimopoulos and S. Kachru, hep-th/0501082.

[67] L. Susskind, "Supersymmetry breaking in the anthropic landscape," In *Shifman, M. (ed.) et al.: From fields to strings, vol. 3* 1745-1749 doi:10.1142/9789812775344-0040 [hep-th/0405189].

[68] M. R. Douglas, "Statistical analysis of the supersymmetry breaking scale," hep-th/0405279.

[69] M. R. Douglas, "The String landscape and low energy supersymmetry," doi:10.1142/9789814412551-0012 arXiv:1204.6626 [hep-th].

[70] M. R. Douglas, "Basic results in vacuum statistics," Comptes Rendus Physique **5** (2004) 965 doi:10.1016/j.crhy.2004.09.008 [hep-th/0409207].

[71] H. Baer, V. Barger and S. Salam, "Naturalness versus stringy naturalness (with implications for collider and dark matter searches," Phys. Rev. Research. **1** (2019) 023001 doi:10.1103/PhysRevResearch.1.023001 [arXiv:1906.07741 [hep-ph]].

[72] S. K. Soni and H. A. Weldon, "Analysis of the Supersymmetry Breaking Induced by N=1 Supergravity Theories," Phys. Lett. **126B** (1983) 215. doi:10.1016/0370-2693(83)90593-2

[73] V. S. Kaplunovsky and J. Louis, "Model independent analysis of soft terms in effective supergravity and in string theory," Phys. Lett. B **306** (1993) 269 doi:10.1016/0370-2693(93)90078-V [hep-th/9303040].

[74] A. Brignole, L. E. Ibanez and C. Munoz, "Towards a theory of soft terms for the supersymmetric Standard Model," Nucl. Phys. B **422** (1994) 125 Erratum: [Nucl. Phys. B **436** (1995) 747] doi:10.1016/0550-3213(94)00600-J, 10.1016/0550-3213(94)00068-9 [hep-ph/9308271].

[75] M. Dine, E. Gorbatov and S. D. Thomas, "Low energy supersymmetry from the landscape," JHEP **0808** (2008) 098 doi:10.1088/1126-6708/2008/08/098 [hep-th/0407043].

[76] V. Agrawal, S. M. Barr, J. F. Donoghue and D. Seckel, "The Anthropic principle and the mass scale of the standard model," Phys. Rev. D **57**, 5480 (1998); V. Agrawal, S. M. Barr, J. F. Donoghue and D. Seckel, "Anthropic considerations in multiple domain theories and the scale of electroweak symmetry breaking," Phys. Rev. Lett. **80**, 1822 (1998).

[77] H. Baer, V. Barger, H. Serce and K. Sinha, "Higgs and superparticle mass predictions from the landscape," JHEP **1803**, 002 (2018).

[78] A. Falkowski, O. Lebedev and Y. Mambrini, JHEP **0511** (2005) 034 doi:10.1088/1126-6708/2005/11/034 [hep-ph/0507110].

[79] K. Choi, K. S. Jeong, T. Kobayashi and K. i. Okumura, Phys. Rev. D **75** (2007) 095012 doi:10.1103/PhysRevD.75.095012 [hep-ph/0612258].

[80] The ATLAS collaboration [ATLAS Collaboration], ATLAS-CONF-2017-022; T. Sakuma [CMS Collaboration], PoS LHCP **2016** (2017) 145 [arXiv:1609.07445 [hep-ex]].

[81] The ATLAS collaboration [ATLAS Collaboration], ATLAS-CONF-2017-037; A. M. Sirunyan *et al.* [CMS Collaboration], arXiv:1706.04402 [hep-ex].

[82] D. S. Akerib *et al.* [LUX Collaboration], Phys. Rev. Lett. **118** (2017) no.2, 021303.

[83] X. Cui *et al.* [PandaX-II Collaboration], Phys. Rev. Lett. **119** (2017) no.18, 181302.

[84] E. Aprile *et al.* [XENON Collaboration], Phys. Rev. Lett. **119** (2017) no.18, 181301.

[85] M. L. Ahnen *et al.* [MAGIC and Fermi-LAT Collaborations], JCAP **1602** (2016) no.02, 039.

[86] N. Arkani-Hamed, A. Delgado and G. F. Giudice, Nucl. Phys. B **741** (2006) 108; H. Baer, A. Mustafayev, E. K. Park and X. Tata, JCAP **0701** (2007) 017; H. Baer, A. Mustafayev, E. K. Park and X. Tata, JHEP **0805** (2008) 058; M. Badziak, M. Olechowski and P. Szczerbiak, Phys. Lett. B **770** (2017) 226.

[87] J. L. Feng, K. T. Matchev and F. Wilczek, Phys. Lett. B **482** (2000) 388.

[88] H. Baer, C. Balazs, A. Belyaev and J. O'Farrill, JCAP **0309** (2003) 007.

[89] H. Baer, V. Barger and H. Serce, Phys. Rev. D **94** (2016) no.11, 115019.

[90] T. Cohen, M. Lisanti, A. Pierce and T. R. Slatyer, JCAP **1310** (2013) 061.

[91] J. Fan and M. Reece, JHEP **1310** (2013) 124.

[92] H. Baer, C. Balazs and A. Belyaev, JHEP **0203** (2002) 042

[93] [Planck Collaboration] P. A. R. Ade *et al.* Astronom. and Astrophys. **A13** (2016) 594 [arXiv:1502.01589]

[94] H. Baer, K. Y. Choi, J. E. Kim and L. Roszkowski, Phys. Rept. **555** (2015) 1.

[95] E. J. Chun and A. Lukas, Phys. Lett. B **357** (1995) 43; J. E. Kim and M. S. Seo, Nucl. Phys. B **864** (2012) 296.

[96] H. Baer, A. Lessa and W. Sreethawong, JCAP **1201** (2012) 036; K. J. Bae, H. Baer and A. Lessa, JCAP **1304** (2013) 041; K. J. Bae, H. Baer and E. J. Chun, JCAP **1312** (2013) 028; K. J. Bae, H. Baer, A. Lessa and H. Serce, JCAP **1410** (2014) no.10, 082.

[97] H. Baer and A. Lessa, JHEP **1106** (2011) 027.

[98] T. Moroi and L. Randall, Nucl. Phys. B **570** (2000) 455.

[99] G. B. Gelmini and P. Gondolo, Phys. Rev. D **74** (2006) 023510.

[100] B. S. Acharya, G. Kane, S. Watson and P. Kumar, Phys. Rev. D **80** (2009) 083529.

[101] G. Kane, K. Sinha and S. Watson, Int. J. Mod. Phys. D **24** (2015) no.08, 1530022.

[102] B. Dutta, L. Leblond and K. Sinha, Phys. Rev. D **80**, 035014 (2009); R. Allahverdi, B. Dutta and K. Sinha, Phys. Rev. D **86**, 095016 (2012).

[103] H. Baer, C. Balazs, A. Belyaev and J. O'Farrill, JCAP **0309** (2003) 007.

[104] J. R. Ellis, K. A. Olive and C. Savage, Phys. Rev. D **77** (2008) 065026; J. Ellis, N. Nagata and K. A. Olive, Eur. Phys. J. C **78** (2018) no.7, 569.

[105] J. Hisano, K. Ishiwata and N. Nagata, JHEP **1506** (2015) 097.

[106] C. Amole *et al.* [PICO Collaboration], Phys. Rev. Lett. **118** (2017) no.25, 251301.

[107] M. G. Aartsen *et al.* [IceCube Collaboration], JCAP **1604** (2016) no.04, 022.

[108] Talk by C. Krauss for the Pico collaboration, ICHEP 2016 meeting, Chicago, IL, August 2016.

[109] H. Baer, V. Barger, D. Mickelson, A. Mustafayev and X. Tata, JHEP **1406** (2014) 172.

[110] G. Giesen, M. Boudaud, Y. Génolini, V. Poulin, M. Cirelli, P. Salati and P. D. Serpico, JCAP **1509** (2015) no.09, 023.

[111] A. Cuoco, J. Heisig, M. Korsmeier and M. Krämer, arXiv:1711.05274 [hep-ph].

[112] J. Bramante, N. Desai, P. Fox, A. Martin, B. Ostdiek and T. Plehn, Phys. Rev. D **93** (2016) no.6, 063525.

[113] L. Aparicio, M. Cicoli, B. Dutta, S. Krippendorf, A. Maharana, F. Muia and F. Quevedo, JHEP **1505** (2015) 098; L. Aparicio, M. Cicoli, B. Dutta, F. Muia and F. Quevedo, JHEP **1611** (2016) 038.

[114] H. Baer, V. Barger, J. S. Gainer, H. Serce and X. Tata, Phys. Rev. D **96** (2017) no.11, 115008.

[115] K. Kowalska, L. Roszkowski, E. M. Sessolo and S. Trojanowski, JHEP **1404** (2014) 166.

[116] K. Kowalska and E. M. Sessolo, arXiv:1802.04097 [hep-ph].

[117] H. Baer, V. Barger, P. Huang, D. Mickelson, M. Padeffke-Kirkland and X. Tata, Phys. Rev. D **91** (2015) no.7, 075005.

[118] M. van Beekveld, W. Beenakker, S. Caron, R. Peeters and R. Ruiz de Austri, Phys. Rev. D **96** (2017) no.3, 035015; for other studies with non-universal gaugino masses, see also I. Gogoladze, F. Nasir and Q. Shafi, JHEP **1311** (2013) 173; M. Abdughani, L. Wu and J. M. Yang, Eur. Phys. J. C **78** (2018) no.1, 4; W. Ahmed, X. J. Bi, T. Li, J. S. Niu, S. Raza, Q. F. Xiang and P. F. Yin, arXiv:1709.06371 [hep-ph]; W. Ahmed, L. Calibbi, T. Li, S. Raza, J. S. Niu and X. C. Wang, arXiv:1711.10225 [hep-ph]; M. A. Ajaib and I. Gogoladze, arXiv:1710.07842 [hep-ph].

[119] K. J. Bae, H. Baer and H. Serce, JCAP **1706** (2017) no.06, 024.

[120] For an early review, see *e.g.* N. Polonsky, hep-ph/9911329.

[121] G. F. Giudice and R. Rattazzi, Phys. Rept. **322** (1999) 419.

[122] A. Arbey, M. Battaglia, A. Djouadi, F. Mahmoudi and J. Quevillon, Phys. Lett. B **708** (2012) 162.

[123] H. Baer, V. Barger and A. Mustafayev, JHEP **1205** (2012) 091.

[124] G. G. Ross, K. Schmidt-Hoberg and F. Staub, JHEP **1703** (2017) 021.

[125] A. E. Nelson and T. S. Roy, Phys. Rev. Lett. **114** (2015) 201802.

[126] S. P. Martin, Phys. Rev. D **92** (2015) no.3, 035004.

[127] G. F. Giudice and A. Masiero, Phys. Lett. B **206** (1988) 480.

[128] J. A. Casas and C. Munoz, Phys. Lett. B **306** (1993) 288.

[129] Saul Ramos-Sanchez, Fortsch.Phys. 58 (2010) 748-752 DESY-10-028

[130] R. Kappl, H. P. Nilles, S. Ramos-Sanchez, M. Ratz, K. Schmidt-Hoberg and P. K. S. Vaudrevange, Phys. Rev. Lett. **102** (2009) 121602; F. Brummer, R. Kappl, M. Ratz and K. Schmidt-Hoberg, JHEP **1004** (2010) 006.

[131] K. Choi, E. J. Chun and H. D. Kim, Phys. Rev. D **55** (1997) 7010.

[132] L. J. Hall, Y. Nomura and A. Pierce, Phys. Lett. B **538** (2002) 359.

[133] H. P. Nilles, M. Ratz and P. K. S. Vaudrevange, Fortsch.Phys. 61 (2013) 493-506.

[134] M. Dine and J. Kehayias, Phys. Rev. D **82** (2010) 055014.

[135] K. S. Babu, I. Gogoladze and K. Wang, Nucl. Phys. B **660** (2003) 322.

[136] H. M. Lee, S. Raby, M. Ratz, G. G. Ross, R. Schieren, K. Schmidt-Hoberg and P. K. S. Vaudrevange, Phys. Lett. B **694** (2011) 491.

[137] H. M. Lee, S. Raby, M. Ratz, G. G. Ross, R. Schieren, K. Schmidt-Hoberg and P. K. S. Vaudrevange, Nucl. Phys. B **850** (2011) 1.

[138] K. Harigaya, M. Ibe, K. Schmitz and T. T. Yanagida, Phys. Rev. D **88** (2013) no.7, 075022.

[139] P. Sikivie, Phys. Rev. Lett. **48** (1982) 1156.

[140] S. E. Larsson, S. Sarkar and P. L. White, Phys. Rev. D **55** (1997) 5129.

[141] M. Dine, F. Takahashi and T. T. Yanagida, JHEP **1007** (2010) 003.

[142] K. J. Bae, H. Baer, H. Serce and Y. F. Zhang, JCAP **1601** (2016) 012.

[143] L. E. Ibanez and A. M. Uranga, JHEP **0703** (2007) 052.

[144] D. Green and T. Weigand, arXiv:0906.0595 [hep-th].

[145] B. S. Acharya, K. Bobkov, G. L. Kane, J. Shao and P. Kumar, Phys. Rev. D **78** (2008) 065038.

[146] E. Witten, hep-ph/0201018.

[147] B. S. Acharya, G. Kane, E. Kuflik and R. Lu, JHEP **1105** (2011) 033.

[148] H. P. Nilles, M. Srednicki and D. Wyler, Phys. Lett. **120B** (1983) 346; J. M. Frere, D. R. T. Jones and S. Raby, Nucl. Phys. B **222** (1983) 11; J. P. Derendinger and C. A. Savoy, Nucl. Phys. B **237** (1984) 307; for a recent review, see M. Maniatis, Int. J. Mod. Phys. A **25** (2010) 3505; U. Ellwanger, C. Hugonie and A. M. Teixeira, Phys. Rept. **496** (2010) 1; U. Ellwanger, J. F. Gunion and C. Hugonie, JHEP **0502**

(2005) 066; V. Barger, G. Shaughnessy and B. Yencho, Phys. Rev. D **83** (2011) 055006.

[149] J. Bagger and E. Poppitz, Phys. Rev. Lett. **71** (1993) 2380; J. Bagger, E. Poppitz and L. Randall, Nucl. Phys. B **455** (1995) 59.

[150] J. R. Ellis, K. Enqvist, D. V. Nanopoulos, K. A. Olive, M. Quiros and F. Zwirner, Phys. Lett. B **176** (1986) 403; B. Rai and G. Senjanovic, Phys. Rev. D **49** (1994) 2729; S. A. Abel, S. Sarkar and P. L. White, Nucl. Phys. B **454** (1995) 663; J. McDonald, Nucl. Phys. B **530** (1998) 325.

[151] S. A. Abel, Nucl. Phys. B **480** (1996) 55; C. Panagiotakopoulos and K. Tamvakis, Phys. Lett. B **446** (1999) 224; T. Han, P. Langacker and B. McElrath, hep-ph/0402064; A. Mazumdar, K. Saikawa, M. Yamaguchi and J. Yokoyama, Phys. Rev. D **93** (2016) no.2, 025002.

[152] C. Balazs, M. Carena, A. Freitas and C. E. M. Wagner, JHEP **0706** (2007) 066.

[153] L. J. Hall, D. Pinner and J. T. Ruderman, JHEP **1204** (2012) 131.

[154] C. Panagiotakopoulos and K. Tamvakis, Phys. Lett. B **469** (1999) 145.

[155] C. Panagiotakopoulos and A. Pilaftsis, Phys. Rev. D **63** (2001) 055003.

[156] A. Dedes, C. Hugonie, S. Moretti and K. Tamvakis, Phys. Rev. D **63** (2001) 055009.

[157] A. Menon, D. E. Morrissey and C. E. M. Wagner, Phys. Rev. D **70** (2004) 035005.

[158] V. Barger, P. Langacker, H. S. Lee and G. Shaughnessy, Phys. Rev. D **73** (2006) 115010.

[159] V. Barger, P. Langacker and G. Shaughnessy, Phys. Lett. B **644** (2007) 361.

[160] J. Cao, H. E. Logan and J. M. Yang, Phys. Rev. D **79** (2009) 091701.

[161] D. E. Lopez-Fogliani and C. Munoz, Phys. Rev. Lett. **97** (2006) 041801; N. Escudero, D. E. Lopez-Fogliani, C. Munoz and R. Ruiz de Austri, JHEP **0812** (2008) 099; J. Fidalgo, D. E. Lopez-Fogliani, C. Munoz and R. Ruiz de Austri, JHEP **0908** (2009) 105; for a review, see C. Munoz, AIP Conf. Proc. **1200** (2010) 413.

[162] K. Y. Choi, D. E. Lopez-Fogliani, C. Munoz and R. Ruiz de Austri, JCAP **1003** (2010) 028.

[163] P. Ghosh and S. Roy, JHEP **0904** (2009) 069; A. Bartl, M. Hirsch, A. Vicente, S. Liebler and W. Porod, JHEP **0905** (2009) 120; J. Fidalgo, D. E. Lopez-Fogliani, C. Munoz and R. Ruiz de Austri, JHEP **1110** (2011) 020; P. Ghosh, D. E. Lopez-Fogliani, V. A. Mitsou, C. Munoz and R. Ruiz de Austri, Phys. Rev. D **88** (2013) 015009; P. Ghosh, D. E. Lopez-Fogliani, V. A. Mitsou, C. Munoz and R. Ruiz de Austri, JHEP **1411** (2014) 102.

[164] M. Cvetic, D. A. Demir, J. R. Espinosa, L. L. Everett and P. Langacker, Phys. Rev. D **56** (1997) 2861 Erratum: [Phys. Rev. D **58** (1998) 119905].

[165] R. S. Hundi, S. Pakvasa and X. Tata, Phys. Rev. D **79** (2009) 095011.

[166] D. E. Morrissey and J. D. Wells, Phys. Rev. D **74** (2006) 015008.

[167] T. Cohen and A. Pierce, Phys. Rev. D **78** (2008) 055012.

[168] A. Arvanitaki, Phys. Rev. D **81** (2010) 075008.

[169] J. Erler, P. Langacker and T. j. Li, Phys. Rev. D **66** (2002) 015002.

[170] T. Han, P. Langacker and B. McElrath, Phys. Rev. D **70** (2004) 115006.

[171] M. Hirsch and J. W. F. Valle, New J. Phys. **6** (2004) 76.

[172] M. Dine, W. Fischler and M. Srednicki, Phys. Lett. **104B** (1981) 199; A. R. Zhitnitsky, Sov. J. Nucl. Phys. **31** (1980) 260 [Yad. Fiz. **31** (1980) 497].

[173] R. Dermisek and A. Mafi, Phys. Rev. D **65** (2002) 055002.

[174] N. Arkani-Hamed and S. Dimopoulos, hep-ph/9811353; N. Arkani-Hamed, L. Hall, D. Smith and N. Weiner, Phys. Rev. D **63**, 056003 (2001).

[175] K. J. Bae, H. Baer and E. J. Chun, Phys. Rev. D **89** (2014) no.3, 031701;

[176] K. J. Bae, H. Baer and E. J. Chun, JCAP **1312** (2013) 028.

[177] K. J. Bae, H. Baer, A. Lessa and H. Serce, JCAP **1410** (2014) no.10, 082.

[178] H. Baer, A. Lessa and W. Sreethawong, JCAP **1201** (2012) 036.

[179] E. J. Chun, Phys. Rev. D **84** (2011) 043509; K. J. Bae, E. J. Chun and S. H. Im, JCAP **1203** (2012) 013.

[180] M. Tanabashi *et al.* [Particle Data Group], Phys. Rev. D **98** (2018) no.3, 030001.

[181] K. J. Bae, H. Baer and H. Serce, JCAP **1706** (2017) no.06, 024.

[182] J. E. Kim and H. P. Nilles, Phys. Lett. B **263** (1991) 79; E. J. Chun, J. E. Kim and H. P. Nilles, Nucl. Phys. B **370** (1992) 105.

[183] J. E. Kim and H. P. Nilles, Phys. Lett. B **553** (2003) 1; J. E. Kim and H. P. Nilles, JCAP **0905** (2009) 010.

[184] M. Bastero-Gil and S. F. King, Phys. Lett. B **423** (1998) 27.

[185] O. J. Eyton-Williams and S. F. King, Phys. Lett. B **610** (2005) 87.

[186] A. D. Linde, Phys. Lett. B **249** (1990) 18; A. D. Linde, Phys. Lett. B **259**, 38 (1991).

[187] O. J. Eyton-Williams and S. F. King, JHEP **0506** (2005) 040.

[188] J. E. Kim and H. P. Nilles, Phys. Lett. B **730** (2014) 53.

[189] L. M. Krauss and F. Wilczek, Phys. Rev. Lett. **62** (1989) 1221; J. E. Kim and H. P. Nilles, Mod. Phys. Lett. A **9** (1994) 3575; T. Banks, Nucl. Phys. B **323** (1989) 90.

[190] E. J. Chun and A. Lukas, Phys. Lett. B **297** (1992) 298.

[191] K. Y. Choi, E. J. Chun and H. M. Lee, Phys. Rev. D **82** (2010) 105028.

[192] A. H. Chamseddine and H. K. Dreiner, Nucl. Phys. B **458** (1996) 65.

[193] M. C. Chen, M. Fallbacher and M. Ratz, Mod. Phys. Lett. A **27** (2012) 1230044.

[194] J. E. Kim, Phys. Rev. Lett. **111** (2013) no.3, 031801.

[195] H. Baer, V. Barger and D. Sengupta, arXiv:1810.03713 [hep-ph].

[196] M. Dine and A. Nelson, Phys. Rev. D **48** (1993) 1277. M. Dine, A. Nelson, Y. Nir and Y. Shirman, Phys. Rev. D **53** (1996) 2658.

[197] B. Carter, "The general theory of the mechanical, electromagnetic and thermodynamic properties of black holes," p. 294-369.

[198] S. B. Giddings and A. Strominger, Nucl. Phys. B **306** (1988) 890; G. Gilbert, Nucl. Phys. B **328** (1989) 159.

[199] R. Kallosh, A. D. Linde, D. A. Linde and L. Susskind, Phys. Rev. D **52** (1995) 912.

[200] B. A. Dobrescu, Phys. Rev. D **55** (1997) 5826.

[201] M. Kamionkowski and J. March-Russell, Phys. Lett. B **282** (1992) 137; see also S. M. Barr and D. Seckel, Phys. Rev. D **46** (1992) 539; R. Holman, S. D. H. Hsu, T. W. Kephart, E. W. Kolb, R. Watkins and L. M. Widrow, Phys. Lett. B **282** (1992) 132.

[202] C. Vafa, hep-th/0509212.

[203] H. Baer, V. Barger, D. Sengupta and X. Tata, Eur. Phys. J. C **78** (2018) no.10, 838.

[204] R. D. Peccei and H. R. Quinn, Phys. Rev. Lett. **38** (1977) 1440; R. D. Peccei and H. R. Quinn, Phys. Rev. D **16** (1977) 1791.

[205] M. Tanabashi *et al.* [Particle Data Group], Phys. Rev. D **98** (2018) no.3, 030001.

[206] L. F. Abbott and P. Sikivie, Phys. Lett. B **120** (1983) 133; J. Preskill, M. B. Wise and F. Wilczek, Phys. Lett. B **120** (1983) 127; M. Dine and W. Fischler, Phys. Lett. B **120** (1983) 137; M. S. Turner, Phys. Rev. D **33** (1986) 889; K. J. Bae, J. H. Huh and J. E. Kim, JCAP **0809** (2008) 005; L. Visinelli and P. Gondolo, Phys. Rev. D **80** (2009) 035024.

[207] K. Choi and J. E. Kim, Phys. Lett. **154B** (1985) 393.

[208] P. Svrcek and E. Witten, JHEP **0606** (2006) 051.

[209] A. D. Linde, Phys. Lett. B **201** (1988) 437.

[210] S. Hellerman and J. Walcher, Phys. Rev. D **72** (2005) 123520.

[211] F. Wilczek, In *Carr, Bernard (ed.): Universe or multiverse* 151-162 [hep-ph/0408167]; see also F. Wilczek, Class. Quant. Grav. **30** (2013) 193001.

[212] M. Tegmark, A. Aguirre, M. Rees and F. Wilczek, Phys. Rev. D **73** (2006) 023505.

[213] B. Freivogel, JCAP **1003** (2010) 021.

[214] L. Visinelli and P. Gondolo, Phys. Rev. D **80** (2009) 035024.

[215] M. Kawasaki, K. Kohri, T. Moroi and A. Yotsuyanagi, Phys. Rev. D **78** (2008) 065011.

[216] K. Jedamzik, Phys. Rev. D **74** (2006) 103509.

[217] K. J. Bae, K. Choi and S. H. Im, JHEP **1108** (2011) 065; K. J. Bae, E. J. Chun and S. H. Im, JCAP **1203** (2012) 013.

[218] A. Brandenburg and F. D. Steffen, JCAP **0408** (2004) 008.

[219] J. Pradler and F. D. Steffen, Phys. Rev. D **75** (2007) 023509.

[220] H. P. Nilles and P. K. S. Vaudrevange, Mod. Phys. Lett. A **30** (2015) no.10, 1530008.

[221] Z. Han, G. D. Kribs, A. Martin and A. Menon, Phys. Rev. D **89** (2014) no.7, 075007; H. Baer, A. Mustafayev and X. Tata, Phys. Rev. D **90** (2014) no.11, 115007; C. Han, D. Kim, S. Munir and M. Park, JHEP **1504** (2015) 132; A. M. Sirunyan *et al.* [CMS Collaboration], Phys. Lett. B **782** (2018) 440.

[222] The ATLAS collaboration [ATLAS Collaboration], ATLAS-CONF-2019-014.

[223] F. Gabbiani and A. Masiero, Nucl. Phys. B **322** (1989) 235. doi:10.1016/0550-3213(89)90492-6

[224] J. S. Hagelin, S. Kelley and T. Tanaka, Nucl. Phys. B **415** (1994) 293. doi:10.1016/0550-3213(94)90113-9

[225] F. Gabbiani, E. Gabrielli, A. Masiero and L. Silvestrini, Nucl. Phys. B **477** (1996) 321 doi:10.1016/0550-3213(96)00390-2 [hep-ph/9604387].

[226] M. Misiak, S. Pokorski and J. Rosiek, Adv. Ser. Direct. High Energy Phys. **15** (1998) 795 doi:10.1142/9789812812667-0012 [hep-ph/9703442].

[227] M. Dugan, B. Grinstein and L. J. Hall, Nucl. Phys. B **255** (1985) 413. doi:10.1016/0550-3213(85)90145-2

[228] S. P. Martin and M. T. Vaughn, Phys. Rev. D **50** (1994) 2282 Erratum: [Phys. Rev. D **78** (2008) 039903] doi:10.1103/PhysRevD.50.2282, 10.1103/PhysRevD.78.039903 [hep-ph/9311340].

[229] N. Arkani-Hamed and H. Murayama, Phys. Rev. D **56** (1997) R6733 doi:10.1103/PhysRevD.56.R6733 [hep-ph/9703259].

[230] H. Baer, C. Balazs, P. Mercadante, X. Tata and Y. Wang, Phys. Rev. D **63** (2001) 015011 doi:10.1103/PhysRevD.63.015011 [hep-ph/0008061].

[231] H. Baer, C. Balazs, M. Brhlik, P. Mercadante, X. Tata and Y. Wang, Phys. Rev. D **64** (2001) 015002 doi:10.1103/PhysRevD.64.015002 [hep-ph/0102156].

[232] A. G. Cohen, D. B. Kaplan and A. E. Nelson, Phys. Lett. B **388** (1996) 588 doi:10.1016/S0370-2693(96)01183-5 [hep-ph/9607394].

[233] S. L. Glashow, J. Iliopoulos and L. Maiani, Phys. Rev. D **2** (1970) 1285. doi:10.1103/PhysRevD.2.1285

[234] M. K. Gaillard and B. W. Lee, Phys. Rev. D **10** (1974) 897. doi:10.1103/PhysRevD.10.897

[235] S. Dimopoulos and D. W. Sutter, Nucl. Phys. B **452** (1995) 496 doi:10.1016/0550-3213(95)00421-N [hep-ph/9504415].

[236] J. R. Ellis and D. V. Nanopoulos, Phys. Lett. **110B** (1982) 44. doi:10.1016/0370-2693(82)90948-0

[237] J. F. Donoghue, H. P. Nilles and D. Wyler, Phys. Lett. **128B** (1983) 55. doi:10.1016/0370-2693(83)90072-2

[238] M. J. Duncan and J. Trampetic, Phys. Lett. **134B** (1984) 439. doi:10.1016/0370-2693(84)91380-7

[239] A. Bouquet, J. Kaplan and C. A. Savoy, Phys. Lett. **148B** (1984) 69. doi:10.1016/0370-2693(84)91613-7

[240] A. M. Baldini *et al.* [MEG Collaboration], Eur. Phys. J. C **76**, no. 8, 434 (2016) doi:10.1140/epjc/s10052-016-4271-x [arXiv:1605.05081 [hep-ex]].

[241] S. Kachru, R. Kallosh, A. D. Linde and S. P. Trivedi, Phys. Rev. D **68** (2003) 046005.

[242] K. Choi, A. Falkowski, H. P. Nilles, M. Olechowski and S. Pokorski, JHEP **0411** (2004) 076 doi:10.1088/1126-6708/2004/11/076 [hep-th/0411066].

[243] O. Loaiza-Brito, J. Martin, H. P. Nilles and M. Ratz, AIP Conf. Proc. **805** (2005) no.1, 198 doi:10.1063/1.2149698 [hep-th/0509158].

[244] K. Choi, K. S. Jeong and K. i. Okumura, JHEP **0509** (2005) 039 doi:10.1088/1126-6708/2005/09/039 [hep-ph/0504037].

[245] K. Choi, A. Falkowski, H. P. Nilles and M. Olechowski, Nucl. Phys. B **718** (2005) 113 doi:10.1016/j.nuclphysb.2005.04.032 [hep-th/0503216].

[246] H. Baer, V. Barger, M. Savoy, H. Serce and X. Tata, JHEP **1706** (2017) 101 doi:10.1007/JHEP06(2017)101 [arXiv:1705.01578 [hep-ph]].

[247] H. Baer, V. Barger, J. S. Gainer, P. Huang, M. Savoy, D. Sengupta and X. Tata, Eur. Phys. J. C **77** (2017) no.7, 499 doi:10.1140/epjc/s10052-017-5067-3 [arXiv:1612.00795 [hep-ph]].

[248] H. Baer, V. Barger, J. S. Gainer, D. Sengupta, H. Serce and X. Tata, Phys. Rev. D **98** (2018) no.7, 075010 doi:10.1103/PhysRevD.98.075010 [arXiv:1808.04844 [hep-ph]].

[249] X. Cid Vidal *et al.* [Working Group 3], arXiv:1812.07831 [hep-ph].

[250] K. J. Bae, H. Baer, N. Nagata and H. Serce, Phys. Rev. D **92** (2015) no.3, 035006 doi:10.1103/PhysRevD.92.035006 [arXiv:1505.03541 [hep-ph]].

[251] H. Baer, V. Barger, D. Mickelson, A. Mustafayev and X. Tata, JHEP **1406** (2014) 172; S. L. Lehtinen, H. Baer, M. Berggren, K. Fujii, J. List, T. Tanabe and J. Yan, arXiv:1710.02406 [hep-ph]; K. Fujii *et al.*, arXiv:1702.05333 [hep-ph]; H. Baer, M. Berggren, K. Fujii, J. List, S. L. Lehtinen, T. Tanabe and J. Yan, to appear.

[252] H. Baer, V. Barger, P. Huang, D. Mickelson, A. Mustafayev, W. Sreethawong and X. Tata, Phys. Rev. Lett. **110** (2013) no.15, 151801 doi:10.1103/PhysRevLett.110.151801 [arXiv:1302.5816 [hep-ph]].

[253] H. Baer, V. Barger, J. S. Gainer, M. Savoy, D. Sengupta and X. Tata, Phys. Rev. D **97** (2018) no.3, 035012 doi:10.1103/PhysRevD.97.035012 [arXiv:1710.09103 [hep-ph]].

[254] K. Choi and H. P. Nilles, JHEP **0704** (2007) 006 doi:10.1088/1126-6708/2007/04/006 [hep-ph/0702146 [HEP-PH]].

[255] The ATLAS collaboration [ATLAS Collaboration], ATLAS-CONF-2019-014.

[256] H. Baer, V. Barger, S. Salam, H. Serce and K. Sinha, JHEP **1904** (2019) 043 doi:10.1007/JHEP04(2019)043 [arXiv:1901.11060 [hep-ph]].

[257] R. M. Barnett, J. F. Gunion and H. E. Haber, UCD-88-30, LBL-26204, SCIPP-88-36; H. Baer, X. Tata and J. Woodside, Phys. Rev. D **41** (1990) 906; H. Baer, X. Tata and J. Woodside, Phys. Rev. D **45** (1992) 142; R. M. Barnett, J. F. Gunion and H. E. Haber, Phys. Lett. B **315** (1993) 349.

[258] H. Baer, V. Barger, P. Huang, D. Mickelson, A. Mustafayev, W. Sreethawong and X. Tata, JHEP **1312** (2013) 013 Erratum: [JHEP **1506** (2015) 053].

[259] U. Chattopadhyay, A. Datta, A. Datta, A. Datta and D.P. Roy, Phys. Lett. B **493** (2000) 127; P. Mercadante, J. K. Mizukoshi and X. Tata, Phys. Rev. D **72** (2005) 035009; R.H.K. Kadala, P. Mercadante, J. K. Mizukoshi and X. Tata, *Eur. Phys. J.* **C 56** (() 2008) 511.

[260] H. Baer, V. Barger, M. Savoy and X. Tata, Phys. Rev. D **94** (2016) no.3, 035025.

[261] J. Alwall, M. Herquet, F. Maltoni, O. Mattelaer and T. Stelzer, JHEP **1106** (2011) 128; J. Alwall, R. Frederix, S. Frixone, V Herschi, F. Maltoni, O. Mattelaer, H.-S. Shao, T. Stelzer, P. Torrielli and M. Zaro, JHEP **1407** (2014) 079.

[262] T. Sjöstrand *et al.*, Comput. Phys. Commun. **191** (2015) 159.

[263] J. de Favereau *et al.* [DELPHES 3 Collaboration], JHEP **1402** (2014) 057.

[264] W. Beenakker, R. Hopker and M. Spira, hep-ph/9611232.

[265] M. Czakon, P. Fiedler and A. Mitov, Phys. Rev. Lett. **110**, 252004 (2013).

[266] J. M. Campbell, R. K. Ellis and C. Williams, JHEP **1107**, 018 (2011).

[267] J. M. Campbell and R. K. Ellis, JHEP **1207**, 052 (2012).

[268] A. Kardos, Z. Trocsanyi and C. Papadopoulos, Phys. Rev. D **85**, 054015 (2012).

[269] T. Melia, K. Melnikov, R. Rontsch and G. Zanderighi, JHEP **1012**, 053 (2010).

[270] Y. B. Shen, R. Y. Zhang, W. G. Ma, X. Z. Li and L. Guo, Phys. Rev. D **95**, no. 7, 073005 (2017).

[271] M. Cacciari, G. P. Salam and G. Soyez, JHEP **0804**, 063 (2008).

[272] M. Cacciari, G. P. Salam and G. Soyez, Eur. Phys. J. C **72**, 1896 (2012).

[273] CMS Collaboration [CMS Collaboration], CMS-PAS-BTV-15-001.

[274] M. Cacciari and G. P. Salam, Phys. Lett. B **659**, 119 (2008).

[275] S. Corréad, V. Kostioukine, J. Levêque, A. Rozanov, J. B. de Vivie, ATLAS Note, ATLAS-PHYS-2004-006, and V. Kostioukine, ATLAS Note, ATLAS-PHYS-2003-033.

[276] V. D. Barger, T. Han and R. J. N. Phillips, Phys. Rev. D **36**, 295 (1987).

[277] C. G. Lester and D. J. Summers, Phys. Lett. B **463**, 99 (1999); A. Barr, C. Lester and P. Stephens, J. Phys. G **29**, 2343 (2003).

[278] V. D. Barger, R. W. Robinett, W. Y. Keung and R. J. N. Phillips, Phys. Lett. **131B** (1983) 372; H. Baer, X. Tata and J. Woodside, Phys. Rev. D **42** (1990) 1568; H. Baer, C. h. Chen, M. Drees, F. Paige and X. Tata, Phys. Rev. D **58** (1998) 075008.

[279] H. Baer, V. Barger, N. Nagata and M. Savoy, Phys. Rev. D **95** (2017) no.5, 055012.

[280] H. Baer, A. Mustafayev and X. Tata, Phys. Rev. D **89** (2014) no.5, 055007. See also, C. Han, A. Kobakhidze, N. Liu, A. Saavedra, L. Wu and J. M. Yang, JHEP **1402** (2014) 049; P. Schwaller and J. Zurita, JHEP **1403**, 060 (2014).

[281] Z. Han, G. D. Kribs, A. Martin and A. Menon, Phys. Rev. D **89** (2014) no.7, 075007; H. Baer, A. Mustafayev and X. Tata, Phys. Rev. D **90** (2014) no.11, 115007; C. Han, D. Kim, S. Munir and M. Park, JHEP **1504** (2015) 132.

[282] CMS Collaboration [CMS Collaboration], CMS-PAS-SUS-16-048.

[283] M. Aaboud *et al.* [ATLAS Collaboration], Phys. Rev. D **97** (2018) no.5, 052010.

[284] H. Baer, V. Barger, P. Huang, D. Mickelson, A. Mustafayev, W. Sreethawong and X. Tata, Phys. Rev. Lett. **110** (2013) no.15, 151801; H. Baer, V. Barger, P. Huang, D. Mickelson, A. Mustafayev, W. Sreethawong and X. Tata, JHEP **1312** (2013) 013, Erratum: [JHEP **1506** (2015) 053]; H. Baer, V. Barger, J. S. Gainer, M. Savoy, D. Sengupta and X. Tata, Phys. Rev. D **97** (2018) no.3, 035012.

[285] H. Baer, V. Barger, J. S. Gainer, P. Huang, M. Savoy, H. Serce and X. Tata, Phys. Lett. B **774** (2017) 451.

[286] C. Borschensky, M. Krämer, A. Kulesza, M. Mangano, S. Padhi, T. Plehn and X. Portell, Eur. Phys. J. C **74** (2014) no.12, 3174.

[287] The ATLAS collaboration [ATLAS Collaboration], ATLAS-CONF-2017-022.

[288] A. M. Sirunyan *et al.* [CMS Collaboration], Phys. Rev. D **97**, no. 1, 012007 (2018) doi:10.1103/PhysRevD.97.012007; A. M. Sirunyan *et al.* [CMS Collaboration], Eur. Phys. J. C **77**, no. 10, 710 (2017) doi:10.1140/epjc/s10052-017-5267-x.

[289] The ATLAS collaboration [ATLAS Collaboration], ATLAS-CONF-2017-037.

[290] A. M. Sirunyan *et al.* [CMS Collaboration], arXiv:1706.04402 [hep-ex].

[291] See, *e.g.* ATLAS Phys. PUB 2013-011; CMS Note-13-002.

[292] H. Baer, A. Lessa, S. Rajagopalan and W. Sreethawong, JCAP **1106** (2011) 031; K. J. Bae, H. Baer and E. J. Chun, Phys. Rev. D **89** (2014) no.3, 031701; H. Baer, V. Barger and H. Serce, Phys. Rev. D **94** (2016) no.11, 115019; K. J. Bae, H. Baer and H. Serce, JCAP **1706** (2017) no.06, 024; H. Baer, V. Barger, D. Sengupta and X. Tata, arXiv:1803.11210 [hep-ph].

[293] T. Han, S. Mukhopadyay and X. Wang, arXiv:1805.00015 [hep-ph].

[294] Talk by L. Shchutska, Moriond EW 2017. See also Ref. [282].

[295] H. Baer, V. Barger, G. Shaughnessy, H. Summy and L. t. Wang, Phys. Rev. D **75** (2007) 095010.

[296] W. S. Cho, K. Choi, Y. G. Kim and C. B. Park, Phys. Rev. Lett. **100** (2008) 171801; M. M. Nojiri, Y. Shimizu, S. Okada and K. Kawagoe, JHEP **0806** (2008) 035; K. Agashe, R. Franceschini and D. Kim, JHEP **1411** (2014) 059; M. Burns, K. Kong, K. T. Matchev and M. Park, JHEP **0903** (2009) 143; W. S. Cho *et al.* JHEP **1408** (2014) 070.

[297] W. Beenakker, R. Hopker, M. Spira and P. M. Zerwas, Nucl. Phys. B **492**, 51 (1997) doi:10.1016/S0550-3213(97)80027-2 [hep-ph/9610490].

[298] W. Beenakker, S. Brensing, M. n. Kramer, A. Kulesza, E. Laenen, L. Motyka and I. Niessen, Int. J. Mod. Phys. A **26**, 2637 (2011) doi:10.1142/S0217751X11053560 [arXiv:1105.1110 [hep-ph]].

[299] K. J. Bae, H. Baer and E. J. Chun, Phys. Rev. D **89** (2014) no.3, 031701; K. J. Bae, H. Baer and E. J. Chun, JCAP **1312** (2013) 028; K. J. Bae, H. Baer, A. Lessa and H. Serce, JCAP **1410** (2014) no.10, 082.

[300] B. Altunkaynak, H. Baer, V. Barger and P. Huang, Phys. Rev. D **92** (2015) no.3, 035015.

[301] A. Bredenstein, A. Denner, S. Dittmaier and S. Pozzorini, Phys. Rev. Lett. **103** (2009) 012002.

[302] F. Febres Cordero, L. Reina and D. Wackeroth, Phys. Rev. D **80**, 034015 (2009) doi:10.1103/PhysRevD.80.034015 [arXiv:0906.1923 [hep-ph]].

[303] G. Bevilacqua and M. Worek, JHEP **1207**, 111 (2012) doi:10.1007/JHEP07(2012)111 [arXiv:1206.3064 [hep-ph]].

[304] `https://twiki.cern.ch/twiki/bin/view/LHCPhysics/SingleTopRefXsec` (Accessed January 10, 2017.)

[305] A. Bredenstein, A. Denner, S. Dittmaier and S. Pozzorini, JHEP **1003**, 021 (2010) doi:10.1007/JHEP03(2010)021 [arXiv:1001.4006 [hep-ph]].

[306] M. Aliev, H. Lacker, U. Langenfeld, S. Moch, P. Uwer and M. Wiedermann, "HATHOR: HAdronic Top and Heavy quarks crOss section calculatoR," Comput. Phys. Commun. **182**, 1034 (2011) doi:10.1016/j.cpc.2010.12.040 [arXiv:1007.1327 [hep-ph]]; P. Kant, O. M. Kind, T. Kintscher, T. Lohse, T. Martini, S. Mölbitz, P. Rieck and P. Uwer, "HatHor for single top-quark production: Updated predictions and uncertainty estimates for single top-quark production in hadronic collisions," Comput. Phys. Commun. **191**, 74 (2015) doi:10.1016/j.cpc.2015.02.001 [arXiv:1406.4403 [hep-ph]].

[307] I. Hinchliffe, F. E. Paige, M. D. Shapiro, J. Soderqvist and W. Yao, Phys. Rev. D **55** (1997) 5520; H. Bachacou, I. Hinchliffe and F. E. Paige, Phys. Rev. D **62** (2000) 015009.

[308] H. Baer, V. Barger, A. Lessa, X. Tata, Phys. Rev. D **86** (2012) 117701.

[309] U. Chattopadhyay, A. Datta, A. Datta, A. Datta, and D. P. Roy, *Phys. Lett.* **B 493** (2000) 127; J. K. Mizukoshi, P. Mercadante and X. Tata , *Phys. Rev.* **D 72** (2005) 035009; R. Kadala, J. K. Mizukoshi, P. Mercadante and X. Tata, Eur. Phys. J C **56** (2008) 511.

[310] `https://twiki.cern.ch/twiki/bin/view/LHCPhysics/SUSYCrossSections13TeVgluglu`; C. Borschensky, M. Krämer, A. Kulesza, M. Mangano, S. Padhi, T. Plehn and X. Portell, Eur. Phys. J. C **74**, no. 12, 3174 (2014) doi:10.1140/epjc/s10052-014-3174-y [arXiv:1407.5066 [hep-ph]].

[311] Y. Gershtein *et al.*, arXiv:1311.0299 [hep-ex].

[312] A. Fowlie, arXiv:1510.07319 [hep-ph].